THE UNIVERSITY
of EDINBURGH

Activity-Dependent Bulk Endocytosis: Control by Molecules and Signalling Cascades. Vol. 1

Jessica Nicholson-Fish

Submitted for a PhD in Biomedical Sciences

The University of Edinburgh

March 2017

Table of Contents

Table of Figures

Acknowledgements

The last 5 years of my life are contained in this book, or at least it seems so. I have grown from a gullible, lazy adolescent into a logical, cynical and fairly lazy adult (science can't fix everything). In all honesty, I started my Ph.D. on a whim. I wasn't ready to make those decisions which adults are expected to make outside of education. However, I don't believe I could have made a better decision if it was one over which I had agonised for months. The skills I have acquired through the infuriating business of scientific inquiry will stay with me for the rest of my life and I've had a marvellous time.

Everything I have accomplished I owe to my amazingly patient supervisors, Mike Cousin and Karen Smillie. They guided me every day and were always at hand to explain something my frazzled mind was not understanding. They were supportive and generous with their time in a way I had no right to expect and I would like to sincerely thank them for all of it. I think in the end that we made a great team, despite (or perhaps because of) the need for Karen to translate between Mike and my overly-excited conversations. Karen will also notice that I'm exhausting my flowery vocabulary in this section, since I restrained myself from using many of my more flamboyant expressions in the main body of this thesis (honest, I did). Looking back through it, I would like to thank her for this. I also owe a special thank you to Mike for sending me the e-mail which inspired my academic whimsy, half a decade ago.

Thank you too to my fellow lab members, both past and present. Every one of them has had some part in my work. Ranging from supporting data (thank you Alex Kokotos for your all-important blotting!), to insight, or to that occasionally essential

wind-down pint (or four...Sarah Gordon, you were a terrible influence). It has been so much fun and I will sincerely miss the Cousin lab, we were definitely the best ones!

I also need to thank my loving, chaotic and brilliant family. My visits always served to take my mind off my work, even when they weren't supposed to. I love you all and thank you so much for making me laugh during those most stressful periods.

A very special thank you to my Mum. She was always listening to my worries and giving me help wherever I needed it. I'm sorry this was so often. I promise that I'll make it up to you when I'm rich and famous. But for now, I thank you from the bottom of my heart for your seemingly boundless generosity and encouragement.

Lastly, thank you to Scott… I can't fail to mention how you helped me with my work. Your name on that paper forever confirms that you had a pivotal role in my favourite brainchild. It would have been so much harder without your insane Excel skills.

I know this will probably be the only page of my thesis you will ever read, but you've succeeded in pretending to follow so many of my lab-related rants that I think I can forgive you this last, bound version. Thank you for being a perfect combination of unyielding support and wonderful distraction. And thank you for making me happy, you really did make all the difference.

Declaration

I, Jessica Nicholson-Fish, have composed this thesis myself. The work and the results reported herein are my own except where indicated, and have not been submitted for any other degree or professional qualification

 .

Abstract

Synaptic vesicle (SV) recycling in the presynapse is essential for the maintenance of neurotransmission. During mild stimulation clathrin-mediated endocytosis (CME) dominates, however during intense stimulation activity-dependent bulk endocytosis (ADBE) is the dominant form of membrane retrieval.

The aim of this thesis was to determine how the signalling molecule GSK3 controlled ADBE, with the hypothesis that this enzyme was required at multiple stages of this endocytosis mode. I also hoped to identify a specific cargo for ADBE.

I found that during intense action potential stimulation, a localised calcium increase is necessary for the activation of Akt, which inhibited GSK3. This activation was mediated via a phosphatidylinositol 3-kinase (PI3K)-dependent mechanism. Furthermore, I found that phosphatidylinositol 4-kinaseIIα (PI4KIIα), a molecule whose abundance is regulated by GSK3, had a key role in ADBE. Specifically, I found that the absence of PI4KIIα accelerated CME but inhibited ADBE and that PI4KIIα controls CME and ADBE via distinct mechanisms.

The PI4KIIα study revealed potential cross-talk between CME and ADBE. To determine whether modulation of either endocytosis mode impacts on the other, the retrieval of genetically-encoded reporters of SV cargo was monitored during intense stimulation during inhibition of either CME or ADBE. The recovery of almost all SV cargo was unaffected by ADBE inhibition but was arrested by abolishing CME. In contrast, VAMP4-pHluorin retrieval was perturbed by inhibiting ADBE and not by blocking CME. Knockdown of VAMP4 also arrested ADBE, indicating that in

addition to being the first identified ADBE cargo, it is also essential for this endocytosis mode to proceed.

Publications

The following papers were published during the course of this PhD;

1. Nicholson-Fish, J.C., Smillie, K.J & Cousin, M.A., 2016. Monitoring activity-dependent bulk endocytosis with the genetically-encoded reporter VAMP4-pHluorin. *Journal of Neuroscience Methods*, Volume 266, Pages 1–10. Available at: http://www.sciencedirect.com/science/article/pii/S0165027016300176

2. Nicholson-Fish, J.C. et al., 2015. VAMP4 Is an Essential Cargo Molecule for Activity-Dependent Bulk Endocytosis. *Neuron*, pp.1–12. Available at: http://linkinghub.elsevier.com/retrieve/pii/S089662731500937X

Nicholson-Fish, J.C., Cousin, M.A. & Smillie, K.J., 2015. Phosphatidylinositol 3-Kinase Couples Localised Calcium Influx to Activation of Akt in Central Nerve Terminals. *Neurochemical research*, 3. Available at: http://www.ncbi.nlm.nih.gov/pubmed/26198194

List of Abbreviations

ADBE	Activity-Dependent Bulk Endocytosis
ADP	Adenosine diphosphate
AM	Acetoxymethyl
AMPA	α-amino-3-hydroxy-5-methyl-4-isoxazolepropionic acid
ANTH	AP180 N-terminal homology
AP	Action Potential
AP-1,2,3	Adaptor Protein-1,2,3
AP180	Adaptor Protein 180
AP-5	(2R)-amino-5-phosphonovaleric acid
Arp	Actin-Related Proteins
ATP	Adenosine triphosphate
BAPTA	1,2-bis(o-aminophenoxy)ethane-N,N,N′,N′-tetraacetic acid
BAR	Bin/Amphiphysin/Rvs
BDNF	Brain-Derived Neurotrophic Factor
BFA	Brefeldin A
BLOC-1	Biogenesis of Lysosome-related Organelles Complex 1
CALM	Clathrin-Assembly Lymphoid Myeloid
CaMKII	Calcium/Calmodulin-Dependent Protein Kinase II
CCP	Clathrin-Coated Pit
CCV	Clathrin-Coated Vesicle
cdk5	Cyclin-Dependent Kinase 5
CFP	Cyan Fluorescent Protein
CGN	Cerebellar Granule Neurons
CHC	Clathrin Heavy Chain
CLC	Clathrin Light Chain
CME	Clathrin-Mediated Endocytosis
CNQX	6-Cyano-7-nitroquinoxaline-2,3-dione
CNS	Central Nervous System
DAG	Diacylglycerol
EGFP	Enhanced Green Fluorescent Protein
EGTA	Ethylene Glycol-bis(β-aminoethyl ether)-N,N,N',N'-tetraacetic Acid
EM	Electron Microscopy
ENTH	Epsin N-terminal homology
FCH	Fer/Cip4 homology domain
FCHO	Fer/Cip4 homology domain-only
GABA	Gamma-Aminobutyric Acid
GFP	Green fluorescent protein
GTP	Guanosine triphosphate

HFS	High Frequency Stimulation
HRB	HIV-1 Rev Binding Protein
HRP	Horseradish Peroxidise
Hsc70	Heat Shock Cognate 70
KD	Knockdown
KO	Knock-out
LDCV	Large Dense Core Vesicles
LFS	Low Frequency Stimulation
NSF	N-ethylmalemide Sensitive Factor
OCRL	oculocerebrorenal syndrome of Lowe
OH-Group	Hydroxy-Group
PC12	Phaeochromocytoma Cell-12
PDK1	Phosphoinositide-dependent kinase-1
PFA	Paraformaldehyde
PH	Pleckstrin homology
PI	Phosphoinositide
PI3K	Phosphoinositide 3-Kinase
PI4K	Phosphoinositide 4-Kinase
PIP_2	PtdIns 4,5-bisphosphate
PIPK1γ	Phosphatidylinositol Phosphate Kinase Type 1γ
PM	Plasma Membrane
PNS	Peripheral Nervous System
PRD	Proline Rich Domain
RP	Reserve Pool
RRP	Readily-Releasable Pool
SH3	Src Homology 3
SNAP	Soluble NSF Attachment Protein
SNARE	SNAP and NSF Attachment Receptors
SNX9	Sorting Nexin 9
SV	Synaptic Vesicle
Syndapin	Synaptic, Dynamin-Associated Protein
t-SNARE	Target SNARE
TTX	Tetrodotoxin
UV	Ultra Violet
VAMP	Vesicle-Associated Membrane Protein
v-GAT	Vesicular GABA Transporter
VGCC	Voltage-Gated Calcium Channel
v-Glut	Vesicular Glutamate Transporter
v-SNARE	Vesicular SNARE
WT	Wildtype

Introduction

1. Introduction

Neurons are electrically excitable cells which are responsible for the transmission of information through electrical and chemical signals. Neurons are connected to form a neural network and vary in structure and function depending on their roles. Examples include sensory neurons which can respond to physical stimulus such as sound, touch or light via the sensory organs they innervate; interneurons which form connections between neurons within the central nervous system (CNS) or between the CNS and peripheral nervous system (PNS), enabling communication between different neuronal types; and motor neurons which receive signals from the brain or spinal cord to affect a muscular or glandular response.

Typically, a neuron consists of a soma or cell body which houses the nucleus of the cell, a number of dendrites through which an electrical input is conducted into the cell and an axon through which a collated electrical input from the dendrites progresses on to the next neurite.

1.1 Synapse Structure and Function

A synapse is the junction of two neurons. Through this junction an electrical impulse (action potential) is transmitted from one neuron to the other via a chemical intermediate, termed a neurotransmitter. The synapse consists of a presynaptic terminal (in which quanta of neurotransmitter are contained in synaptic vesicles (SVs)); a synaptic cleft (an extracellular space separating the two cells); and the post-synaptic terminal (on which resides membrane-bound receptors for neurotransmitter detection) (see Figure 1.1). The post-synaptic membrane is a component of a dendrite of the next neuronal cell.

Action potentials are transmitted down axons of presynaptic neurons via the controlled exchange of charged ions, creating a difference in membrane potential which travels extremely quickly toward the presynapse. The arrival of an action potential in the presynaptic terminal depolarises the cell membrane and causes an influx of extracellular calcium (Ca^{2+}) (Figure 1.1 A). This influx mainly occurs at a site called the active zone, an area enriched with voltage-gated Ca^{2+} channels (VGCCs). A population of neurotransmitter-containing SVs are tethered to the plasma membrane (PM) in close proximity to these Ca^{2+} channels, allowing Ca^{2+}-sensitive machinery to respond rapidly to stimulation of the cell and causing fusion of the SV (Südhof 2013). This fusion allows the neurotransmitter to be released into the synaptic cleft (Figure 1.1 B), diffusing across to the post-synaptic membrane and binding to receptors. Depending on the type of neurotransmitter released this has one of two effects: 1) For excitatory presynaptic cells, postsynaptic binding of neurotransmitter increases the probability of an action potential being transmitted

down the axon of the post-synaptic cell by changing its cross-membrane potential. For example, the postsynaptic binding glutamate or acetylcholine causes the opening of channels, allowing influx of positively charged ions and causing depolarisation of the postsynaptic cell and the procession of the action potential down the dendrite. 2) For inhibitory presynaptic cells, the binding of neurotransmitter decreases the possibility of an action potential progression. For example, postsynaptic GABA causes the opening of chloride channels allowing influx of negatively charged ions and causing hyperpolarisation of the postsynaptic cell. This has the effect of making it less likely that input from an excitatory presynaptic cell will depolarise the postsynaptic cell sufficiently to transmit the action potential onwards.

To enable the release of vesicles for a subsequent stimulus, and to avoid inflation of the cell due to insertion of membrane, SVs are formed directly or via an endosomal intermediate from the edge of the active zone or the peri-active zone (Figure 1.1 C, D and F) and are refilled with neurotransmitter (Figure 1.1 E) for future cycles of synaptic communication.

1.2 Synaptic Vesicle Pools

Within the presynapse, SVs have been proposed to reside within functionally discrete groupings referred to as "pools". The hypothesis of distinct vesicle pools was first developed when observing acetylcholine release from feline sympathetic ganglia (Birks & MacIntosh 1961). Upon stimulation, a small "readily releasable" fraction of acetylcholine was observed which depleted rapidly during stimulation at high frequencies as well as a larger, "non-readily releasable" fraction (Birks & MacIntosh 1961). These observations led to the idea of SVs with different release probabilities residing within a synapse which were undergoing fusion only when their specific release criteria had been met.

A universally agreed model on the identity and function of different SV pools has not yet been developed, and terminology differs between laboratories. Most groups concur that there is a pool of vesicles from which SVs are rapidly released on stimulation: the readily-releasable pool (RRP). However, during prolonged activity the number of vesicles which fuse with the PM can greatly exceed the number of vesicles docked at the active zone (Betz 1970). It is agreed that there is another pool of vesicles which are mobilised only during prolonged stimulation: the reserve pool (RP). Together, these two pools can be termed as the recycling pool i.e. the collection of all SVs which are available for release (Südhof 2000). SVs outwith these populations of releasable vesicles are therefore classified as belonging to the "resting pool" of SVs.

A typical hippocampal synapse contains somewhere in the vicinity of 200 SVs (Schikorski & Stevens 1997). Using SV proteins which have been lumenally-tagged

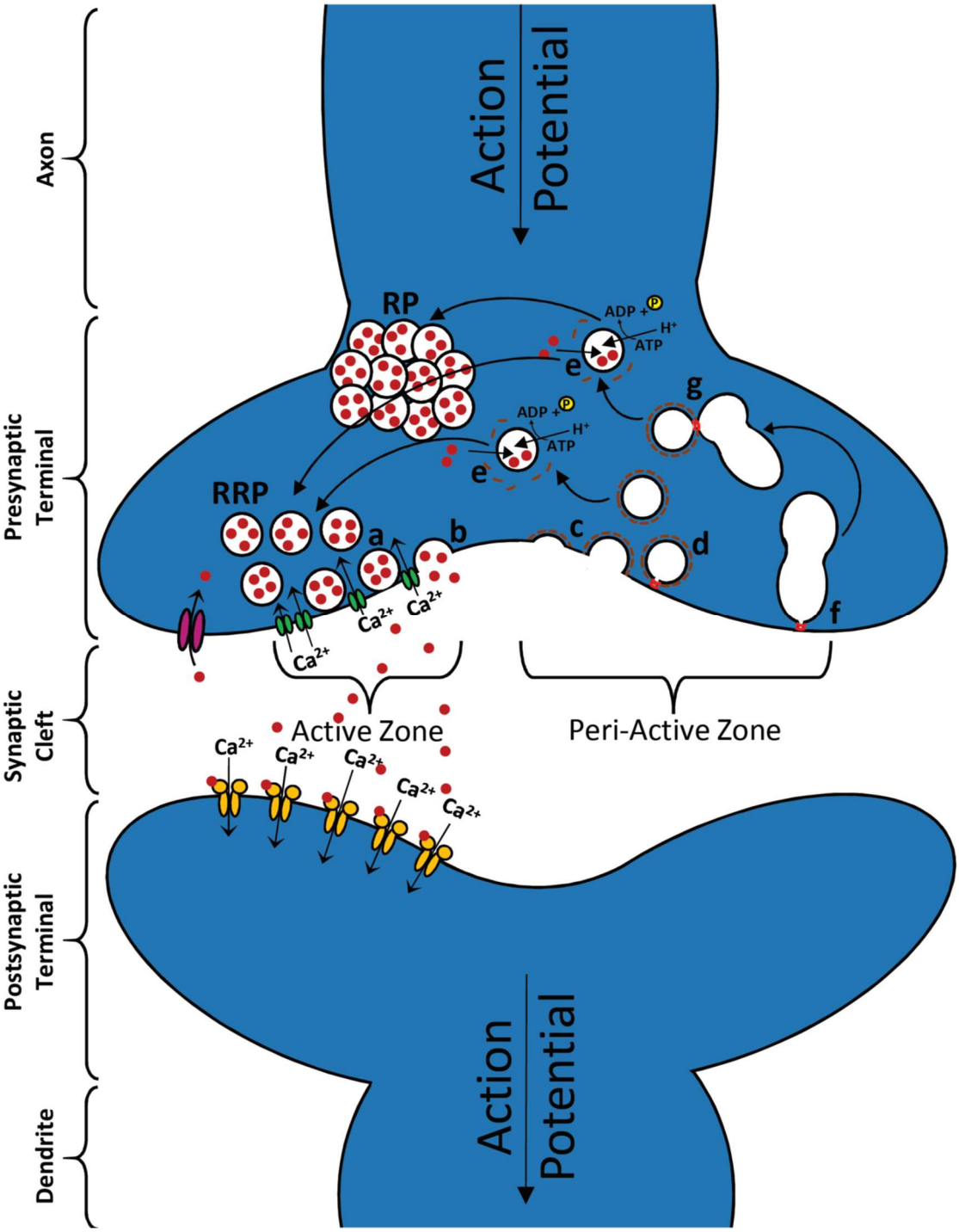

Figure 1.1 Synaptic Vesicle Recycling in the Presynaptic Terminal

An action potential arriving via an axon of the presynaptic terminal depolarises the synaptic membrane and causes the opening of calcium channels, leading to an influx of Ca^{2+} molecules (a). This Ca^{2+} interacts with fusion machinery and causes the exocytosis of docked and primed SVs (b). Coupled tightly to this is the endocytosis of SVs via CME. SVs or formed via a clathrin coat (c) and scissioned from the membrane via dynamin (d). Newly formed SVs are then uncoated, acidified and filled with neurotransmitter (e). During intense activity, larger sections of membrane are invaginated via ADBE (f).

with a pH-sensitive GFP molecule (pHluorin), one can track the relative amount of a certain protein to be exposed to the exterior of the cell compared to its total population. Using pHluorins it has been demonstrated that within a given population, the number of SVs available for release (recycling pool) during a prolonged stimulation is around 50% in neurons (Kim & Ryan 2010).

It is worth noting that other models propose that nearly all SVs are available for release in the synapse with sustained activity. With regards to these models the three pools are classified as such: the readily releasable pool (1%) – SVs docked and primed at the active zone and primed for release; the recycling pool (5-20%) – the pool of vesicles that maintain release during moderate stimulation; and the reserve pool – the remaining 80-90% of vesicles which are only released during intense stimulation (Rizzoli & Betz 2005). This model was, however, developed around data acquired from goldfish retinal bipolar cells as well as frog neuromuscular junction (NMJ) cells which are much larger and have a greatly increased number of SVs: around 700,000 and 500,000 per synapse respectively. It was also noted in these studies that the frequencies needed to stimulate the exocytosis of these SVs was most likely not representative of physiological stimulation (Rizzoli & Betz 2005).

The RRP is tethered in close proximity to the active zone, allowing for rapid fusion upon arrival of an action potential to the synapse. The reserve pool however is immobilised and away from the active zone membrane. Actin has been implicated in the clustering of these SVs (Doussau & Augustine 2000) and several studies have shown a dynamic modification of actin filaments in the presynapse in response to activity (Morales et al. 2000; Colicos et al. 2001; Sankaranarayanan et al. 2003).

Depolymerisation of actin via lantrunculin A increases neurotransmitter release without affecting the size of the RRP (Morales et al. 2000) showing a role for actin in the restraint of SVs separate from the RRP during stimulation.

Further interference with actin function has shown a role for actin filaments in the recycling of SVs after endocytosis back to this vesicle cluster (Shupliakov et al. 2002). Other work has shown an active recruitment of actin from the axon to presynaptic vesicle clusters during stimulation in hippocampal neurons (Sankaranarayanan et al. 2003). However, despite disrupting this recruitment, interference with actin dynamics using lantrunculin A does not inhibit SV formation as measured by uptake of styryl dyes (Sankaranarayanan et al. 2003). As such it would seem that actin recruitment is not essential for SV formation and it is likely it plays a role as a scaffolding protein for regulatory molecules involved in SV formation.

Actin does not interact with SV membrane directly (Doussau & Augustine 2000) and as such the regulation of the mobilisation and release of SVs held within this actin filament structure is mediated via an intermediate: synapsin (Hilfiker et al. 1999). Synapsins are a family of peripheral SV phospho-proteins which are capable of binding both actin and SVs simultaneously (Benfenati et al. 1992).

The necessity for synapsin in the assembly and/or maintenance of a reserve pool has been demonstrated in synapsin knockout mice; mouse models deficient in all isoforms of synapsin (I a and b, II a and b and III a and b) have shown a decrease in the number of SVs clustered away from the PM, with no effect on the number of SVs docked at the PM (Gitler et al. 2004), showing a role for synapsin in the maintenance

of a pool of vesicles distinct from the RRP, similar to if not overlapping with the role performed by actin. Similar studies in mouse models devoid of only one or two synapsin isoforms have shown similar effects on the clustering of SVs (L. Li et al. 1995; Takei et al. 1995). On an ultrastructural level, synapsins have been shown to localise specifically to SVs distal to the active zone (De Camilli et al. 1983; Hirokawa et al. 1989; Torri-Tarelli et al. 1990; Pieribone et al. 1995; Bloom et al. 2003), possibly indicating a specificity for reserve pool SVs.

The release of SVs from this synapsin-actin matrix is dependent on phosphorylation. The affinity of synapsin for SVs is dramatically decreased when synapsin is phosphorylated by cAMP-dependent protein kinase (PKA), Ca^{2+} /calmodulin-dependent kinase I (CaM kinase I) or Ca^{2+} /calmodulin-dependent kinase II (CaM kinase II) (Schiebler et al. 1986; Hosaka et al. 1999; Menegon et al. 2006); whereas phosphorylation of synapsin by mitogen-activated protein kinase (MAP kinase) decreases its affinity for actin (Jovanovic et al. 1996).

During periods of prolonged activity an increase in internal calcium concentration ($[Ca^{2+}]_i$) causes an activation of Ca^{2+}-dependent kinases such as CaM kinase I/II and those forms of PKA which are Ca^{2+}-sensitive. This causes a decrease in the affinity of synapsin for SVs and mobilisation of those vesicles held within the matrix (Chi et al. 2001; Chi et al. 2003; Menegon et al. 2006). Increased $[Ca^{2+}]_i$ during periods of high activity also causes the activation of calcineurin which dephosphorylates those sites phosphorylated by MAP kinase and increases the affinity of synapsin for actin. This adaptable interaction may be responsible for modulating actin dynamics during high synaptic activity (Jovanovic et al. 1996; Jovanovic et al. 2001). Together this

shows that the reserve pool of vesicles is held within an actin-synapsin matrix designed to change shape during periods of intense activity, freeing these SVs and allowing continued SV fusion and therefore synaptic transmission when the RRP has been depleted.

1.3 Synaptic Vesicle Life Cycle

The cycle of fusion (exocytosis) and formation (endocytosis) of SVs in the presynapse is essential for efficient neuronal signalling and therefore function of the nervous system. Mutations or abnormal expression of proteins integral to this process have been linked to a variety of neurological conditions. Examples include: a single point mutation in synaptic protein synapsin I and familial epilepsy (Garcia et al. 2004); decreased expressions of essential endocytic proteins synaptotagmin, AP-2, AP180 and dynamin I in Alzheimer's disease (Yao 2004); and mutations of the presynaptic phosphatase synaptojanin 1 in certain cases of mania or depression (Saito et al. 2001; Stopkova et al. 2004).

1.3.1 Synaptic Vesicle Exocytosis

Exocytosis of a vesicle is not as simple as two membranes colliding and fusing. It occurs via a series of tightly regulated processes. All of which; docking, priming and fusion and require a multitude of proteins to facilitate each stage.

1.3.1.1 Docking and Priming of Synaptic Vesicles

The current model for the docking and priming of SVs hypothesises that SVs connect ("dock") to the active zone within the presynapse. Subsequent to this the SVs undergo a process allowing them to become capable of fusion ("primed"). These SVs form the RRP, the docking and priming of these SVs in such close vicinity to the calcium channels of the active zone allows them to be rapidly fused with the PM upon an increase in $[Ca^{2+}]_i$ (Südhof 2013).

Although the necessity for each of these processes is accepted, the conclusions drawn from studies into the molecular processes belying them remains relatively inconclusive. For example, one theory derived from work in chromaffin cells stated that the SV protein synaptotagmin-1 functions as calcium-sensitive machinery during docking through its interactions with membrane-bound synaptosomal-associated protein 25 (SNAP-25)/syntaxin complexes (de Wit et al. 2009). This model is popular and yet contentious as other work in synaptotagmin-1 KO mice showed that though a phenotype was observed in the docking of large dense-core vesicles in chromaffin cells, this defect was not recapitulated in the fusion of secretory vesicles (Schonn et al. 2008). Work in synapses utilising synaptotagmin KO or mutant mice have shown deficits in the release of neurotransmitter with little to no corresponding defects in the size or location of the RRP (Geppert et al. 1994; Liu et al. 2009). These results would disagree with the model of synaptotagmin as a component for docking but instead imply more of a role in the fusion of a SV.

The variety of models, cell types, methods of fixation, definitions and terminology used in the study of the docking and priming of vesicles across the field of study make a consensus difficult to gauge. The accurate identification of docked vesicles has been argued to require the measurement of intermembrane differences in the order of nanometres (Verhage & Sørensen 2008), resulting in a morphological rather than functional definition of docked vesicles which can only be studied reliably via electron microscopy.

The docking of a SV at the active zone requires an interaction of both vesicular and membrane proteins. The process of priming organises these proteins in such a way to facilitate a rapid fusion upon Ca^{2+} entry to the active zone.

The initial recruitment of SVs to an available space at the active zone is likely driven by the binding of SV proteins (e.g. Rab3/27) to Rab-interacting molecules (RIMs) (Haucke et al. 2011) and RIM-binding proteins (Liu et al. 2011). RIMs directly associate with a large portion of active zone and SV proteins including calcium channels themselves (Mittelstaedt et al. 2010) and have been shown to be essential for SV docking and priming (Koushika et al. 2001; Schoch et al. 2002; Schoch et al. 2006; Gracheva et al. 2008), though their exact mechanism of action is unknown.

The docking and priming of SVs to the active zone after their recruitment is facilitated through the association of membrane proteins. The collective name for the proteins which assemble between SV and PM during docking and priming is SNARE proteins (for Soluble N-ethylmaleimide-sensitive factor {NSF}-Attachment protein REceptors). The SNARE complex, formed upon docking, consists of proteins both on the vesicle (v-SNARES) and on the PM (t-SNARE) (Söllner et al. 1993).

t-SNAREs consist of syntaxin-1 and SNAP-25 and the v-SNARE is synaptobrevin II. Although SNARE proteins are varied in size and structure each protein shares a SNARE motif in their cytosolic domain. This is a 60-70 amino acid region that contains heptad repeats which are able to form coiled-coil structures. SNAP-25 is unique in that it has two SNARE motifs. Once assembled the SNARE proteins form a complex consisting of four α-helix domains, with one each of synaptobrevin and syntaxin and both SNAP-25 motifs contributed (Sutton et al. 1998; Stein et al. 2009).

The incorporation of syntaxin into this SNARE complex is the rate limiting step of this interaction. Syntaxin is held in a "closed" state by Munc-18 in which it is incapable of interacting with other SNARE proteins (Burkhardt et al. 2008); t-SNAREs syntaxin and SNAP-25 must first form a dimer before v- and t-SNARE binding can successfully occur to form a trans-SNARE complex (Fasshauer et al. 2002; Rickman et al. 2004).

Munc-18 is one of the family of Sec1/Munc18-like (SM) proteins. Munc18 was first linked to membrane fusion through the discovery of its association with syntaxin (Hata et al. 1993) and is essential for exocytosis of SVs (Verhage et al. 2000) though its exact function is not exactly understood. Its arch-shaped structure contains a central cavity with a high-affinity for the t-SNARE syntaxin (Misura et al. 2000; Burkhardt et al. 2008). However, it is thought that Munc-18 has a role in the initiation of the fusion machinery assembly (Jahn & Fasshauer 2012) and it remains associated with a SNARE complex throughout assembly and disassembly (Khvotchev et al. 2007).

However, the binding of Munc-18 to the individual t-SNARE syntaxin occludes part of the SNARE motif and therefore inhibits SNARE -complex formation; this is referred to as a "closed" conformation of syntaxin (Dulubova et al. 1999; Misura et al. 2000). The consequences of this interaction would suggest a contradictory suppressive action of Munc-18 on SNARE complex formation. It has been hypothesised therefore that Munc-18 firstly acts as a chaperone for syntaxin-1 to a prospective fusion site (Jahn & Fasshauer 2012) and the closed formation of syntaxin

is necessary to prevent the formation of ectopic SNARE complexes before its arrival at the active zone (Medine et al. 2007).

Another hypothesis for the purpose of Munc18 observes the similarities between a closed syntaxin structure and a complete SNARE complex. In addition to its coiled SNARE motif, syntaxin also contains a three-helix bundle comprising its globular, N-terminal "Habc" domain. This domain folds back and binds the helical SNARE motif to form the closed syntaxin conformation (Dulubova et al. 1999; Misura et al. 2000). In this closed configuration, syntaxin forms a four helix bundle which is clasped by Munc-18. The Habc domain of Munc-18 is also able to bind to a fully formed four helix SNARE complex (Dulubova et al. 2007). It has been proposed that Munc-18 releases syntaxin during SNARE-complex assembly allowing the opening of its structure and subsequent incorporation into the SNARE complex, it then forms an association with the four helix bundle of the SNARE complex, possibly helping to form this transmembrane SNARE complex when the three SNARE proteins are brought into proximity.

The SNARE/Munc-18 complex, is not the only release machinery involved in priming a SV for exocytosis. Complexin (also known as synaphin) is a highly charged, hydrophilic protein (Ishizuka et al. 1995) which binds with high affinity only to partly or fully formed SNARE complexes. It is possible that the binding of complexin to a SNARE complex allows its associated SV to become what is termed as "superprimed"; and that it is in this formation that a SNARE complex becomes a substrate for the Ca^{2+}-sensitive component of SV release machinery synaptotagmin I – all synaptotagmin-controlled fusion reactions examined to date appear to require

complexin (Südhof 2013). It is also possible that the integration of complexin into this complex allows the stabilisation of the correctly orientated syntaxin-synaptobrevin allowing more efficient fusion (Tang et al. 2006; Jahn & Fasshauer 2012) and that complexin binding has no effect on synaptotagmin as it is independent from the SNARE complex.

The role of complexin in the priming of SVs is somewhat confused by the presence of both an N-terminal head, which is directed towards the PM and is required to facilitate fusion (Maximov et al. 2009) but also a central helix which plays an inhibitory role in fusion (Giraudo et al. 2009). This has led to two main theories of the molecular mechanism of complexin and its seemingly dual stimulatory and inhibitory roles (Brose 2008; Stein & Jahn 2009; Sudhof & Rothman 2009; Sørensen 2009; Neher 2010a). Firstly, the addition of complexin to an assembling SNARE complex may promote the "zippering" of the separate helices and sensitise them to the action of synaptotagmin in the presence of calcium. Secondly, the addition of complexin to a zippering complex may act as a clamp and block further progression and spontaneous fusion. A block which is relieved by the calcium-triggered action of synaptotagmin.

These two functions are not necessarily mutually exclusive; if SVs are not held in a stable configuration the potential for spontaneous firing and depletion of the RRP is greatly increased and complexin has been shown to inhibit spontaneous exocytosis (Wragg et al. 2013). With this in mind, a SV must be capable of rapid fusion when a synaptic stimulus arrives. As such complexin serves the dual purposes of facilitating

the action of Ca^{2+}-sensitive machinery whilst maintaining the stability of the SNARE complex.

Complexin is not essential for exocytosis to proceed, however complexin knockout mice show a greatly reduced release of RRP SVs demonstrating a facilitative role of the protein in the maintenance of a population of primed SVs (Reim et al. 2001).

1.3.1.2 Fusion

After the docking and priming of a SV, the SNARE proteins embedded in each membrane form a *trans*-complex which undergo a zippering together of the four helical SNARE motifs which progresses from N- to C-terminal on each motif (Hanson et al. 1997).

This zippering action is triggered by entry of Ca^{2+} to the active zone. This Ca^{2+} -dependent response is mediated via a protein complex consisting of RIM, RIM-BP and Munc-13. This complex binds SVs via Rab proteins Rab3 and Rab 27 whilst simultaneously binding VGCCs (Südhof 2013), effectively tethering one to the other. The close proximity of the SV and its SNARE complex to this entering Ca^{2+} allows a rapid fusion of membrane after stimulation. The calcium-sensitive element of SV release machinery has been identified as synaptotagmin 1 (Fernández-Chacón et al. 2001; Sørensen et al. 2003; Pang et al. 2006). There are 16 different synaptotagmins expressed in the brain and eight of these bind Ca^{2+}. Synaptotagmin 1, 2 and 9 all have roles in some form of synchronous SV exocytosis and all with slightly different kinetics which are suited for the particular cell type in which they are expressed (Xu et al. 2007).

Synaptotagmin is a transmembrane protein with two cytoplasmic C2 domains (Perin et al. 1990) which contain Ca^{2+} binding sites (Brose et al. 1992): C2A- which can bind three Ca^{2+} ions and C2B which can bind two (Südhof 2004). These C2 domains are connected to each other and the membrane by flexible linkers (Jahn & Fasshauer 2012) and have the ability to bind Ca^{2+} in a manner which increases their affinity for phospholipids (Brose et al. 1992; C. Li et al. 1995). These C2 domains also facilitate folding of synaptotagmin (Perin et al. 1990; Davletov & Sudhof 1993; Sutton et al. 1995; Südhof 2004) as well as binding to syntaxin and SNARE complexes (Bennett et al. 1992; Söllner et al. 1993; C. Li et al. 1995) in a manner which is increased in the presence of Ca^{2+}. These facts together create a model for Ca^{2+}-mediated fusion being facilitated by synaptotagmin bound to a *trans*-SNARE complex, and undergoing a conformational shift implemented by Ca^{2+} binding to its C2 domains and completing the zippering of the SNARE complex helices. This zippering action forces the vesicular and PM into close proximity and consequently destabilises their hydrophilic surfaces, opening a fusion pore.

This is not the only current model as to the role of synaptotagmin in SV fusion. There is evidence that synaptotagmin does not bind to SNARE complexes *in vivo* due to the presence of polyvalent ions such as ATP and Mg^{2+} and that it is actually synaptotagmins association with the phospholipid PIP_2 which mediates the fusion of SVs upon Ca^{2+} entry (Park et al. 2015). In this model, the addition of Ca^{2+} ions to the C2 domains of synaptotagmin causes their insertion into the lipid bilayer of the PM, bringing it and the SV membrane into closer proximity and causing fusion.

Despite the general acknowledgement of synaptogamin's role as the calcium sensitive effector for SV release, it is still controversial as to how the influx of calcium implements the rapid, synchronous exocytosis of SVs. It is widely agreed that a primed SV is tethered by a SNARE complex in a partially zipped state which is somehow prevented from full co-ordination. This could be either by an energy barrier or by an interfering protein (such as complexin or possibly synaptotagmin). It is also possible that Munc-18 is still bound to the SNARE complex at this stage. Some believe that this complex is strained, storing energy that could be released during exocytosis. Others believe that this complex is relaxed allowing a flexibility of the linkers connecting the zippered section of the complex and the membrane (Jahn & Fasshauer 2012).

The model of synaptotagmin-mediated fusion therefore would differ depending on which conformation SNARE complex is perceived. The reaction of synaptotagmin after Ca^{2+} binding could progress in any of the following ways:

1. Ca^{2+} binding allows synaptotagmin to disengage from SNAREs, thereby removing itself as an inhibitory device (fusion clamp model – synaptotagmin) (Chicka et al. 2008).
2. Ca^{2+} binding allows synaptotagmin to bind the SNARE complex, thereby displacing the inhibitory complexin (fusion clamp model – complexin) (Yang et al. 2010) and/or…
3. …Ca^{2+} binding allows synaptotagmin to bind the SNARE complex, thereby promoting the completion of SNARE motif zippering (energy barrier model) (Yang et al. 2010).

4. Ca^{2+} binding allows synaptotagmin to bind to PM adjacent to partially zipped SNARE complex, causing destabilisation at the fusion site (energy barrier model) (Stein et al. 2007; Xue et al. 2008; Lee et al. 2010).
5. Ca^{2+} binding allows synaptotagmin to increase curvature stress by displacing lipids in the PM (energy barrier model) (Martens et al. 2007; Hui et al. 2009).
6. Ca^{2+} binding allows synaptotagmin to bind to PM, therefore accelerating fusion by charge compensation due to the positive electrostatic potential of its C2 domains (energy barrier model) (Araç et al. 2006).

Currently none of these models uniformly fit the wealth of gathered evidence (Jahn & Fasshauer 2012) and hence the method of Ca^{2+}-activated synaptotagmin-mediated fusion remains elusive.

1.3.1.3 SNARE Complex Disassembly and Retrieval

Upon fusion, the SV collapses into the PM, hence the SNARE complex formed of v-SNAREs and t-SNAREs is no longer a *trans*-SNARE complex residing on two distinct membranes but a *cis*-SNARE complex – tightly bound via the SNARE motifs and residing entirely on the PM. To ensure a sustainable pool of t-SNARE proteins on the PM, and to allow the uptake of v-SNAREs onto newly forming SVs, these *cis*-SNARE complexes must be broken apart into their constituent parts.

The process of "unzipping" the assembled SNARE motifs requires energy. This is supplied via the ATPase N-ethylmaleimide-sensitive fusion (NSF) protein which binds to SNARE complexes via adaptors called soluble NSF-attachment proteins (SNAPs). NSF is a member of a AAA+ family of ATPases (Erzberger & Berger

2006) and forms homomeric hexamers with each protomer containing two ATPase domains and one amino-terminal domain which is responsible for SNAP and possibly SNARE binding (Whiteheart et al. 2001). Together the NSF hexamer, SNAPs and SNARE complex bind to form a “20S” complex prior to ATP hydrolysis (Söllner et al. 1993).

It has been hypothesised that in any given 20S structure there contains up to four molecules of SNAP, one hexameric ring of NSF and one SNARE complex (Zhao et al. 2015). This hypothesis has given rise to the following model: firstly, a barrel of SNAP molecules surrounds the SNARE helices. After this NSF attaches to form a complete 20S structure, and its ATPase rings tighten like a loaded spring (Zhao et al. 2015). This model suggests that the 20S complex utilises ATP hydrolysis to twist and exert a torque force to unwind the SNARE helices (Zhao et al. 2015).

After this disassembly, all components of this SNARE complex become available for future rounds of exocytosis. t-SNAREs remain on the PM and v-SNARES are retrieved via endocytosis onto new SVs along with all other SV cargo. Failure to clear the active zone of these proteins leads to an inhibition of neurotransmitter release and clearance has been proposed to be a rate-limiting step in SV fusion (Neher 2010b)

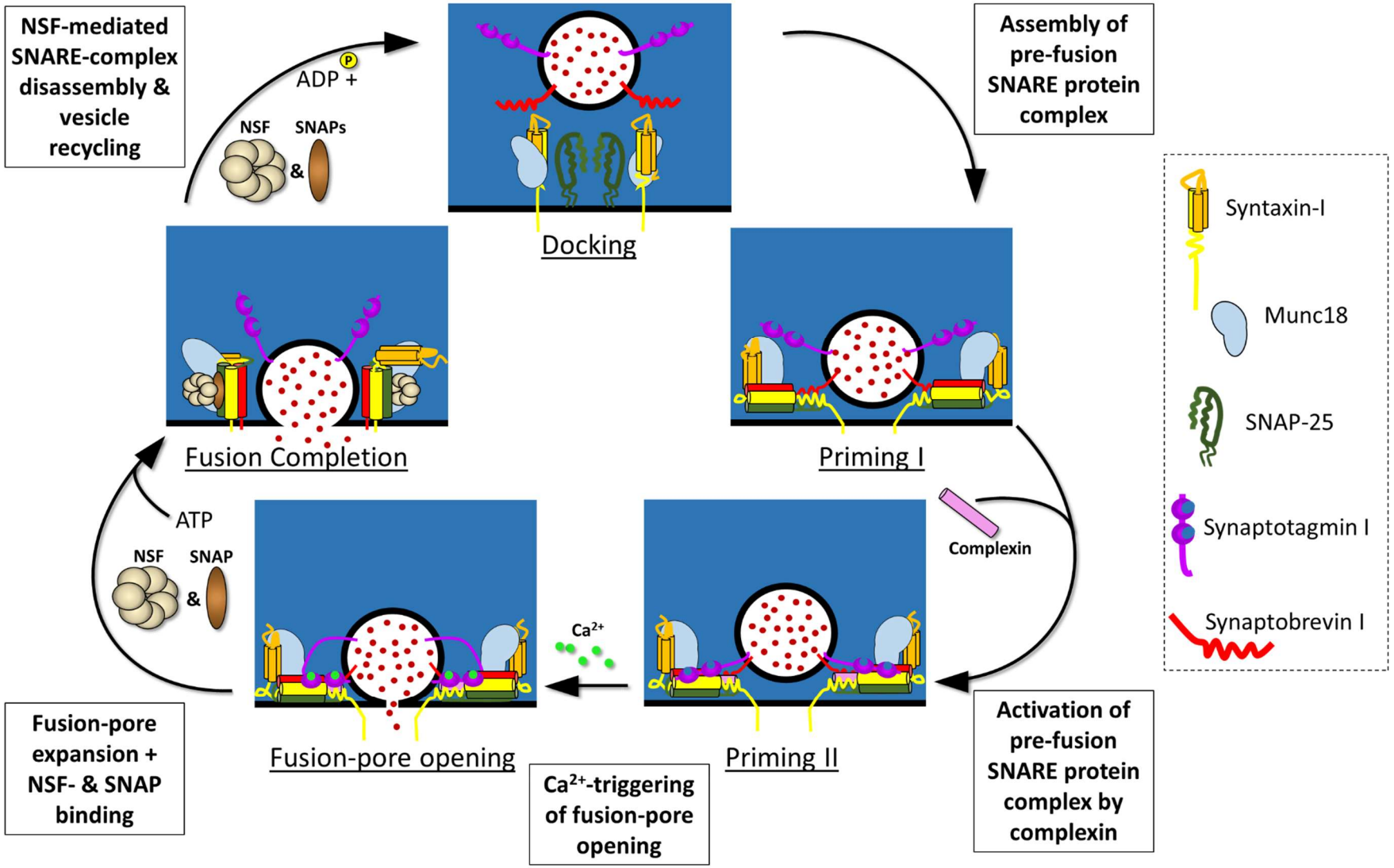
NSF-mediated SNARE-complex disassembly & vesicle recycling
ADP +
P
NSF
SNAPs
&
Docking
Assembly of pre-fusion SNARE protein complex
Syntaxin-I
Munc18
SNAP-25
Synaptotagmin I
Synaptobrevin I
Fusion Completion
Priming I
ATP
NSF
SNAP
&
Complexin
Ca2+
Fusion-pore opening
Priming II
Fusion-pore expansion + NSF- & SNAP binding
Ca2+-triggering of fusion-pore opening
Activation of pre-fusion SNARE protein complex by complexin

Figure 1.2 Fusion of Synaptic Vesicles – Exocytosis

Schematic showing the docking, priming and fusion of synaptic vesicles. Beginning from the top panel and going clockwise: Box 1: a SV is brought into the vicinity of the active zone. On the plasma membrane, the t-SNARE syntaxin (orange) is held in its closed formation by Munc18 (blue). Box 2: Priming I – Syntaxin opens and a SNARE complex is formed via the SNARE motif of syntaxin, the two of SNAP-25 (green) (t-SNAREs) and synaptobrevin II (red) (v-SNARE). Munc18 then binds this four helix bundle. Box 3: Priming II – after this formation complexin (pink) inserts itself into the complex, facilitating the future fusion of the two membranes, possibly by association with synaptotagmin (purple). Box 4: Fusion-pore opening – during stimulation, Ca^{2+} binds synaptotagmin and causes an alteration in its association with the SNARE complex, bringing the two membranes into contact and forcing fusion. Box 5: Fusion completion - The SV collapses into the plasma membrane and neurotransmitter is released into the extracellular space. The SNARE complex is now residing bound on one membrane. NSF (cream) and SNAPs (brown) bind the complex and utilise ATP hydrolysis to break apart the complex. Individual components of the complex are then free to recycle for further rounds of fusion. Adapted from (Südhof 2013).

1.3.2 Synaptic Vesicle Endocytosis

1.3.2.1 Clathrin Mediated Endocytosis

Clathrin mediated endocytosis (CME) is required for the uptake of not only SNAREs but all SV cargo from the presynaptic PM. This endocytic route is the best characterised method of synaptic membrane retrieval and utilises a host of accessory proteins, allowing the uptake of a variety of cargo proteins into each internalised SV. CME can be separated into several stages: nucleation, cargo selection, invagination, fission and uncoating. The process of endocytosis of a single SV after stimulation has been measured using fluorescent-tagged SV proteins such as synaptophysin-pHluorin and estimated to take a time of around 15 seconds (Granseth et al. 2007) for a SV to become entirely separated from the PM.

However, this model of initiation has recently been called into question. Several studies have shown a role for the formation of a nucleation module, which appear to label those sites on the PM to which clathrin and its adaptor proteins will be recruited (Henne et al. 2010; Stimpson et al. 2010).

This nucleation module consists of FCH domain only (FCHO) proteins, EGFR pathway substrate 15 (eps15) and intersectins (Henne et al. 2010; Stimpson et al. 2010; Reider et al. 2009) and its assembly at the PM is thought to be facilitated by an affinity for PIP_2 (McMahon & Boucrot 2011). Depletion of either FCHO, eps15 or intersectins inhibits clathrin coat recruitment in yeast (Henne et al. 2010; Stimpson et al. 2010; Reider et al. 2009).

FCHO proteins contain curvature-sensing F-BAR domains which act to create very low curvatures. Deletion of this F-BAR domain inhibits the formation of clathrin-coated pits (Henne et al. 2010) showing a necessity for membrane curvature even before the recruitment of adaptor proteins and clathrin molecules. However, it has been suggested that the role played by FCHO proteins is not essential in all CME as and at least partially redundant with that played by Eps15 (Wang et al. 2016).

1.3.2.1.1 Cargo Selection

Once the nucleation module is formed, generating a slight membrane curvature, it is now thought to be responsible for the recruitment of AP-2 (Henne et al. 2010; McMahon & Boucrot 2011) via its interactions with module component eps15 (Benmerah et al. 1998). AP-2 is a tetramer and consists of two large subunits (α2 and β2), an intermediate size subunit (μ2) and a small subunit (σ2). AP-2 anchors itself to the PM through a direct interaction with PIP_2 via the α2 subunit (Gaidarov & Keen 1999). The β2 subunit of AP-2 binds directly to the SV scaffold protein clathrin, recruiting it to an invaginating SV (Shih et al. 1995).

AP-2 also binds to epsin (Chen et al. 1998), an ENTH-domain protein which binds to PIP_2 and inserts an amphipathic helix into the PM, inducing further membrane curvature (Ford et al. 2002). It is possible that both ENTH-domain proteins epsin and eps15 work in concert. Epsin and eps15 interact via their carboxy-terminal and EH domains respectively (Chen et al. 1998) both are capable of binding multiple copies of AP-2 and both are displaced from AP-2 upon clathrin binding (Morgan et al. 2003; Praefcke et al. 2004) and move to the rim of growing coated pits.

AP-2 acts as the major hub for protein interactions in the growing clathrin-coated pit, the μ- and σ-subunits are capable of interacting directly with the cytoplasmic tails of transmembrane receptors as well as indirectly with other SV cargo using appendage domains to bind accessory adaptor proteins (Collins et al. 2002; Kelly et al. 2008). A variety of accessory adaptor proteins are responsible for the retrieval of different cargo (see Table 1.1). For example, human immunodeficiency virus Rev-binding protein (HRB) retrieves vesicle-associated membrane protein 7 (VAMP7) (Pryor et al. 2008). Importantly though, these cargo-specific adaptors all bind AP-2 (McMahon & Boucrot 2011) ensuring a targeted and co-ordinated accumulation of cargo and adaptor proteins.

One example of these accessory adaptor proteins is AP180 which contains both an ANTH domain, which is responsible for the association of this protein with the PM, and a "membrane-bending" ENTH domain (Ford et al. 2001). AP180 binds to clathrin and has a role as a chaperone of the SV cargo protein synaptobrevin. Synapses expressing mutant AP180 show a wider dispersal of synaptobrevin with less concentration at active zones (Dittman & Kaplan 2006). AP180 is also important in its role as an assembler of clathrin molecules (Hao et al. 1999).

Stonin 2 is another adaptor protein which is known to retrieve synaptotagmin (Haucke & De Camilli 1999). However, more recent work has implied a larger role for this adaptor in the retrieval of vesicles and their cargo. The knockdown of stonin 2 in hippocampal cells lead to a much larger effect on pHluorin retrieval than any AP-2 subunit knockdown with these results recapitulated using an acute method of protein removal (Willox & Royle 2012).

The plethora of interactions of AP-2 with necessary SV cargo proteins would imply that the recruitment of AP-2 is the step of cargo selection in CME. Though, as its removal via rerouting does not cause a severe effect on the retrieval of SV proteins in comparison to clathrin or Stonin 2 (Willox & Royle 2012) it is possible that its role is complementary in nature. Also, FCHO proteins contain a possible ligand-binding domain (Stimpson et al. 2010; Reider et al. 2009) and as such it is possible that some cargo sorting occurs as early as nucleation.

1.3.2.1.2 Clathrin Coat Assembly

Clathrin is a triskelion shaped scaffolding protein consisting of three heavy and three light chains. Clathrin cannot directly bind to the PM and as such is only tethered to the SV via its interactions with adaptor proteins such as AP180, epsin and AP-2 (McMahon & Boucrot 2011). AP180 interacts with the heavy chains in clathrin triskelion (Prasad & Lippoldt 1988; Lindner & Ungewickell 1991), clathrin triskelia are therefore directed to sites of adaptor protein concentration. When clustered, individual triskelia aggregate to form a polyhedral lattice and form coats of 60-70 nm diameter around the invaginating vesicle (Ahle & Ungewickell 1986; Prasad & Lippoldt 1988; Morris et al. 1993). The formation of this coat stabilises the curvature of the invaginating SV, it also displaces some curvature effectors such as eps15 and epsin (Tebar et al. 1996; Saffarian et al. 2009) allowing them to perform their membrane-bending function most effectively at the neck of the vesicle.

In a clathrin-depleted cell, AP-2 remains in puncta co-localised with the nucleation complex but this site does not mature into an invagination (Henne et al. 2010).

Whereas the disruption of AP-2 recruitment to the active zone via the knockdown of the AP-2 μ2 subunit results in the successful assembly of a nucleation complex but no recruitment of clathrin, resulting in a lack of vesicle formation (Motley et al. 2003; Boucrot et al. 2010; Henne et al. 2010). These results would appear to reveal the sequence of events in which cargo selection and clathrin recruitment occur at the active zone. A nucleation complex on the PM binds AP-2 which then recruits clathrin along with other essential proteins to allow successful endocytosis of a clathrin-coated vesicle.

1.3.2.1.3 Fission

The scission of a clathrin-coated vesicle is dependent on the GTPase dynamin (Kosaka & Ikeda 1983). Dynamin must be recruited to the neck of invaginating structures to perform its function. This is performed via a number of membrane-sensing (BAR-domain) proteins which recognise the curvature of the vesicle neck (Wigge et al. 1997; Ferguson et al. 2009; Sundborger et al. 2011). These include amphiphysin, endophilin and sorting nexin 9 (SNX9). All of these proteins contain SRC homology 3 (SH3) domains which bind to the proline rich domain of dynamin (McMahon & Boucrot 2011).

The mechanistic action responsible for the fission of SV from the PM occurs after polymerisation of dynamin around the neck of the invaginating vesicle. This arrangement causes activation of GTPase activity of dynamin (Hinshaw & Schmid 1995; Sweitzer & Hinshaw 1998). The exact mechanism of dynamin-mediated scission is unclear. However it is known that the dynamin ring undergoes a GTP

hydrolysis-dependent conformational change causing subsequent fission of the vesicle (Sweitzer & Hinshaw 1998; Stowell et al. 1999; Roux et al. 2006; Bashkirov et al. 2008). Several models for dynamin function in scission have been proposed since it was first discovered as an essential fission protein. The higher-order structure and its construction into a helical collar around the neck of an invaginating vesicle suggested a mechanism of constriction of the neck until it fused (Roux 2014). Other mechanisms such as a lengthening of the dynamin collar to "pop" off the SV have also been proposed. Though the constriction model remains the one with the most experimental support to date (Roux 2014).

Numerous dynamin disruptions have been utilised to demonstrate the necessity for dynamin in vesicle scission. For example, the expression of mutant forms of dynamin I unable to hydrolyse GTP causes an arrest of endocytosis at a stage after clathrin-coat recruitment (Van Der Bliek et al. 1993). Dynasore is a small molecule which interferes with the GTPase activity of dynamin. Pharmacological inhibition of dynamin GTPase activity by dynasore also rapidly arrested endocytosis of SVs (Macia et al. 2006) resulting in half- or fully-formed SVs remaining attached to the membrane. Though, as this drug was shown to block other, dynamin-independent forms of endocytosis in triple dynamin knockout fibroblasts (Park et al. 2013) these results should be treated with caution.

1.3.2.1.4 Uncoating

After scission from the PM the clathrin coat must be converted from its polymerised lattice configuration into its individual triskelia to "uncoat" the SV. This is achieved

through the action of the ATPase heat shock cognate 70 (HSC70) and auxilin (Schlossman et al. 1984; Ungewickell et al. 1995). Auxilin initially binds to a clathrin coated vesicle after scission and then recruits HSC70 (Barouch et al. 1997; McMahon & Boucrot 2011). The uncoating of a vesicle is known to be ATPase dependent as the addition of ATP greatly increases the complex of HSC70 and clathrin whereas the addition ADP decreases this interaction (Prasad et al. 1994). Auxilin also functions as a potentiator of the ATPase activity of HSC70 (Jiang et al. 1997).

The binding of Auxilin to a clathrin cage weakens the structure of the lattice by disturbing the contacts between the heavy chains in each triskelion. This weakening facilitates the disassembly of the clathrin cage via the action of HSC70 (Fotin et al. 2004). It is likely that auxilin is only recruited to a clathrin coated vesicle after fission as the area of the SV which was previously occupied by the connective neck will now exhibit a gap in its clathrin coat. This may allow for easier access of these molecules and therefore more effective destruction of the lattice (McMahon & Boucrot 2011). *In vitro* experiments have shown that per clathrin triskelion one auxilin and up to three HSC70 molecules are required for optimum disassembly of a clathrin lattice (Böcking et al. 2011; Rothnie et al. 2011).

Clathrin is not the only protein which requires removal from a budded vesicle. After scission, the SV has a coat of both clathrin scaffold and the host of adaptor proteins responsible for retrieving cargo during endocytosis. These proteins are removed via changes in phosphoinositide composition. Synaptojanin is a lipid phosphatase which converts $PI(4,5)P_2$ into PI(4)P. The activity of this phosphatase works in a curvature

sensitive manner and as such has a much a higher level of activity on an internalised SV than on the PM (Chang-Ileto et al. 2011).

After endocytosis synaptojanin works to deplete levels of $PI(4,5)P_2$ on the SV membrane, disrupting the binding of epsin, AP180 as well as the cargo hub AP-2 which are all bound to the vesicular membrane in a $PI(4,5)P_2$-dependent manner. This will cause a dissociation of adaptor molecules from the SV, allowing them to be recycled for further use. A further method of action of synaptojanin may be to create a lipid environment suitable to increase the binding of auxilin (Massol et al. 2006), therefore initiating the assembly of uncoating machinery. The uncoating of a clathrin-coated vesicle releases individual triskelia back into the cytoplasm to be reused for further rounds of CME.

The refilling of an SV with neurotransmitter for use in further rounds of transmission requires the acidification of its lumen. Acidification is the result of the Vacuolar-type H^+ (V-type) ATPase proton pump which uses the energy from converting ATP to transport protons (H^+) across the SV membrane (creating a vesicle membrane potential – $\Delta\psi$). The membrane potential gradient caused by this pump is responsible for the accumulation and neurotransmitters (Maycox et al. 1990). All types of neurotransmitter are loaded into an SV via pumps which exchange protons for molecules of neurotransmitter (Gasnier 2000). Inhibition of the ATPase function of the proton pump via bafilomycin A1, has been demonstrated to inhibit the vesicular accumulation of neurotransmitter (Haigh et al. 1994; Roseth et al. 1995) showing the essential role played by V-type ATPase.

This stage is not necessary for the fusion competence of an SV: vesicles which have not been acidified/refilled can still be released via exocytosis (Cousin & Nicholls 1997), however this should not occur naturally as acidification occurs within seconds after scission (Atluri & Ryan 2006). The exact sequence of uncoating and acidification is ill-defined. There is evidence that the two occur simultaneously as coated SVs have been seen to be filled with neurotransmitter (Prior & Clague 1997). If this is true it would allow for rapid re-entry of SVs into the recycling pool after uncoating.

1.3.2.2 Ultrafast Endocytosis

Ultrafast endocytosis is clathrin-independent mode of membrane retrieval and is named for its rapid onset after stimulation. Using a novel "flash-and-freeze" protocol (Watanabe et al. 2013) it was possible to compare different forms of membrane retrieval over very small incremental time points after an optogenetic stimulation leading to the relatively recent discovery of a possible new form of endocytosis.

Endosomes formed via ultrafast endocytosis were seen to be formed within 50-100 ms of a single, short light stimulus (eliciting one action potential) in hippocampal cell synapses (Watanabe et al. 2013b) whereas smaller SVs and other endocytic structures were not yet formed. The formation of SVs via CME is widely agreed to take between 15-20 seconds (Balaji & Ryan 2007; Granseth et al. 2006; Wienisch & Klingauf 2006; Miller & Heuser 1984; Jockusch et al. 2005), a timescale around 200-fold longer than ultrafast endocytosis. This would suggest that ultrafast endocytosis is specialised to rapidly restore cell surface area during initial exocytosis of docked

vesicles which occurs as quickly as 30 ms after the beginning of stimulation (Watanabe et al. 2013).

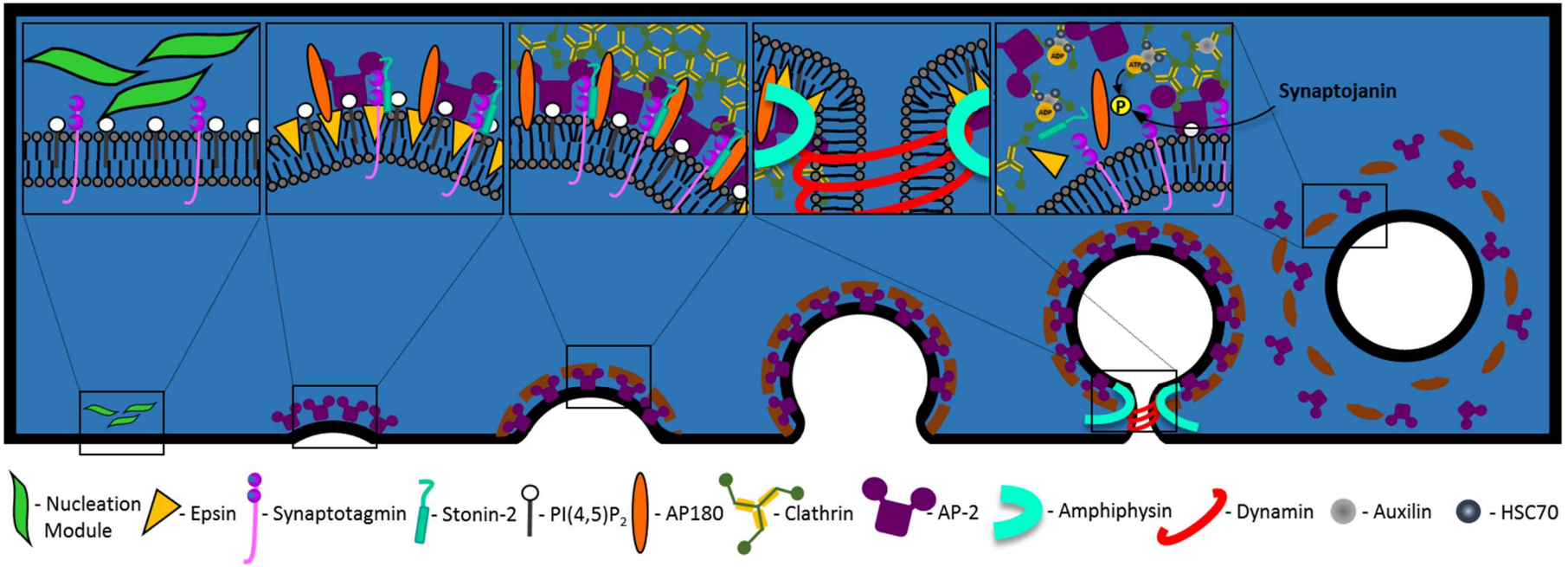

Figure 1.3 Key Stages of Clathrin-Mediated Endocytosis

Left to right: Box 1: Site of endocytosis is saturated with PIP_2 and SV cargo molecules such as synaptotagmin. Nucleation modules formed of FCHO molecules, Eps15 and intersectins recognise saturated sites. Box 2: Membrane curvature is initiated via Epsin molecule insertions which cause a larger disturbance on the cytoplasmic side of the phospholipid bilayer of the plasma membrane causing curvature. AP-2 and AP180 bind to both cargo molecules (such as synaptotagmin via stonin-2) and PIP_2. Box 3: Clathrin molecules bind to AP2 and form a scaffold around the invaginating SV and displacing epsin to the neck of the vesicle. Box 4: Amphiphysin senses membrane curvature and recruits dynamin I to the neck of the vesicle. Box 5: After GTP hydrolysis dynamin alters configuration and the SV is scissioned from the plasma membrane.

Core Components

Protein	Function
Clathrin	Three light chains and three heavy chains form clathrin triskelion. Self-polymerisation forms lattices which serve as a scaffolding cage around an invaginating vesicle.
FCHO	F-BAR domain-containing proteins that generate the initial membrane curvature for endocytosis and nucleate clathrin-coated pits.
AP2	Heterotetrameric adaptor complex made up of α2, β2, μ2 and σ2 subunits. Responsible for linking membrane cargo to clathrin and accessory proteins.
Eps15	Part of the nucleation complex which binds AP-2.
Intersectin	Scaffolding protein, links components of clathrin machinery.
AP180 (brain), CALM (ubiquitous)	ANTH domaining-containing PIP_2-binding protein that binds AP-2 and clathrin.
Epsin	ENTH domain-containing membrane-bending protein.
Amphiphysin	N-BAR domain-containing protein that bends plasma membrane and recruits dynamin to clathrin-coated pits.
SNX9	BAR domain-containing protein that binds AP-2 and dynamin.
Dynamin	Self-polymerising mechanoenzyme that triggers vesicle scission upon GTP-hydrolysis
Auxillin (brain) GAK (ubiquitous)	J domain-containing protein that recruits HSC70 to clathrin cages for uncoating.
HSC70	ATPase which triggers uncoating of clathrin cages.
Stonin-2	Recruits synaptotagmin to AP-2. Also possibly acts as a hub for SV protein retrieval.
HRB	Recruits the SNARE protein VAMP7 to AP-2.

Inositol 5-phosphatases

Protein	Function
Synaptojanin	Lipid phosphatase recruited to clathrin-coated pits by AP-2 and endophilin.
SHIP2	Lipid phosphatase recruited to clathrin-coated pits by intersectins.
OCRL	Lipid phosphatase recruited to mature clathrin-coated pits by AP-2 and clathrin.

Protein Kinases

Protein	Function
AAK1	Phosphorylates the μ-chain of AP-2.
CVAK104	Phosphorylates the β2 subunit of AP-2.
DYRK1A	Phosphorylates several proteins involved in CME.

Actin-nucleation at clathrin-coated vesicles

Protein	Function
HIP1/HIP1R	ANTH domain-containing proteins that bind clathrin, actin, AP-2 (HIP1 only) and cortactin (HIP1R only)
Cortactin	Recruits actin polymerisation machinery to budding clathrin-coated vesicle through dynamin and HIP1R

Other proteins potentially involved in clathrin-mediated endocytosis

Protein	Function
Endophilin	N-BAR domain-containing protein that bends the membrane and recruits dynamin and synaptojanin

Table 1.1 CME Machinery

A list of proteins making up the machinery of CME. Adapted from (McMahon & Boucrot 2011). Abbreviations: AAK1, AP2-associated kinase 1; ANTH, AP180 amino-terminal homology domain; AP-2, adaptor protein 2; CALM, clathrin assembly lymphoid myeloid leukaemia; CVAK104, coated vesicle associated kinase of 104 kDa; DYRK1A, dual-specificity Tyr phosphorylation-regulated kinase; ENTH, epsin N-terminal homology domain; EPS15, EGFR pathway substrate 15; FCHO, FCH domain only; GAK, cyclin G-associated kinase; HIP1, huntingtin-interacting protein 1; HIP1R, HIP1-related; HSC70, heat shock cognate 70; OCRL, oculocerebrorenal syndrome of Lowe; SHIP2, SH2 domain-containing inositol phosphatase 2; SNX9, sorting nexin 9; VAMP7, vesicle-associated membrane protein 7.

Ultrafast endocytosis only occurs in synapses at physiological temperatures (34-37 ^{o}C), in these conditions ultrafast endocytosis appears to take the dominant role in membrane retrieval with little evidence of the clathrin-coated pits which denote active CME (Watanabe et al. 2014). However, at room temperature (22^{o}C) there is no evidence of ultrafast endocytosis (Watanabe et al. 2014) this is possibly due to the effect of lower (non-physiological) temperatures on the kinetics of actin polymerisation in mammalian cells (Kane 1976; Hartmann-Petersen et al. 2000; Gisselsson et al. 2005; Jensen et al. 2007) which would inhibit the advantageous rapidity of ultrafast endocytosis as an instantaneous corrector of the increase in surface area caused by exocytosis. In these conditions the slower endocytic mode of CME becomes dominant (Watanabe et al. 2014).

The formation of ultrafast endosomes from the plasma membrane does not appear to rely on clathrin, however clathrin is essential for the formation of individual SVs from ultrafast endosomes. Use of a clathrin heavy chain shRNA resulted in identical numbers of ultrafast endosomes after a stimulus, however these endosomes remained whole and were not broken down into SVs over time as was observed in the scrambled control (Watanabe et al. 2014). This suggests a role for clathrin in the budding of ultrafast endosomes but not in invagination.

Ultrafast endocytosis is actin-dependent. The role of actin was discovered with application of latrunculin-A, a disrupter of actin polymerisation (Spector et al. 1983). Actin polymerisation was shown to be an essential step in the formation of these structures using the same methods of optogenetic stimulation and immediate freezing

with or without this agent, with no ultrafast endosomes or endocytic pits observed in synapses with interrupted actin polymerisation (Watanabe, Rost, et al. 2013).

To probe the role of the GTPase dynamin in ultrafast endocytosis, dynasore was used. In the presence of dynasore, ultrafast endosomes were still observed after stimulation however they appeared to be still anchored to the PM, showing an inhibition of membrane scission (Watanabe, Rost, et al. 2013). This demonstrates that dynamin is essential for the cleavage, but not the formation of, ultrafast endosomes from the PM.

1.3.2.3 Activity Dependent Bulk Endocytosis

During high frequency stimulation, CME lacks the capacity to compensate for the large addition of membrane being inserted via exocytosis during these conditions. Activity-dependent bulk endocytosis (ADBE) was theorised after the observations that a "bulk" section of membrane was internalised from the PM in neuronal cells during intense stimulation (Heuser & Reese 1973; Gad et al. 1998; Takei et al. 1998; Richards et al. 2000; Holt et al. 2003). Large areas of membrane are internalised direct from the PM and scissioned forming an endosome which is later "budded" to form SVs to replenish the reserve pool (Clayton & Cousin 2009; Cousin 2009). ADBE is the dominant form of endocytosis during high frequency stimulation (HFS) and is a rarer event at low frequencies (Clayton et al. 2008; Wenzel et al. 2012). Without the initiation of ADBE, a presynaptic cell would be delayed in its recovery from intense stimulation conditions and unable to sustain high frequency communication.

This implies that ADBE could play an important role in neuronal events in which high frequency stimuli are integral such the physiological mechanisms long-term potentiation or injurious events such as epileptic seizures.

1.3.2.3.1 Methods of Monitoring ADBE

There are many different assays which can be used to specifically monitor ADBE and its roles in the refilling of SV pools. Initiation, scission and budding can all be monitored via electron microscopy. If stimulated in the presence of the electron-dense HRP at high frequencies, distinct endocytic structures (both vesicular and endosomal) can be viewed which have taken up HRP from the extracellular medium and their number and progression can be examined. For example, one can determine if a manipulation results in more bulk endosomes, if the endosomes are still attached to the membrane or if they have begun to bud. The same can be done for investigating any process which internalises extracellular medium such as CME. This form of investigation is of most use for pharmacological intervention or for mutant or knockout mouse lines. It is less useful for transfected cell conditions which have a low efficiency within a culture if using non-viral delivery methods. Though immuno-EM, which utilises antibodies tagged with electron-dense gold particles, can be used to identify transfected cells in electron microscopy investigations.

Tetramethylrhodamine-dextran (dextran) is 40kDa and large enough that it is very unlikely to be internalised via CME, it therefore selectively labels bulk endosomes in a non-releasable fashion (Clayton et al. 2008; Clayton & Cousin 2009). Unfortunately, dextran uptake assays provide insight only as to how many nerve

terminals are undergoing ADBE. It does not provide information as to whether bulk endosomes formed but were not severed from the membrane, allowing dextran molecules to be washed out. It also does not provide information as to how many endosomes have been formed per nerve terminal. However, this assay gives a clear indication of ADBE disruption and can be used in transfected neurons which make it a very useful and simple tool.

Another tool for investigating ADBE are the styryl dyes FM1-43 and FM2-10 which exhibit differential labelling of CME and ADBE (Richards et al. 2000; Evans & Cousin 2007; Clayton & Cousin 2008). FM2-10 preferentially labels SVs formed via CME whereas FM1-43 labels both SVs and bulk endosomes. This disparity allows the observer to distinguish between effects on endocytosis and effects on ADBE specifically. The uptake of FM dyes is often monitored, as is the unloading of dye as SVs which internalised the dye are recycled and released. This method can be used for transfected or culture-wide conditions and can be used to investigate an array of parameters such as vesicle pool replenishment as discussed below.

1.3.2.3.2 Initiation

During periods of high activity, when ADBE is initiated, CME reaches a saturation point (Sankaranarayanan & Ryan 2000) and can no longer compensate for the additional surface area of the cell caused by SV exocytosis. Saturation of CME is possibly caused due to a limited number of clathrin molecules in a presynapse (López-Murcia et al. 2014), meaning only a set number of clathrin cages can be formed at any one time.

Increased SV fusion during intense stimuli is thought to be one of the factors which triggers ADBE. There are two main sets of evidence for this: firstly, the inhibition of SV fusion using tetanus toxin during HFS results in an inhibition of ADBE as viewed via EM and dextran uptake (Morton et al. 2015). However, ablating exocytosis will have an equal effect of ablating endocytosis via CME as well as ADBE and as such this evidence could also argue a role for CME saturation as an ADBE trigger. The exposure to tetanus toxin however does not inhibit Ca^{2+} influx, and as such this shows that increased $[Ca^{2+}]_i$ alone is not sufficient to initiate ADBE.

Secondly, ADBE does not continue after stimulation terminates (Clayton & Cousin 2009b). If ADBE was triggered due to an increased surface area of the cell or a saturation in the rate of CME, one would expect it to continue after stimulus termination until either of these variables was corrected. The fact that this is not the case could indicate a more important role for SV fusion, which ceases after stimulation, than CME in ADBE initiation. The model of CME saturation as a trigger for ADBE is also flawed due to the immediate onset of ADBE upon HFS (Clayton & Cousin 2009b).

As discussed above, the interference of SV fusion in isolation from Ca^{2+} influx inhibits ADBE. It is also true that inhibiting an increase in cytosolic Ca^{2+} (i.e. outside the active zone) with the calcium chelator EGTA-AM does not affect SV fusion but does inhibit ADBE as viewed by EM (Morton et al. 2015). Both SV fusion and cytosolic calcium increase are therefore essential but not individually sufficient for the process of ADBE.

The initiation of ADBE, like CME, appears to have a reliance on lipid composition of the PM. Phosphatidylinositol (4,5) biphosphate ($PI(4,5)P_2$) is enriched at the site of ADBE (Gormal et al. 2015). Several enzymes known to control the levels of this specific phospholipid have also been implicated in ADBE such as synaptojanin (Clayton & Cousin 2009b), the primary lipid phosphatase in nerve terminals.

The main protein interaction partner of synaptojanin is endophilin. (Micheva et al. 1997; Ringstad et al. 1997), a BAR domain-containing protein. Mutant synaptojanins incapable of binding endophilin expressed in synaptojanin KO mice were capable of rescuing SV endocytosis only during a brief stimulus (Mani et al. 2007). This implies a role for synaptojanin-endophilin binding in ADBE. What is interesting about the necessity for both the 5-phosphatase activity of synaptojanin and its interaction with endophilin is that they are both controlled by its phosphorylation status i.e. dephosphorylation enhances both phosphatase activity and binding (Lee et al. 2004). Not only this, but said dephosphorylation occurs via the activation of calcineurin during prolonged stimulation (McPherson et al. 1994; Marks & McMahon 1998). Together these observations convey a potential mechanism for endophilin-mediated recruitment of synaptojanin and subsequent modification of membrane phospholipids all facilitated via the activity-dependent dephosphorylation of synaptojanin by calcineurin.

Another key player in the maintenance of $PI(4,5)P_2$ levels in neurons is phosphatidylinositol (4) phosphate 5 kinase type I γ (PIPKIγ), the major PIP kinase at the synapse (Di Paolo et al. 2004). PIPKIγ is dephosphorylated by activated calcineurin during prolonged stimulation (Lee et al. 2005) culminating in the

activation of the kinase via interaction with talin (Lee et al. 2005). HFS and calcineurin activation therefore causes both the synthesis and the metabolism of $PI(4,5)P_2$ at the synapse.

The importance of $PI(4,5)P_2$ metabolism in endocytosis is exemplified in the temperature-sensitive Rolling Blackout mutant in *Drosophila* (Huang et al. 2004). Rolling blackout is a membrane lipase integral in the conversion of $PI(4,5)P_2$ into inositol triphosphate (IP_3) and diacylglycerol (DAG) (Huang et al. 2004). *Drosophila* expressing this mutant form of Rolling Blackout displayed paralysis within minutes of being exposed to the restrictive temperature (37 ºC) (Huang et al. 2006) and an activity-dependent accumulation of $PI(4,5)P_2$ and concurrent depletion of DAG. This indicates a role in the regulation of $PI(4,5)P_2$ levels as well as its metabolites in SV endocytosis. It would seem however that this lipase activity of Rolling Blackout is only essential for endocytosis in non-neuronal cells as an inactivated form of the lipase was sufficient to restore endocytosis in neuromuscular junction cells (Vijayakrishnan et al. 2010). This indicates another function of Rolling Blackout is necessary for neuronal endocytosis.

There is strong evidence for a specific role of Rolling Blackout in ADBE. In neuromuscular synapses expressing temperature-sensitive mutant Rolling Blackout display a pronounced inhibition in FM1-43 uptake (Vijayakrishnan et al. 2009). Using neuronal cultures and Garland cells this inhibition was seen to be facilitated via a significantly decreased endosome formation upon stimulation (Vijayakrishnan et al. 2009) implying a specific role of Rolling Blackout in ADBE. A concomitant

increase in the number of newly-formed SVs over control (Vijayakrishnan et al. 2009) also indicated an attempt in compensation through single vesicle endocytosis.

As it has been shown that the lipase function of Rolling Blackout is not essential for synaptic endocytosis other aspects of the protein were examined. EFR3 is a homolog of Rolling Blackout found in yeast and has integral function as a scaffolding protein as well as a recruiter of PI4P kinase, therefore regulating PM phosphoinositide signalling (Baird et al. 2008). It is therefore possible that the role played by Rolling Blackout in ADBE is facilitated by its scaffolding, rather than lipase, ability. This is not unheard of for a synaptic enzyme, for example calmodulin-dependent protein kinase II has dual functions as a Ca^{2+}-dependent kinase as well as independent roles as a membrane scaffold (Hojjati et al. 2007).

1.3.2.3.3 Scission

After the initiation of ADBE, an infolded structure has been formed and is attached to the membrane. This structure must undergo scission to become an endosome. This process is facilitated via the GTPase action of dynamin I much like the scission of SVs via CME. The necessity for dynamin in ADBE has been demonstrated via EM images in neuronal cells utilising the GTPase inhibitor dynasore during HFS. Under these conditions both CME and ADBE were almost completely ablated (Clayton et al. 2009). However, as previously stated dynasore is known to be a rather non-specific inhibitor of dynamin.

Further experiments have been performed utilising the more potent and specific Dyngo4a™ (Mccluskey et al. 2013) in NMJs in which a complete block in bulk

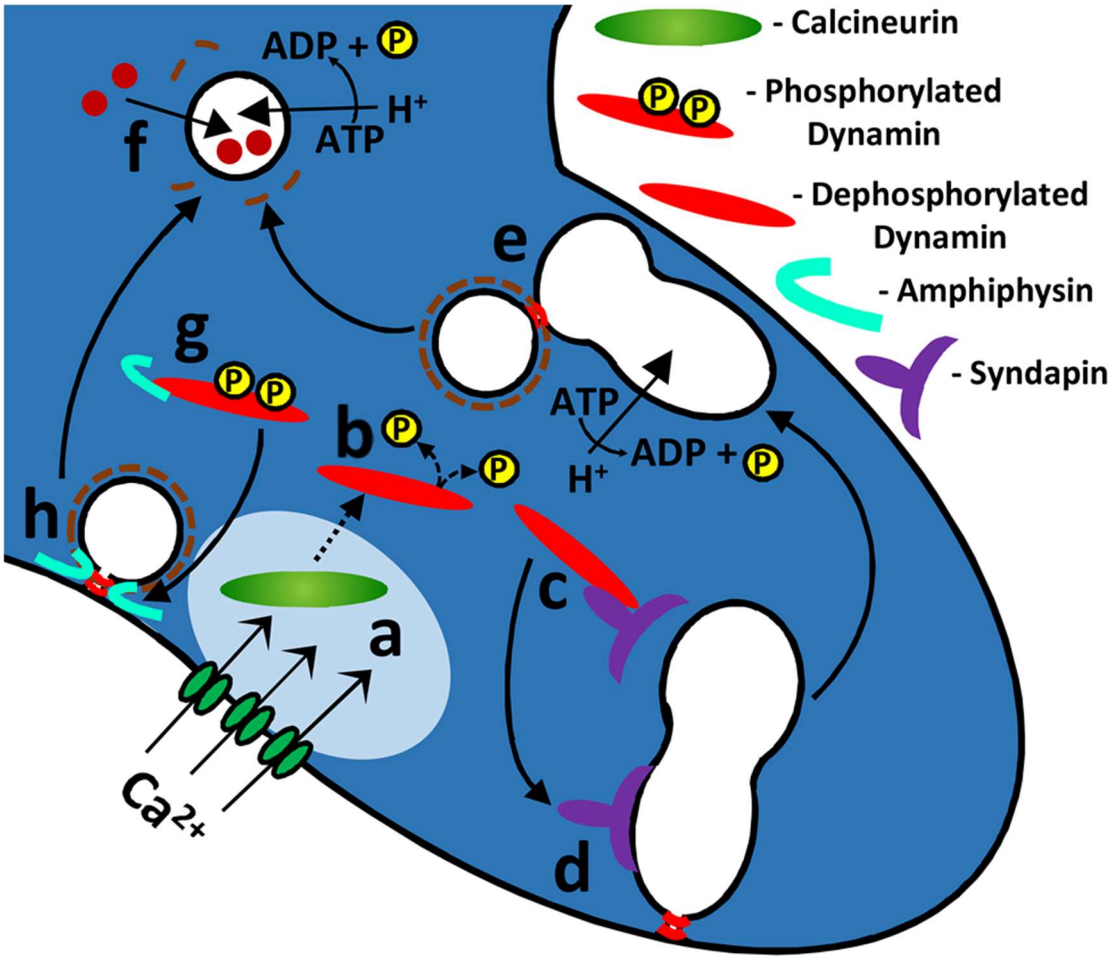

Figure 1.4 - Schematic of Key Events in Activity Dependent Bulk Endocytosis

a) Neuronal activity causes large influx of calcium ions (Ca^{2+}) into the synapse. During high frequency stimulation, the $[Ca^{2+}]_i$ increases above the threshold required to activate the phosphatase calcineurin. b) Activated calcineurin de-phosphorylates dynamin I on two serine residues (774 and 778). c) This dephosphorylation facilitates the interaction of dynamin I with syndapin. d) The shallow membrane-sensing F-BAR domain of syndapin allows it to recognise and recruit dynamin I to the invaginating endosome. Dynamin polymerises in around the neck of the endosome and its GTPase function causes a conformational change forcing scission of the endosome from the plasma membrane. e) After the endosome acidifies SVs are budded via a clathrin and dynamin-dependent mechanism. f) Budded SVs uncoat and are filled with neurotransmitter to rejoin the recycling vesicle pool. g) During periods of mild stimulation, the $[Ca^{2+}]_i$ does not increase sufficiently to activate calcineurin, dynamin is not dephosphorylated and therefore will not bind with syndapin. Phosphorylated dynamin I binds the BAR domain-containing amphiphysin (as does dephosphorylated dynamin I). h) Amphiphysin recruits dynamin I to the neck of a SV undergoing CME. Dynamin I polymerises around the neck of the vesicle and the GTPase function of dynamin causes a conformational change leading to vesicle scission. These SVs then uncoat, are filled with neurotransmitter (f) and rejoin the recycling pool.

endosome formation was observed (Nguyen et al. 2012). It should be noted though that treatment with these drugs creates greater endocytic phenotypes than those seen in mouse synapses lacking all three isoforms of synaptic dynamin (Park et al. 2013). Normal bulk endocytosis was seen to continue in these conditions (Park et al. 2013). As such the results of these specific studies should be treated with caution and the role of dynamin in ADBE is still slightly contentious.

Calcineurin is activated during high frequencies due to a high cytoplasmic Ca^{2+} concentration (Morton et al. 2015). The function of calcineurin in ADBE was investigated using the styryl dyes FM1-43 and FM2-10. Inhibition of calcineurin by

cyclosporine A decreases loading of FM1-43 but not FM2-10, showing an essential role for calcineurin activation in ADBE (Evans & Cousin 2007). Activated calcineurin dephosphorylates the GTPase responsible for SV scission dynamin I on two serine sites (serine 774 and serine 778). Dephosphorylation of these sites only occurs at stimulation frequencies at which ADBE is triggered (Clayton et al. 2009).

Dynamin I binds to the ADBE-essential protein syndapin I only after dephosphorylation on these two residues (Anggono et al. 2006). Inhibition of this interaction by competitive peptides or by expressing dominant negative dynamin I mutants incapable of syndapin binding effectively inhibits ADBE as demonstrated by EM, dextran uptake and FM1-43 analysis (Clayton et al. 2009), showing this interaction is essential for the progression of a bulk endosome.

Syndapin is a member of a family of dynamin I-binding proteins which contain an N-terminal bin-amphiphysin-RVS (BAR) domain along with endophilin and

amphiphysin. BAR domains sense membrane curvature and also have roles in the tubulation of membrane (Gallop & McMahon 2005; Dawson et al. 2006). Other binding partners of dynamin I such as amphiphysin and endophilin contain an N-BAR domain which are sensitive to a tight curvature in membrane (Peter et al. 2004) allowing them to fulfil their role in the invagination of single SVs. Syndapin contains an F-BAR domain which is sensitive to a more shallow membrane curvature (Henne et al. 2007; Shimada et al. 2007) such as that exhibited by an invaginating endosome. It is unknown if syndapin is purely an escort for dynamin I or if it plays a more active role in ADBE scission as may be implied by the presence of a BAR domain.

The de- and re-phosphorylation cycle of dynamin I has been shown to be of critical importance for the continuation of ADBE, expression of both phospho-mimetic and phospho-null forms of the proteins resulted in an inhibition of ADBE as measured by dextran uptake (Clayton et al. 2010) showing that in order for dynamin to perform its function it must be able to be modified at these sites.

After cessation of a high frequency stimulus, dynamin I is rephosphorylated by cyclin-dependent kinase 5 (Cdk5) on serine 778 and then by glycogen synthase kinase 3 (GSK3) on serine 774 (Clayton et al. 2010). Cdk5 is constitutively active and performs its action first on the dynamin I protein (Clayton et al. 2010) whereas GSK3 is inhibited via phosphorylation on Ser 9 (β isoform) or 21 (α isoform) (Frame & Cohen 2001). This activity-dependent phosphorylation occurs via the activity-dependent kinase Akt during HFS.

Akt activity is also modulated by its phosphorylation but in the opposite direction. Phosphorylation on Ser 473 and Thr 308 cause activation of Akt (Alessi et al. 1997;

Sarbassov et al. 2005). Both GSK3 and Akt show phosphorylation on two serine sites in response to high frequency stimulation and in correlation with dynamin dephosphorylation (Smillie & Cousin 2012). This system ensures maximal dephosphorylation of dynamin I via the inhibition of GSK3 and therefore maximal ADBE (Smillie & Cousin 2012).

If GSK3 or cdk5 are inhibited via application of CT99021 (CT) or roscovitine respectively, there is no effect on ADBE during a single HFS as dynamin I is dephosphorylated normally under these conditions. However, if inhibition is continued throughout a second high frequency stimulus there is a significant inhibition of ADBE (Clayton et al. 2010). This suggests that dynamin I must be rephosphorylated after stimulation by GSK3 and cdk5 to be used in further rounds of ADBE.

This signalling cascade was determined to have no role in CME during HFS. The unloading of CME-specific styryl dye, FM2-10 (Clayton et al. 2009), an indicator of the number of SVs formed during stimulation, was not affected by the expression of constitutively active from of Akt in CGNs (Smillie & Cousin 2012) whereas the same overexpression caused a significant reduction in ADBE as seen by dextran uptake (Smillie & Cousin 2012). As these cells would experience a consistent phosphorylation of GSK3 due to heightened Akt activity, this showed a requirement for the modulation, but not chronic inhibition, of GSK3 activity specifically in ADBE.

Although it would appear that Akt activation and GSK3 inhibition ensures an efficient and maximal dephosphorylation of dynamin during HFS, an acute inhibition

of Akt did not cause an inhibition of dextran uptake in the same cells (Smillie & Cousin 2012). This shows that the less efficient dephosphorylation of dynamin that would be seen with a higher level of GSK3 activity is still sufficient to allow ADBE.

Monitoring the uptake of fluorescent markers in conjunction with the disruption of actin filaments with cytochalasin D or latrunculin A shows a need for actin dynamics in the process of bulk endosome formation (Kuromi & Kidokoro 1998; Holt et al. 2003; Richards et al. 2004; Nguyen et al. 2012). However, it is unknown at which point actin may play its role. Only one such study has implied a role for actin filaments in the initiation of ADBE prior to a role in the scission of an endosome (Nguyen et al. 2012).

As discussed above dynamin I has an essential role in the scission of both SVs and bulk endosomes, it has also been shown to play an essential role in actin polymerisation in endocytosis (Kessels et al. 2001; Gu et al. 2010). Syndapin I can form homo-oligomers via it F-BAR domain and as such can simultaneously bind dynamin I and a protein known to initiate actin polymerisation via the recruitment the arp2/3 complex, neuronal Wiskott-Aldrich syndrome protein (N-WASP) (Kessels & Qualmann 2006; Halbach et al. 2007). It is possible that this association allows syndapin to form a complex with both dynamin and actin to recruit and even co-ordinate actin dynamics via N-WASP interactions at the sites of ADBE (Kessels & Qualmann 2002). In support of this theory, the perturbation of syndapin binding in lamprey reticulospinal synapses caused a reduction in actin accumulation at endocytic sites (Andersson et al. 2008).

Recent work in neurosecretory cells has indicated a role for actin-myosin rings in the scission of endosomes after secretagogue stimulation. Rings of GFP-labelled actin were observed around the necks of invaginating endosomal structures which then contracted before scission (Gormal et al. 2015). Inhibitors of myosin II were used to demonstrate a necessity for myosin as well as actin for the formation of these contracting rings around endosomal necks.

1.3.2.3.4 Budding

After a bulk endosome has been severed from the PM it undergoes "budding". This is a process in which smaller vesicles are generated from the larger endosome to re-enter the recycling pool of SVs, possibly after shuttling through other endosomal structures. SVs formed via bulk endosomes have been shown to preferentially refill a pool of vesicles termed the "reserve pool" which are only mobilised during periods of intense activity which correlate to the activation of ADBE.

During mild stimulation, newly formed SVs are preferentially recruited to the RRP in a process termed "reuse" (Pyle et al. 2000; Kavalali 2006). This process of reusing newly formed SVs to refill the RRP is conserved during HFS (Sara et al. 2002). However, in amphibian neuromuscular junctions it was observed that those SVs formed via ADBE were not immediately available for release unlike these reused SVs (Richards et al. 2000; Richards et al. 2004). This observation along with the preferential use of the reserve pool during high intensity stimulation (Südhof 2000) led to the hypothesis that SVs formed via ADBE are directed to replenish the reserve pool after intense stimulation.

Work using the styryl dyes FM1-43 and FM2-10 in primary neuron cultures, showed an increase in labelling of the reserve pool by FM1-43 over FM2-10 after identical HFS (as seen by monitoring the unloading of dye during stimulation protocols tailored to unload the RRP or RP separately – the "FM unloading protocol") in a manner not observed after mild stimulation (Cheung et al. 2010). As both of these dyes label CME, but only FM1-43 labels bulk endosomes. The increase in labelling of the reserve pool by FM1-43 during intense stimulation therefore suggests a significant contribution of SVs formed via ADBE into the reserve pool.

Further work utilising EM allowed observations as to the time taken for a bulk endosome to bud into vesicles after scission. Neurons were stimulated at high frequencies in the presence of HRP so that any SVs and bulk endosomes formed during this stimulation were distinct. These cells were then washed of HRP and depleted of both the readily-releasable and reserve pool, leaving only bulk endosomes which were formed during the first stimulation as visible structures. The cells were then left to rest for 30 minutes - this will hereafter be referred to as the "HRP budding protocol". After this 30-minute period, HRP-labelled SVs were visible. As all labelled SVs formed via CME had been depleted, the only possible provenance of these SVs is from bulk endosomes meaning that bulk endosomes have begun to or have completed budding SVs within 30 minutes of their formation (Cheung et al. 2010).

Calcium plays an essential role in the budding of SVs from bulk endosomes. This is perhaps not surprising as the Ca^{2+}-dependent phosphatase calcineurin has been shown to perform essential roles in both the initiation and the budding of endosomes.

Interestingly, it is the efflux of intra-endosomal calcium which dictates normal budding. This was manipulated via the addition of calcium chelators during the HRP budding assay. BAPTA-AM was used to chelate Ca^{2+} which had escaped the endosome after HRP loading and caused an inhibition in SV budding (Cheung & Cousin 2013). To deplete intra-endosomal Ca^{2+} a chelator was conjugated onto a dextran molecule which were not internalised by single SVs (Holt et al. 2003; Clayton et al. 2008) and utilised in the HRP budding assay. Depletion of endosomal Ca^{2+} inhibited the formation of SVs from bulk endosomes (Cheung & Cousin 2013) demonstrating the necessity of internal Ca^{2+} and the logical extension that the internalisation of extracellular Ca^{2+} via ADBE is also essential for SV budding.

It has been shown that endosome acidification via vacuolar-type H^{+}-ATPase (V-type ATPase) is essential for budding to occur (Cheung & Cousin 2013). Inhibition of this proton transporter via bafilomycin A1 (Gerasimenko et al. 1998) causes a depletion in SVs formed by the budding of bulk endosomes as viewed by the HRP budding protocol and a consequential depletion of the reserve pool of vesicles as denoted by FM unloading protocol (Cheung & Cousin 2013). It is unknown if the presence of V-type ATPases on bulk endosomes is a result of cargo retrieval in ADBE or of a fusion even between a bulk endosome and another structure containing V-type ATPases such as a SV and as such one cannot speculate as to the ability of endosomes to retrieve cargo from these results alone. However, it does offer an insight into the directionality of events preceding budding. These results in conjunction with those indicating that endosomal Ca^{2+} efflux is necessary for SV budding also indicates that endosomal acidification by V-type ATPases is the trigger for Ca^{2+} efflux.

Several other components have been found to be essential for bulk endosome budding. Calcineurin was first observed as a component of ADBE initiation. However, if the calcineurin inhibitor cyclosporine A is present in the HRP budding protocol after the formation of bulk endosomes but throughout the rest period, there is a significant reduction in the number of HRP-labelled, budded SVs (Cheung & Cousin 2013). This shows a necessity for calcineurin activity in the budding of SVs from bulk endosomes in a role totally separate from that which it plays in the initiation or scission of bulk endosomes. This result was recapitulated using the FM unloading assay (Cheung & Cousin 2013), reinforcing the hypothesis that SVs budded from bulk endosomes go on to refill the RP.

Budding requires the formation of SVs from bulk endosome membrane, a process which must require the efficient sorting of any membrane cargo present in bulk endosomes. During CME protein sorting is largely facilitated through the adaptor protein AP-2 (Royle & Lagnado 2003). Rapid inactivation of clathrin light or heavy chains using fluorescein-assisted light inactivation (FALI) has shown a potential role for clathrin coat assembly in the budding of bulk endosomes (Heerssen et al. 2008; Kasprowicz et al. 2008). As clathrin depends on its interactions with adaptor proteins to co-ordinate itself and any cargo this would imply a necessity for AP complexes in bulk endosome budding.

Of the five known adaptor protein complexes, AP-1 and AP-3 were of interest when trying to identify the adaptor proteins responsible for SV budding from bulk endosomes for several reasons: Both AP-1 and AP-3 are enriched in nerve terminals (Glyvuk et al. 2010; Newell-Litwa et al. 2010) and are found on SVs (Takamori et al.

2006) which implies a role in SV formation which cannot be attributed to CME. Mice lacking an essential subunit of AP1-B display decreased endosome numbers as well as a delay in recycling pool recovery after strong stimulation (Glyvuk et al. 2010). Also, endosomal vesicle budding in other cell types has been shown to be inhibited by brefeldin A (BFA) (Drake et al. 2000) though in neuronal cultures SV endocytosis was only inhibited during intense stimulation (Voglmaier et al. 2006; Kim & Ryan 2009). This is of significance as BFA inhibits the GTPase ADP-ribosylation factor 1 (ARF1) which is essential in the recruitment of both AP-1 and AP-3 to membrane (Faúndez et al. 1998; Pagano et al. 2004; Newell-Litwa et al. 2007)

The budding of SVs from bulk endosomes has also been shown, via HRP budding assays, to be inhibited by exposure to BFA in CGNs (Cheung & Cousin 2012). This block in SV budding also translated into a deficit in the refilling of the reserve pool as observed via the FM unloading protocol (Cheung & Cousin 2012). These results imply a role for AP-1 and/or AP-3 in SV budding.

Knockdowns of subunits of either AP-1 or AP-3 showed an equal inhibition on the budding of SVs, however this could not be observed via HRP budding assay due to the nature of transfection and as such this was only observed via the effects on FM labelling of the RRP (Cheung & Cousin 2012). Neither knockdown resulted in a reduction of bulk endosome formation as measured by dextran (Cheung & Cousin 2012) and as such the defect in RP refilling was due to an inhibition of budding and not initiation of ADBE.

It is possible that the process of ADBE requires little to no sorting of SV cargo at the PM and that cargo sorting occurs at later stage. The individual impact of each of these knockdowns implied a lack functional redundancy between with adaptor complexes i.e. they would seem to be performing separate, possibly sequential roles. It was theorised that the budding of SVs from bulk endosomes is not a single process. Instead, "immature" SVs bud from the bulk endosome in a process dependent on one adaptor protein and go on to fuse with another endosomal intermediate such as an early endosome. "Mature" SVs with a full complement of SV cargo are then budded from the early endosome via a mechanism dependent on the second adaptor protein (Cheung & Cousin 2012).

Further work is required to identify any specific cargo which interacts with these adaptors during bulk endosome budding. An example of a protein of interest would include phosphatidylinositol 4-kinase II α (PI4KIIα) which is shuttled from the cell body to the synapse via AP-3 or BLOC-1. Another would be VAMP7 which is involved in the fusion of late endocytic compartments with other membranes (Chaineau et al. 2009) and is a binding partner of AP-3 (Martinez-Arca et al. 2003).

1.4 Phosphoinositides

Lipids are small, hydrophobic molecules with the ability to assemble autonomously into complex structures in an aqueous environment. The nervous system has an especially enriched and diverse lipid composition compared to other tissues (Sastry 1985; Bozek et al. 2015) and variation in the neural lipodome has been associated with a variety of diseases such as Alzheimer's, Parkinson's and Huntington's (Lauwers et al. 2016).

Phosphoinositides (PIs) belong to a subset of membrane lipids which are amphiphilic and due to their negatively charged head groups (which reside on the cytosolic membrane surface) and a non-polar backbone and tails (Lauwers et al. 2016). Other members of this family include phosphatidylserine, sphingomyelin and phosphatidylcholine. PIs can be phosphorylated to make seven different lipids. Phosphatidylinositol (PtdIns) is the unphosphorylated form of a PI and contains an inositol ring containing six, phosphorylatable -OH groups. The nomenclature to distinguish these groups was originally designed to allow a simple visualisation of a body of a turtle, with its six -OH groups (D1-D6) forming its head, four legs and tail (Agranoff 1978). Only three of these OH- sites (D3, D4, and D5) are phosphorylated in naturally occurring PIs, allowing for seven known combinations of PtdIns phosphorylation comprising of all known PIs (Figure 1.5). The different phosphorylation states of a population of PIs is regulated by a host of kinases and phosphatases with specificity to each -OH group (see Figure 1.5)

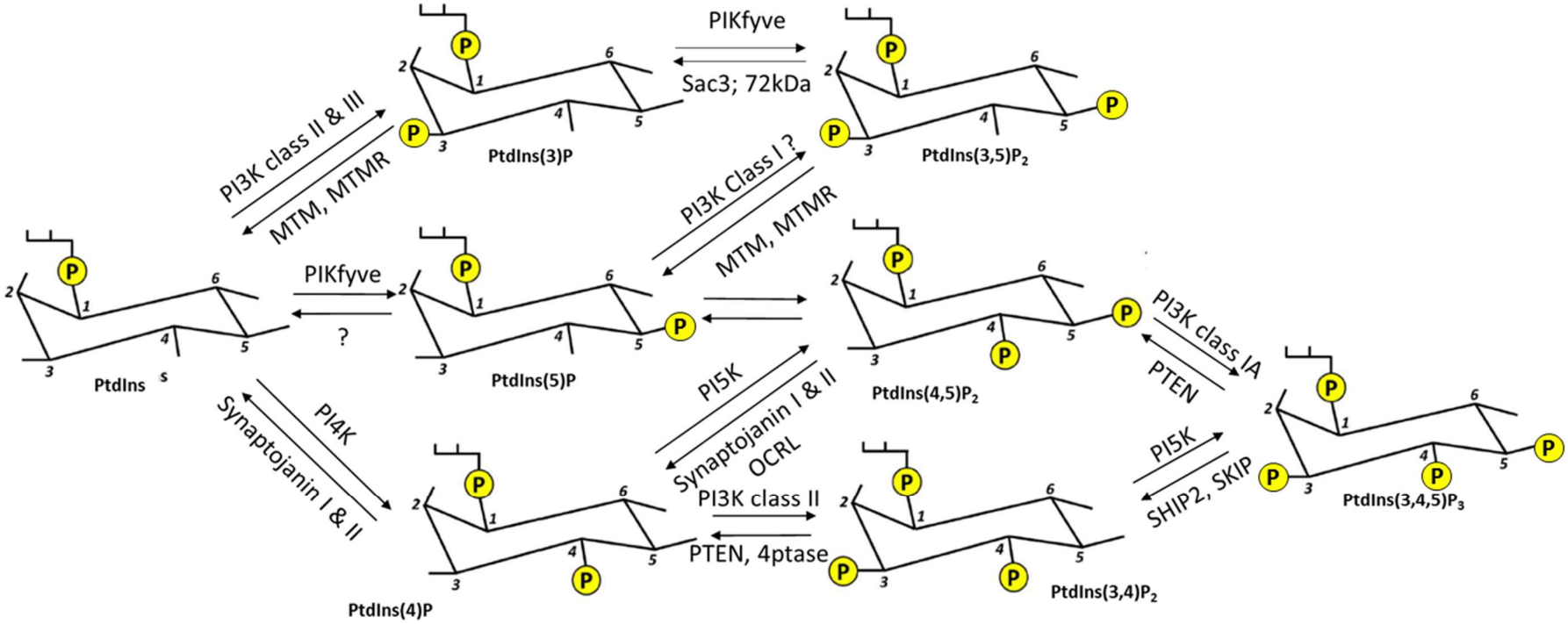

Figure 1.5 Phosphorylation Cycle of Phosphoinositides

Schematic showing common kinases, phosphatases and actions involved in the production of phosphoinositides (PtdIns). PtdIns have an inositol ring with 6 hydroxyl groups (D1-6). D1 alone is phosphorylated in PtdIns (left). Kinases add phosphate groups to groups D2-D5. E.g. Actions of any of the 4 mammalian phosphatidylinositol 4-kinases (PI4Ks) can phosphorylate PtdIns on D4 creating PtdIns(4)P. Further phosphorylation on either D3 or D5 will create PtdIns(3,4)P_2 or PtdIns(4,5)P_2 respectively. PtdIns(3,4,5)P_3 can be created from either of these via phosphorylation of the remaining position. The addition of any of these phosphate groups is reversible by the actions of phosphatases. D2 and D6 are not typically phosphorylated due to steric hindrance. Adapted from data in (Shisheva 2008)

1.4.1 Importance of PI Levels in SV Recycling

The transmission of information via synapses requires extensive remodelling of membrane, although this process is largely driven by protein machinery the lipids of the membrane play key roles (Davletov & Montecucco 2010; Puchkov & Haucke 2013). Phosphoinositides have essential roles in multiple stages of the SV cycle, in exo- and endocytosis as well as the coupling of the two processes (Koch & Holt 2012) with their electrostatic charge being of central importance to its functions (Lauwers et al. 2016).

As well as its membranes being enriched with lipid components, the synapse contains a host of lipid metabolising enzymes which are capable of locally altering lipid structures. Although PIs are low-abundance membrane lipids (only making 10-20% of total cellular phospholipids (Balla 2013)) they are of crucial importance for the localisation of certain proteins to different membrane compartments.

1.4.1.1 Exocytosis

Of particular importance at the presynaptic terminal is the PI phosphorylated at the D4 and D5 positions; PI(4,5)P_2. The necessity for PI(4,5)P_2 in SV fusion has been demonstrated via many different methods. For example, via the application of high-affinity pleckstrin homology (PH) domain probes which effectively shield sites on specific PIs, inhibiting their interaction with binding partners. Use of these PH domain probes to specifically block PI(4,5)P_2 interactions resulted in a block of exocytosis as measured by both electrochemical and electrophysiological techniques

in chromaffin cells (Holz et al. 2000). Another, specific, method of interfering with $PI(4,5)P_2$ binding is via the HIV-1Tat protein which has a 20 fold higher affinity for $PI(4,5)P_2$ than PH domain probes (Debaisieux, S. 2012). The use of these proteins in PC12 cells also demonstrated a block in exocytosis due to inhibited $PI(4,5)P_2$ interactions (Tryoen-Toth et al. 2013).

PI levels can also be manipulated by altering the expression or location of the metabolising kinases or phosphatases. PI(4)P5-kinase Iγ (PIPK1γ) is a major regulator of $PI(4,5)P_2$, converting PI4P via the addition of a phosphate group to the OH group at the D5 position (see Figure 1.5). In a PIPK1γ knockout mouse the abundance of $PI(4,5)P_2$ is significantly decreased but PI4P levels are unaffected (Di Paolo et al. 2004). In this model a host of synaptic transmission deficits were detected in cortical neurons, amongst them a smaller RRP and a reduced rate of exocytosis (Di Paolo et al. 2004). Conversely, the increased synthesis of $PI(4,5)P_2$ via overexpression of PIPK1γ caused an increase in sustained rates of evoked exocytosis in PC12 cells (Aikawa & Martin 2003; Milosevic et al. 2005).

There are different theories as to the mechanism by which $PI(4,5)P_2$ is essential for SV fusion. At the PM of neuroendocrine cells there are distinct microdomains of $PI(4,5)P_2$ at fusion sites (Martin et al. 2012) which may suggest a role for the membrane curvature qualities of this PI provided by its conical structure. However, other cellular processes performed by $PI(4,5)P_2$ are achieved via the recruitment and activation of $PI(4,5)P_2$-binding proteins so it is also possible that $PI(4,5)P_2$ exerts its main function in SV fusion in the same manner.

Active zones contain the many proteins which form the machinery for exocytosis. These include Q-SNARES Syntaxin 1 and SNAP-25 as well as proteins such as RIM and unc-13 which mediate SV docking and priming as well as VGCC recruitment (Südhof 2012). The interaction of these proteins with PIs are mediated mostly by organised, positively charged motifs such as C2 domains which allow Ca^{2+}-dependent and -independent binding to $PI(4,5)P_2$ and are found in cytosolic proteins such as unc-13 and RIM (Südhof 2012).

$PI(4,5)P_2$ binds directly with syntaxin 1A and is found to be concentrated within the active zone in subdomains corresponding with syntaxin 1A clusters and docked dense core vesicles (Aoyagi et al. 2005). Overexpression of the $PI(4,5)P_2$- and $PI(3,4,5)P_3$-metabolising enzyme synaptojanin causes a dispersion of syntaxin 1A across the PM (Murray & Tamm 2009) and shows that this association is specific to lipid composition of the active zone. These results do not specifically link $PI(4,5)P_2$ to syntaxin 1A clustering however and it is possible that $PI(3,4,5)P_3$, which has a greater negative charge, could be playing a similar role in syntaxin clustering. Indeed, studies have shown that lowering the availability of $PI(3,4,5)P_3$ causes a similar effect on syntaxin 1A clustering as well as a reduction in neurotransmitter release (Khuong et al. 2013).

$PI(4,5)P_2$ microdomains only co-localise with a subset of docked SVs and are known to cluster and activate several proteins involved in the docking and priming of SVs. Studies in neuroendocrine cells have shown roles for $PI(4,5)P_2$ in the activation or recruitment of SNARE-binding proteins such as calcium-dependent activator protein for secretion (CAPS), a Ca^{2+}-dependent regulator for the exocytosis of large dense

core vesicles (LDCVs) (Loyet et al. 1998), Munc-13, and synaptotagmin (Martin 2014).

Synaptotagmin, the Ca^{2+}-sensitive activator of SV fusion, undergoes an altered affinity for PIs in the presence or absence of Ca^{2+}. In the absence of Ca^{2+}, synaptotagmin binds preferentially to $PI(3,4,5)P_3$. In the presence of Ca^{2+} however, synaptotagmin binds $PI(3,4)P_2$ or $PI(4,5)P_2$ (Schiavo et al. 1996). It is possible that $PI(4,5)P_2$-binding is of primary importance however, as inhibition of $PI(3,4)P_2$ synthesis does not affect the priming of large core dense vesicles (LCDVs) in PC12 cells (Martin et al. 1997).

Synaptotagmin and Doc2-β (a modulator of spontaneous release of SVs (Groffen et al. 2010)) both contain a C2 domain and are responsible for bridging the SV membrane with the PM (Davletov & Sudhof 1993; Wen et al. 2011). These protein-bridge membrane interactions may be regulated by other negatively charged lipid molecules such as phosphatidylserine (PtdSer) which compete with PIs for protein interactions. PtdSer is actually much more abundant in synaptic membranes (Takamori et al. 2006) than PIs and has known roles in facilitating vesicle fusion in PC12 cells. *In vitro* studies suggest that PIs and PtdSer compete for binding and the successful lipid determines whether synaptotagmin binds to SV membrane in a *cis* formation, or to PM in a *trans* formation (Chapman 2002; Vennekate et al. 2012)

The issue of $PI(3,4,5)P_3$ involvement is confused by conflicting results of the effects of interfering with the function or availability of the lipid. The inhibition of Ca^{2+} activated exocytosis by phospholipase C (Hay et al. 1995) (a phospholipid enzyme which specifically cleaves $PI(4,5)P_2$ and not $PI(3,4,5)P_3$) implies a lack of role for

$PI(3,4,5)P_3$ in PC12 cells. This finding is further strengthened by the lack of effect of PI3K inhibition by LY294002 in PC12 cells on ATP-dependent priming (Martin et al. 1997). However, LY294002 has been reported to cause an inhibition of evoked exocytosis in other studies (Chasserot-Golaz et al. 1998). This finding should be treated with caution though as LY294002 also has an inhibitory effect on type III PI4-kinases (Balla 2013). Furthermore, work using PH domains specific to $PI(3,4,5)P_3$ have also resulted in a decrease in neurotransmitter release (Khuong et al. 2013).

1.4.1.1.1 Ion Channel Activity

Ion channel activity is tightly regulated by PIs. The conformation of ion channels is so strongly controlled by $PI(4,5)P_2$-binding that in many cases only a proteo-lipid ($PI(4,5)P_2$-bound) form of the complex will conduct ions (Gamper & Shapiro 2007). The mechanism responsible for this regulation in the inward rectifying potassium channels (Kir2.2) (responsible for the maintenance of a neuronal resting potential (Lauwers et al. 2016)) has been revealed via visualisation of the crystal structure of both the $PI(4,5)P_2$-bound and unbound forms of the channel. This investigation showed a shift in the whole carboxy-terminal domain toward the membrane as well as a rotation of its helices following $PI(4,5)P_2$-binding (Hansen et al. 2011; Li et al. 2015). This modified confirmation is then capable of conducting potassium ions. In accordance with this, the ability of the family of Kir2 channels to conduct ions is inhibited by increases in lipid phosphatases or by exposure to anti-$PI(4,5)P_2$ antibodies which inhibit their interaction (Lauwers et al. 2016).

It is unknown if this regulatory conformational change is universal across ion channels. However, a similar change is seen in Kir7.1 channels (Zaydman et al. 2013) suggesting a broadly relevant mechanism. It has been proposed that this reliance on $PI(4,5)P_2$-binding ensures a channel is only active once it has been trafficked to the $PI(4,5)P_2$-rich environment of the active zone (Lauwers et al. 2016). For calcium channels this would mean their ability to conduct ions is only activated once in the vicinity of the Ca^{2+}-dependent membrane-remodelling machinery.

Further work in T-cells has also raised the theory that Ca^{2+} serves to neutralise the negative charge of PIs to release protein-PI interactions (Shi et al. 2013). If this is true, $PI(4,5)P_2$-binding of ion channels may function not only to activate them specifically at the active zone but also to provide a Ca^{2+}-sensitivity.

This collective data supports a model of enriched domains of lipids such as $PI(4,5)P_2$ defining the function and/or localisation of exocytic proteins to presynaptic active zones. $PI(4,5)P_2$ organises SV fusion sites and clusters with the SNARE molecule syntaxin. The same lipid is also responsible for regulating interactions leading to SV docking and priming as well as ion channel activity and, by extension, neuronal excitability and presynaptic release efficacy.

1.4.1.2 Endocytosis

Subsequent to exocytosis, membrane-essential lipids and proteins are retrieved via endocytosis. This occurs within milliseconds of exocytosis via ultrafast endocytosis in the area directly surrounding the active zone or within seconds via CME or ADBE in the peri-active zone (L. Zhou et al. 2014; Kononenko & Haucke 2015).

$PI(4,5)P_2$ is known to play an important role in CME due to its affinity for many endocytic factors including the clathrin adaptors AP2, AP180, CALM, and Epsins (Lauwers et al. 2016). Inhibiting the interactions between $PI(4,5)P_2$ and these binding partners results in a disrupted localisation of these endocytic adaptors on the PM (Lauwers et al. 2016). The specific interactions of $PI(4,5)P_2$ in CME-mediated cargo retrieval has been discussed more fully previously (see 1.3.2.1).

Using PH domain probes to disrupt $PI(4,5)P_2$-binding in perforated A431 cells (a model system used to reconstitute receptor-mediated endocytosis) resulted in the inhibition of clathrin-coated vesicle (CCV) formation after stimulation (Jost et al. 1998), implying a role for $PI(4,5)P_2$-binding in CME.

Levels of PIs at specific areas of the cell such as the active zone can be manipulated using rapamycin-mediated redirection of specific phosphatases or kinases to particular membranes. Redirecting inositol 5-phosphatase to the PM using this method results in a dephosphorylation of both $PI(4,5)P_2$ and $PI(3,4,5)P_3$ on the PM at the D5 position. Reducing levels of these PIs resulted in a reduction in clathrin-coated pit formation and a concurrent block in transferrin uptake in COS-7 cells (Zoncu et al. 2007), these results indicate a role for PIs in the early stages of CME.

The role of PIs in CME is not only limited to the early stages of nucleation and invagination. $PI(4,5)P_2$ also binds a host of CME accessory proteins, including the GTPase dynamin via its PH domain. Upon binding the GTPase activity of dynamin is dramatically increased (around 1000 fold) and this binding may also serve to direct dynamin to the PM (Lin & Gilman 1996; Barylko et al. 1998; Klein et al. 1998; Achiriloaie et al. 1999). In addition to this $PI(4,5)P_2$ binds many actin regulatory

proteins such as Arp2/3 (Zoncu et al. 2007). Redirection of inositol 5-phosphatases to the PM also results in a disruption of dynamin and Arp2/3 localisation (Zoncu et al. 2007) showing a necessity for a specific PI enrichment to guarantee proper organisation of the machinery responsible for scission of a vesicle as well as a variety of other endocytic proteins.

Little is known about essential molecules in the process of ultrafast endocytosis (discussed in 1.3.2.2). However, as it is known that clathrin is responsible for the formation of SVs from these ultrafast endosomes (Watanabe et al. 2014). Since clathrin requires adaptor proteins to facilitate in the formation of vesicles and these adaptor proteins require the presence of $PI(4,5)P_2$ on the membrane for their recruitment, it can be assumed that $PI(4,5)P_2$ plays a role in this process. The same may be true of SV budding from endosomes formed either directly via ADBE or from other endosomal structures with which bulk endosomes have fused. More is known about the contribution of PIs in ADBE and has been discussed earlier in this thesis (see 1.3.2.3.2).

1.4.2 Phosphoinositide 3-Kinase

Phosphatidylinositol 3-kinases (PI3Ks) are responsible for the phosphorylation of PtdIns at the D3 position to create PI3P as well as the modification of other forms of PI in the same location. PI3Ks are activated in response to cell stimulation by growth factors, hormones and insulin (Cantley 2002; Smillie & Cousin 2011). This activation sets a co-ordinated series of events in motion leading to a variety of functions in cells including cell cycle initiation, growth, migration and survival

(Cantley 2002). This is mediated via a host of signalling proteins including protein tyrosine kinases, serine-threonine kinases and exchange factors which contain domains which specifically recognise and bind to D3 phosphorylated phosphoinositides (Cantley 2002). During resting conditions, these signalling proteins are located in the cytosol of a cell. However, in response to PI3K stimulation and subsequent D3 phosphorylation they accumulate at the PM. The active, membrane-bound proteins then initiate various localised responses via the regulation of heterotrimeric guanosine triphosphate (GTP)-binding proteins. The results of these regulatory roles include the polymerisation of actin, assembly of signalling complexes and the priming of protein kinase cascades (Cantley 2002).

Upon stimulation by growth factors, activation of PI3K leads to the conversion of $PI(4,5)P_2$ into $PI(3,4,5)P_3$. Those signalling proteins containing a PH domain will accumulate at sites of $PI(3,4,5)P_3$ synthesis via direct binding. Of these proteins the serine-threonine kinases Akt and phosphoinositide-dependent kinase I (PDK1) are of particular interest. Akt and PDK1 both bind $PI(3,4,5)P_3$ directly and as such, growth factor stimulation brings the two into close proximity allowing the phosphorylation and therefore activation of Akt by PDK1 (Lawlor & Alessi 2001).

Akt activation leads to the phosphorylation (and usually inhibition) of a variety of proteins involved in cell cycle entry, growth and survival. An important target of Akt enzyme activity is GSK3. GSK3 is constitutively active during basal conditions but is inhibited by phosphorylation (Frame & Cohen 2001). GSK3 activity in SV recycling is discussed more thoroughly elsewhere in this thesis (see 1.3.2.3.3 and 3.1) but this protein has roles in many other signalling cascades usually in an

inhibitory capacity until its phosphorylation. One example of its function outside of SV turnover is in the establishment of axonal polarity in immature nerve terminals. Active GSK3 phosphorylates collapsing response mediator protein 2 (CRMP-2) and adenomatous polyposis coli (APC), inhibiting their interaction with actin microtubules. The phosphorylation and inhibition of GSK3 via PI3K-mediated activation of Akt (during growth factor stimulation) prevents the phosphorylation of CRMP2 and APC and allows microtubule polymerisation (Zumbrunn et al. 2001; Yoshimura et al. 2005). This results in the prevention of axonal polarisation and the promotion of axonal growth.

1.4.3 Phosphoinositide 4-Kinase

Phosphatidylinositol 4-kinases (PI4Ks) are responsible for the phosphorylation of PtdIns at the D4 position to create PI4P, it also phosphorylates other PIs at the same region to create lipids such as $PI(3,4)P_2$. PI4P is the predominant lipid determinant of the Golgi and trans-Golgi network (McCrea & De Camilli 2009) it also contributes to the acidic nature of the PM (Hammond et al. 2012).

PI4P was originally believed to hold no specific function of its own, and only serve as a precursor for $PI(4,5P)_2$ and $PI(3,4,5)P_3$ (Boura & Nencka 2015). However, studies with yeast revealed many essential functions of PI4P in signalling and cellular trafficking which are conserved in human physiology (Boura & Nencka 2015).

Eukaryotes express two families of PI4K; type II and type III (Balla & Balla 2006) and each possesses a unique domain organisation. PI4K type II (PI4KII) is known as

“atypical” as it is dissimilar from other known lipid kinases whereas PI4K type III is known as “typical” as it is very similar in structure to PI3Ks.

Humans, unlike yeast, express two isoforms of type II PI4Ks: PI4KIIα and PI4KIIβ. The kinase domain of both isoforms contain a CCPCC motif. Palmitoylation of this region causes a stable association with a membrane along with activation of kinase activity and is therefore the main method of regulation of the enzyme (Boura & Nencka 2015).

PI4KIIα is the more active of the two isoforms and is responsible for the synthesis of around 50% PI4P in humans (Boura & Nencka 2015). It is predominantly located on the Golgi and plays a role in vesicle trafficking. It is also enriched on endosomes where both the AP-3 sorting motif on PI4KIIα and its kinase domain are required for its function in endosome trafficking (Craige et al. 2008). PI4KIIα-mediated synthesis of PI4P is needed for the recruitment of clathrin adaptors to endosomes (Salazar et al. 2005) as well as the trans-Golgi network (Wang et al. 2007). PI4KIIα also has specific functions in the endosomal sorting of the R-SNARE VAMP3 (Jović et al. 2014).

PI4KIIα is involved in the regulation of Wnt signalling via its production of PI4P (Boura & Nencka 2015). The trans-Golgi network/endosomally localised E3 ubiquitin ligase Itch has been identified as a direct binding partner as well as regulator of PI4KIIα enzyme activity (Mössinger et al. 2012). It appears that ubiquitination of PI4KIIα by Itch inhibits its production of PI4P which limits the Wnt signalling response (Mössinger et al. 2012). As well as this, ubiquitination by Itch enhances the interaction of PI4KIIα with endosomal sorting proteins such as

Tom1 and myoferlin while inhibiting interactions with endocytic proteins such as endophilin, SNX9, SNX18 and SGIP1 (Mössinger et al. 2012). This implies an Itch-mediated switch that redirects PI4KIIα from the PM to a degradative endosomal pathway.

PI4KIIα is not only involved in the trafficking of endosomal and Golgi-derived vesicles. As previously mentioned, $PI(4,5)P_2$ is an essential component of SV retrieval at the PM. PI4KIIα has been identified as the isoform responsible for PI4K activity on SVs (Guo et al. 2003), creating the PI4P substrate for the synthesis of $PI(4,5)P_2$. This makes PI4KIIα an important component of the SV cycle as well as endosomal and Golgi trafficking. The phosphorylation of this PI4P at the D5 position most likely only occurs once SVs have fused with the PM, possibly explaining the lack of clathrin-coat formation on SVs prior to exocytosis.

It is well known that proteins are capable of modifying the physical properties as well as the shape of biological membranes (Boura & Nencka 2015). Interestingly though, analysis of PI4KIIα structure and function has revealed a reversal of this role. It appears that the current state of membrane regulates the enzyme activity of PI4KIIα and this regulation is possibly determined by the fluidity (i.e. the cholesterol content) of the membrane (Zhou et al. 2014; Sun et al. 2014).

Less is currently known about the isoform PI4KIIβ. It is mostly localised to an inactive cytoplasmic pool which is stabilised by heat shock protein 90 (Jung et al. 2011) and is known to be activated by platelet-derived growth factor (Wei et al. 2002). This isoform has also been noted as an integral signalling component of early T-cell activation (Sinha et al. 2013).

1.5 Hypothesis of the Project

The activity-dependent regulation of GSK3 makes it an interesting candidate for research in the field of ADBE. Increased levels of synaptic activity result in an inhibition of its high basal activity and it has many substrates in the presynapse. The hypothesis of this project is that GSK3 has another essential role in ADBE other than dynamin I phosphorylation via the regulation of certain key substrates such as PI4KIIα.

1.6 Aims and Objectives

1.6.1 To determine how neuronal activity is translated into GSK3 inactivation

I aimed to determine which effects of HFS on the presynapse culminates in the phosphorylation and inactivation of GSK3. As it is known that GSK3 activity is essential for continued rounds of ADBE, a knowledge of those factors which modulate its activity could be of great use in future work into the modulation of ADBE.

1.6.2 To determine whether PI4KIIα regulation has any relevance to ADBE

GSK3 activity is responsible for the downregulation of PI4KIIα. As this activity is so intrinsically linked with the activity of a neuron and the continuation of ADBE it was

my aim to determine if PI4KIIα had any role in the process of ADBE. This could also indicate another distinct role for GSK3 in the process of ADBE.

1.6.3 To determine whether CME and ADBE are bi-directionally coupled

It is known that exo- and endocytosis are coupled to ensure optimal recycling of PM as well as SV proteins. As CME and ADBE work together during HFS it is possible that these two modes also possess a degree of coupling. It is possible that, if such a relationship exists, that it could be used to manipulate the speed or incidence of either mode by facilitating or inhibiting the other. This would be a convenient way of manipulating ADBE without damaging the health of a neuron.

Materials and Methods

2. Materials and Methods

2.1 Materials

Foetal bovine serum was from Biosera (Sussex, UK). Neurobasal media, B-27 supplement, Penicillin /streptomycin and Minimum Essential Medium and lipofectamine 2000 were from Invitrogen (part of ThermoFisher, Massachusetts, USA).

The primary antibodies phospho-Akt Ser473, GSK3α/β Ser21/9 and clathrin heavy chain (CHC) were from Cell Signalling (Massachusetts, USA). Bovine serum albumin was from Roche (West Sussex, UK). BAPTA-AM, CNQX and AP-5 were from Tocris. EGTA-AM was from Cambridge Bioscience (Cambridge, UK).

Fluorsave reagent, Roscovitine and ionomycin were from Merck Chemicals (Nottingham, UK). CT92001 was from R&D Systems (Minnesota, USA).

Pitstop2-AM and antibodies for Synaptotagmin 1 and Synaptobrevin-II were from AbCam (Cambridge, UK). 40kDa tetramethylrhodamine dextran, was from Life technologies (part of ThermoFisher). FM1-43 and advasep-7 were from Biotium Inc. (California, USA). The VAMP-4 antibody was from Synaptic Systems (Göttingen, Germany).

Secondary antibodies, β-Actin antibody, LY294002, Wortmannin, acrylamide and all other chemicals were bought from Sigma (Missouri, USA).

Nitrocellulose was from Bio-Rad Laboratories Ltd (California, USA).

The pHluorin expression vectors were obtained from the following sources - Synaptophysin-pHluorin - Prof. L. Lagnado (University of Sussex, UK), Synaptotagmin1-pHluorin - Prof. V. Haucke (Leibniz Institute of Molecular Pharmacology, Berlin, Germany); vGLUT1-pHluorin - Prof. R. Edwards (University of California, San Francisco, USA); synaptobrevinII-pHluorin - Prof. G. Miesenbock (Oxford University, UK); VAMP4-pHluorin - Prof. Ege Kavalali (UT South-western Medical Centre, Texas, USA).

The sequence encoding VAMP4-pHluorin was cloned into a Clontech EGFP-N1 mammalian expression vector by first removing EGFP and then inserting VAMP4-pHluorin using AgeI and NotI enzymes. The VAMP4-pHluorin L25A vector was created by Alexandros Kokotos of Edinburgh University via site-directed mutagenesis. The pSuper neo vector was engineered to express mCerulean (Rizzo et al. 2004) (mCer) by removing GFP with the enzymes AgeI and BsrGI and replacing with pre-digested mCerulean (Cheung et al. 2010). mCer N1 empty vector was made using a Clontech EGFP-N1 backbone in which the sequence encoding EGFP was replaced by mCer using AgeI and BsrGI enzymes (Anggono et al. 2006). For species and vector information see Table 2.1.

shRNA against syndapin I was designed using the pSUPER vector system (pSUPER neo-GFP, OligoEngine) (Cheung et al. 2010). shRNAs and their scrambled controls against VAMP4 and Clathrin Heavy Chain (CHC) were made using previously validated oligos (Bal et al. 2013; Royle et al. 2005) inserted into a pSuper neo backbone, the shRNA sequences were inserted using AgeI and Not I or BglII and XhoI enzymes respectively. PI4KIIα shRNA and its scrambled control as well as all

PI4KIIα rescue vectors were provided by Dr. Adam Cole (Garvan Institute of Medical Research, Sydney, Australia). For vector backbones and nucleotide sequences see Table 2.2 shRNA Plasmids.

.

Table 2.1 Protein Expression Plasmids

Expressed Protein	Species	Vector	Reference
Synaptophysin-pHluorin	Rat	pEGFP-C1	(Granseth et al. 2006)
Synaptotagmin-pHluorin	Rat	pcDNA3	(Kononenko et al. 2014)
vGlut-pHluorin	Rat	PCAGGS	(Voglmaier et al. 2006)
Superecliptic SynaptobrevinII-pHluorin	Mouse	pC1-neo	(Miesenbock et al. 1998)
VAMP-4-pHluorin WT	Human	Clontech EGFP-N1	(Nicholson-Fish et al. 2015)
VAMP-4-pHluorin L25A	Human	Clontech EGFP-N1	(Nicholson-Fish et al. 2015)
GFP- N1	N/A	Clontech EGFP-N1	(Andres et al. 2004)
mCer N1 empty vector	N/A	Clontech EGFP-N1	(Anggono et al. 2006)
mCer pSuper neo	N/A	pSuper neo	(Cheung et al. 2010)
PI4KIIα Wild-Type	Human	pRK5 - FLAG-tagged	(Robinson et al. 2014)
PI4KIIα QUAD-D	Human	pRK5 - FLAG-tagged	(Robinson et al. 2014)
PI4KIIα S9/51A	Human	pRK5 - FLAG-tagged	(Robinson et al. 2014)
PI4KIIα L60/61A	Human	pRK5 - FLAG-tagged	(Robinson et al. 2014)
PI4KIIα K152A	Human	pRK5 - FLAG-tagged	

Table 2.2 shRNA Plasmids

Target	Species	Vector	shRNA Sequence	Reference
PI4KIIα	Mouse/Rat	pSuper	5’-GATTTGATTC TTCCAAAGA-3’	(Robinson et al. 2014)
PI4KIIα Scrambled	N/A	pSuper		(Robinson et al. 2014)
Syndapin I	Mouse/Rat	pSuper	5’-AGAAGAAAC TTGTGGATAA-3’	(Cheung et al. 2010)
Clathrin Heavy Chain	Mouse	pSuper neo	5’-TCCAATTCGAAGACCAAT-3’	(Royle et al. 2005)
Clathrin Heavy Chain Scrambled	N/A	pSuper neo	5’-GACCTCGAATCATAACTA-3’	(Royle et al. 2005)
VAMP4	Rat	pSuper neo	5’-AGATAATATTACCAAGGTAAT-3’	(Bal et al. 2013)
VAMP4 Scrambled	N/A	pSuper neo	5’-GATATGATACGATAATAAGCA-3’	(Raingo et al. 2012)

Table 2.3 Drugs and Small Molecules

Name	Concentration	Pre-Incubation	Exposure	Source	Catalogue
Ionomycin	2.5 µM	N/A	1 min	Calbiochem	407950
LY294002	10 µM	10 min	During Stimulation	Sigma Aldrich	L9908
Wortmannin	200 nM	10 min	During Stimulation	Sigma Aldrich	W1628
BAPTA-AM	100 µM	30 min	N/A	Calbiochem	196419
EGTA-AM	100 µM	30 min	N/A	Calbiochem	324628
CT99021	2 µM	10 min	During Stimulation	Tocris	4423/10
Roscovitine	10 µM	10 min	During Stimulation	Calbiochem	557360
Pitstop2	15 µM	≤ 8 seconds	During Stimulation	Abcam	ab120687
AP5	50 µM	10 min (Lysis only)	During Stimulation	Abcam	ab120271
CNQX	10 µM	10 min (Lysis only)	During Stimulation	Abcam	ab120044
Tetrodotoxin	100 nM	48 hr	N/A		

Table 2.4 Primary Antibodies

Antigen	Host Species	Dilution	Incubation	Use	Manufacturer	Catalogue #	Reference
Phospho Akt Ser 473 Rabbit	Rabbit Rabbit	1:1000 1:1000	2 hours 2 hours	WB WB	Cell Signalling Cell Signalling	D9E D7F10	(Yuan et al. 2011) (Andres et al. 2013)
Phospho-GSK3 α/β Ser 21/9	Rabbit	1:1000	2 hours	WB	Cell Signalling	9331S	(Smillie & Cousin 2012)
β-Actin (HRP-Coupled)	Mouse	1:50000	30 min	WB	Sigma	A3854	(Gao et al. 2008)
Clathrin Heavy Chain	Rabbit	1:50	30 min	IF	Cell Signalling	P1663	(Popova et al. 2011)
PI4KIIα	Mouse	1:4	30 min	IF	Dr. Shane Minogue, UCL	N/A	(Simons et al. 2009)

Antigen	Host Species	Dilution	Incubation	Use	Manufacturer	Catalogue #	Reference
VAMP-4	Rabbit	1:100	30 min	IF	Synaptic Systems	136 002	(Wilhelm et al. 2014)
GFP	Chicken	1:2000	30 min	IF	Abcam	ab13970	(Hori et al. 2014)

Table 2.5 Secondary Antibodies

Conjugate	Antigen	Host Species	Incubation	Dilution	Use	Manufacturer	Catalogue #
Alexa Fluor 568	Chicken	Goat	30 min	1:500	IF	Invitrogen	A11041
Alexa Fluor 568	Rabbit	Goat	30 min	1:500	IF	Invitrogen	A21069
Alexa Fluor 568	Mouse	Goat	30 min	1:500	IF	Invitrogen	A11004
Alexa Fluor 488	Chicken	Goat	30 min	1:500	IF	Invitrogen	A11039
HRP	Rabbit	Goat	1 hour	1:5000	WB	Sigma Aldrich	A6154

2.2 Methods

2.2.1 Cell Culture

2.2.1.1 Rat Cerebellar Granule Neurons

Autoclaved coverslips were pre-coated by immersion and constant agitation in a poly-D-lysine solution (50 μg/mL in 0.1 M Borate buffer in autoclaved sterile H_2O {from a MilliQ Academic Ultrapure Water System, Millipore} pH 8.5) for at least 3 hours. Coverslips were then washed three times with sterile H_2O before drying on sterilised paper.

Cerebella were removed from P7 Sprague-Dawley rat pups (killed by euthatal injection – Schedule 1) and run twice through a McIlwain tissue chopper (Mickle Laboratory Eng. Co. Ltd. Surrey, UK) using 375μM intervals at 90˚ angles. The tissue was then placed Solution B (14 mM glucose, 50 μM bovine serum albumin {fatty acid free} (BSA), 3 mM $MgSO_4$, 153 mM Na^+, 4 mM K^+, 139 mM Cl^-, 10 mM PO_4^{2-}) supplemented with 0.25 mg/mL trypsin and kept at 37 ºC for 20 minutes. After trypsinisation 20 mL of solution W (3.2:16.8 Solution C (defined below): Solution B) containing 8 μg/mL soybean trypsin inhibitor and 8 U/mL DNase was added and the sample was centrifuged at 1000g for 60 seconds. The supernatant was removed and ~1 mL solution C (50 U/mL DNase, 50 μg/mL soybean trypsin inhibitor, 3 mM MgSO4 in solution B) was added and flame-polished Pasteur pipettes with bore sizes of decreasing diameters were then used to disaggregate the cells. The cell suspension was then layered onto an Earle's Balanced Salt Solution + 4% BSA solution and centrifuged at 1500g for 5 minutes. The pellet was

resuspended in culture medium (Minimal Essential Medium, 10% foetal bovine serum, 100 U/mL penicillin 100 µg/mL, 25 mM KCl, 33 mM glucose and 2 mM L-glutamine) and a cell density calculation performed using a haemocytometer: 10 µL of cell suspension was diluted in 90 µL culture medium and pipetted into the haemocytometer. A cell count of a 1 mm^2 area (containing 100 nL of 1:10 cell suspension) is repeated 4 times and an average taken. This cell count is then inserted into the following equation:

$$\frac{\boldsymbol{Cell\ Count \times 100 \times Suspension\ Volume\ (\mu L)}}{\boldsymbol{7,500,000}} = \boldsymbol{Volume\ required\ for\ \frac{7.5 \times 10^5\ cells}{100\ \mu L}}$$

This cell suspension was then diluted in culture medium to a density of $7.5x10^6$ cells/100 µL. A droplet of 50 or 75 µL (lysis experiments: action potential or ionomycin respectively) at this density was then plated or diluted to a density of 1.406×10^5 cells/ 75 µL (imaging experiments) and a droplet of 75 µL pipetted onto the centre of a pre-coated 25 mm coverslip each. After 1 hour each coverslip was covered in 2 mL of culture medium. After 24 hours this medium was removed and replaced with culture medium supplemented with 10 µM cytosine-β-D-arabinofuranoside (Ara-C), this inhibits cell proliferation and thereby prevents astrocyte growth. Cells were kept in an incubator at 5% CO_2, 37 ºC and used between 8-14 days in vitro (DIV).

2.2.1.2 Mouse Hippocampal Neurons

Hippocampal cells were prepared by the Cousin Laboratory. Coverslips were prepared as described for Rat CGNs. Dissociated primary hippocampal enriched neuronal cultures were prepared from both male and female E17.5 C56BL/6J mouse

embryos taken from mothers culled by cervical dislocation- Schedule 1. Isolated hippocampi were kept in ice-cold phosphate buffered saline supplemented with 1 % v/v penicillin/streptomycin before being transferred to 10 U/mL papain and incubated at 37 ºC for 20 minutes. Excess papain was removed and replaced with Supplemented DMEM/F12 (Dulbecco's Modified Eagle Medium: Nutrient Mixture F-12) supplemented with 1% v/v penicillin/streptomycin solution and 10% w/v foetal bovine serum and triturated to obtain a single-cell suspension. The suspension was centrifuged (1500rpm, room temp, 5 min). Any insoluble material was carefully removed. The supernatant was discarded and the pellet resuspended in Neurobasal supplemented with 2% B-27, 0.5 mM L-glutamine, and 1% v/v penicillin/streptomycin. A cell density calculation was then performed using a haemocytometer to assess initial concentration ($Concentration^{A}$) and the suspension was then diluted to a density 0.5 x 10^7 cells/mL ($Concentration^{B}$) using the equation:

$$\boldsymbol{ConcentrationA\ x\ VolumeA\ =\ ConcentrationB\ x\ VolumeB}$$

10 µL of this solution was then seeded onto previously prepared 25 mm coverslips into a pre-placed 50 µL spot of supplemented Neurobasal enriched with laminin (0.1 µg/mL). The cells were allowed to attach to the coverslip substrate in a 37 ºC / 5% CO_2 incubator for 1 hour before a further 1.5 mL of supplemented Neurobasal media was added. After 72 hours, cultures were further supplemented with 1 µM Ara-C to inhibit glial proliferation.

2.2.2 Transfection

2.2.2.1 Rat Cerebellar Granule Neurons

Rat cerebellar granule neurons (CGNs) were transfected after 5-8 days in culture with Lipofectamine 2000: conditioned culture medium was removed and replaced with MEM (single or co-transfections) or opti-MEM (triple transfections) for 2 hours with 2 µL of lipofectamine and 1/0.7µg DNA per construct (single or double/ triple respectively) per coverslip. Cells were subsequently washed with MEM before replacement of conditioned culture medium. Cells were imaged at 8-11 days in culture (3 days after transfection).

2.2.2.2 Mouse Hippocampal Neurons

Cells were transfected after 6-8 days in culture with Lipofectamine 2000 just as CGNs with the following alterations: conditioned neurobasal medium was removed and replaced with MEM for 2 hours with 2 µL of lipofectamine and 1 µg DNA construct per coverslip. Cells were subsequently washed with MEM before replacement of conditioned Neurobasal. Cells were imaged at 13-15 days in culture (7 days after transfection).

2.2.3 CGN Lysis

CGNs were removed from culture medium and repolarised in "imaging buffer" (170 mM NaCl, 3.5 mM KCl, 400 µM KH_2PO_4, 20 mM TES [N-tris[hydroxy-methyl]-methyl-2-aminoethane-sulfonic acid], 5 mM $NaHCO_3$, 5 mM glucose, 1.2 mM Na_2SO_4, 1.2 mM $MgCl_2$, 1.3 mM $CaCl_2$ at pH 7.4) for 10 minutes. This medium was

then replaced by imaging buffer supplemented with (2*R*)-amino-5-phosphonovaleric acid (AP-5, 50 μM), 6-cyano-7-nitroquinoxaline-2,3-dione (CNQX, 10 μM) and the relevant drug of interest if preincubation was required (Table 2.3). For electrical field stimulation experiments coverslips were placed in a Warner imaging chamber with embedded parallel platinum wires (RC-21BRFS, Warner Instruments, Connecticut, USA) and either challenged with a train of 800 action potentials delivered at 80 hertz (Hz) (100 mA at 1 msec pulses) or no stimulus (basal). In experiments using ionomycin, cells were treated in an identical manner, with the exception that the challenge with 2.5 μM ionomycin or a vehicle control (DMSO) was for 1 min.

In all experiments drugs were present during stimulation with the exception of those using either BAPTA-AM or EGTA-AM (see Table 2.3 for incubation times and concentrations). Low calcium imaging buffer had the following alterations, $CaCl_2$ was reduced to 100 μM, $MgCl_2$ was increased to 10 mM and EGTA was added at 50 μM. After stimulation with either action potentials or ionomycin, CGNs were immediately lysed in 25 μL of SDS sample buffer (67 mM Tris, 9.3% glycerol, 2 mM EGTA, 67 mM SDS, bromophenol blue, 12% β-mercaptoethanol) and boiled at 95˚C for at least 5 min.

2.2.4 Western Blotting

CGN lysates were separated using a 10 % polyacrylamide gel using a Bio-Rad Protean 3 system and transferred onto nitrocellulose using a Wet Western blot transfer apparatus from Bio-Rad Laboratories and transfer buffer (25 mM Tris, 192 mM Glycine in 1:4 methanol to H_2O solution) the membrane was exposed to Ponceau stain to confirm a successful transfer. The membrane was then blocked for 1

hour using tris-buffered saline (20mM Tris, 137 mM NaCl, pH 7.6) with 0.1% Tween (TBST) supplemented with 5% semi-skimmed milk powder. Membranes were then washed with TBST for 3 washes of 5 minutes with constant agitation before being placed in primary antibody (see Table 2.4). After primary antibody incubation membranes were washed with TBST for 3 washes of 5 minutes with constant agitation and then exposed to secondary antibodies (see Table 2.5) where required. Following a further 3 washes of 5 minutes with TBST membranes were covered with a 1:1 mixture of luminol solution (0.1M Tris pH 8.5,2.5 mM luminol, 396 nM P-coumaric acid) and peroxide solution (0.1M Tris pH 8.5, 0.06% hydrogen peroxide) for enhanced chemiluminescence (ECL). Kodak BioMax X-ray film was used to determine chemiluminescence on the membrane for each blot.

2.2.4.1 Western Blotting Analysis

The intensity of the detected chemiluminescence signal was determined using Image J (NIH): boxes were superimposed over the images to encompass all bands (Figure 2.1 B), and a histogram of greyscale intensity was created (Figure 2.1 C). Sections of the histogram corresponding to each band were then separated and measured giving raw densitometry values. Raw densitometry values were normalised firstly to the highest value within an individual blot and then to individual corresponding loading controls (β-Actin) (which was also normalised to the highest value). All Western blot data was displayed after normalisation to basal signal from each drug condition within a blot. All data was analysed using Microsoft Excel with statistical analysis performed using GraphPad Prism. Student's t-tests were performed comparing all data sets to their corresponding basal condition unless otherwise stated.

2.2.5 Fluorescence Microscopy

Fluorescence microscopy is of use in cell imaging as it allows defined spatial resolution in fixed cells as well as temporal resolution in live cells as it allows the visualisation of trafficking and recycling of fluorescent markers in real time. Live cell imaging experiments were all conducted with hippocampal or CGN cultures. CGN cultures were repolarised for 10 minutes in imaging buffer before being loaded onto a Warner chamber and placed onto the stage of a microscope. Fixed cells to be imaged were mounted on slides and cured (see 2.2.5.2) before being loaded onto the stage of an inverted epifluorescence microscope.

All experiments except for those utilising fura2-AM (see 2.2.5.1.1) were imaged on a Zeiss Axio Observer A1 epifluorescence microscope. Cultures were visualised with a Zeiss Plan Apochromat x40 oil immersion objective (NA 1.3). Single images or time-lapse images at 4 second intervals were captured using a Zeiss AxioCam MRm Rev.3 digital camera. All images were processed offline using Image J 1.43 software. Timelapse videos were processed using the ImageJ plugin Time Series Analyser (http://rsb.info.nih.gov/ij/plugins/time-series.html). Identically sized regions of interest (ROIs) were placed over boutons and the total fluorescence recorded over time. All statistical analyses were performed using Microsoft Excel and GraphPad Prism software.

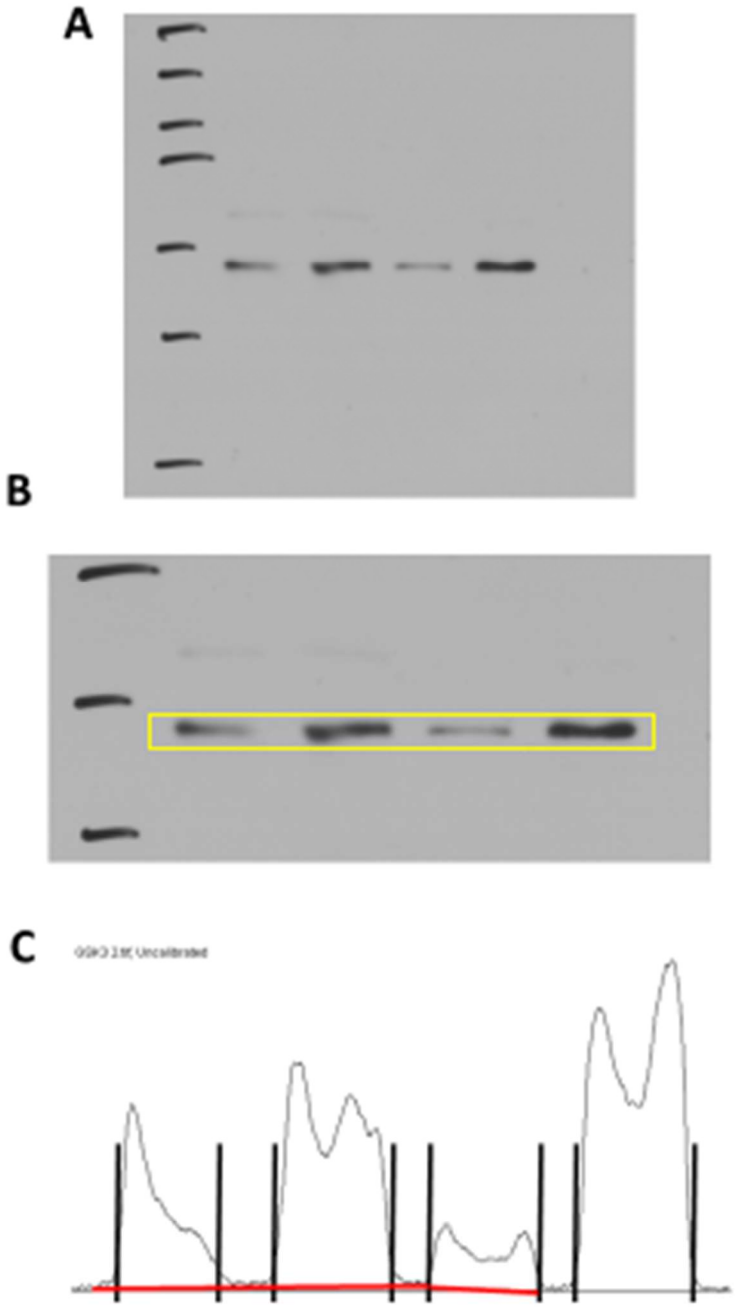

Figure 2.1 Example of Western Blot Analysis:

Levels of chemiluminescence were detected using X-ray film (A). Densitometry was then performed using ImageJ: a box was drawn around the relevant bands as closely as possible (B) and a histogram of greyscale intensity was created (C). The bands were separated (black lines, C) and the background intensity removed when needed (red lines, C). The area of each band was then measured.

2.2.5.1 Calcium Imaging

2.2.5.1.1 FURA 2-AM Assay

Fura-2 is a ratiometric fluorescent dye that is excited by different wavelengths of light depending whether or not it has bound a calcium ion. In its bound state it is maximally excited by a 340 nM wavelength but in its unbound state it is maximally excited by 380 nM (Tsien et al. 1985). The ratio of emissions between these wavelengths can give a comparative representation of calcium concentration within a cell ($[Ca^{2+}]_i$) with the added advantage of any value being independent of amount of dye loaded into the cell. The acetoxymethyl (AM) region makes the Fura dye cell permeable, this region is then cleaved by esterases within the cell, trapping the Fura intracellularly.

After repolarisation, imaging buffer was removed and then replaced with imaging buffer supplemented with 10 μM Fura2-AM for 30 minutes. After this the cultures were washed twice in imaging buffer. The coverslips were then mounted onto a Warner imaging chamber, covered with 200 μL of imaging buffer and viewed on a Nikon Diaphot TMD inverted epifluorescence microscope fitted with a 20x NA 0.75 air objective lens. Cells were excited with light of wavelengths 340 nm and 380 nm in sequential 6 second cycles with emissions captured for 0.5 seconds at 505 nm using a Hamamatsu ORCA-ER CCD (Hamamatsu City, Japan) camera and the software C- imaging PCI (HC image, Pennsylvania, USA). A baseline fluorescence was acquired for 30 seconds before addition of 50 μL imaging buffer alone (control) or supplemented with either 1 μM, 2.5 μM, or 5 μM ionomycin (final) and imaged

continuously for 90 seconds. Imaging was then paused for 10 minutes to allow maximal calcium influx and resumed for a further 5 minutes.

2.2.5.1.1.1 Fura 2-AM Assay Analysis

Time-series stacks were acquired as a composite of emissions at 505 nm from excitation in both 340 and 380 nm (Figure 2.2 C, F). The stack was split into two channels – emissions when excited by 340 nm or by 380 nm light (Figure 2.2 A, B, D, E). One hundred identically sized (5 x 5 pixel) regions of interest (ROIs) were placed on the neurites of the image and superimposed onto each channel. The total pixel intensity was calculated within each ROI for each frame and the ratios between the individual readings for each frame on either channel was then calculated using ImageJ with the Time Series analyser plugin. The values were then expressed as a ratio of 340/380 i.e. the higher the ratio value, the more calcium-bound Fura (Figure 2.2 G). For these experiments n refers to the number of coverslips examined.

2.2.5.1.2 Fluo3-AM Imaging

Fluo-3 has an affinity for calcium ($K_d\{Ca^{2+}\}$) of 335 nM. When internalised within the cell its fluorescence can be used as a measure of $[Ca^{2+}]_i$. Fluo-3 has a low fluorescence when unbound which sharply increases (typically > 100-fold) upon binding a calcium ion. Its structure was based upon that of conventional rhodamines and fluoresceins (Minta et al. 1989). It is a preferable calcium indicator to Fura-2 for

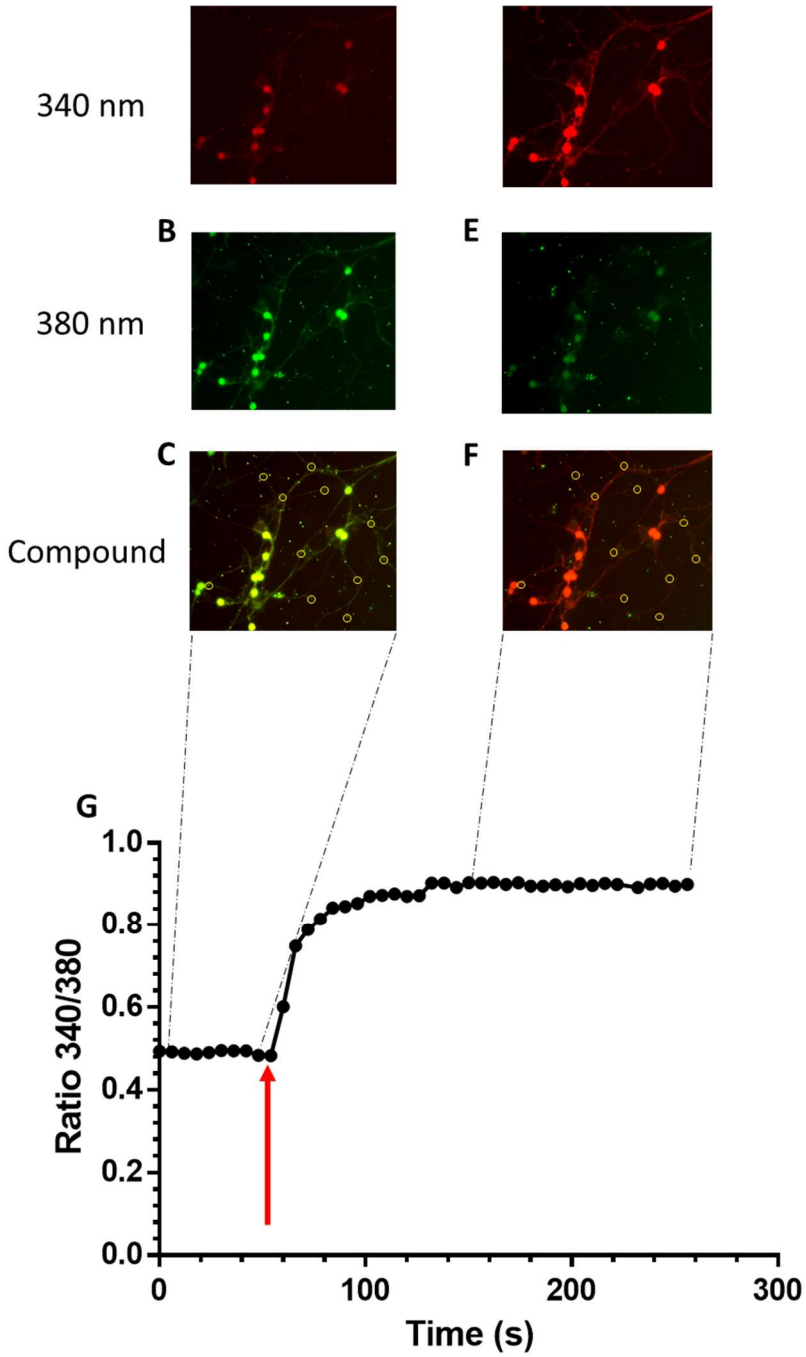

Figure 2.2 Example of Fura2-AM Analysis:

Fura loaded cultures were imaged using 340 nm (A and D) and 380 nm (B and E) UV filters, after baseline acquisition ionomycin was added to the imaging buffer (red arrow, G). Stacks were aligned and identically sized ROIs were placed over neurites in the composite images (yellow circles, C and F). Fluorescence within these ROIs in each wavelength was measured throughout the stack and screened for responsive synapses. For each frame a ratio of fluorescence intensity between 340 and 380 nm was calculated and plotted against time. Traces were then averaged together (G).

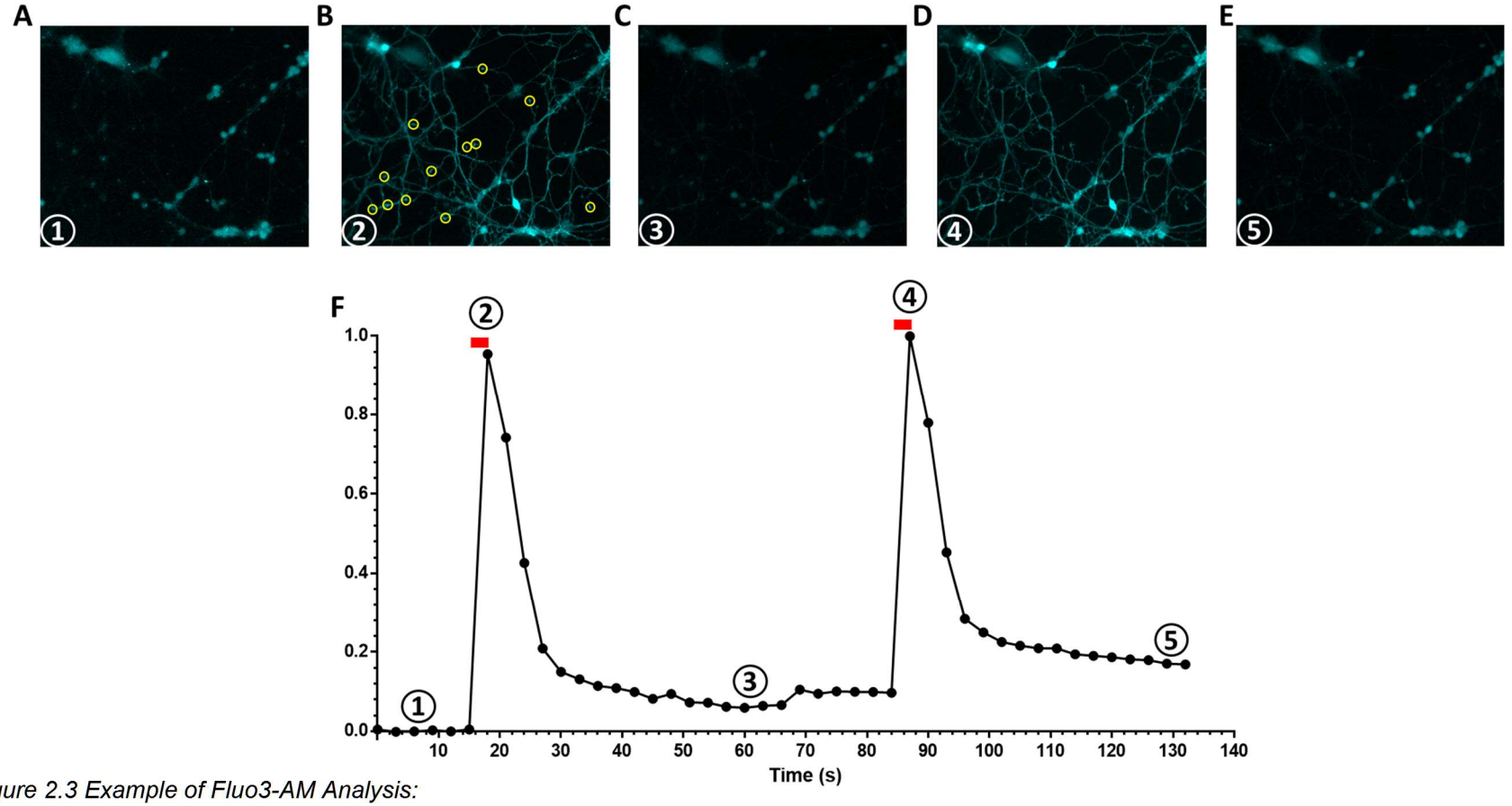

Figure 2.3 Example of Fluo3-AM Analysis:

Neurons loaded were Fluo3 were imaged using CFP filter set. Cultures were stimulated twice (red bars, F) while imaging. Timelapse stacks were aligned (A-E) and identically sized ROIs were place over neurites responsive to the first stimulation (yellow circles, B). Fluorescence within these ROIs was measured throughout the stack and normalised to baseline and maximum fluorescence (1 and 4). Remaining traces were then averaged together (F) and peak heights compared as S1/S2

our purposes due to its excitation wavelength. Fura-2 requires excitation at 340 and 380 nm wavelengths which are in the ultraviolet (UV) spectrum and nearing the limit for transmission through glass, UV excitation of living cells is also potentially injurious. Fluo-3 is maximally excited at 506 nm which is in the visible spectrum and more compatible with common filter sets.

CGN cultures were removed from culture medium and placed into imaging buffer supplemented with 10 µM fluo3-AM for 30 minutes. Cultures were then washed twice in imaging buffer before being placed into a Warner imaging chamber, covered with 200 µL of imaging buffer and placed on the stage of the Zeiss Axio Observer A1 epifluorescence microscope. A dichroic 455 nm and a band-pass emission filter, 535 nm (Zeiss filter set 46 YFP) were used. A baseline of 30 seconds was acquired before a stimulation train of 400 action potential at 40 Hz. Cells were imaged for a further minute before imaging was paused. 5 minutes after initiation of imaging, 50 µL of imaging buffer supplemented with 5 times concentration of the relevant antagonist (see Table 2.3) was added directly to the Warner imaging chamber. After 10 minutes of drug incubation an identical protocol of imaging and stimulation as described above was performed (Figure 2.3).

2.2.5.1.2.1 Fluo3-AM S1 S2 Assay Analysis

Only traces from ROIs that increased in fluorescence in response to the first action potential stimulation were analysed. The fluorescence change was calculated as:

$$\text{Change in fluorescence } (F\Delta) \,/\, \text{Baseline fluorescence } (F_0)$$

with difference between baseline and stimulation peak fluorescence measured for each stimulation (S1 and S2) and compared for each experiment. Values are expressed as ΔF S2/ ΔF S1 and n refers to the number of individual coverslips examined.

2.2.5.1.3 pHluorin Imaging

The genetically encoded reporters called pHluorins allow the investigation of synaptic vesicle recycling. A pH-sensitive version of a GFP molecule was made by Miesenböck et al. (1998) via the following mutations: S147D, N149Q, T161I, S202F, Q204T and A206T and fused to the luminal domain of a synaptic vesicle protein, making a pHluorin. The lumen of a synaptic vesicle has a pH of around 5.5, pHluorins are quenched when in an acidic (<6) pH and therefore have minimal fluorescence when encapsulated inside a vesicle. When the GFP molecule is exposed to the neutral pH of the extracellular environment (i.e. via exocytosis) it dramatically increases in fluorescence (20-fold) and when the pHluorin is re-acidified inside a vesicle (after endocytosis) this fluorescence is re-quenched (Figure 2.4).

A method of normalisation utilised with pHluorins is exposure to an (alkaline) "ammonium imaging buffer" (imaging buffer with 50 mM NH_4Cl substituted for 50 mM NaCl), this allows visualisation of all pHluorin molecules present in a given cell. This is possible by NH^+ diffusing across the SV membrane and neutralising the lumen, causing the pHluorin molecules to fluoresce despite their internalisation. The proportion of surface-bound pHluorin molecules can also be determined by pulsing an impermeant acidic imaging buffer (imaging buffer with 20 mM MES substituted for 20 mM TES, pH 5.5) over the cell, quenching any accessible pHluorin molecules.

All pHluorins with the exception of synaptobrevin II- and synaptophysin-pHluorin constructs were co-transfected with an empty mCer-tagged vector to allow identification of transfected cells for pHluorins with a low baseline fluorescence. Transfected neurons were visualised at 436 nm excitation (to illuminate mCer where present) using a dichroic 455 nm and a band-pass emission filter, 480 nm (Zeiss filter set CFP), whereas pHluorin reporters were visualised at 500 nm using a dichroic 455 nm and a band-pass emission filter, 535 nm (Zeiss filter set 46 YFP). This allowed separation of mCer fluorescence from pHluorin fluorescence. During all experiments cells were subject to continuous perfusion with imaging buffer. A baseline of one minute was acquired prior to each stimulation with action potentials (300 AP at 10 Hz or 400 AP at 40 Hz) and imaged for at least 3 minutes after. At the end of each experiment cultures were challenged with alkaline imaging buffer to reveal total pHluorin fluorescence (Figure 2.4).

Imaging of hippocampal cultures was performed in essentially the same manner except for the absence of a 10 min repolarisation period and the use of an altered "hippocampal imaging buffer" (136 mM NaCl, 2.5 mM KCl, 2 mM $CaCl_2$, 1.3 mM $MgCl_2$, 10 mM glucose, 10 mM HEPES, pH 7.4 supplemented with 10 μM CNQX and 50 μM AP-5) and alkaline imaging buffer (50 mM NH_4Cl substituted for 50 mM NaCl).

Only regions that showed an increase of fluorescence in response to action potential stimulation and exhibited an alkaline buffer fluorescence greater than stimulation intensity were selected for analysis. The average trace from each experiment was normalised to baseline and alkaline wash maximum fluorescence to 0 and 1

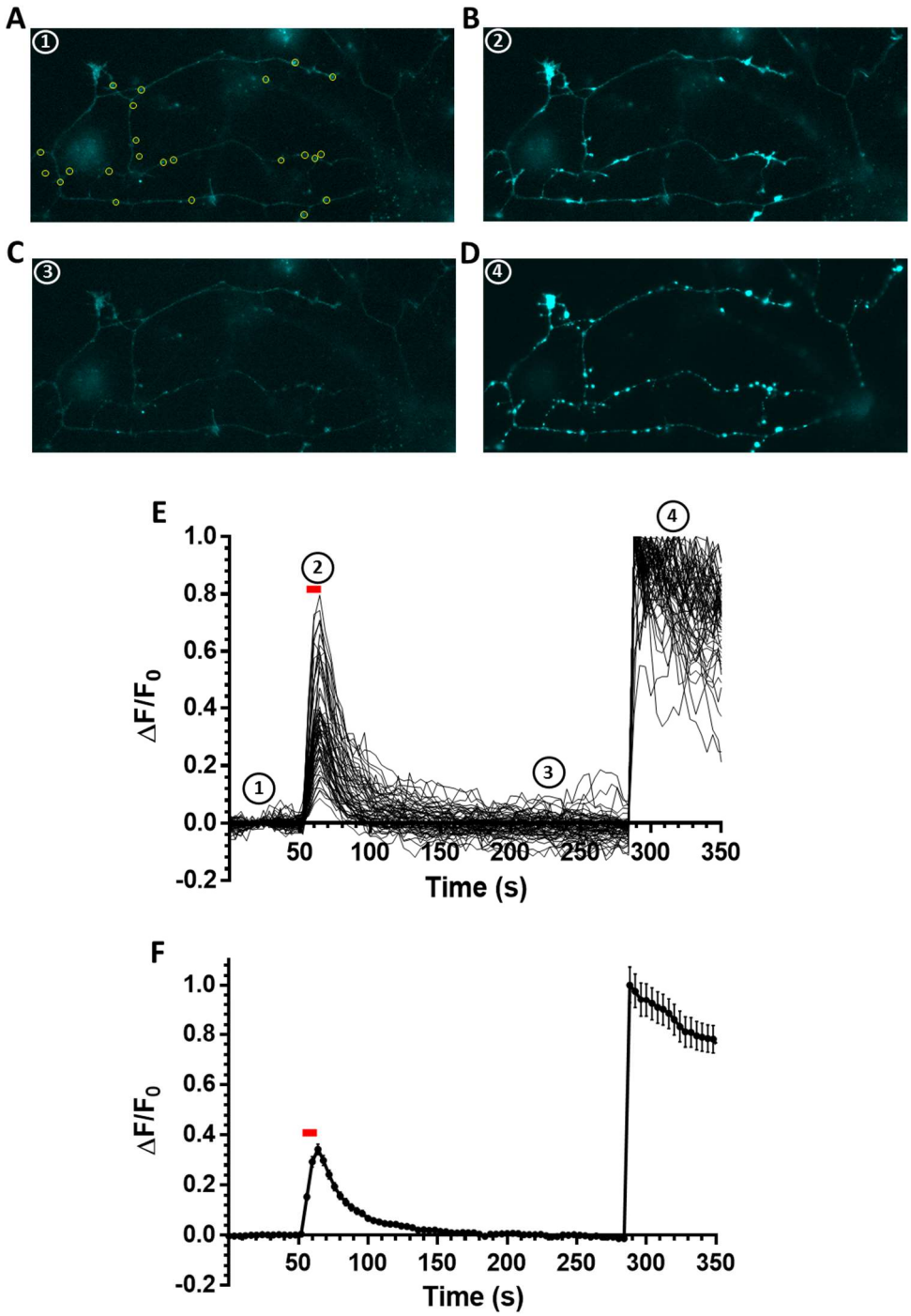

Figure 2.4 Example of pHluorin Analysis:

Images of pHluorin transfected neuron were acquired with YFP filter set. Timelapse images were aligned (A-D) and identically sized ROIs were placed over boutons on transfected cells (yellow circles, A). Fluorescence within these ROIs was measured throughout the stack and screened for responsive synapses and normalised to baseline and maximum fluorescence (E). Remaining traces were then averaged together (F) and any measurements of τ or peak height were made from this average. Red bar represents time of stimulation. Error bars represent SEM.

respectively (Figure 2.4 E). The pHluorin fluorescence change was calculated as $F\Delta/F_0$. A non-linear regression curve-fit was fitted to the endocytic decay of the pHluorin trace using GraphPad Prism and the tau (τ) value calculated for each stimulation. Peak height was measured using Microsoft Excel and calculated as $F\Delta/F_0$ in comparison to alkaline maximum fluorescence. In all cases n refers to the number of individual coverslips examined.

VAMP4-pHluorin analysis differs from the above protocol in the following ways: a 3 x 3 pixel binning was implemented in either Axiovision or Zen Pro software during acquisition. This was due to the low basal fluorescence of a VAMP4-pHluorin transfected neuron. VAMP4-pHluorin undergoes significant photo bleaching over time; in GraphPad Prism a non-linear regression curve was fitted to the first 19 frames of baseline acquisition for each trace, the equation of these curves were then subtracted from the original data to compensate for fluorescence lost through decay (see Figure 2.5 A and B). Trace acquisition, decay correction and screening for responsive synapses occurred in an identical manner to that described above however VAMP4-pHluorin data also requires an additional step of analysis. Screened traces (Figure 2.5 C) were inserted into a Microsoft Excel spreadsheet which firstly normalised each trace to the maximum fluorescence given with alkaline imaging buffer and secondly separated those traces which increased in fluorescence upon stimulation from those which decreased (Figure 2.5 D) using the following calculation:

"IF('Normalised Traces'!BH5<AVERAGE('Normalised Traces'!B5:O5),▼,▲))"

Meaning:

If, after 2 minutes of recovery, fluorescence intensity is lower than the average value of its baseline, classify as Down (▼) if not classify as Up (▲).

When an experiment required two stimulations this spreadsheet was modified to separate out traces based on both stimulations, creating four subsets:

1) **S1 Up, S2 Up**

2) **S1 Up, S2 Down**

3) **S1 Down, S1 Down**

4) **S1 Down, S2 Up**

These subsets were then averaged. The proportion of each subset within each experiment was also calculated and compared.

2.2.5.1.3.1 Single Stimulation pHluorin Assay

Cultures were subjected to stimulation with a train of either 400 action potentials delivered at 40 Hz or 300 action potentials delivered at 10 Hz (100 mA, 1 ms pulse width) where indicated. Where the drug pitstop2 was utilised the cell was exposed to the drug 4-8 seconds before stimulation.

Comparisons between traces were performed using a 2-way ANOVA in GraphPad Prism. Peak Heights and Tau values were compared using t-tests or one-way ANOVAs where stated using GraphPad Prism.

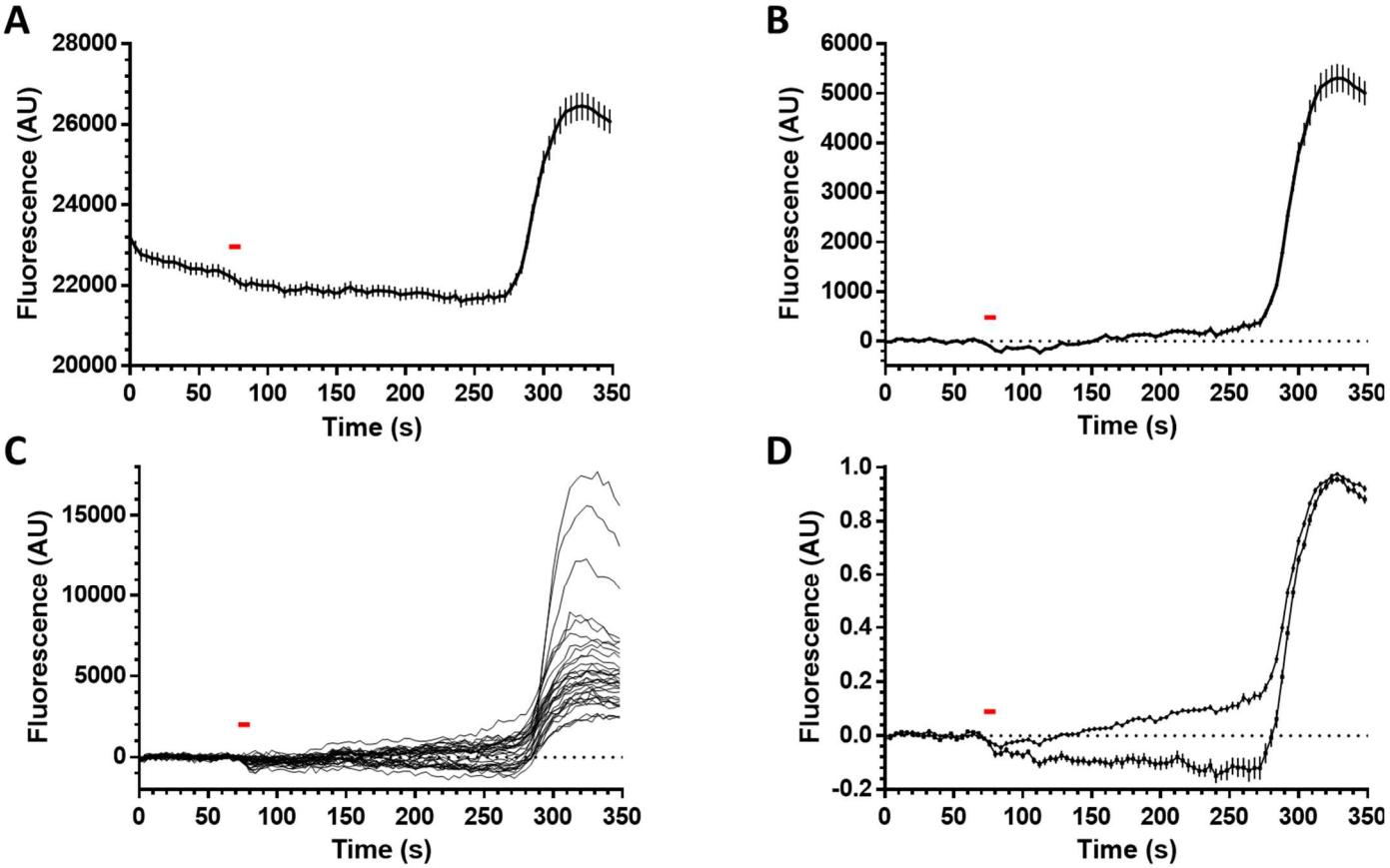

Figure 2.5 Example of VAMP4-pHluorin Analysis

Raw data from timelapse images (A - average) were fit with non-linear regression curves and decay corrected (B - average). Individual decay corrected traces (C) were then separated into two subsets: those which had a relative decrease in fluorescence 2 minutes after stimulation and those which had a relative increase (D). Red bar represents point of stimulation, error bars represent SEM.

2.2.5.1.4 S1 S2 pHluorin Assay

For experiments blocking ADBE, cells were incubated with the relevant drug or imaging buffer alone (control) for 10 minutes after initial repolarisation. Cultures were subjected to continuous perfusion with imaging buffer plus/minus the relevant drug. A baseline of 1 minute was acquired before cells were stimulated with a train of 400 action potentials delivered at 40 Hz (100 mA, 1 ms pulse width) “S1”. Cultures were allowed to recover for 10 minutes in total with images acquired for 3 minutes after S1 before a second identical stimulus train and imaging protocol “S2”. In experiments using pitstop-2 (to block CME) the first stimulation serves as an internal control with the drug only being applied 4-8 seconds before the second stimulation.

2.2.5.1.4.1 S1 S2 Assay pHluorin Analysis

Peak height and τ values were noted for each stimulation within the experiment and a ratio of S1/S2 calculated per value. Ratios between conditions were compared using Microsoft Excel and GraphPad Prism.

2.2.5.1.5 Acid Wash pHluorin Assay

Perfusion of an impermeant acidic imaging buffer over a cell expressing pHluorins allows one to isolate the fraction of pHluorin molecules residing on the cell surface in relation to the total pool as revealed by alkaline imaging buffer. It can also be used to reveal any pHluorin which has been internalised into a neutral-pH environment after stimulation via comparison to a control acid wash.

Cells transfected with syp-pH were imaged for 40 seconds with constant perfusion of imaging buffer before perfusion of acidic imaging buffer for a further 40 seconds. This is the control acid wash, which provides a baseline of minimum fluorescence. Acidic buffer was replaced with imaging buffer via perfusion before a stimulus train of 400 action potentials delivered at 40 Hz (100 mA, 1 ms pulse width). Thirty seconds after stimulation, during the recovery period, acidic buffer was pulsed over the culture for 30 seconds and then replaced with imaging buffer. This is the first post-stimulation acid wash. After 90 seconds, acidic buffer was again pulsed over the culture and again replaced with imaging buffer, this is the second post-stimulation acid wash.

2.2.5.1.6 Acid Wash pHluorin Assay Analysis

The difference in fluorescence between control acid wash to stimulation intensity was determined ($F\Delta_0$) and compared to difference in fluorescence between first ($F\Delta_1$) or second ($F\Delta_2$) post-stimulation acid wash and stimulation intensity. Values are expressed as percentage of control acid wash difference e.g.:

$$\frac{(F\Delta_1)}{(F\Delta_0)} \times 100$$

This experiment was repeated using VAMP4-pHluorin using an identical protocol as described above with the following alterations. After stimulation only one post-stimulation acid wash was performed immediately after stimulation had ceased. The experiment was performed with stimulus trains of either 400 AP at 40 Hz or 300 AP at 10 Hz.

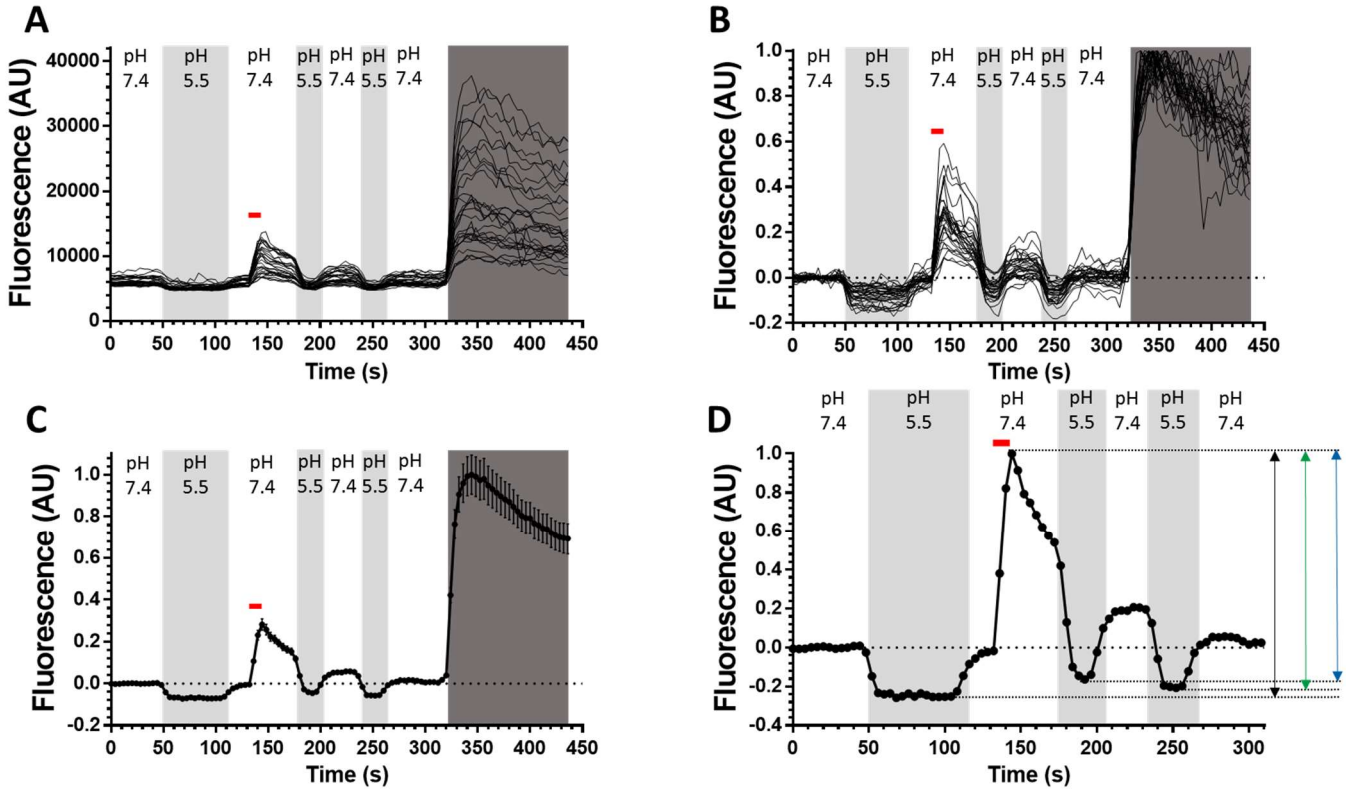

Figure 2.6 Example of Acid Wash Analysis

Neurons transfected with pHluorin were exposed to acidic imaging buffer (light grey bands) to reveal surface fraction. The cell was then stimulated with 40 HZ 10 sec and exposed to acidic buffer twice more at set time points to reveal any sequestered pHluorin. Raw data from timelapse images was screened for responsive synapses (A) and normalised to its baseline and alkaline pulse (dark grey bands) fluorescence (B) and averaged together (C). This averaged trace was then normalised to the stimulation peak height and the differences between the peak height and the control acid wash (black arrow, D), first post-stimulation wash (green arrow, D) and second post-stimulation wash (blue arrow, D) was calculated and compared. Red line indicates stimulation time point, error bars represent SEM.

2.2.5.1.7 Vesicle Acidification Assay

Cultures were perfused with imaging buffer for 1 minute and then exposed to alkaline imaging buffer. The alkaline buffer was then replaced with either imaging buffer alone (control) or supplemented with 15 μM Pitstop-2. This solution was then perfused for the length of a typical one stimulation experiment (4 minutes) and challenged with another exposure to alkaline imaging buffer alone (control) or with Pitstop-2. The culture was then left for 5 minutes in either imaging buffer alone (control) or with Pitstop-2 before renewing acquisition. A third alkaline buffer wash was then executed (control) with Pitstop-2.

2.2.5.1.8 Vesicle Acidification Assay Analysis

Only regions that responded to all alkaline imaging buffer challenges were selected for analysis. The differences between baseline and total fluorescence was calculated for all 3 exposures and compared between control and Pitstop-2 conditions. Values were normalised to the greatest difference in fluorescence and all $F\Delta/F_0$ values were expressed as a percentage of the largest.

2.2.5.2 Immunofluorescent Antibody Assay

CGN or hippocampal cultures were removed from culture medium and washed twice in PBS solution (0.1 M phosphate buffer, 2.7 mM KCl, 137 mM NaCl, pH 7.4) before fixing in 4% PFA in PBS for 20 minutes. The PFA was then quenched with two 5 minute washes in PBS solution supplemented with 50 mM NH_4Cl. Cells were permeabilised to allow labelling of intracellular structures via 2 washes of 4 minutes

in PBS solution supplemented with 0.1% Triton X-100. Cells were then placed in blocking solution (PBS solution with 2% BSA) for ≥10 minutes.

Primary antibodies were made up in blocking solution to the correct concentration (see Table 2.4). Fixed, permeabilised and blocked cultures were exposed to the primary antibody solution in a humidifying chamber at room temperature for 30 minutes. The antibody was then removed with 3 washes of PBS solution.

Secondary antibodies were made up in blocking solution to the correct concentration (see Table 2.5) and antibody exposure was conducted in an identical manner to that of the primary antibody. For every primary antibody investigated 2 controls were performed (primary or secondary antibody alone).

After secondary antibody exposure coverslips were submerged in sterile H_2O in 3 separate containers to remove any unbound antibody, dried and placed on slides with Fluorsave reagent mountant and left to cure in the dark overnight. Slides were left in a 4 ^{o}C environment until imaged.

CGN cultures were placed on the stage of Zeiss Axio Observer A1 epifluorescence microscope. Transfected neurons were located with a Zeiss Plan Apochromat x40 oil immersion objective (NA 1.3) at 436 nm excitation to illuminate mCerulean using a dichroic 455 nm and a band-pass emission filter, 480 nm (Zeiss filter set 47 CFP) or at 500 nm where Alexa Fluor 488-bound GFP antibody was present using a dichroic 455 nm and a band-pass emission filter, 535 nm (Zeiss filter set 46 YFP). Antibodies labelled with an Alexa Fluor 568 secondary were visualised at 546 nm using a

dichroic 560 nm and a band-pass emission filter, 608 nm (Zeiss filter set 20 Rhodamine). A least 8 fields were imaged per coverslip.

2.2.5.2.1.1 Immunofluorescence Assay Analysis

Images from each region were overlaid and ROIs of identical sizes were placed over transfected synaptic boutons and the fluorescence in the rhodamine channel of each ROI was taken using ImageJ with the Time Series analyser plugin. Equal-sized ROIs were then placed over non-transfected synaptic boutons as visualised in the rhodamine channel and the fluorescence of each ROI taken. ROIs of equal size were also placed over synaptic bouton-adjacent areas devoid of neurons to acquire an accurate representation of average background fluorescence intensity. This background intensity was then subtracted from each value for both transfected and non-transfected ROI set and the remainders averaged for each image. These averages were then expressed normalised to the non-transfected value, giving the transfected values as a percentage of the non-transfected. n represents number of transfected cells imaged.

2.2.5.3 Dextran Imaging

CGN cultures were repolarised in imaging buffer and then placed into a Warner imaging chamber. Imaging buffer (200 µL) supplemented with 50 µM 40kDa tetramethylrhodamine-Dextran (dextran) was then added to the chamber and cultures were challenged with a stimulus train of 400 action potentials at 40 Hz, dextran was removed and replaced with imaging buffer. Hippocampal cultures were treated in the same manner with previously stated alterations (see 0). The Warner chamber was

then mounted onto the stage of a Zeiss Axio Observer A1 epifluorescence microscope and any non-internalised dextran was washed off with imaging buffer via perfusion for at least 1 minute. dextran was imaged at 546 nm using a 560 nm dichroic and a 608 nm band-pass emission filter (Zeiss filter set 20 Rhodamine). At least 8 fields were imaged per coverslip.

2.2.5.3.1 Field Dextran Assays

For a single stimulation CGN cultures were repolarised for 10 minutes in imaging buffer before being placed in in a Warner imaging chamber and covered with 200 µL of 50 µM dextran in imaging buffer alone (control) or supplemented with the relevant drug and subjected to a stimulus train of 400 action potentials at 40 Hz and treated as stated above.

For S1 S2 experiments, repolarised CGN cultures were incubated for 10 minutes with imaging buffer alone (control) or supplemented with 2 µM CT92001 or 10 µM roscovitine. Coverslips were then placed in a Warner imaging chamber and stimulated with 400 AP at 40 Hz (S1) and left to recover for 10 minutes before an identical dextran loading protocol as that stated above (S2).

2.2.5.3.1.1 Field Dextran Assay Analysis

The number of dextran puncta per image were assessed using a macro: a threshold of fluorescence was set using the plugin Auto Threshold (https://github.com/fiji/Auto_Threshold/) to eliminate lowly fluorescing or overexposed bodies. It then counted bodies of circular shapes (puncta) within the

defined fluorescence range with a diameter of between 4 and 14 pixels in each image using the command “Analyze Particles”. The number of valid puncta in each image were averaged within coverslips and then within conditions. Values are expressed as a percentage of control (n represents number of coverslips imaged).

2.2.5.3.2 Dextran with Transfected Cell Assay

After an identical dextran loading and washing protocol as described in 2.2.5.3, transfected cells were located at 436 nm excitation to illuminate mCerulean using a dichroic 455 nm and a band-pass emission filter, 480 nm (Zeiss filter set 47 CFP). Images were acquired in both CFP and Rhodamine.

2.2.5.3.2.1 Dextran with Transfected Cell Assay Analysis

Lengths of transfected neurites were measured in pixels using the Fiji (ImageJ analogue) plugin Simple Neurite Tracer (http://fiji.sc/Simple_Neurite_Tracer) (Figure 2.7 C). Images of transfected neurons and dextran were overlaid and any dextran puncta which overlaid entirely with a transfected neurite were counted (Figure 2.7). Puncta per pixel were calculated and normalised to the control condition. Data is expressed as puncta/pixel as a percentage of control (n represents transfected cell number).

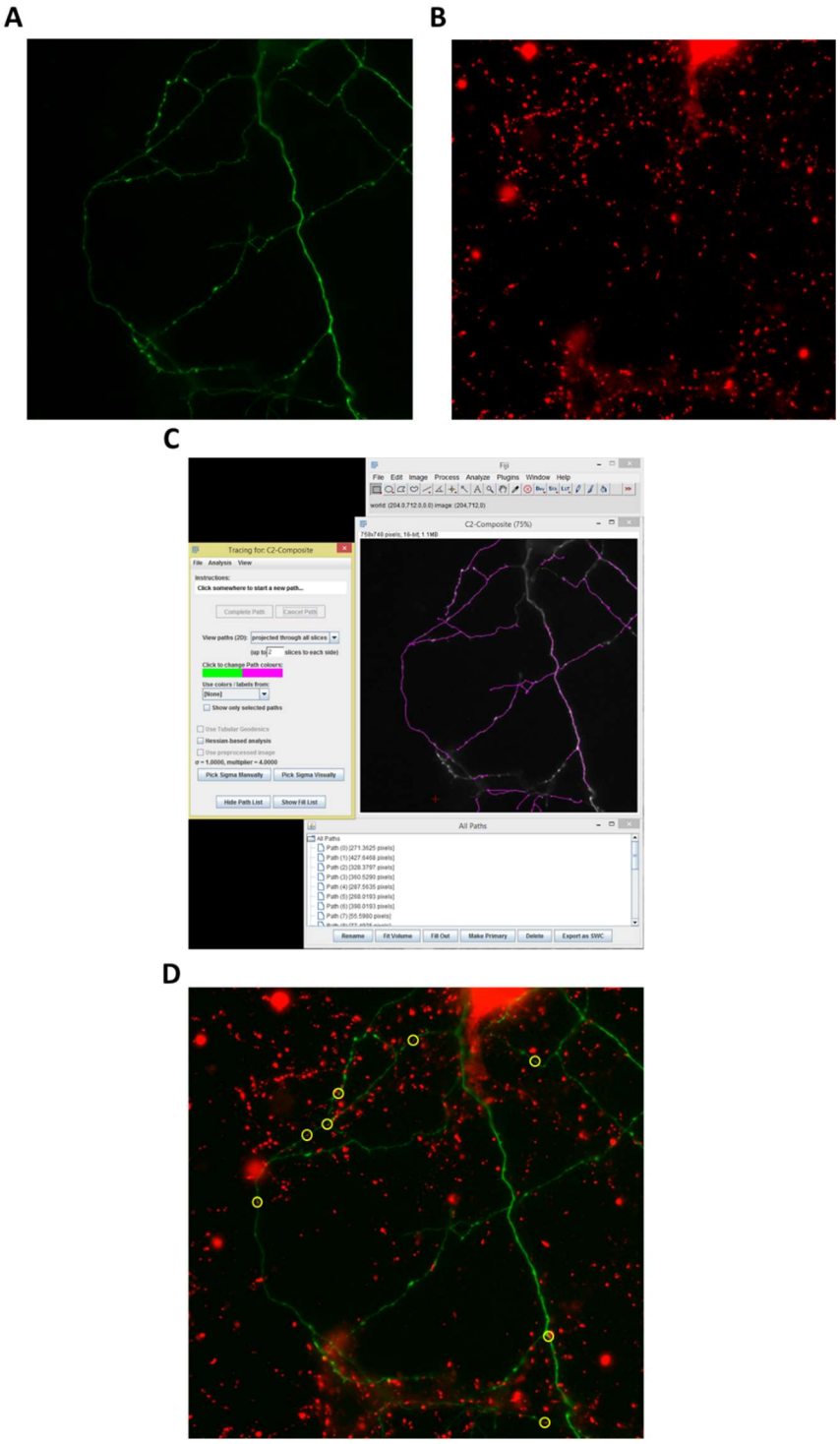

Figure 2.7 Example of Transfected Dextran Analysis:

Images were captured with both CFP (mCer) and Rhodamine (Dextran) filter sets (A and B respectively). Neurite length was measured in pixels using “Simple Neurite tracer” (C). Images were then overlaid (D) and puncta co-localising with transfected neurites were counted (yellow circles, D).

Results

Phosphatidylinositol 3-Kinase Couples Localised Calcium Influx to Akt Activation in Central Nerve Terminals

3. PI3K couples localised calcium influx to Akt activation in central nerve terminals

3.1 Introduction

During intense stimulation an additional form of endocytosis is initiated alongside single SV retrieval via CME, activity-dependent bulk endocytosis (ADBE). ADBE is triggered immediately during high frequency stimulation and is a rare event during low frequencies. This mode permits dramatically increased retrieval capacity via the formation of large endosomes direct from the PM. These bulk endosomes then undergo "budding", a clathrin-dependent process which forms SVs from the larger endosome. These SVs are capable of repopulating the recycling pool (Clayton & Cousin 2009; Kokotos & Cousin 2015).

Initiation of ADBE is dependent on the dephosphorylation of the large GTPase dynamin I at two serine residues (Ser774 and Ser778) (Clayton et al. 2009). This event is mediated by the calcium-dependent protein phosphatase calcineurin and only occurs during intense activity (Clayton et al. 2009). In order to maintain ADBE across multiple trains of stimuli the two serine residues of dynamin I must be rephosphorylated by cyclin-dependent kinase 5 (cdk5) on Ser778 and then subsequently by glycogen synthase kinase 3 (GSK3) on Ser774 (Clayton et al. 2010). Expression of both phospho-null and phospho-mimetic Ser774 mutant versions cause an inhibition of ADBE (Clayton et al. 2010). This demonstrates the need for both de- and rephosphorylation in the initiation of this process.

Although Cdk5 is constitutively active, the high basal activity of GSK3 is modulated via its phosphorylation status (Frame & Cohen 2001). Phosphorylation of Ser 21/9 of GSK3β/α by upstream cascades inhibit its protein kinase activity. GSK3 phosphorylation can occur as a consequence of many different signalling cascades (Eldar-Finkelman 2002). GSK3 is phosphorylated in central nerve terminals in response to stimulation only during high levels of neuronal activity, coincident with dynamin I dephosphorylation (Smillie & Cousin 2012). This activity-dependent phosphorylation of GSK3 is performed by Akt (also known as protein kinase B {PKB}). During periods of intense neuronal activity Akt is activated via phosphorylation on Ser473 and Thr308. This activity-dependent inhibitory signalling cascade of Akt activation leading to GSK3 de-activation ensures efficient and maximal dephosphorylation of Ser-774 on dynamin I during periods of intense activity (Smillie & Cousin 2012). Importantly, either expression of constitutively active Akt or addition of signalling molecules capable of activating Akt, such as brain-derived neurotrophic factor (BDNF), reduces incidence of ADBE as measured by dextran uptake in cultured neurons (Smillie & Cousin 2012; Smillie et al. 2013). Together, this suggests that this activity-dependent signalling cascade is essential for efficient presynaptic endocytosis during intense neuronal activity.

It is unknown what specific factors of HFS are responsible for the phosphorylation of Akt and GSK3, and which specific upstream components are responsible for the procession of the cascade. To address this, the phosphorylation status of both Akt and GSK3 was monitored utilising phospho-specific antibodies with Western blotting whilst manipulating elements such as intracellular free calcium ($[Ca^{2+}]_i$) as well as inhibiting potential contributors.

3.2 Results

3.2.1 An Intracellular Free Calcium Increase is Essential for Phosphorylation of Akt/GSK3

It is currently unclear how action potential stimulation is transduced into activation of Akt. The pronounced activity-dependence of Akt and GSK3 phosphorylation could suggest an essential requirement for increased $[Ca^{2+}]_i$, an event which is also essential for the initial dephosphorylation of dynamin I.

To assess the importance of increased $[Ca^{2+}]_i$ on both Akt and GSK3 phosphorylation the calcium ionophore ionomycin was employed to uniformly increase $[Ca^{2+}]_i$ throughout the presynaptic bouton independent of depolarisation. To assess the duration for which neurons should be exposed to this ionophore in order to elicit a significant $[Ca^{2+}]_i$ increase, a preliminary experiment was performed using the ratiometric calcium reporter Fura-2.

Independent cultures which had been loaded with Fura-2 and then washed to remove any un-internalised reporter were incubated with different concentrations of ionomycin (1, 2.5 and 5 μM) and the rate of $[Ca^{2+}]_i$ increase was monitored and assessed using timelapse imaging. The time taken to reach 75% of maximum $[Ca^{2+}]_i$ was determined to be consistently between 30 and 60 seconds for ionomycin concentrations of both 2.5 and 5 μM (Figure 3.1). Based on these data it was decided that these concentrations would be utilised for further experiments and an appropriate exposure time was determined to be 1 minute.

To test the effect of an artificially increased $[Ca^{2+}]_i$ on Akt and GSK3 phosphorylation, cultures were exposed to 5 μM ionomycin for 1 minute in the presence and absence of extracellular Ca^{2+} and immediately lysed. These lysed cell samples were then Western blotted using phospho-specific antibodies for those activity-dependent phosphorylation states of Akt and GSK3.

Significant phosphorylation of both Akt and GSK3 was observed when CGNs were exposed to ionomycin in the presence of extracellular calcium in comparable amounts to that seen during intense stimulation. However, no evoked increase was observed when this experiment was repeated in low calcium buffer (Figure 3.2). This indicates that increased $[Ca^{2+}]_i$ in the absence of membrane depolarization is sufficient to cause activation of this signalling cascade. The absence of the same phosphorylation in the presence of ionomycin but with no increase in $[Ca^{2+}]_i$ shows that this is not an ionomycin-specific effect. Controls were conducted in the absence of inonomycin and no effect was observed with differing concentrations of extracellular calcium alone.

Increased presynaptic $[Ca^{2+}]_i$ during action potential stimulation is usually a result of activation of VGCCs. To assess if these channels are responsible for the increased $[Ca^{2+}]_i$ leading to Akt/GSK phosphorylation during HFS the nonselective calcium channel inhibitor flunarizine was employed (Cousin et al. 1993).

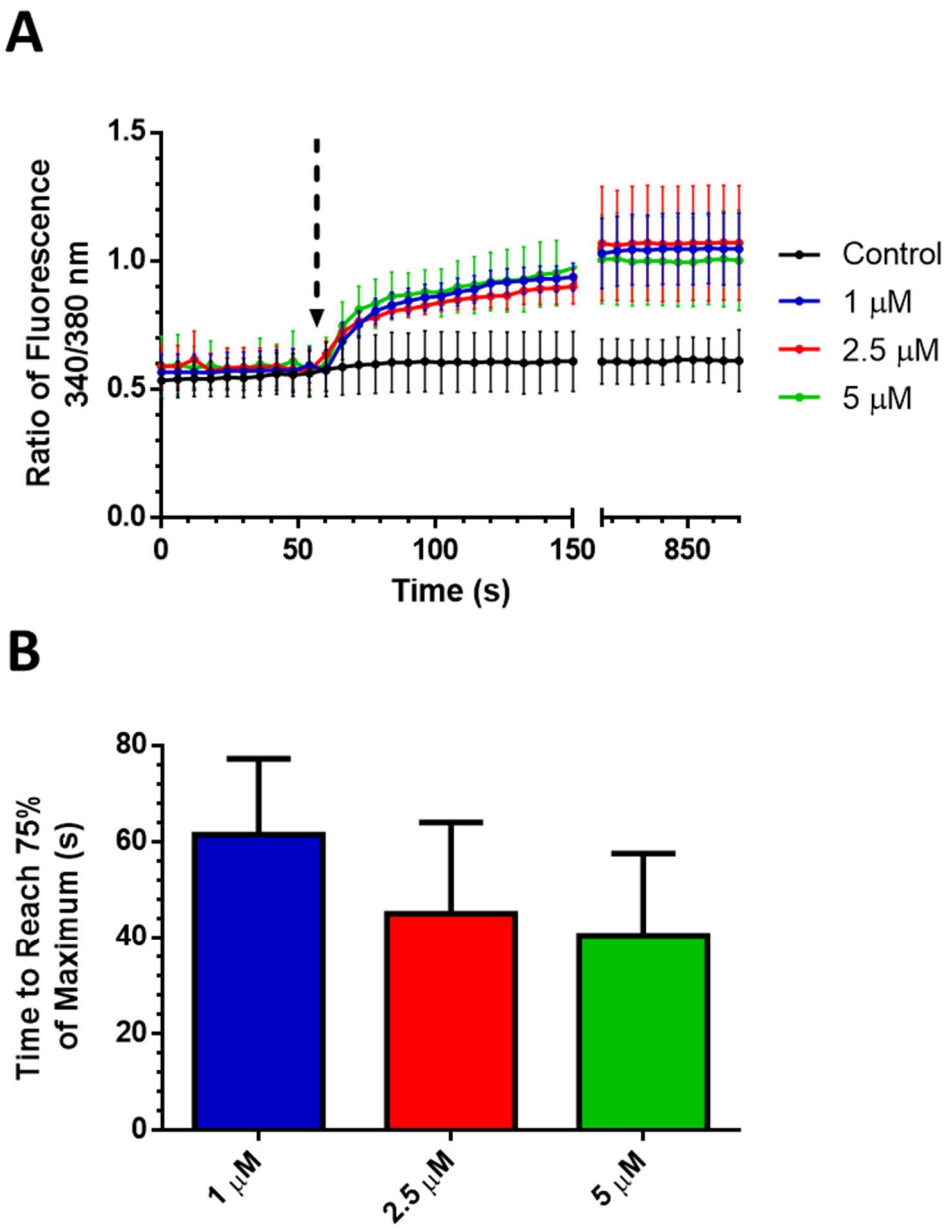

Figure 3.1$[Ca^{2+}]_i$ reaches high levels within 1 minute of ionomycin exposure

CGN cultures were loaded with Fura2-AM and excited at both 340 (to illuminate Ca2+ bound Fura) and 380 nm (to illuminate unbound Fura). A baseline was acquired before the addition of 1, 2.5 or 5 µM ionomycin (arrow, A). Cultures were imaged for a further 2 minutes, imaging was paused for 10 minutes and resumed for a further 5 minutes. A) Average traces of ratio of illumination from both 340 and 380 nm excitation ± SEM against time is displayed. B) The average time taken for the ratio to increase by 75% of total increase ± SEM. Control n = 3, all other conditions n = 4.

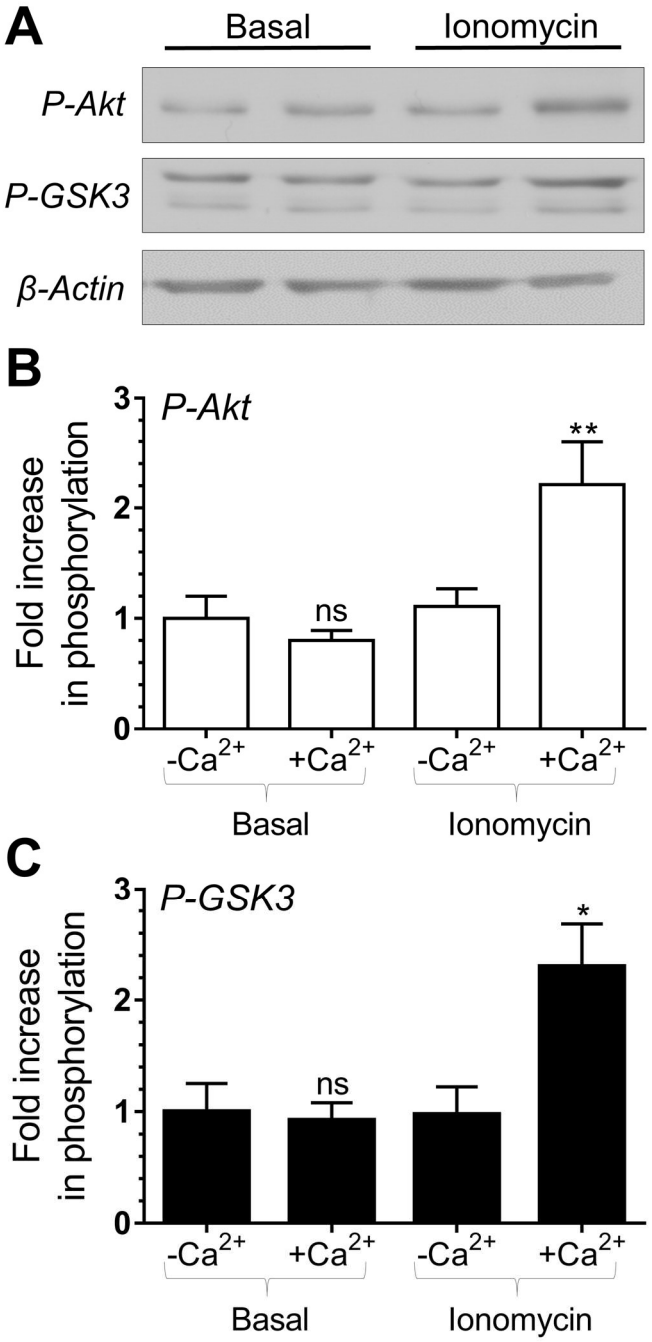

Figure 3.2 $[Ca^{2+}]_i$ increases are essential for Akt/GSK3 phosphorylation.

CGN cultures were either rested (Basal) or stimulated with 5 μM ionomycin for 1 minute in imaging buffer containing either 1.3 mM ($+Ca^{2+}$) or low ($-Ca^{2+}$) calcium. A) Representative blots are displayed showing either Akt Ser473 phosphorylation (*P-Akt*), GSK3 α/β Ser21/9 phosphorylation (*P-GSK3*) or β-Actin levels (*β-Actin*). B,C) The fold increase in phosphorylation of either Akt Ser473 (B, open bars) or GSK3 α/β Ser21/9 (C, closed bars) is displayed after corrected for protein levels using β-Actin and normalisation to the low calcium control. All error bars represent ± SEM; n=5 for P-Akt and n=4 for P-GSK3 (Student's t test. *$p<0.05$, $-Ca^{2+}$ to $+Ca^{2+}$ per condition)

To confirm that flunarizine was effectively blocking calcium entry during intense stimulation in CGNs, a fluorescent calcium indicator was employed. To avoid any injury to cells from UV illumination (such as is required with Fura-2) the reporter Fluo3-AM was used, which requires excitation by light in the visible spectrum. CGN cultures were loaded with Fluo-3 for 30 minutes. After this the cultures were washed to remove any un-internalised Fluo-3 and then subjected to a stimulation train of 800 AP at 80 Hz whilst taking timelapse images. After 5 minutes of recovery, cultures cells were incubated with or without flunarizine for 10 minutes and stimulated again (Figure 3.3 A). Flunarizine was successful in blocking calcium entry during intense stimulation (Figure 3.3 B and C).

After confirming that flunarizine was effective in ablating $[Ca^{2+}]_i$ increase via VGCC during HFS, I next sort to determine if $[Ca^{2+}]_i$ increase leading to Akt and GSK3 phosphorylation upon intense stimulation was dependent on entry through VGCCs. CGN cultures were incubated for 10 minutes with or without flunarizine and then stimulated with a train of 800 action potentials (80 Hz), a stimulus protocol that ensures maximal Akt and GSK3 phosphorylation (Smillie & Cousin 2012). As expected, a large activity-dependent phosphorylation of both Akt and GSK3 was observed in the absence of flunarizine. In contrast, incubation with flunarizine (10 μM) resulted in a complete block of activity-dependent Akt and GSK3 phosphorylation (Figure 3.4 A-C).

To ensure that this inhibition was due to blockade of calcium channels, these experiments were repeated with ionomycin exposure, causing increased $[Ca^{2+}]_i$ independently of calcium channel activation. Flunarizine had no effect on

ionomycin-evoked Akt/GSK3 phosphorylation (Figure 3.4 D-F), illustrating that its inhibition of activity-dependent phosphorylation was not due to off-target effects. Therefore, influx of extracellular calcium via VGCCs is essential for activation of the Akt/GSK3 phosphorylation cascade during intense neuronal activity.

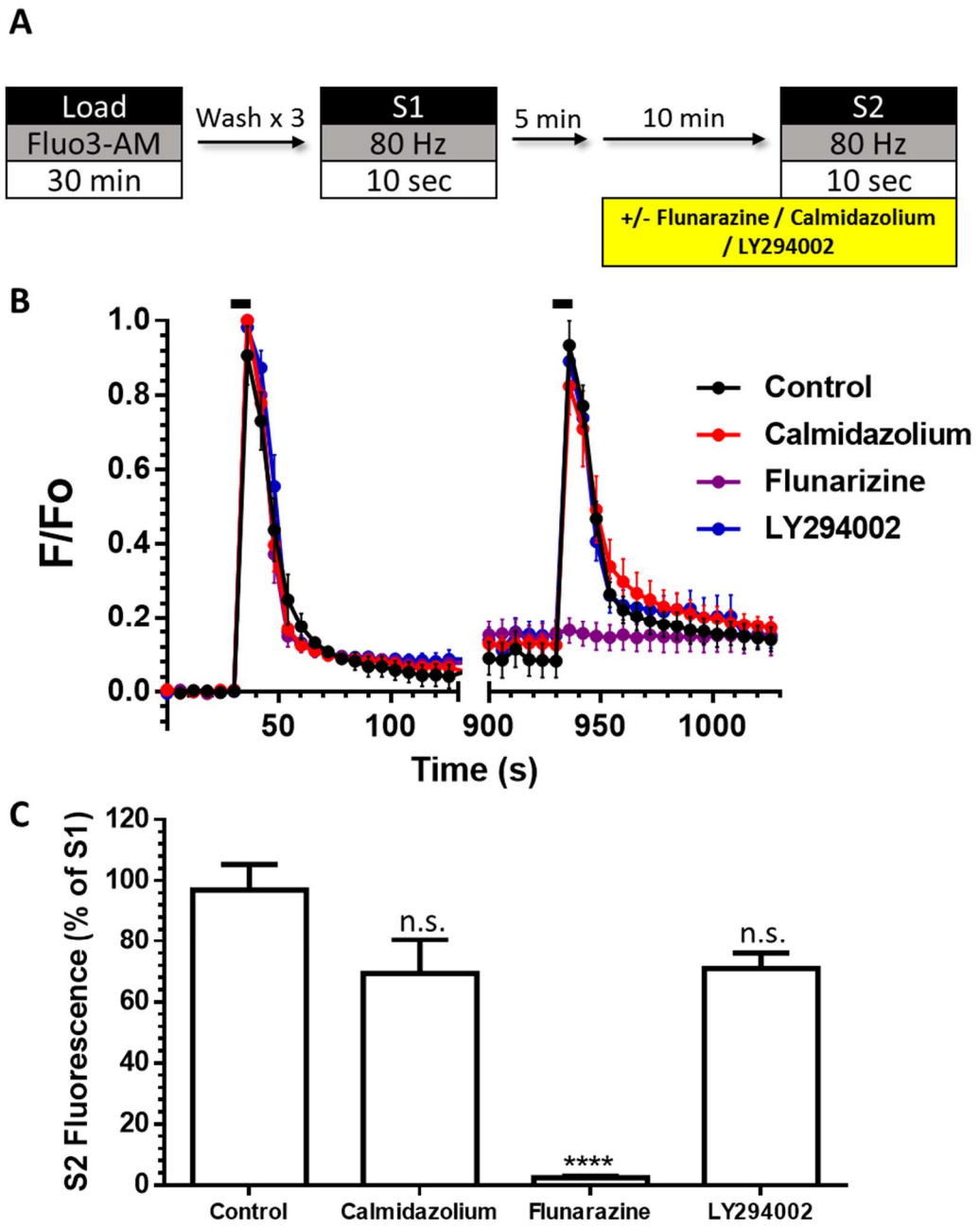

Figure 3.3 Flunarizine Effectively Blocks $[Ca^{2+}]_i$ Increase on Stimulation

A) Protocol of experiment: CGN cultures were loaded with Fluo3-AM before a stimulus train of 800 AP at 80 Hz (S1), cells were left to recover for 5 minutes before being incubated for 10 minutes with imaging buffer (control) supplemented with flunarizine, calmidazolium or LY294002 (10 µM each) and stimulated again (S2). B) Average time traces ± SEM of Fluo-3 fluorescence for all conditions. C) Peak heights were measured, Average value of S2 measured as a percentage of S1 is displayed + SEM. In all cases, fluorescence was normalised to a baseline acquired before S1 and the highest peak fluorescence. n = 4 for all conditions. One-way ANOVA to control, ****=p<.0001

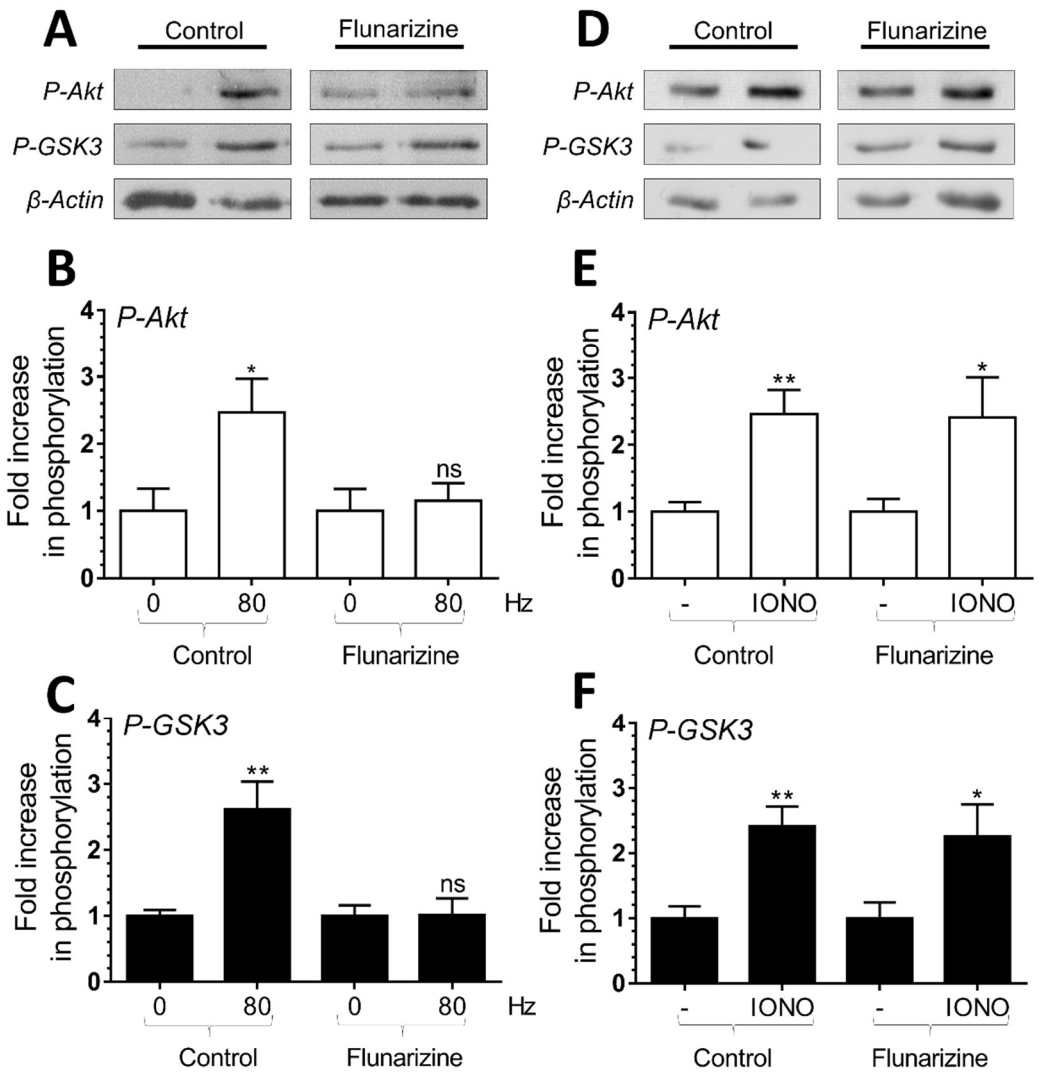

Figure 3.4 Ca^{2+} influx via voltage-gated calcium channels is essential for Akt/GSK3 phosphorylation.

CGNs cultures were incubated in imaging buffer (control) supplemented with 10 μM flunarizine for 10 min. After this point CGNs were left to rest (0 Hz/-) or challenged with either 800 action potentials (80 Hz) or ionomycin (IONO, 2.5 μM for 1 minute). A,D) Representative blots showing either Akt Ser473 phosphorylation (*P-Akt*), GSK3 α/β Ser21/9 phosphorylation (*P-GSK3*) or β-Actin levels (*β-Actin*) after either action potential (A) or ionomycin (D) stimulation. B, E) The average fold increase in phosphorylation of Akt Ser473 (open bars) in response to either action potentials (B) or ionomycin (E) is displayed + SEM. C, F). The average fold increase in phosphorylation of GSK3 α/β Ser21/9 (closed bars) in response to either action potentials (B) or ionomycin (E) + SEM. In all cases phosphorylation levels were corrected for protein levels using β-Actin and normalisation to the basal controls. n=5 for both P-Akt and P-GSK3 with 80 Hz, n=6 for P-Akt IONO and n=7 for P-GSK3 IONO. Student's t test. *=$p<0.05$, **=$p<0.01$ either basal to 80 Hz or basal to ionomycin per condition.

3.2.2 A Localised Intracellular Calcium Concentration Increase is Essential for Akt/GSK3 Phosphorylation

In central nerve terminals VGCCs are clustered at the active zone. During action potential stimulation the opening of these channels generates a localised microdomain of high $[Ca^{2+}]_i$ which is required for neurotransmitter release (Adler et al. 1991). I next sought to determine whether this localised microdomain and not cytoplasmic increase in $[Ca^{2+}]_i$ is required for Akt and GSK3 phosphorylation during intense neuronal activity.

To assess this, CGNs were challenged with a train of 800 action potentials at 80 Hz and then immediately lysed after prior treatment with the calcium chelators BAPTA-AM and EGTA-AM for 30 minutes (both 100 μM, cells were washed of any un-internalised chelator before stimulation). Both chelators have the same affinity for calcium but each has a different on-rate for its binding. This means that BAPTA-AM effectively buffers $[Ca^{2+}]_i$ increases at the active zone, whereas EGTA-AM does not (Adler et al. 1991). Both chelators, however, efficiently buffer activity dependent $[Ca^{2+}]_i$ increases outside of the active zone.

Interestingly, CGNs treated with EGTA-AM displayed a robust activity-dependent phosphorylation of both Akt and GSK3 after stimulation (Figure 3.5 A-C). CGNs treated with the active zone-buffering BAPTA-AM however displayed an abolishment of action potential-evoked increase in both Akt and GSK3 phosphorylation (Figure 3.5 A-C). This confirms a requirement for an increased

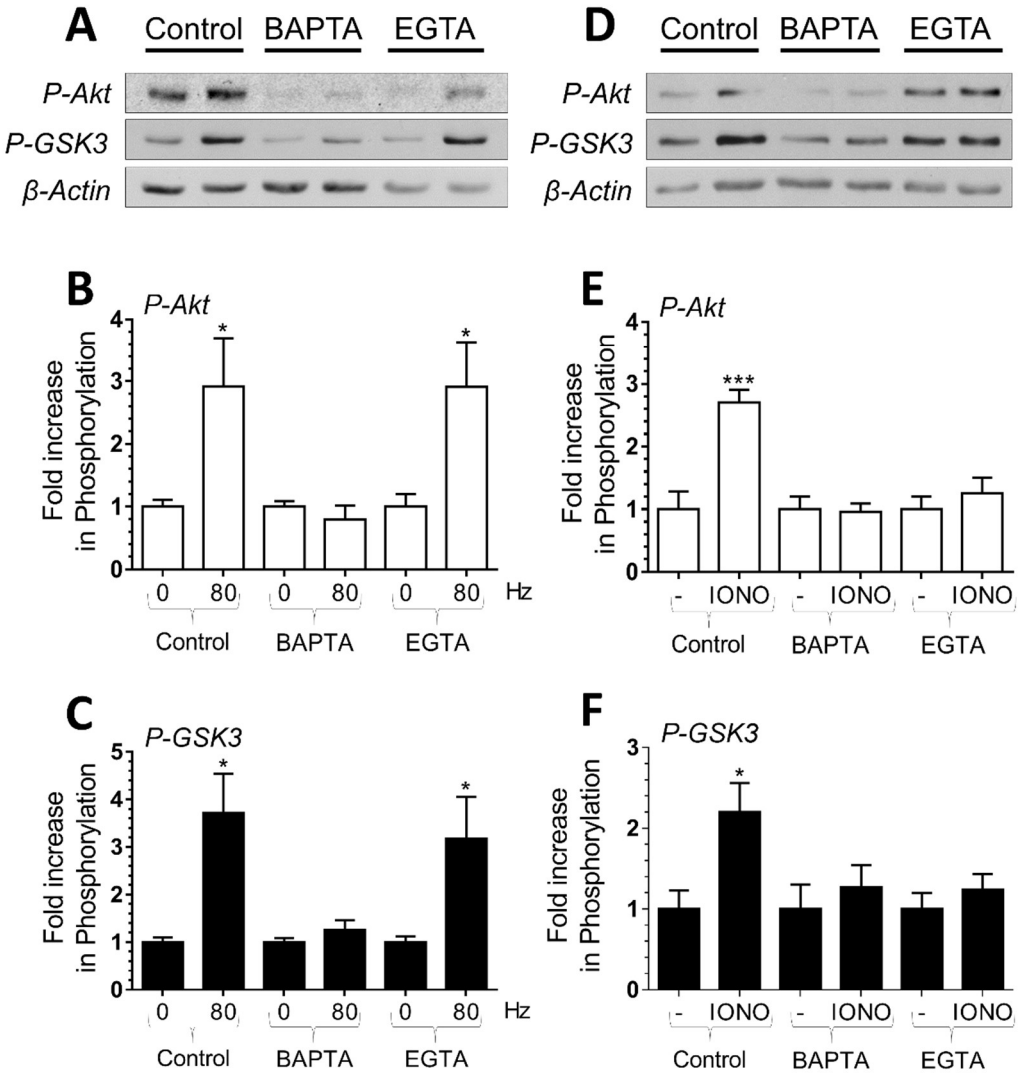

Figure 3.5 Localised Ca^{2+} influx is essential for Akt/GSK3 phosphorylation.

CGN cultures were incubated in imaging buffer (control) supplemented with either 100 μM BAPTA-AM or EGTA-AM for 30 min. After this point CGNs were left to rest (0 Hz/-) or challenged with either 800 action potentials (80 Hz) or ionomycin (IONO, 2.5 μM for 1 minute). A,D) Representative blots showing either Akt Ser473 phosphorylation (*P-Akt*), GSK3 α/β Ser21/9 phosphorylation (*P-GSK3*) or β-Actin levels (*β-Actin*) after either action potential (A) or ionomycin (D) stimulation. B, E). The average fold increase in phosphorylation of Akt Ser473 (open bars) in response to either action potentials (B) or ionomycin (E) + SEM. C, F). The fold increase in phosphorylation of GSK3 α/β Ser21/9 (closed bars) in response to either action potentials (B) or ionomycin (E) + SEM. In all cases phosphorylation levels were corrected for protein levels using β-Actin and normalisation to the basal controls. n=4 for P-Akt 80 Hz, n=5 for P-GSK3 80 Hz, n=7 for P-Akt IONO and n=6 for P-GSK3 IONO. Student's t test. *=p<0.05, **=p<0.01, ***=p<0.001 basal to 80 Hz or basal to ionomycin per condition.

$[Ca^{2+}]_i$ specifically in the active zone for Akt/GSK3 phosphorylation during action potential stimulation.

Importantly, both BAPTA-AM and EGTA-AM arrested phosphorylation of Akt and GSK3 when $[Ca^{2+}]_i$ increase in CGNs was evoked by ionomycin exposure (Figure 3.5 D-F). This was expected, ionomycin increases $[Ca^{2+}]_i$ globally across the nerve terminal with no predilection for the active zone meaning this microdomain is not formed. This also provides proof that EGTA is functioning as a calcium chelator. Thus during intense neuronal activity, a localised increase in $[Ca^{2+}]_i$ at the active zone is essential for triggering both Akt and GSK3 phosphorylation.

3.2.3 PI3K Activity is Required for Activity-Dependent Akt and GSK3 Phosphorylation

To understand how activity-dependent calcium influx is coupled to downstream Akt and GSK3 phosphorylation, the role of PI3K was examined. PI3K activity plays a key role in phosphorylation of Akt and subsequently GSK3 in the presence of the signalling molecule BDNF in CGNs (Smillie & Cousin 2012). However, it is not known whether action potentials activate the same signalling pathway.

To determine the role for PI3K in activity-dependent Akt and GSK3 phosphorylation, the PI3K inhibitor LY294002 (10 μM) was used. CGNs were incubated in basic imaging buffer with or without a supplement of LY294002 for 10 minutes before a stimulation of 800 action potentials at 80 Hz. Inhibition of PI3K resulted in an arrest of activity-dependent Akt phosphorylation. LY294002 also significantly reduced GSK3 phosphorylation (Figure 3.6 A-C). This block in Akt and

GSK3 phosphorylation did not appear to be caused by an inhibition of [Ca2+]i increase, which was measured during an identical stimulation protocol whilst monitored using the reporter Fluo-3 (Figure 3.3 B and C). Thus intense neuronal activity results in activation of PI3K, which triggers activity-dependent Akt and GSK3 phosphorylation.

To ensure the effect on Akt and GSK3 phosphorylation via LY294002 was in fact caused by its inhibition of PI3K and not due to an off-target effect of the drug another PI3K inhibitor, Wortmannin (200 nM), was utilised using an identical protocol as with LY294002. Inhibiting PI3K function with Wortmannin resulted in an identical block in phosphorylation of both Akt and GSK3 during HFS (Figure 3.6 D-F). This means the outcomes observed using both drugs are most likely due to their PI3K inhibition and not due to off-target effects of the drugs

In order to transduce activity-dependent calcium influx into activation of PI3K, a calcium sensor must be present in nerve terminals, most probably at the active zone as this is the location of the essential increase in $[Ca^{2+}]_i$. One potential candidate for this role is the calcium binding protein calmodulin (Chin & Means 2000). Calmodulin can directly activate PI3K on elevation of $[Ca^{2+}]_i$ (Joyal et al. 1997) and is required for calcineurin activation during intense neuronal activity (Wu et al. 2009) resulting in dynamin I dephosphorylation.

To determine whether calmodulin can transduce increased $[Ca^{2+}]_i$ into PI3K activation (and downstream Akt/GSK3 phosphorylation) the calmodulin antagonist calmidazolium was used. An identical protocol was used to that of PI3K inhibition with the substitution of calmidazolium (10 μM). Inhibition of calmodulin however

had no significant effect on the activity-dependent phosphorylation of either Akt or GSK3 after 800 action potentials at 80 Hz (Figure 3.7 A-C) and no significant effect on $[Ca^{2+}]_i$ as reported by Fluo-3 (Figure 3.3). Interestingly when $[Ca^{2+}]_i$ was raised globally with ionomycin (using an identical protocol as previously with flunarizine), calmidazolium abolished both Akt and GSK3 phosphorylation (Figure 3.7 D-F).

Thus the activity-dependent calcium sensor for activation of the PI3K/Akt/GSK3 cascade is not calmodulin, however this cascade can be activated via calmodulin via global $[Ca^{2+}]_i$ increases.

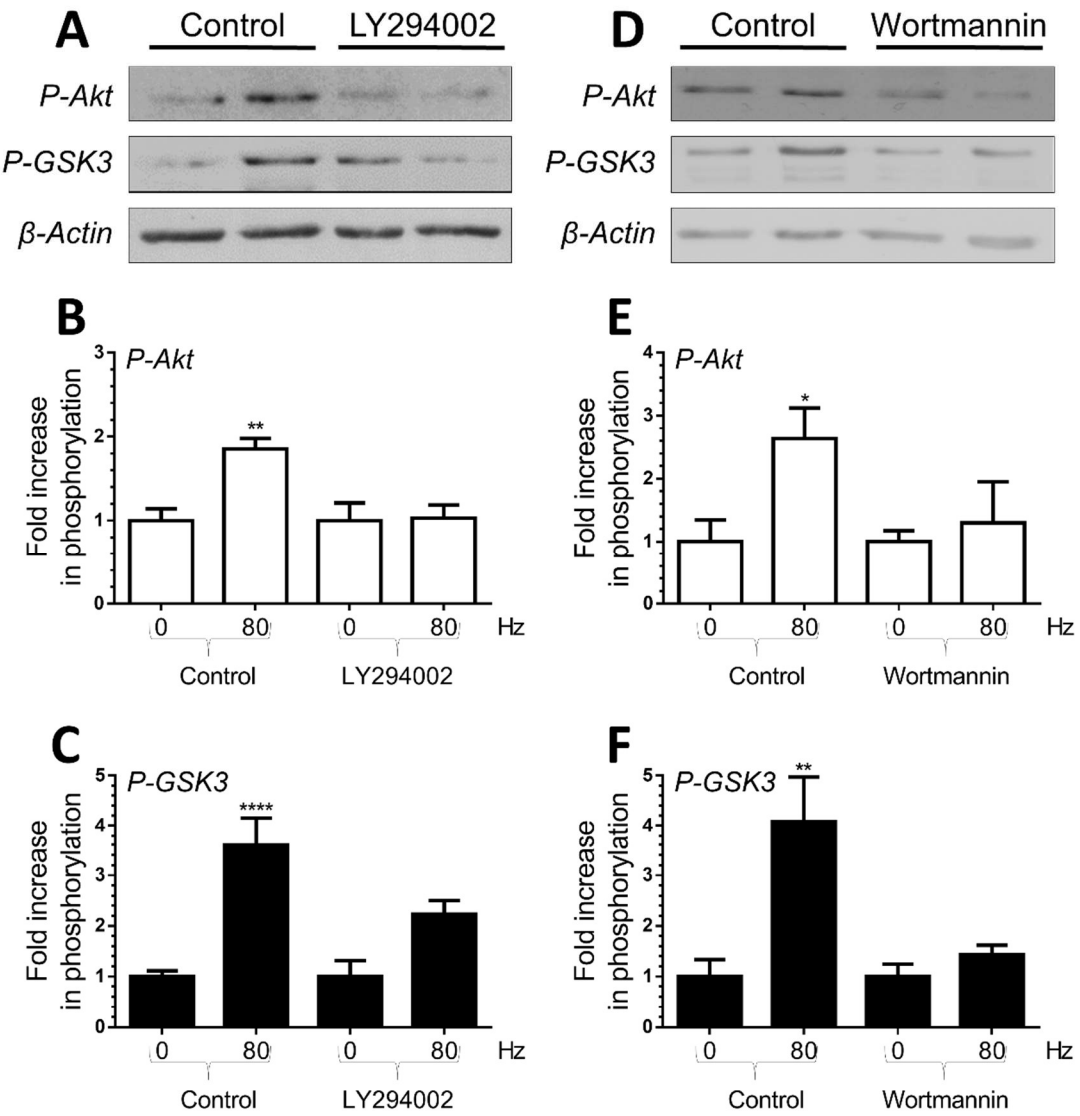

Figure 3.6 PI3K activity is essential for activity-dependent Akt/GSK3 phosphorylation.

CGN cultures were incubated in imaging buffer (control) supplemented with 10 μM LY294002 for 10 min. After this point CGNs were left to rest (0 Hz) or challenged with either 800 action potentials (80 Hz). A) Representative blots are displayed showing either Akt Ser473 phosphorylation (*P-Akt*), GSK3 α/β Ser21/9 phosphorylation (*P-GSK3*) or β-Actin levels (*β-Actin*) after either action potential stimulation. B, C). The average fold increase in phosphorylation of Akt Ser473 (B, open bars) or GSK3 α/β Ser21/9 (C, closed bars) in response to action potential stimulation + SEM. In all cases phosphorylation levels were corrected for protein levels using β-Actin and normalisation to the basal controls. n=6 for P-Akt, n=16 for P-GSK3. Student's t test. *=p<0.05, **p=<0.01, ****p<0.0001 0 to 80 Hz per condition and between 80 Hz data.

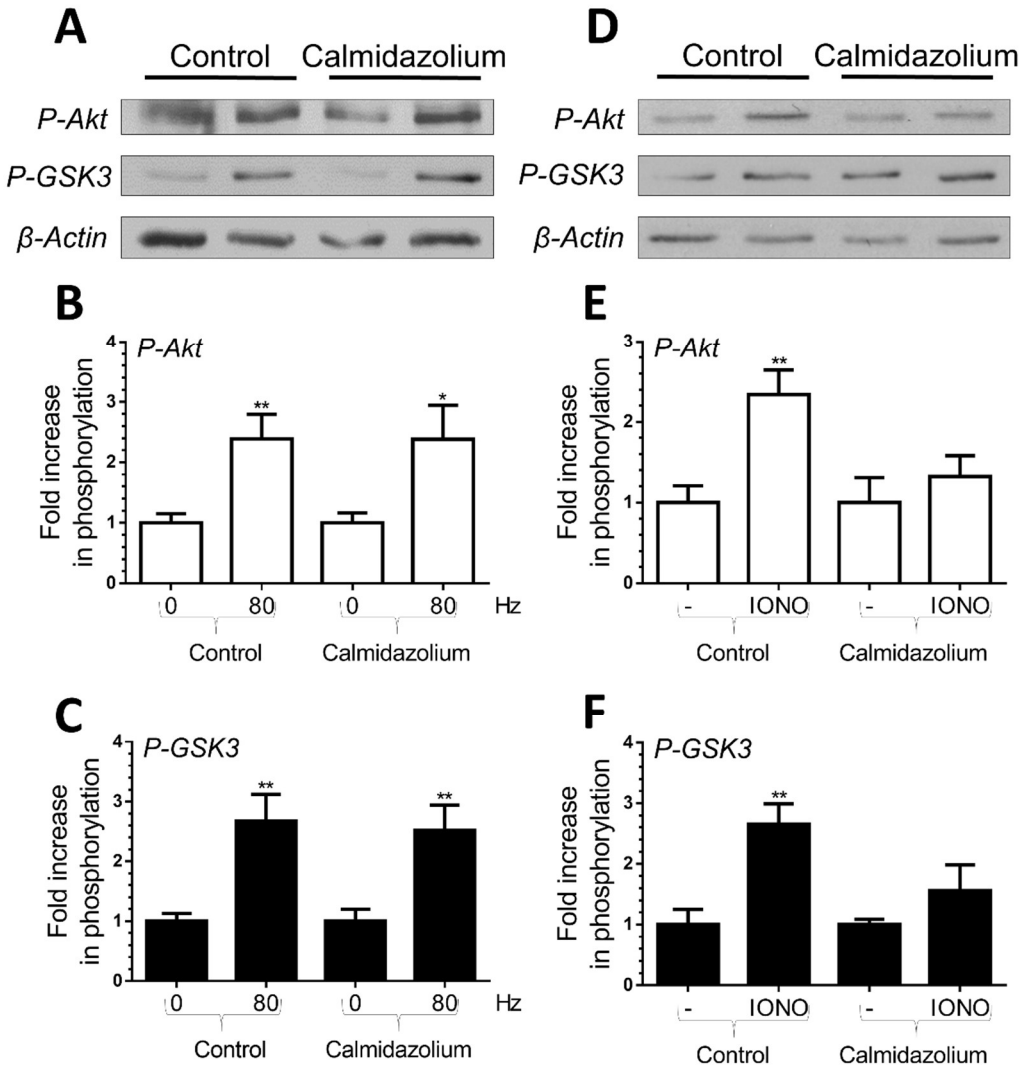

Figure 3.7 Calmodulin is not the calcium sensor for activity-dependent Akt/GSK3 phosphorylation.

CGN cultures were incubated in imaging buffer (control) supplemented with 10 μM calmidazolium for 10 min. After this point CGNs were left to rest (0 Hz/-) or challenged with either 800 action potentials (80 Hz) or ionomycin (IONO, 2.5 μM for 1 minute). A,D) Representative blots showing either Akt Ser473 phosphorylation (*P-Akt*), GSK3 α/β Ser21/9 phosphorylation (*P-GSK3*) or β-Actin levels (*β-Actin*) after either action potential (A) or ionomycin (D) stimulation. B, E). The average fold increase in phosphorylation of Akt Ser473 (open bars) in response to either action potentials (B) or ionomycin (E) + SEM. C, F). The average fold increase in phosphorylation of GSK3 α/β Ser21/9 (closed bars) in response to either action potentials (B) or ionomycin (E) + SEM. In all cases phosphorylation levels were corrected for protein levels using β-Actin and normalisation to the basal controls. n=6 for P-Akt 80 Hz, n=9 for P-GSK3 80 Hz, n=8 for P-Akt IONO and n=9 for P-GSK3 IONO. Student's t test. *=$p<0.05$, **=$p<0.01$ basal to 80 Hz or basal to ionomycin per condition.

3.3 Discussion

The maintenance of neurotransmission during intense neuronal activity is reliant on the integration of activity-dependent calcium influx, multiple signalling cascades and several SV endocytosis modes (Kononenko & Haucke 2015; Clayton & Cousin 2009). One such cascade is the activity-dependent inhibition of GSK3 via Akt, which is essential for the efficient dephosphorylation of dynamin I, a key event in the triggering of ADBE (Smillie & Cousin 2012; Smillie et al. 2013). It is shown here that localised calcium influx via VGCCs is essential for this event to occur.

Furthermore, a key role for PI3K, but not calmodulin, has been demonstrated in the transduction of activity-dependent calcium influx into activation of Akt.

PI3K is implicated in the regulation of secretion and membrane trafficking in a variety of systems (Balla 2013; Chasserot-Golaz et al. 2010; Osborne et al. 2006; Mazza & Maffucci 2011). One member of this family, PI3K-Class 2 α (PI3K-C2α), regulates exocytosis either indirectly via modulation of signalling pathways (Leibiger et al. 2010) or directly via control of the molecular fusion machinery (Meunier et al. 2005; Dominguez et al. 2011). The enzymatic activity of PI3K-C2α is stimulated by calcium (Wen et al. 2008), suggesting that PI3K-C2α is a good candidate for participation in transduction of activity-dependent calcium influx to the Akt signalling cascade. However, PI3K-C2α is insensitive to LY294002 and wortmannin at the concentrations used in this study (Domin et al. 1997), making it unlikely that PI3K-C2α is involved in the activity-dependent activation of Akt.

LY294002 and wortmannin sensitive Class I PI3Ks have been implicated at several stages of SV recycling in central nerve terminals, including replenishment of the RRP from the reserve pool (Cousin et al. 2003), generation of bulk endosomes (Holt et al. 2003) and SV generation from bulk endosomes (Richards et al. 2004). PI3K is also required for the negative regulation of ADBE via BDNF (Smillie et al. 2013). Therefore, it would be of interest to determine the specific activity-dependent role of PI3K in both dynamin I dephosphorylation and ADBE.

3.3.1 Activity-dependent Akt phosphorylation at nerve terminals

The inhibition of GSK3 and activation of Akt respectively was assessed by monitoring their phosphorylation status. Inhibition of GSK3 occurs via phosphorylation of either Ser9 of GSK3β or Ser21 of GSK3β (Frame & Cohen 2001). In this study it was found that GSK3α and GSK3β behaved in an identical manner across all stimulation conditions and pharmacological manipulations. The activation of Akt was assessed by determining the phosphorylation status of Ser473. Phosphorylation of both Ser473 and Thr308 are required for maximal Akt activity (Alessi et al. 1997; Sarbassov et al. 2005) and it has previously been shown that the phosphorylation status of both sites respond in a similar manner to action potential stimulation in CGNs (Smillie & Cousin 2012).

Interestingly, these sites are proposed to be phosphorylated by different protein kinases. Thr308 is a PDK1 substrate, which is activated by PI3K (Alessi et al. 1997; Brazil & Hemmings 2001), whereas Ser473 can be phosphorylated by either the mTORC2 complex (Sarbassov et al. 2005) or DNA-PK (Bozulic & Hemmings

2009). However, here it is shown that the PI3K antagonist LY294002 inhibits the activity-dependent phosphorylation of Ser473.

There are several explanations as to how these findings can be reconciled; one explanation is that LY294002 inhibits a distinct protein kinase that phosphorylates Ser473. In agreement, LY294002 inhibits mTORC2 in cellular systems within the same concentration range for PI3K antagonism (Brunn et al. 1996). This is unlikely however, since mTORC2 it is currently only known to be activated via either ribosomes (which are absent in nerve terminals) or growth factors (Oh & Jacinto 2011). Similarly DNA-PK is activated during DNA damage (Bozulic & Hemmings 2009) making it unlikely that it is the Akt kinase in central nerve terminals. This suggests that the LY294002- dependent inhibition of Akt phosphorylation is mediated via PI3K and studies that attempt to model this process should take this into account.

Akt and GSK3 have a wide cellular distribution, suggesting that the increased phosphorylation observed during action potential stimulation may not be occurring at nerve terminals. However, the modulation of both Akt and GSK3 activity-dependent phosphorylation directly impact on the phosphorylation status of dynamin I and ADBE (Smillie & Cousin 2012; Smillie et al. 2013) and both dynamin I expression and ADBE are restricted to nerve terminals (Clayton & Cousin 2009; Ferguson & De Camilli 2012). With this in mind, the activity-dependent changes in Akt and GSK3 phosphorylation can be reasonably attributed to be presynaptic signalling. This statement is almost certainly not true for ionomycin-evoked changes, since this ionophore will raise $[Ca^{2+}]_i$ uniformly throughout the neuron. Ionomycin is used

throughout this study as a positive control to confirm the specificity of both flunarizine and EGTA-AM in inhibiting calcium channels and global $[Ca^{2+}]_i$ increases respectively. The inhibition of ionomycin-evoked Akt and GSK3 phosphorylation by calmidazolium is intriguing however, this may reflect an altered activity of these enzymes by postsynaptic calcium as Akt and GSK3 are known to have postsynaptic functions (Li et al. 2010; Peineau et al. 2007).

Many studies have investigated the relationship between both neuronal activity and calcium influx in the activation of Akt. Previous work in CGNs showed that chronic hyperkalemic stimulation resulted in increased Akt phosphorylation, however this was insensitive to PI3K antagonists (Lafon-Cazal et al. 2002). This most likely reflects postsynaptic activation of Akt, since permanent depolarisation will reverse electrogenic glutamate transporters on the PM (Nicholls 1993) raising extracellular glutamate concentrations and thus activating postsynaptic glutamate receptors. In agreement, shorter periods of stimulation with elevated KCl resulted in increased Akt phosphorylation which was reversed by PI3K antagonists (Vaillant et al. 1999).

3.3.2 Transduction of calcium influx into Akt phosphorylation

I have shown that intense neuronal activity causes Akt phosphorylation via localised calcium microdomains. This suggests that a sensor must be located within the vicinity of this microdomain to couple calcium influx to PI3K/Akt activation. It is shown here that calmodulin is unlikely to be the sensor since the antagonist calmidazolium was unable to inhibit action potential-evoked Akt phosphorylation. Furthermore the ability of calmidazolium to arrest ionomycin-evoked Akt

phosphorylation is in agreement with the proposed location of calmodulin in the wider cytosol (Chin & Means 2000).

How could activity-dependent calcium influx be coupled to Akt phosphorylation? One potential candidate for the activity-dependent calcium sensor is the family of Ras-GRFs (Fernández-Medarde & Santos 2011). Ras-GRF activates the small G-protein Ras in a calcium-dependent manner (Farnsworth et al. 1995) and overexpression of dominant negative Ras inhibits Akt phosphorylation evoked by KCl depolarization in peripheral neurons (Vaillant et al. 1999).

Importantly Ras-GRF2 knockout mice display altered paired pulse facilitation, suggesting it is localised in the correct location to be activated by presynaptic calcium influx (Li et al. 2006). However the mechanism via which Ras-GRF is activated by calcium influx is thought to be via calcium-bound calmodulin binding to its IQ domain (Farnsworth et al. 1995; Bähler & Rhoads 2002). Since calmodulin inhibition had no effect on activity-dependent Akt phosphorylation, it may be that Ras-GRF is not the sensor for this event.

A second possibility is that there is no calcium a sensor involved in this process. In this model the requirement for localised calcium increases is an indirect result of the presynaptic release of growth factors such as BDNF. This event only occurs in neurons during intense neuronal activity, very similar to that observed in this study (Matsuda et al. 2009). This is potentially important for Akt phosphorylation, since PI3K can activate either PDK1 or the mTORC2 complex via growth factor receptors (Oh & Jacinto 2011). In support, addition of exogenous BDNF initiates the phosphorylation of Ser473 in CGNs via a potential PI3K-dependent route (Smillie et

al. 2013). Consequently, manipulations resulting in either calcium entry inhibition or the buffering of the calcium microdomain should also arrest BDNF release during intense activity, stopping it feeding back to increase Akt phosphorylation via PI3K. This hypothesis is testable using agents that sequester extracellular BDNF (Chen et al. 2012).

In summary, these results show that during intense neuronal activity phosphorylation of Akt (and subsequent inhibition of GSK3) is dependent on localised calcium microdomains formed by VGCCs. The identity of the sensor or release mechanism which transduces increased $[Ca^{2+}]_i$ remains unidentified. This is an important question to address, since my hypothesis predicts that modulation of these events should impact on the extent of ADBE in central nerve terminals.

PI4KIIα Controls CME and ADBE via Independent Mechanisms

4. PI4KIIα Controls CME and ADBE via Independent Mechanisms

4.1 Introduction

Phosphatidylinositol 4-kinases (PI4Ks) are a family of kinases responsible for phosphorylating the four hydroxyl group (D4) on phosphoinositol (PI) creating PI4P (Balla & Balla 2006) (see Figure 1.5). There are four mammalian PI4Ks: Phosphatidylinositol 4-kinase Type IIα (PI4KIIα), IIβ (PI4K IIβ), Type IIIα (PI4K IIIα) and Type IIIβ (PI4K IIIβ). The expression pattern of each of these isoforms differs both on an anatomical and intracellular level (reviewed in Clayton et al. 2013).

PI4KIIα expression is varied throughout the CNS with particularly high abundance in Purkinje cells and Bergman Glia of the cerebellar molecular layer (Simons et al. 2009) as well as a distinct expression pattern within the hippocampus (Larimore et al. 2011). However, despite this anatomical expression pattern, PI4KIIα has a distinct intracellular enrichment across the CNS on dendrites, Golgi bodies and SVs (reviewed in Clayton et al. 2013) and is the only PI4K located on SVs (Guo et al. 2003).

As the only producer of PI4P on SVs, PI4KIIα is of particular interest due to the role of PI4P in the recruitment of clathrin adaptor proteins AP-1 (Wang et al. 2003) and AP-3 (Craige et al. 2008) during Golgi-endosomal trafficking. As both of these adaptors are known to have roles in the formation of SVs from bulk endosomes (Cheung & Cousin 2012) it is possible that PI4KIIα could play a role in adaptor protein recruitment to facilitate SV budding on bulk endosomes. In support of this

theory, PI2KIIα is especially enriched on vesicles formed via AP-3 (Salazar et al. 2005).

PI4P is an essential precursor for the production of both $PI(4,5)P_2$ and $PI(3,4,5)P_3$ (Minogue & Waugh 2012). $PI(4,5)P_2$ is known to have an integral role in CME as an AP-2 recruiter (Gaidarov & Keen 1999) which could also hint at a supporting role for PI4KIIα in the normal function of CME.

The abundance of PI4KIIα is modulated by the kinase GSK3 (Robinson et al. 2014). GSK3 recognises PI4KIIα via previous priming phosphorylation on Ser9 and Ser51 (Robinson et al. 2014). As is typical with this kinase, GSK3 then phosphorylates PI4KIIα on serine sites separated from the priming sites by 4 residues (Ser5 and Ser47). When all four residues have been phosphorylated, it is thought that the structure of PI4KIIα opens, allowing access to residues 60 and 61 (J. Robinson et al. 2010), two leucines which together form a di-leucine AP-3 sorting motif (Craige et al. 2008). GSK3 enzyme activity is inhibited during periods of high activity in synapses (Frame & Cohen 2001).

AP-3- PI4KIIα binding is essential for both PI4KIIα and AP-3 localisation. Binding of AP-3 to PI4KIIα is necessary for the localisation of both proteins to the membrane of the early endosome with a PI4KIIα knockdown resulting in an increase in cytosolic AP-3 (Craige et al. 2008). The interaction of PI4KIIα and AP-3 has also been shown to facilitate the transport of PI4KIIα to the lysosome for degradation (Robinson et al. 2014). The kinase activity of PI4KIIα as well as its di-leucine motif has been shown to be important for efficient AP-3- PI4KIIα binding and localisation (Craige et al. 2008).

Phosphorylation of PI4KIIα by GSK3 is essential in its regulatory role in trafficking in hippocampal neurons. AMPA receptor subunit GluA1 surface expression was shown to be increased with the knockdown of PI4KIIα in a manner that cannot be rescued by non-phosphorylatable PI4KIIα (Robinson et al. 2014). This demonstrates a necessity for GSK3 phosphorylation of PI4KIIα in AMPA recycling in neurons.

Due to evidence of GSK3 contributing to abundance and function for PI4KIIα in neuronal recycling and the specific action of PI4KIIα on SVs I resolved to investigate the effects of manipulation of PI4KIIα abundance, binding and activity on SV protein recycling in the presynapse.

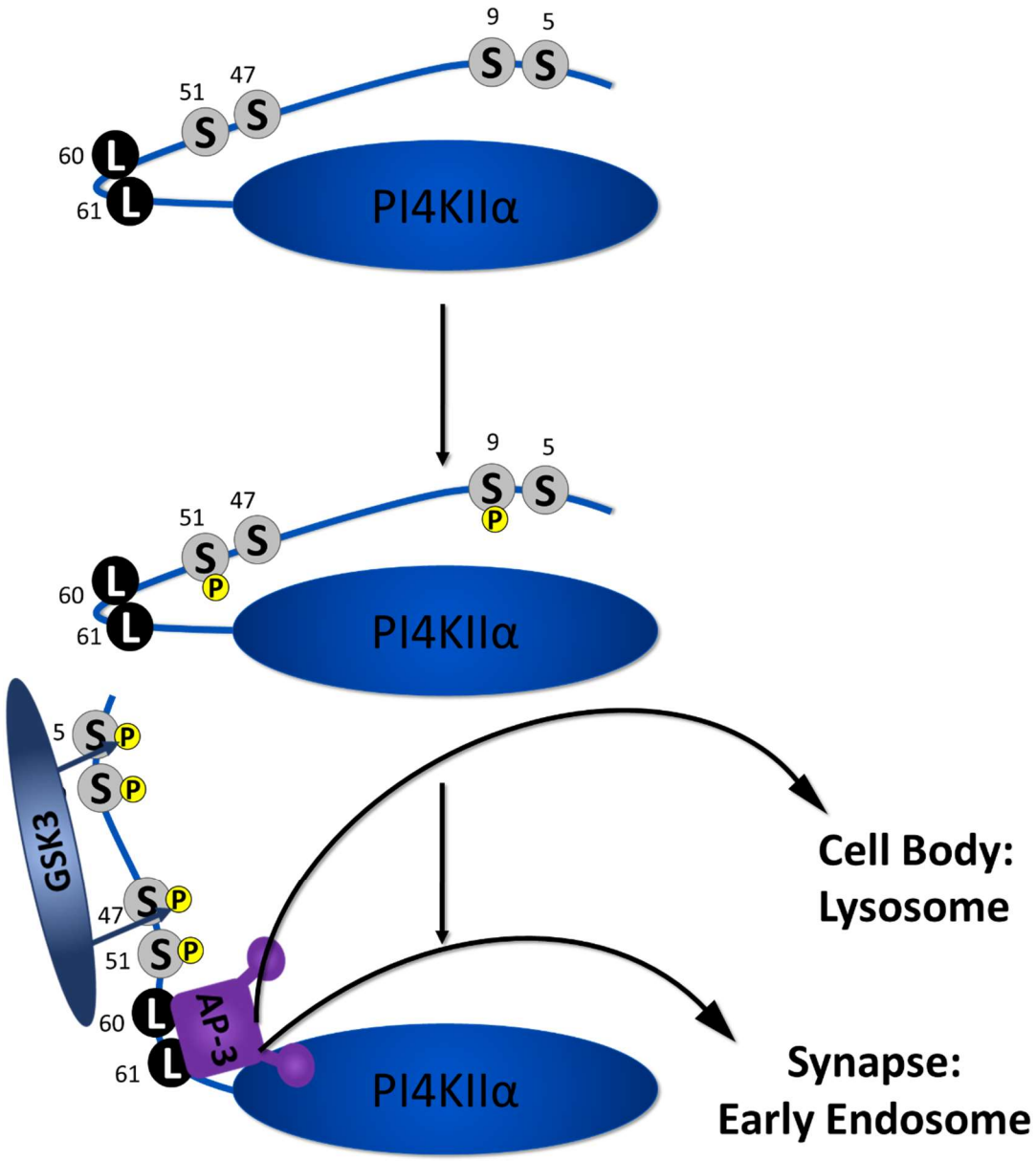

Figure 4.1 Phosphorylation and Conformational Change of PI4KIIα

Membrane-bound PI4KIIα (top) is phosphorylated on residues 9 and 51 (middle). This phosphorylation allows recognition of the protein by GSK3. GSK3 then phosphorylates PI4KIIα on residues 4 and 47 (bottom). This phosphorylation causes the N-terminal of PI4KIIα to open. This structural change allows access to a di-leucine sorting motif by adaptor protein 3 (AP-3). This binding facilitates the relocation of the complex either to the early endosome or out of the synapse to be degraded in the early endosome

4.2 Results

4.2.1 Silencing PI4KIIα Expression Affects Both CME and ADBE

4.2.1.1 CME is Accelerated During HFS in the Absence of PI4KIIα

PI4KIIα is the dominant source of PI4K activity on SVs, suggesting that it may perform a role in SV recycling. Furthermore, the N-terminus of PI4KIIα is phosphorylated on two sites by GSK3 (Robinson et al. 2014), a kinase shown to be inactivated during HFS (Smillie & Cousin 2012), and essential for ADBE (Clayton et al. 2010). Upon phosphorylation, the N-terminal of PI4KIIα alters conformation revealing a di-leucine motif (Robinson et al. 2014). This di-leucine motif is recognised by the adaptor protein AP-3 (Craige et al. 2008), which binds to PI4KIIα. This recognition is essential for the localisation of AP-3 on the early endosome (Craige et al. 2008) as well as facilitating the localisation of PI4KIIα to the lysosome for degradation (Robinson et al. 2014). Given that GSK3 is an activity-dependent kinase, and PI4KIIα degradation is mediated by said activity, firstly PI4KIIα expression was silenced using PI4KIIα shRNA. This protocol may create an exaggerated environment of PI4KIIα clearance such as may be caused by its phosphorylation by GSK3 phosphorylation during periods of low activity. The effects on syp-pH exo- and endocytosis investigated with altered PI4KIIα abundance.

First, the PI4KIIα knockdown system was validated; CGNs were co-transfected with PI4KIIα shRNA (Robinson et al. 2014) or its scrambled control and an empty mCer vector. These cells were then fixed and immunostained with a PI4KIIα antibody. Transfected CGN nerve terminals were located and the relative abundance of

PI4KIIα staining was calculated in comparison to neighbouring, non-transfected nerve terminals.

CGN nerve terminals expressing scrambled shRNA were found to have comparable PI4KIIα levels to those non-transfected cells in the same field of view (Figure 4.2 A and B). In contrast, CGN nerve terminals expressing PI4KIIα shRNA were found to have significantly less PI4KIIα abundance, on average only 25% PI4KIIα when compared to non-transfected cells (Figure 4.2 B and C). Thus the PI4KIIα shRNA vector induced a large depletion of the enzyme in CGNs.

After validating the PI4KIIα shRNA, the effects of reducing PI4KIIα levels on SV recycling were investigated utilising expression of a pHluorin-tagged synaptophysin: synaptophysin-pH (syp-pH).

The expression of pHluorins in cultured neurons allows an observer to quantify the proportion of tagged SV cargo which is deposited in the PM during stimulation in relation to the total expression of that cargo within a synapse. This is accomplished by measuring the fluorescence increase upon stimulation: as SVs release their neurotransmitter content into the synaptic cleft, thereby exposing their lumen to a neutral pH, the fluorescence of a pHluorin molecule which resides on the lumenal domain of a SV protein is unquenched and becomes fluorescent. The fluorescence increase on stimulation is then compared to the fluorescence increase evoked during an ammonia imaging buffer pulse. In solution NH_4Cl is in equilibrium between NH^{4+} and NH_3. NH_3 is free to diffuse across membranes within the synapse. Its entry into an acidic compartment such as a SV causes NH_3 to become protonated and neutralise of the acidic pH. This provides an estimate for the total pool of SVs by revealing the

maximal fluorescence of all resident pHluorin molecules. Acidification of SVs occurs rapidly after endocytosis (Sankaranarayanan & Ryan 2000; Atluri & Ryan 2006), therefore by monitoring the rate of decrease of fluorescence after stimulation the rate of endocytosis/ acidification can also be measured.

CGNs co-transfected with syp-pH and either PI4KIIα shRNA or its scrambled control were challenged with a two stimulus train protocol. A mild stimulation of 20 Hz, 10 sec was delivered to the cells, followed by a recovery of four minutes. Cultures were then exposed to a second, more intense stimulation of 40 Hz, 10 sec (HFS) and again allowed to recover (Figure 4.3 A). After this recovery the culture was perfused with ammonia buffer. Alterations in syp-pH fluorescence at CGN nerve terminals was monitored throughout this experimental protocol to reveal SV turnover during both low and HFS and related to the total SV pool (by normalisation of evoked peak height to the fluorescence after ammonium pulse).

There was no significant difference to the syp-pH fluorescence trace caused by silencing PI4KIIα expression during low frequency stimulation (Figure 4.3 B). When examined, PI4KIIα shRNA had no effect on either rate of endocytosis (Figure 4.3 D) or evoked fluorescence increase (indicative of the extent of SV exocytosis, Figure 4.3 F).

However, the syp-pH response observed after HFS showed a significant difference between control and PI4KIIα knockdown (Figure 4.3 C). The silencing of PI4KIIα expression causes a significant acceleration of syp-pH retrieval after stimulation (Figure 4.3 E). The reduction of PI4KIIα levels did not affect the evoked peak height on stimulation with HFS (Figure 4.3 G). These results indicate that PI4KIIα only has

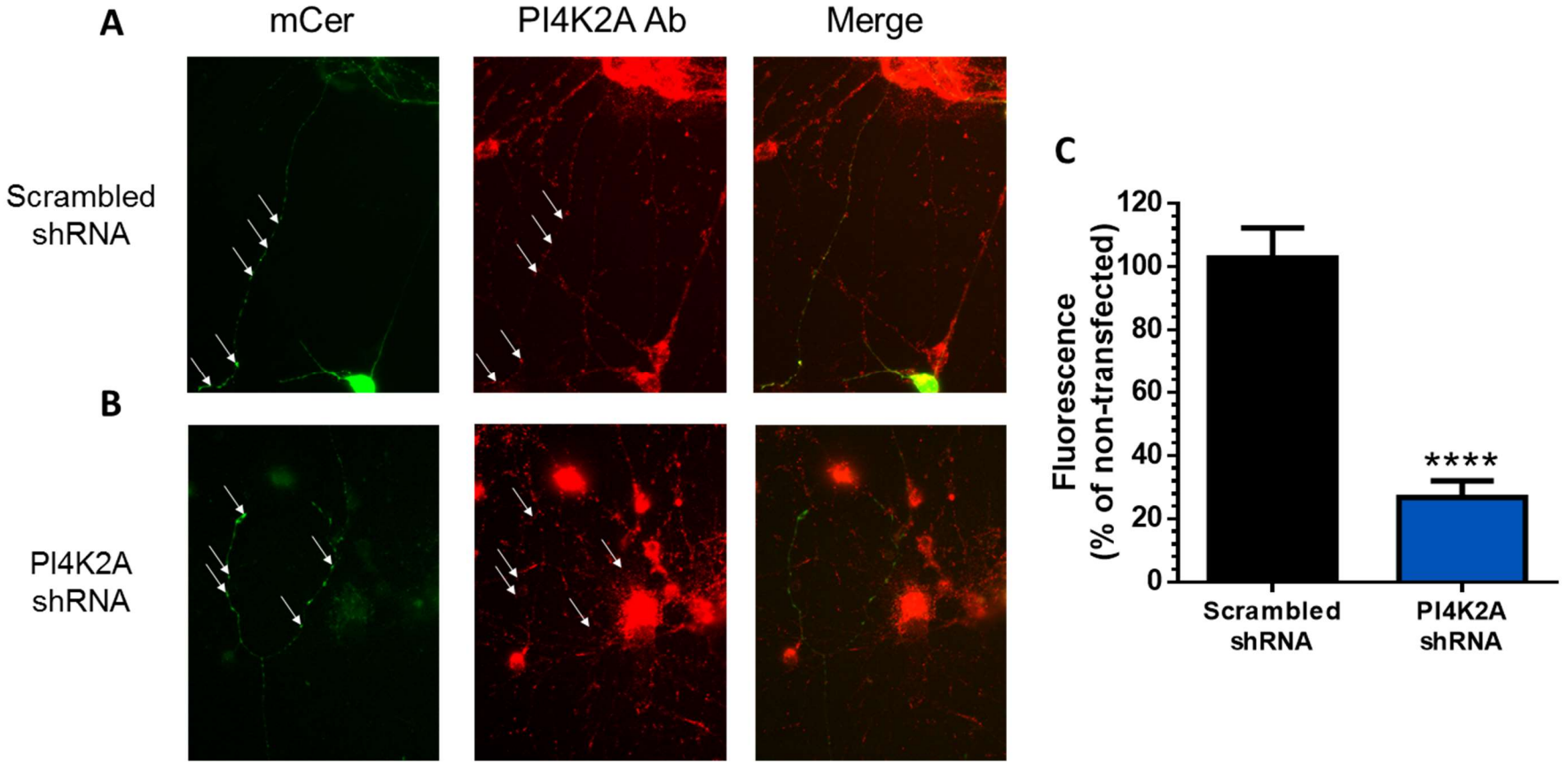

Figure 4.2 PI4KIIα shRNA Effectively Reduces PI4KIIα Expression in CGNs

Images of CGNs transfected with A) Scrambled shRNA or B) PI4KIIα shRNA. CGN culture was labelled with PI4KIIα Ab (middle) and transfected cells were located by mCer fluorescence (left), when overlaid one can see that the synapses of the transfected cell (white arrows) do not exhibit as much PI4KIIα labelling in the presence of PI4KIIα shRNA. Average fluorescence of Scrambled shRNA or PI4KIIα shRNA CGN synapses as a percentage of fluorescence nearby non-transfected synapses of similar size + SEM. Scrambled shRNA n=15, PI4KIIα shRNA n=21. ****= $p<0.0001$. Student's t-test.

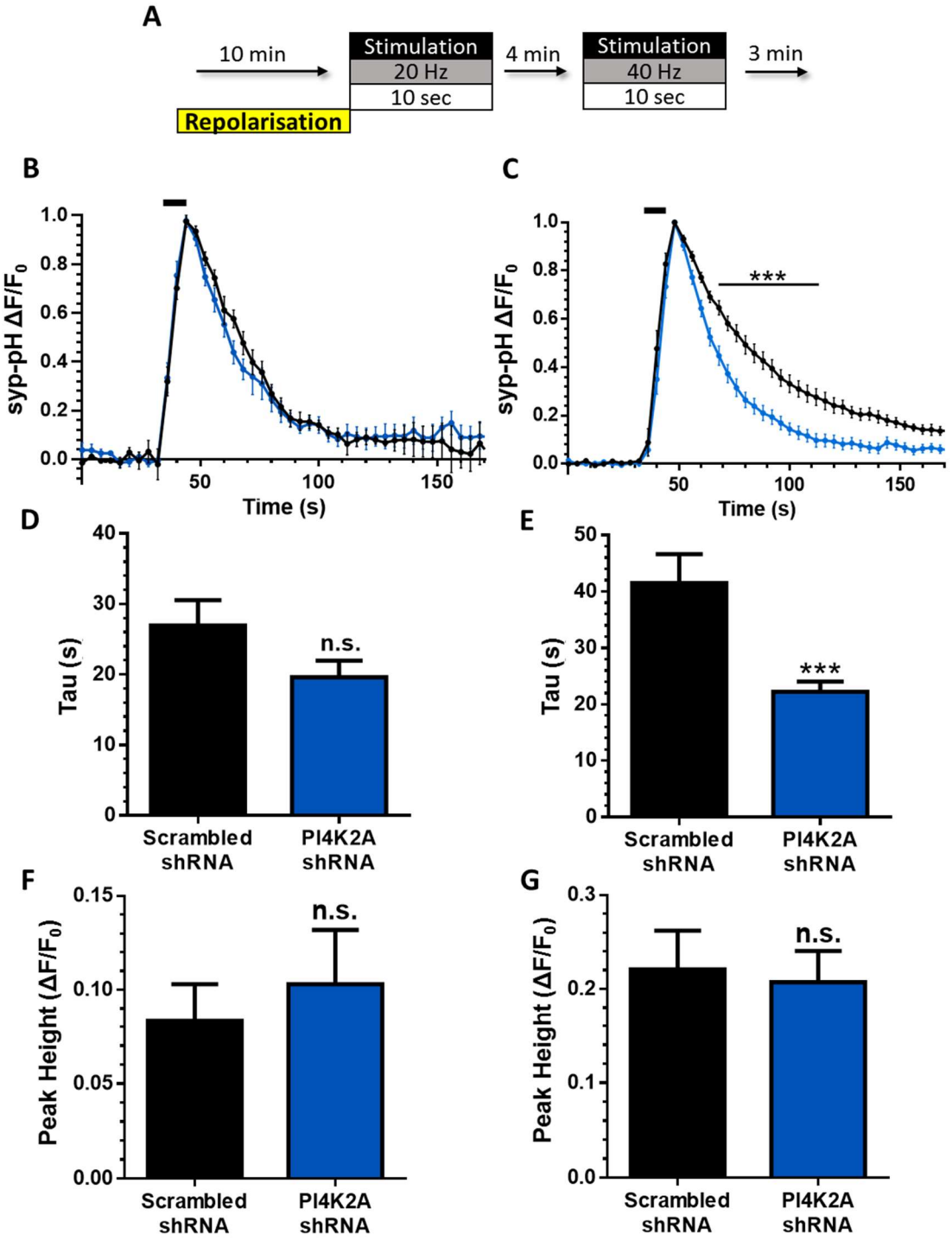
A
10 min
Stimulation
20 Hz
10 sec
4 min
Stimulation
40 Hz
10 sec
3 min
Repolarisation
B
C
syp-pH ΔF/F0
Time (s)
***
D
E
Tau (s)
n.s.
***
Scrambled shRNA
PI4K2A shRNA
F
G
Peak Height (ΔF/F0)
n.s.

Figure 4.3 Silencing PI4KIIα Expression Accelerates SypHy Retrieval During HFS

A) CGNs co-transfected with either PI4KIIα shRNA or scrambled control shRNA and synaptophysin-pHluorin (syp-pH) were incubated with imaging buffer for 10 minutes prior to stimulation and then continuously onwards. Cells were stimulated with a mild stimulation train (200 AP, 20 Hz) and recovered for 4 mins followed by stimulation with HFS train (400 AP, 40 Hz). B and C) Scrambled shRNA (black) Vs. PI4KIIα shRNA (blue) B) Average time trace of mild stimulation (200 AP, 20 Hz) $\pm$ SEM is displayed with stimulation indicated by black bar. C) Average time trace of HFS (400 AP, 40 Hz) $\pm$ SEM is displayed with stimulation indicated by black bar D) Average peak heights on mild stimulation (200 AP, 20 Hz) of each condition (F/F_0) + SEM. E) Average peak heights on HFS of each condition (F/F_0) + SEM. F) Average endocytosis kinetics after mild stimulation (200 AP, 20 Hz) (tau) + SEM. G) Average endocytosis kinetics after HFS (400 AP, 40 Hz) (tau) + SEM. Scrambled shRNA n=5 (20 Hz) 7 (40 Hz) PI4KIIα shRNA n=8 12. Time traces: ***=p<0.001 Two-way

a role in the endocytosis of syp-pH during HFS and may be a negative regulator of SV endocytosis. The loss of PI4KIIα does not have any effect on exocytosis at either mild or intense stimulation as reported by syp-pH fluorescence.

4.2.1.2 ADBE is Inhibited in the absence of PI4KIIα

Due to the specificity of the effect on endocytic kinetics of PI4KIIα knockdown to HFS and not mild stimulation, ADBE was next investigated for an effect (as this is a process which is only activated during HFS). To do this a previously validated 40 kDa dextran-uptake assay (Clayton et al. 2008) was utilised. Dextran is a fluid phase marker of large enough size to make it unlikely to be internalised by single SVs. Dextran therefore only reliably labels the larger invaginations of ADBE and gives a measurement of how many nerve terminals within a culture or in a cell (when using transfected cells) perform ADBE.

CGNs co-transfected with PI4KIIα or its scrambled control and an empty mCer vector were exposed to a HFS in the presence of dextran (50 μM) (Figure 4.4 A). A robust uptake of dextran was observed in neurones expressing the scrambled shRNA (Figure 4.4 B). In contrast, the silencing of PI4KIIα expression had a significant inhibitory effect on the uptake of dextran when compared to the scrambled control (Figure 4.4 B). This would imply that the presence or activity of PI4KIIα is required for ADBE.

As it has now been shown that the absence of PI4KIIα inhibits dextran uptake it can now be deduced that the acceleration of syp-pH retrieval seen previously cannot be attributed to an increase in uptake via ADBE and must therefore represent an

increase in the rate of CME. It is possible that the two phenotypes caused by the silencing of PI4KIIα expression, acceleration of CME and inhibition of ADBE, are functionally related, i.e. the acceleration of CME allows the cell to compensate for surface area increase caused by exocytosis via this mode alone and therefore ADBE is not triggered. It could also be hypothesised that the inhibition of ADBE is the primary effect of PI4KIIα depletion and the rate of CME must be increased to compensate for the loss of this high capacity retrieval mechanism. This hypothesis seems likely as PI4KIIα depletion only affects the rate of CME during HFS when ADBE is activated.

4.2.2 Rescue with Mutant PI4KIIα Reveals Differential Mechanisms for PI4KIIα Influence on Exocytosis, CME and ADBE

Thus, far it has been shown that knockdown of PI4KIIα both accelerates syp-pH retrieval and inhibits ADBE in response to HFS. To determine the molecular basis for these effects a series of shRNA-resistant PI4KIIα mutants was utilised to rescue function in knockdown neurons. These consisted of:

WT - Wild-type PI4KIIα. Homologous to the endogenous form of PI4KIIα, there is no alteration to either the serine residues which serve as the priming sites for GSK3 (Ser9 and Ser51) or the GSK3 phosphorylation sites themselves. As such GSK3 can phosphorylate residues 4 and 47 to open the structure of the WT protein and allow access for AP-3 to recognise its di-leucine motif (Figure 4.5 A).

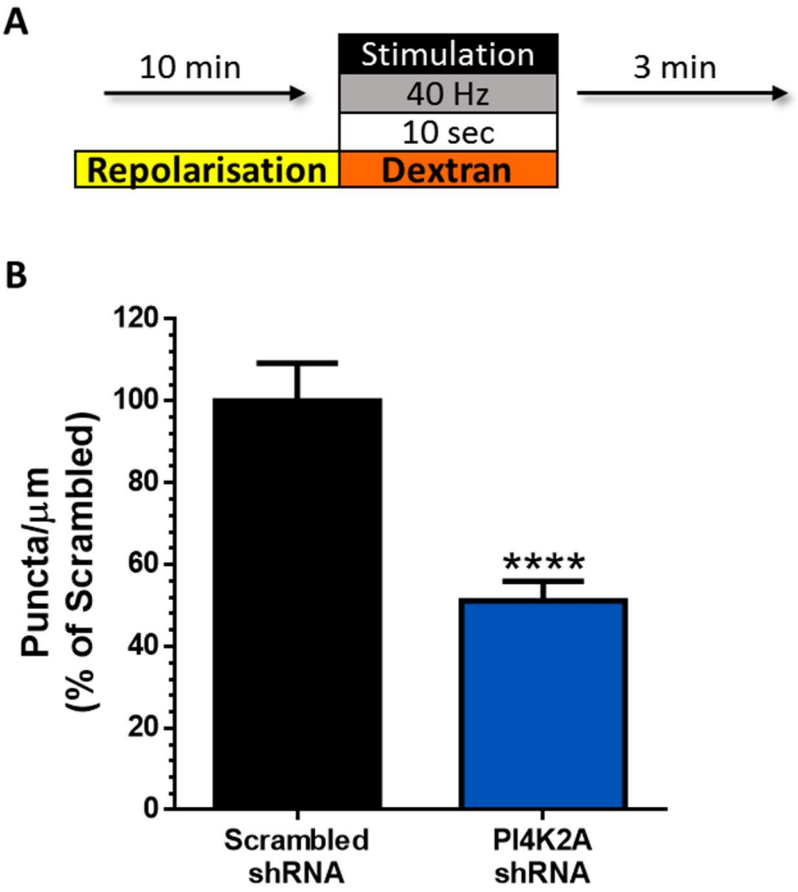

Figure 4.4 Silencing PI4KIIα Expression Inhibits ADBE

A) CGNs transfected with PI4KIIα shRNA or its scrambled control with an empty mCer vector were repolarised in imaging buffer for 10 minutes. Cells were stimulated with a HFS train (400 AP, 40 Hz) in the presence of 50 µM dextran. B) Average number of dextran puncta per µm of axon expressed as a proportion of scrambled shRNA + SEM. Scrambled shRNA n=53, PI4KIIα shRNA n=60. ****=p<0.0001. Student's t-test.

QUAD-D – PI4KIIα with serine residues 5, 9, 47 and 51 mutated to aspartic acid residues (QUAD-D) this phospho-mimetic mutation causes a conformational change of the protein, normally caused via GSK3 phosphorylation. Its structure is innately open and therefore allows unimpeded and constant access for AP-3 to the di-leucine binding site (Figure 4.5 B).

S9/51A – PI4KIIα with the GSK3 priming site serines (Ser9 and Ser51) mutated to alanine residues. This forms phospho-null versions of GSK3 priming sites meaning GSK3 will not recognise and phosphorylate Ser5 and Ser47. Without GSK3 phosphorylation the protein which will retain its "closed" structure making the di-leucine motif less accessible to AP-3 (Figure 4.5 C) and inhibits its degradation.

L60/61A – PI4KIIα in which the di-leucine motif at residues 60 and 61 has been mutated to alanine residues causing a disruption in AP-3 binding. This form of the protein can be either "open" or closed" as GSK3 phosphorylation is not affected (Figure 4.5 D). However, AP-3 will not bind and shuttle PI4KIIα to lysosome for degradation.

K152A – a protein with a lysine residue (Lys152) mutated to an alanine residue. This does not cause a change in structure of the protein however it inhibits kinase activity, creating a kinase-dead version of PI4KIIα. This form of the protein can be either "open" or closed" as GSK3 phosphorylation is not affected (Figure 4.5 E).

To determine level of rescue of expression achieved by these shRNA-resistant PI4KIIα plasmids the following experiment was performed. For a positive control, CGNs were triple-transfected with an mCer empty vector, scrambled shRNA vector

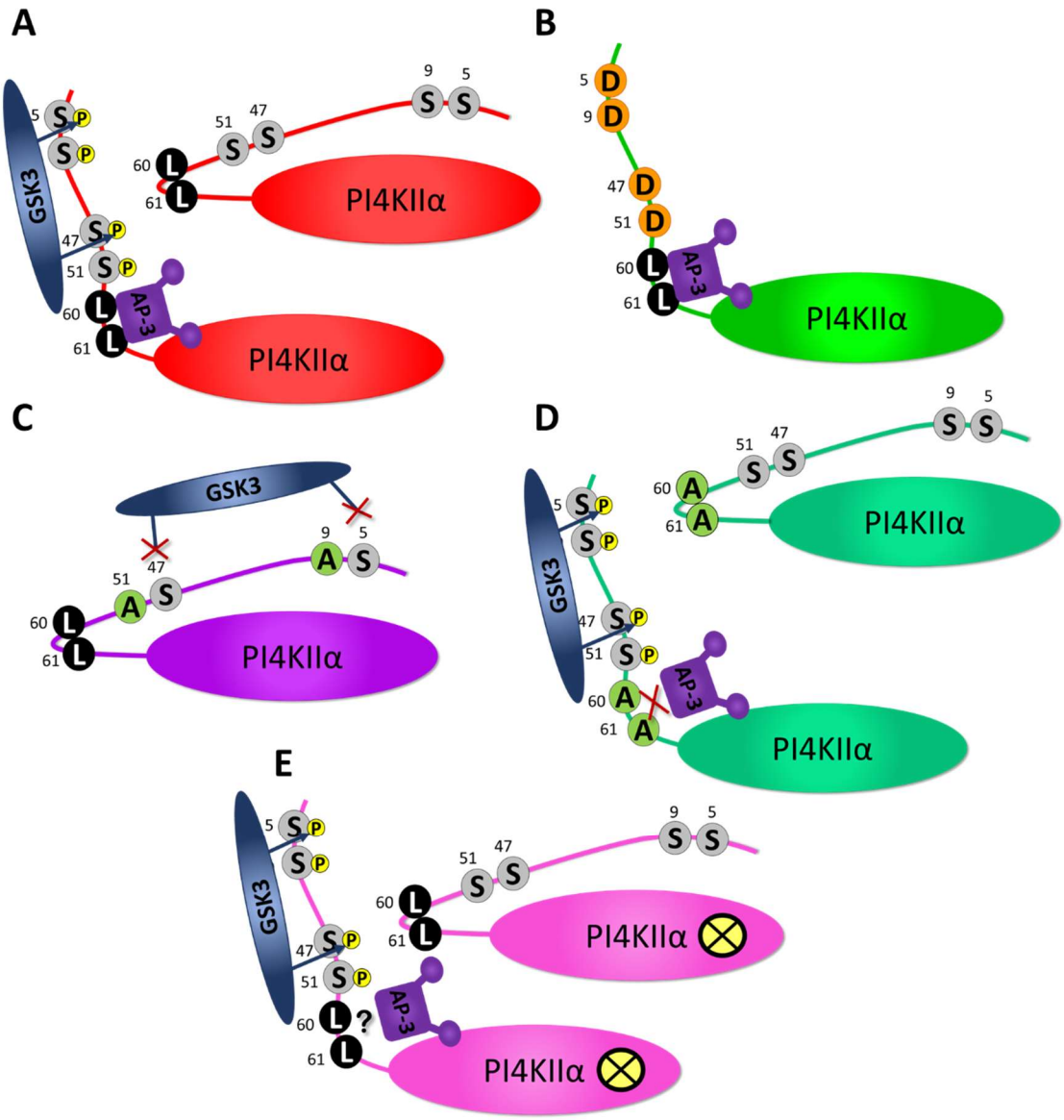

Figure 4.5 shRNA-Resistant PI4KIIα Mutations and Their Functional Implications

A) WT: PI4KIIα in its “closed” (above) or “open” (below) structure. GSK3 phosphorylation of Ser5/47 causes the structure to open and reveals an AP-3 binding site. B) QUAD-D: PI4KIIα mutated at Serines 5,9,47 and 51 to aspartic acid residues. Phospho-mimetic of GSK3 priming and phosphorylation causes constant “open” structure and access to AP-3 binding site. C) S9/51A: PI4KIIα mutated at Serines 9 and 51 to alanine residues. Phospho-null mutations of GSK3 priming sites causes constant “closed” structure obscuring AP-3 binding site, ablating binding. D) L60/61A: PI4KIIα mutated at Leucines 60 and 61 to alanine residues. GSK3 phosphorylation is unaffected and structure can be “open” (above) or “closed” (below) but AP-3 binding site is mutated, ablating AP-3 binding. E) K152A: PI4KIIα with lysine residue at position 152 mutated to an alanine residue, this causes no effect on GSK3 phosphorylation so can be “open” (above) or “closed” (below). AP-3 binding may also be affected. This mutation causes PI4KIIα to lose its kinase function.

and a PRK5 empty vector. For a negative control (knockdown), CGNs were triple-transfected with an mCer empty vector, PI4KIIα shRNA and a PRK5 empty vector. For all rescue conditions CGNs were triple-transfected with mCer empty vector, PI4KIIα shRNA and one of the shRNA-resistant forms of PI4KIIα (WT, QUAD-D, S9/51A, L60/61A or K152A). Cultures were then fixed and immunostained with a PI4KIIα antibody.

As seen previously, the scrambled shRNA had no effect on PI4KIIα abundance compared to non-transfected nerve terminals (Figure 4.6 A and H). The expression of PI4KIIα shRNA resulted in a significant reduction in PI4KIIα abundance in nerve terminals when compared to neighbouring non-transfected nerve terminals and scrambled controls (Figure 4.6 B and H). All other PI4KIIα shRNA-resistant constructs resulted in a significant rescue of PI4KIIα abundance over and above scrambled control levels (Figure 4.6 C-H). Expression of all PI4KIIα mutants (bar QUAD-D PI4KIIα) in a knockdown background were significantly increased above scrambled control PI4KIIα levels (Figure 4.6 H). This shows that all shRNA-resistant PI4KIIα mutants are able to rescue PI4KIIα expression in CGNs when endogenous PI4KIIα expression has been silenced.

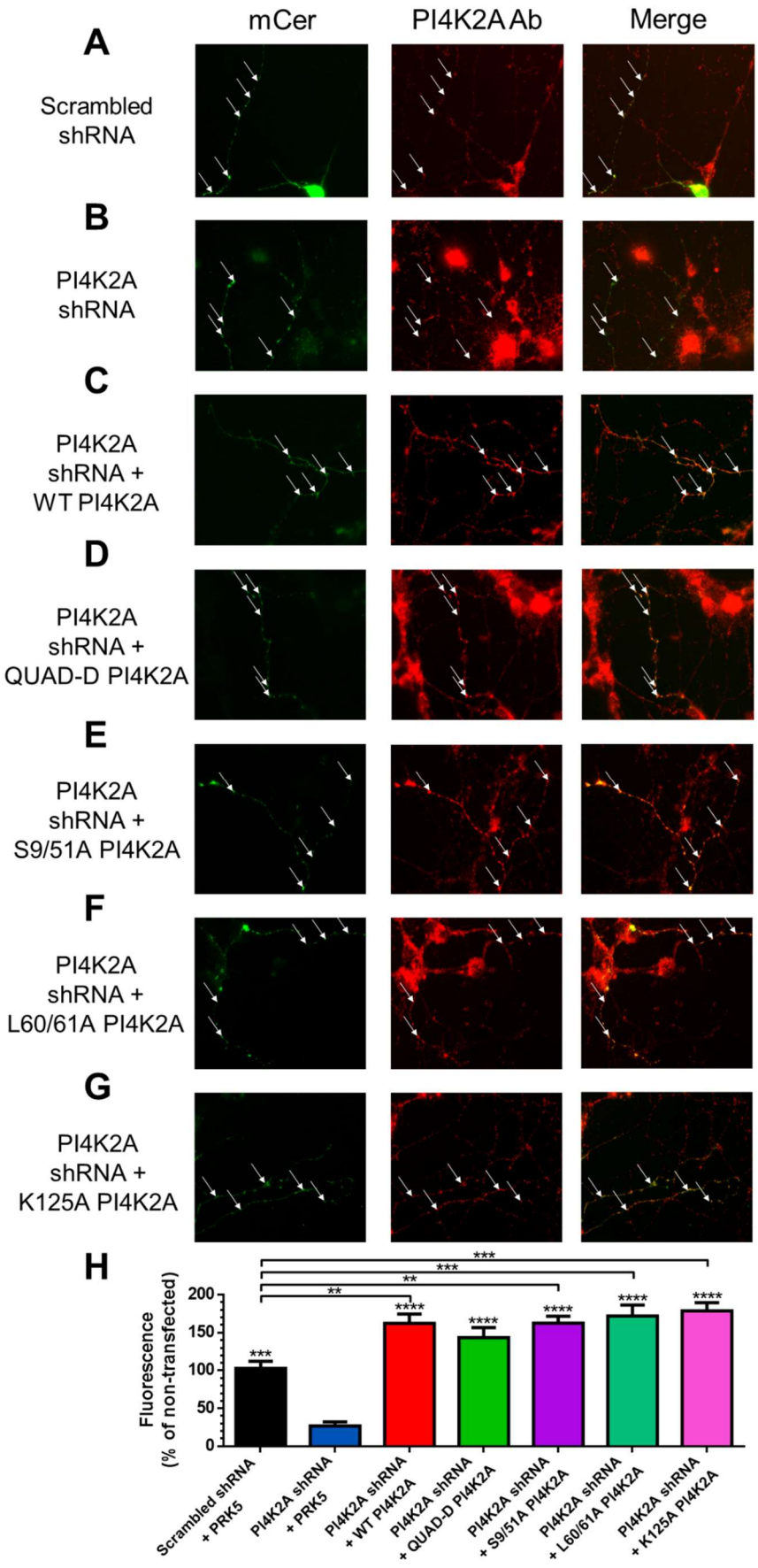
mCer
PI4K2A Ab
Merge
A
Scrambled shRNA
B
PI4K2A shRNA
C
PI4K2A shRNA + WT PI4K2A
D
PI4K2A shRNA + QUAD-D PI4K2A
E
PI4K2A shRNA + S9/51A PI4K2A
F
PI4K2A shRNA + L60/61A PI4K2A
G
PI4K2A shRNA + K125A PI4K2A
H
Fluorescence (% of non-transfected)
200
150
100
50
0
***
**
****
Scrambled shRNA + PRK5
PI4K2A shRNA + PRK5
PI4K2A shRNA + WT PI4K2A
PI4K2A shRNA + QUAD-D PI4K2A
PI4K2A shRNA + S9/51A PI4K2A
PI4K2A shRNA + L60/61A PI4K2A
PI4K2A shRNA + K125A PI4K2A

Figure 4.6 PI4KIIα Expression Levels are Effectively Rescued with shRNA-Resistant PI4KIIα Constructs

Images of CGNs triple-transfected with mCer empty vector, and A) Scrambled shRNA +PRK5 empty vector. B) PI4KIIα shRNA + PRK5 empty vector. C) PI4KIIα shRNA + WT PI4KIIα. D) PI4KIIα shRNA + QUAD-D PI4KIIα. E) PI4KIIα shRNA + S9/51A PI4KIIα. F) PI4KIIα shRNA + L60/61A PI4KIIα. G) PI4KIIα shRNA + K152A PI4KIIα. CGN culture was labelled with PI4KIIα Ab (middle) and transfected cells were located by mCer fluorescence (left), when overlaid one can see that the synapses of the transfected cell (white arrows) do not exhibit as much PI4KIIα labelling in the presence of PI4KIIα shRNA but the expression of shRNA-resistant PI4KIIα rescues protein levels. H) Average fluorescence of CGN synapses transfected with each condition as a percentage of fluorescence nearby non-transfected synapses of similar size + SEM. Scrambled shRNA +PRK5 n=15, PI4KIIα shRNA + PRK5 n=21, PI4KIIα shRNA + WT n=23, PI4KIIα shRNA + QUAD-D n=21, PI4KIIα shRNA + S9/51A n=25, PI4KIIα shRNA + L60/61A n=20, PI4KIIα shRNA + K152A n=23, ***=$p<0.001$, ****= $p<0.0001$. One-way ANOVA to PI4KIIα shRNA + PRK5.

4.2.2.1 CME Kinetics can be Rescued with Wild-Type PI4KIIα

Knockdown of PI4KIIα results in an accelerated rate of CME. To ensure that this effect was not caused by an off-target effect of the shRNA vector I attempted to rescue the phenotype caused by the knockdown using a shRNA-resistant form of WT PI4KIIα.

CGNs were triple-transfected with PI4KIIα shRNA, syp-pH and either a PRK5 empty vector (sypHy PI4KIIα KD) or WT PI4KIIα (sypHy WT rescue) (Figure 4.7 A). As effects on endocytic rate were only seen during intense stimulation, cells were now subjected to a single HFS, with no preliminary mild stimulation (Figure 4.7 B).

Expression of WT PI4KIIα resulted in a significant effect on the retrieval of syp-pH after HFS, which can be visualised by normalising the syp-pH traces of each condition to their peak height (Figure 4.7 C). When endocytic kinetic values (tau) are calculated it is clear that expression of a shRNA-resistant WT PI4KIIα has successfully rescued the increased endocytic kinetics of CME as the tau values are comparable between neurons in which PI4KIIα has been rescued and those where no knockdown has taken place (Figure 4.7 E). This would imply that the effects of PI4KIIα shRNA expression are caused by the loss of PI4KIIα expression in the cell and are not caused by any side effect of expression of the shRNA.

Another interesting observation is that the expression WT PI4KIIα causes a significant increase in the amount of syp-pH exocytosis during stimulation. This can be visualised by normalising the syp-pH fluorescence traces of each condition to total syp-pH (the maximum fluorescence value caused by ammonia buffer after

stimulation) (Figure 4.7 D). This increased exocytosis results in a significantly increased peak height with expression of shRNA-resistant WT PI4KIIα (Figure 4.7 F).

4.2.2.2 ADBE Inhibition can be Rescued with Wild-Type PI4KIIα

Next, the ability of the shRNA-resistant WT PI4KIIα to rescue to inhibition of ADBE seen with the knockdown of PI4KIIα was investigated. CGNs triple-transfected with PI4KIIα shRNA, an empty mCer vector and either an empty PRK5 vector (mCer PI4KIIα KD) or shRNA-resistant WT PI4KIIα (mCer WT Rescue) (Figure 4.8 A) were subjected to a HFS in the presence of dextran (50 μM) (Figure 4.8 B) and the number of puncta per μm of transfected axon was calculated.

Expression of WT PI4KIIα into a PI4KIIα depleted CGN successfully rescues ADBE (Figure 4.8 C). Importantly, the ratio of PI4KIIα shRNA to WT PI4KIIα rescue is comparable to that seen between scrambled shRNA and PI4KIIα shRNA seen previously (see Figure 4.4). This shows that both endocytic phenotypes seen when PI4KIIα expression is silenced by shRNA are due specifically to the loss of PI4KIIα and not due to any off-target effects of the shRNA. The lack of increased ADBE with WT PI4KIIα rescue would imply that overexpression of WT PI4KIIα does not affect ADBE.

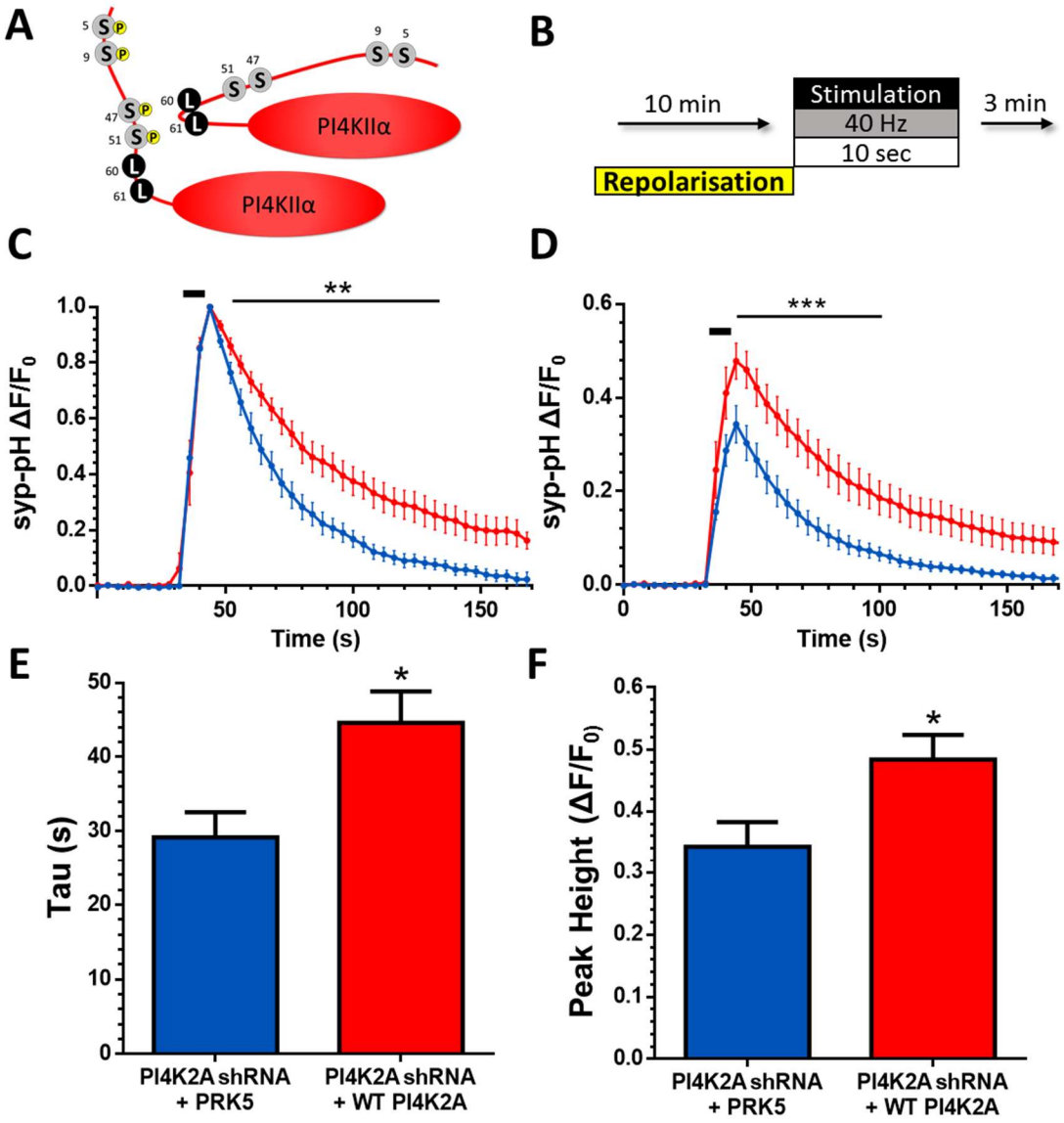

Figure 4.7 shRNA-Resistant WT PI4KIIα Successfully Rescues Accelerated CME Knockdown Phenotype

CGNs were triple-transfected with PI4KIIα shRNA, synaptophysin-pHluorin (syp-pH) and either a PRK5 empty vector or a shRNA-resistant WT PI4KIIα (A). B) Cells were incubated with imaging buffer for 10 minutes prior to stimulation and then continuously onwards. Cells were stimulated with a HFS train (400 AP, 40 Hz). C and D) PI4KIIα shRNA + PRK5 (blue) or + WT PI4KIIα (red). C) Average time trace ± SEM normalised to stimulation peak is displayed with stimulation indicated by black bar. D) Average time trace ± SEM normalised to maximum ammonia pulse fluorescence is displayed with stimulation indicated by black bar E) Average endocytic kinetics (tau) + SEM. F) Average peak heights on HFS of each condition (F/F_0) + SEM. PI4KIIα shRNA + PRK5 n=12, PI4KIIα shRNA + WT PI4KIIα n=5. Time traces: **=p<0.01, ***=p<0.001 Two-way ANOVA, Bonferroni post-test. Bar charts: *=p<0.05 , Student's t-test.

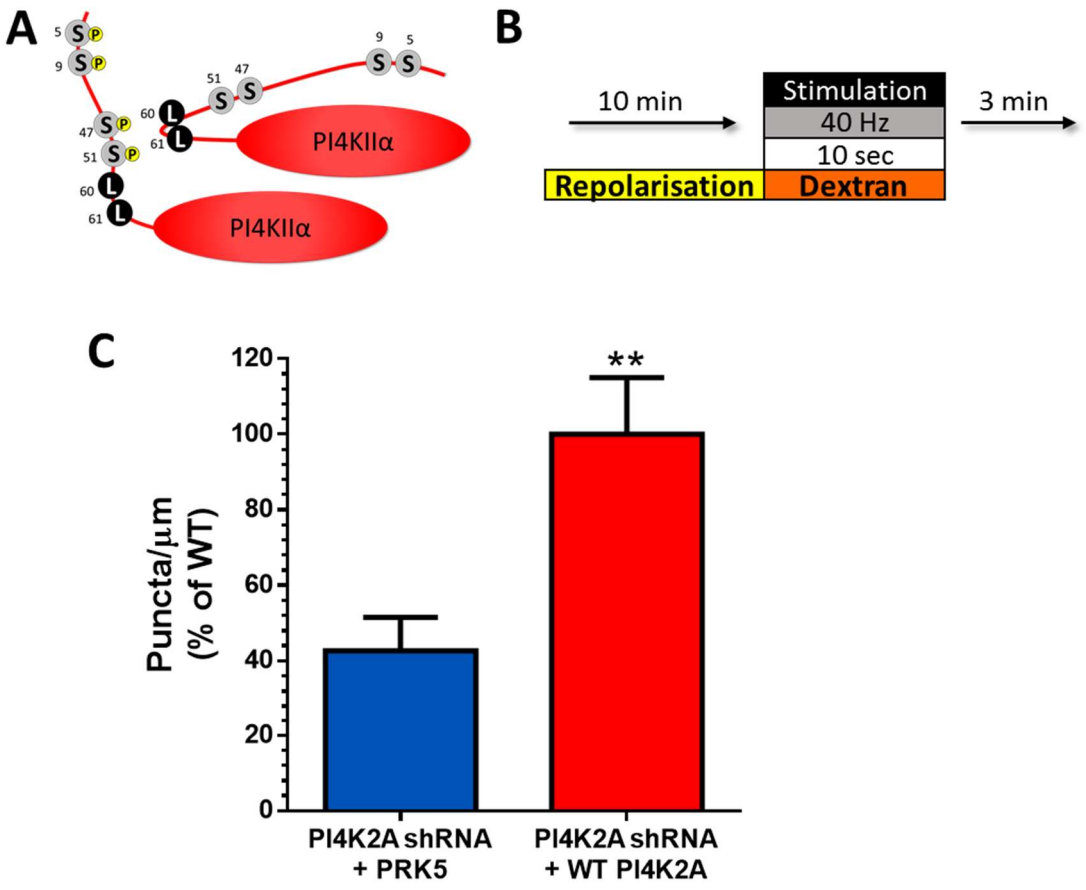

Figure 4.8 shRNA-Resistant WT PI4KIIα Successfully Recues Inhibited ADBE Knockdown Phenotype

CGNs were triple-transfected with PI4KIIα shRNA, an empty mCer vector and either an PRK5 empty vector or shRNA-resistant WT PI4KIIα (A). B) Cells were repolarised in imaging buffer for 10 minutes. Cells were stimulated with a HFS train (400 AP, 40 Hz) in the presence of 50 µM dextran. C) Average number of dextran puncta per µm of axon expressed as a proportion of WT rescue + SEM. PI4KIIα shRNA + PRK5 n=32, PI4KIIα shRNA + WT PI4KIIα n=26. **=p<0.01. Student's t-test.

4.2.2.3 Increased Rate of CME is not Rescued with Phospho-Mimetic PI4KIIα Mutant

I next investigated the importance of GSK3 phosphorylation in the function of PI4KIIα in both CME and ADBE during HFS. Phosphorylation of PI4KIIα by GSK3 causes the di-leucine AP-3-binding motif to become accessible and therefore allows the protein to be recognised by AP-3 and is subsequently shuttled to the lysosome for degradation GSK3 phosphorylates PI4KIIα on serine residues 5 and 47 after being primed by a separate kinase on serine residues 9 and 51 (Robinson et al. 2014). To mimic a PI4KIIα protein which has been phosphorylated on all four serine residues and therefore mimics a GSK3-phosphorylated molecule an shRNA-resistant S5/9/47/51D (QUAD-D) PI4KIIα was expressed.

CGNs triple-transfected with either syp-pH PI4KIIα KD or PI4KIIα shRNA, syp-pH and shRNA-resistant QUAD-D PI4KIIα (syp-pH QUAD-D Rescue) (Figure 4.9 A) were subjected to a single HFS (Figure 4.9 B). No significant difference between PI4KIIα knockdown and QUAD-D rescue was seen on syp-pH retrieval after HFS when traces from each condition were normalised to peak height (Figure 4.9 C). This was also apparent by a lack of significant effect on endocytic kinetics (tau) (Figure 4.9 E). This would suggest that the QUAD-D version of PI4KIIα does not support normal endocytosis like its WT counterpart.

Expression of this phospho-mimetic PI4KIIα does not cause an increase in peak height (Figure 4.9 D and F) as is seen when WT PI4KIIα is expressed in a PI4KIIα

depleted background. Further suggesting that this mutation causes a functional defect in relation to the role of PI4KIIα in normal SV recycling.

4.2.2.4 Inhibition of ADBE is not Rescued with Phospho-Mimetic PI4KIIα Mutant

I examined the ability of QUAD-D PI4KIIα to rescue to phenotype of inhibited ADBE caused by silencing of PI4KIIα expression. CGNs triple-transfected with PI4KIIα shRNA, an mCer empty vector and shRNA-resistant QUAD-D PI4KIIα (mCer QUAD-D Rescue) (Figure 4.10 A) were subjected to HFS in the presence of dextran (50 μM) (Figure 4.10 B).

Expression of QUAD-D PI4KIIα did not rescue the ability of the cell to undergo ADBE during HFS (Figure 4.10 C). Further suggesting a suppressive activity of PI4KIIα phosphorylation by GSK3 in the presynapse.

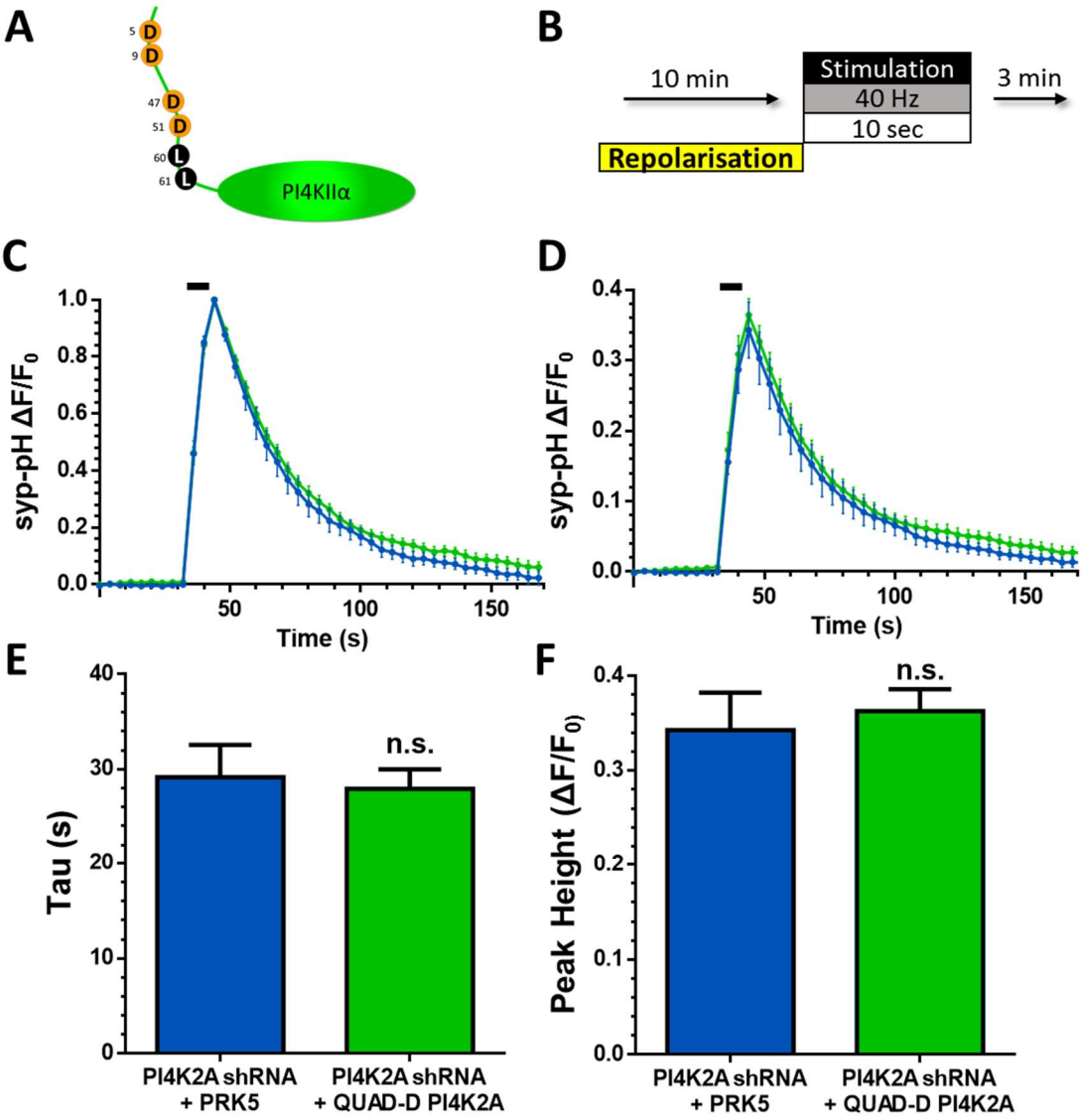

Figure 4.9 shRNA-Resistant QUAD-*D PI4KIIα* does not Rescue Accelerated CME Knockdown Phenotype

CGNs were triple-transfected with PI4KIIα shRNA, synaptophysin-pHluorin (syp-pH) and either a PRK5 empty vector or a shRNA-resistant QUAD-D PI4KIIα (A). B) Cells were incubated with imaging buffer for 10 minutes prior to stimulation and then continuously onwards. Cells were stimulated with a HFS train (400 AP, 40 Hz). C and D) PI4KIIα shRNA + PRK5 (blue) or + QUAD-D PI4KIIα (green). C) Average time trace ± SEM normalised to peak fluorescence is displayed with stimulation indicated by black bar. D) Average time trace ± SEM normalised to maximum ammonia pulse fluorescence is displayed with stimulation indicated by black bar E) Average endocytic kinetics (tau) + SEM. F) Average peak heights on HFS of each condition (F/F_0) + SEM. PI4KIIα shRNA + PRK5 n=12, PI4KIIα shRNA + QUAD-D PI4KIIα n=7. Bar charts: n.s, Student's t-test.

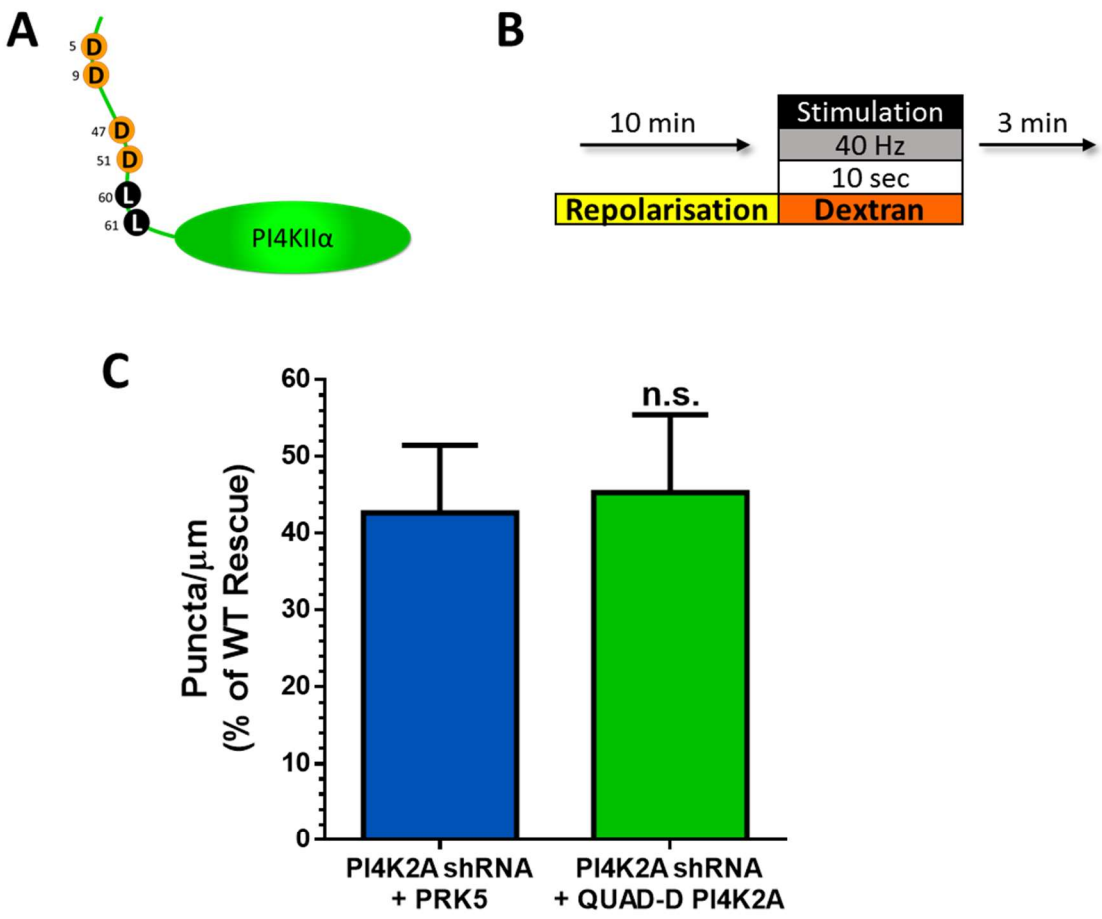

Figure 4.10 shRNA-Resistant QUAD-D PI4KIIα does not Rescue Inhibited ADBE Knockdown Phenotype

CGNs were triple-transfected with PI4KIIα shRNA, an empty mCer vector and either an PRK5 empty vector or shRNA-resistant QUAD-D PI4KIIα (A). B) Cells were repolarised in imaging buffer for 10 minutes. Cells were stimulated with a HFS train (400 AP, 40 Hz) in the presence of 50 µM dextran. C) Average number of dextran puncta per µm of axon expressed as a proportion of WT rescue + SEM. PI4KIIα shRNA + PRK5 n=32, PI4KIIα shRNA + QUAD-D PI4KIIα n=13. n.s.. Student's t-test.

4.2.2.5 Faster Rate of CME is not Rescued But Exacerbated with Phospho-Null PI4KIIα Mutants

I further investigated the importance of GSK3 phosphorylation by employing the shRNA-resistant phospho-null mutant S9/51A. PI4KIIα must be phosphorylated on two priming sites (Ser9 and Ser51) to allow GSK3 phosphorylation. Mutation of these sites to phospho-null alanine residues creates a PI4KIIα protein which will not be recognised by GSK3 and will therefore not be phosphorylated on serines 5 and 47. This will allow the importance of PI4KIIα phosphorylation by GSK3 for both CME and ADBE to be visualised.

CGNs triple-transfected with either syp-pH PI4KIIα KD or PI4KIIα shRNA, syp-pH and shRNA-resistant S9/51A PI4KIIα (syp-pH S9/51A Rescue) (Figure 4.11 A) were stimulated with a single HFS (Figure 4.11 B).

Interestingly, a significant difference in the retrieval of syp-pH after stimulation was observed when fluorescence traces from each condition were normalised to their peak height (Figure 4.11 C). When endocytic kinetics were calculated, there was also a significant difference between the knockdown and rescue with S9/51A. The addition of the phospho-null mutant protein did not rescue the increased CME kinetics but instead increased the rate further. There was no significant difference in evoked peak height (Figure 4.11 D and F) as was seen when rescuing with WT PI4KIIα. This would further suggest that this mutation has altered the function of PI4KIIα.

S9/51A PI4KIIα results in a constitutively "closed" structure of PI4KIIα. This means that the AP-3-binding site is perpetually occluded though AP-3 binding is not entirely ablated (Robinson et al. 2014). To elucidate if this functional consequence of the S9/51A mutation could be causing the further increased rate of CME, another mutant PI4KIIα which is incapable of binding AP-3 – L60/61A was utilised.

AP-3 recognises PI4KIIα via a di-leucine motif (L60 and L61); mutation of these leucine residues to alanine residues disrupts AP-3 binding and therefore should result in a similar phenotype to that seen with S9/51A expression.

CGNs triple-transfected with either mCer PI4KIIα KD or PI4KIIα shRNA, syp-pH and shRNA-resistant L60/61A PI4KIIα (Figure 4.12 A) were stimulated with a single HFS (Figure 4.12 B).

Expression of AP-3-binding deficient PI4KIIα caused a similar and significant difference in syp-pH retrieval after stimulation (Figure 4.12 C) that is clearly seen as an increase in rate of CME when endocytic kinetics are calculated (Figure 4.12 E). Rescue of PI4KIIα abundance with this mutated form did not cause a significant difference in evoked peak height (Figure 4.12 D and F). These results clarify that interfering with PI4KIIα -AP-3 binding in a PI4KIIα knockdown background somehow increases the rate of CME over and above that which is caused by the knockdown itself.

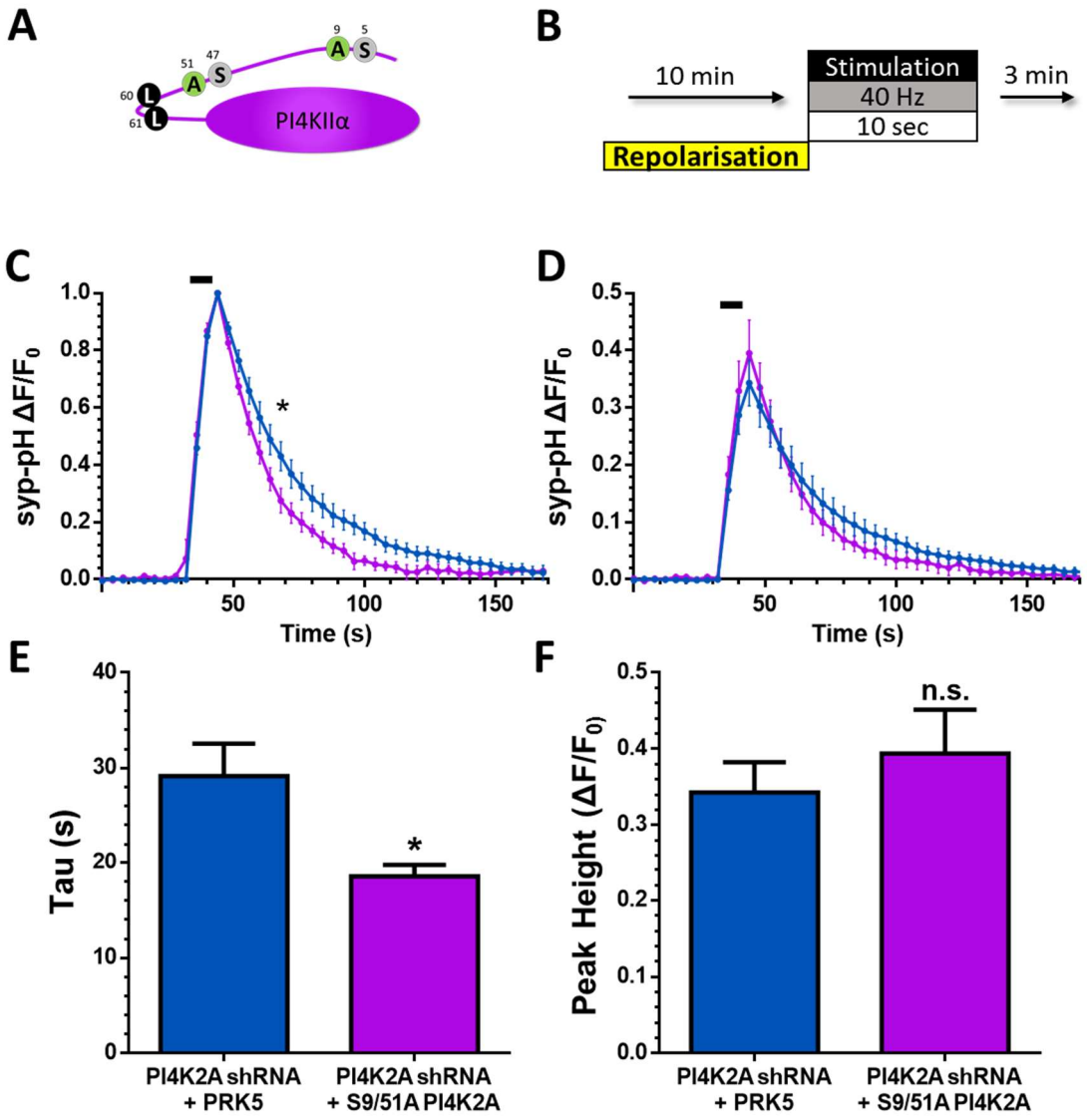

Figure 4.11 shRNA-Resistant S9/51A PI4KIIα Exacerbates Accelerated CME Knockdown Phenotype

CGNs were triple-transfected with PI4KIIα shRNA, synaptophysin-pHluorin (syp-pH) and either a PRK5 empty vector or a shRNA-resistant S9/51A PI4KIIα (A). B) Cels were incubated with imaging buffer for 10 minutes prior to stimulation and then continuously onwards. Cells were stimulated with a HFS train (400 AP, 40 Hz). C and D) PI4KIIα shRNA + PRK5 (blue) or + S9/51A PI4KIIα (purple). B) Average time trace ± SEM normalised to peak fluorescence is displayed with stimulation indicated by black bar. D) Average time trace ± SEM normalised to maximum ammonia pulse fluorescence is displayed with stimulation indicated by black bar E) Average endocytic kinetics of each condition (tau) + SEM. F) Average peak heights of each condition (F/F_0) + SEM. PI4KIIα shRNA + PRK5 n=12, PI4KIIα shRNA + S9/51A PI4KIIα n=6. Time traces: *=$p<0.05$, Two-way ANOVA, Bonferroni post-test. Bar charts: *=$p<0.05$, Student's t-test.

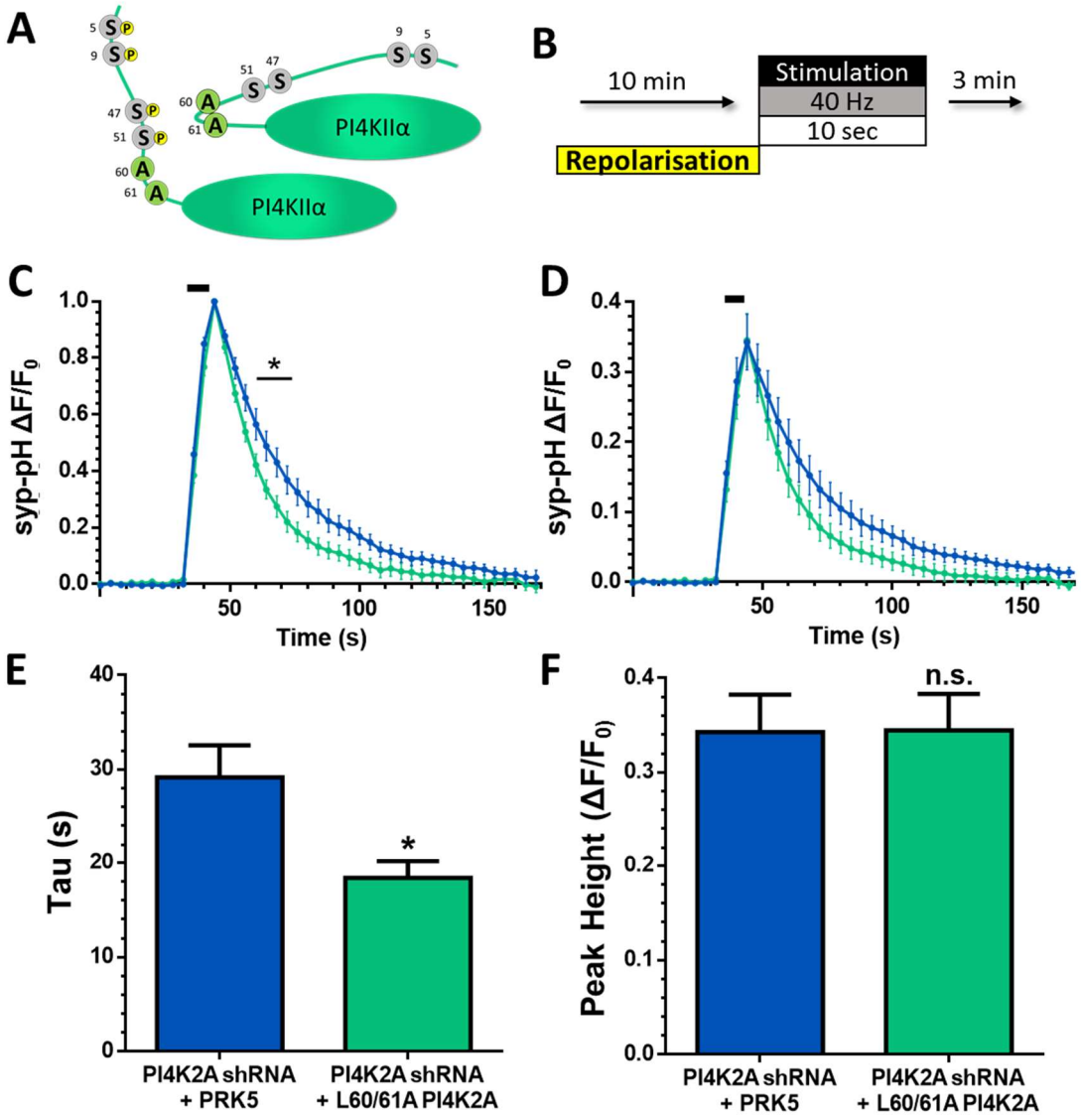

Figure 4.12 shRNA-Resistant L60/61A Exacerbates Accelerated CME Knockdown Phenotype

CGNs were triple-transfected with PI4KIIα shRNA, synaptophysin-pHluorin (syp-pH) and either a PRK5 empty vector or a shRNA-resistant L60/61A PI4KIIα (A). B) Cells were incubated with imaging buffer for 10 minutes prior to stimulation and then continuously onwards. Cells were stimulated with a HFS train (400 AP, 40 Hz). C and D) PI4KIIα shRNA + PRK5 (blue) or + L60/61A PI4KIIα (turquoise). C) Average time trace ± SEM normalised to peak fluorescence is displayed with stimulation indicated by black bar. D) Average time trace ± SEM normalised to maximum ammonia pulse fluorescence is displayed with stimulation indicated by black bar E) Average endocytic kinetics of each condition (tau) + SEM. F) Average peak heights of each condition (F/F_0) + SEM. PI4KIIα shRNA + PRK5 n=12, PI4KIIα shRNA + S9/51A PI4KIIα n=8. Time traces: *=p<0.05, Two-way ANOVA, Bonferroni post-test. Bar charts: *=p<0.05, Student's t-test.

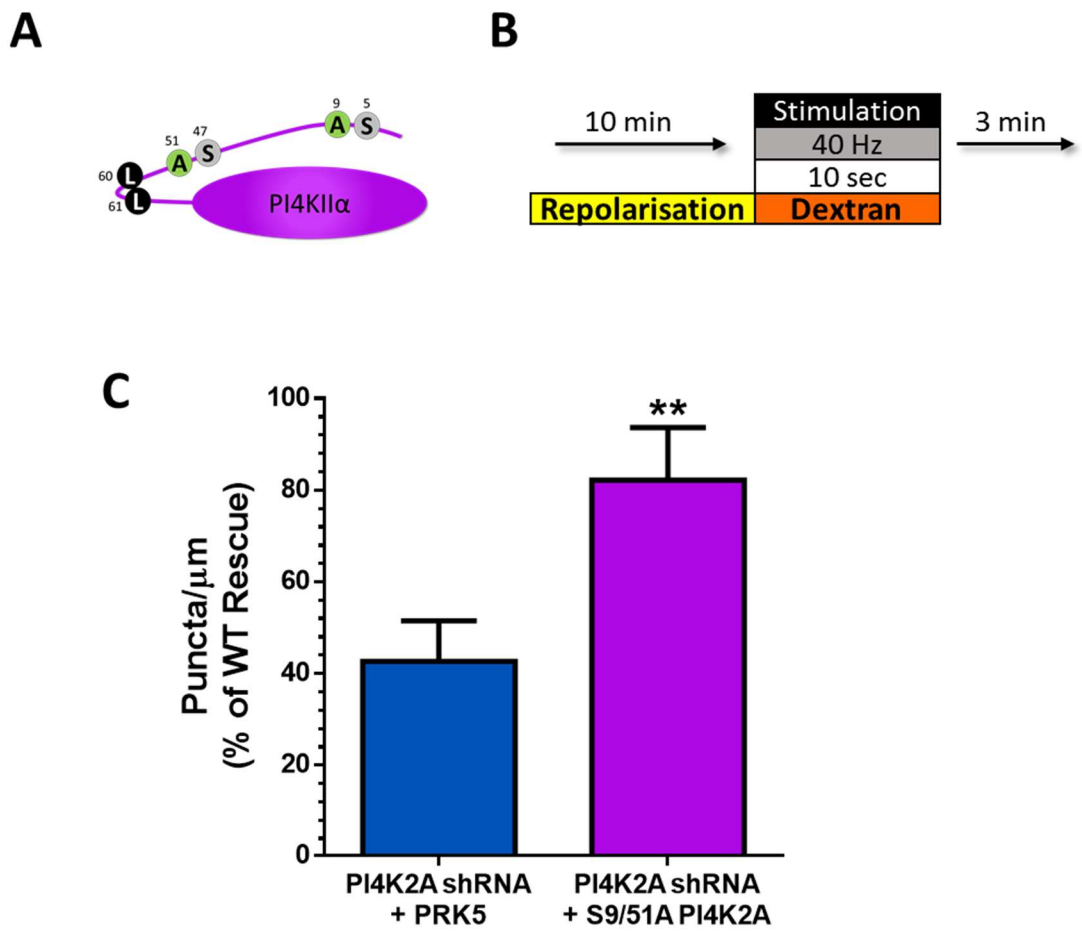

Figure 4.13 shRNA Resistant S9/51A PI4KIIα Successfully Rescues Inhibited ADBE Knockdown Phenotype

CGNs were triple-transfected with PI4KIIα shRNA, an empty mCer vector and either an PRK5 empty vector or shRNA-resistant S9/51A PI4KIIα (A). B) Cells were repolarised in imaging buffer for 10 minutes. Cells were stimulated with a HFS train (400 AP, 40 Hz) in the presence of 50 µM dextran. C) Average number of dextran puncta per µm of axon expressed as a proportion of WT rescue + SEM. PI4KIIα shRNA + PRK5 n=32, PI4KIIα shRNA + S9/51A PI4KIIα n=32. ***=p<0.01, Student's t-test.

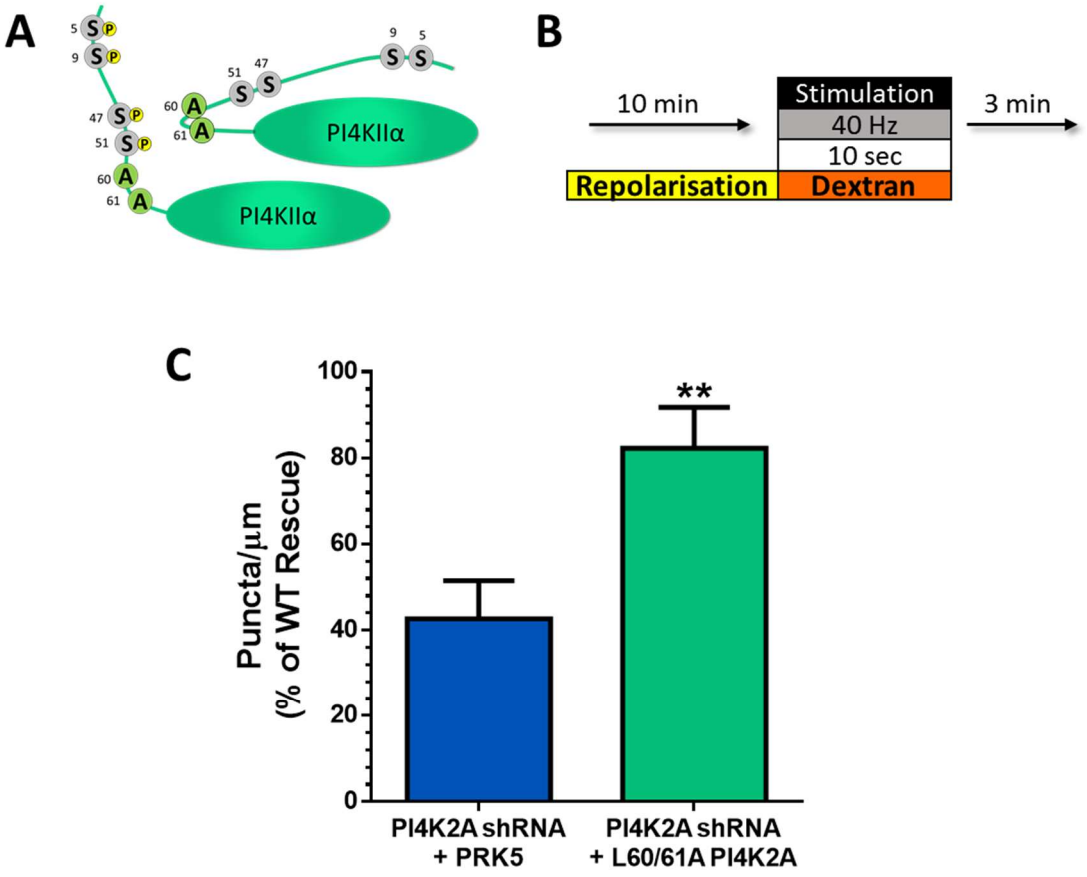

Figure 4.14 shRNA-Resistant L60/61A PI4KIIα Successfully Rescues Inhibited ADBE Knockdown Phenotype

CGNs were triple-transfected with PI4KIIα shRNA, an empty mCer vector and either an PRK5 empty vector or shRNA-resistant L60/61A PI4KIIα (A). B) Cells were repolarised in imaging buffer for 10 minutes. Cells were stimulated with a HFS train (400 AP, 40 Hz) in the presence of 50 µM dextran. C) Average number of dextran puncta per µm of axon expressed as a proportion of WT rescue + SEM. PI4KIIα shRNA + PRK5 n=32, PI4KIIα shRNA + L60/61A PI4KIIα n=33. **=p<0.01, Student's t-test.

4.2.2.6 Inhibition of ADBE is Successfully Rescued with Phospho-Null PI4KIIα Mutants

Both S9/51A and L60/61A caused an exacerbation of the effect seen on CME when PI4KIIα expression is silenced. Silencing of PI4KIIα expression also results in an inhibition of ADBE and as I have hypothesised that the increased rate of CME may be a functionally tied to the reduction of ADBE I next examined what effect these mutant PI4KIIα proteins would have on this phenotype.

CGNs were triple-transfected with either syp-pH PI4KIIα KD or PI4KIIα shRNA, an mCer empty vector and shRNA-resistant S9/51A PI4KIIα (mCer S9/51A Rescue) (Figure 4.13 A) or L60/61A PI4KIIα (mCer L60/61A Rescue) (Figure 4.14 A). Cells were stimulated with a single HFS in the presence of dextran (50 μM) (Figure 4.13. B and Figure 4.14 B).

Interestingly, the expression of both S9/51A and L60/61A did not cause a further inhibition of ADBE as one might have expected if the phenotypes of accelerated CME and inhibited ADBE were coupled. Both mutated proteins caused a significant rescue of inhibited ADBE (Figure 4.13. C and Figure 4.14 C).

Our original hypothesis for the two endocytic phenotypes seen when PI4KIIα expression is silenced (see 4.2.1.2) posited that the observed acceleration of CME was functionally linked to the inhibition of ADBE. This interaction could have been in either direction; ablation of ADBE forcing CME to accelerate to compensate for the lack of this retrieval mechanism; or a lack of triggering of ADBE due to an increased rate of CME, resulting in an increased capacity of the cell to retrieve PM

without the aid of ADBE. However, the results seen here would suggest that this theory is invalid as these two phenotypes can occur independently. AP-3-binding mutants were not able to rescue the accelerated CME caused by PI4KIIα however these same mutants rescued the inhibition of ADBE showing that only the increased rate of CME is reliant on the interaction of PI4KIIα and AP-3 and not ADBE incidence.

4.2.2.7 Faster Rate of CME is not Rescued with Kinase-Dead PI4KIIα Mutant

PI4KIIα activity is especially enriched on SVs and is the only PI4K to synthesis SV PI4P (Guo et al. 2003). PI4KIIα phosphorylates PI on the D4 position, allowing further phosphorylation on the D3 or D5 position by kinases such as PI3K or PIPKγ respectively. The loss of PI4KIIα would therefore presumably have effects in PI production which are separate from its relationship with AP-3. To examine the role of the kinase activity of PI4KIIα in both CME and ADBE the same rescue experiments described above were conducted utilising a kinase-dead mutant form of PI4KIIα – K152A.

CGNs were triple transfected with either syp-pH PI4KIIα KD or syp-pH, PI4KIIα shRNA and shRNA-resistant K152A PI4KIIα (syp-pH K152A Rescue) (Figure 4.15 A). Cells were stimulated with a single HFS and their syp-pH fluorescence was monitored over time (Figure 4.15 B).

When normalised to peak height, CGNs transfected with K152A PI4KIIα did not exhibit much evidence of a rescue of CME kinetics (Figure 4.15 C). When tau values

are quantified there is no significant effect of K152A PI4KIIα expression on the phenotype of accelerated CME caused by PI4KIIα knockdown (Figure 4.15 E).

This would imply that the action of PI4KIIα on the kinetics of CME is dependent on its kinase function, as a kinase-dead PI4KIIα is incapable of rescuing the phenotype of an increased CME rate caused by depleting PI4KIIα.

There was no effect on peak height caused by the expression of PI4KIIα K152A, this could indicate that this phenotype, as seen with the expression of WT PI4KIIα, may be reliant on the ability of PI4KIIα to perform its kinase function.

4.2.2.8 Inhibition of ADBE is not Rescued by Kinase-Dead PI4KIIα

I next investigated any role of PI4KIIα kinase function in the function of ADBE. CGNs were triple-transfected with either mCer PI4KIIα KD or an mCer empty vector, PI4KIIα shRNA and shRNA-resistant PI4KIIα K152A (mCer K152A Rescue) (Figure 4.16 A). Cells were then subjected to a HFS in the presence of dextran (50 μM) (Figure 4.16 B).

Interestingly, the expression of kinase-dead K152A PI4KIIα into a knockdown background effectively rescues ADBE (Figure 4.16 C). This would indicate that though PI4KIIα does play a role in ADBE, this role is not dependent on the ability of PI4KIIα to phosphorylate its substrates.

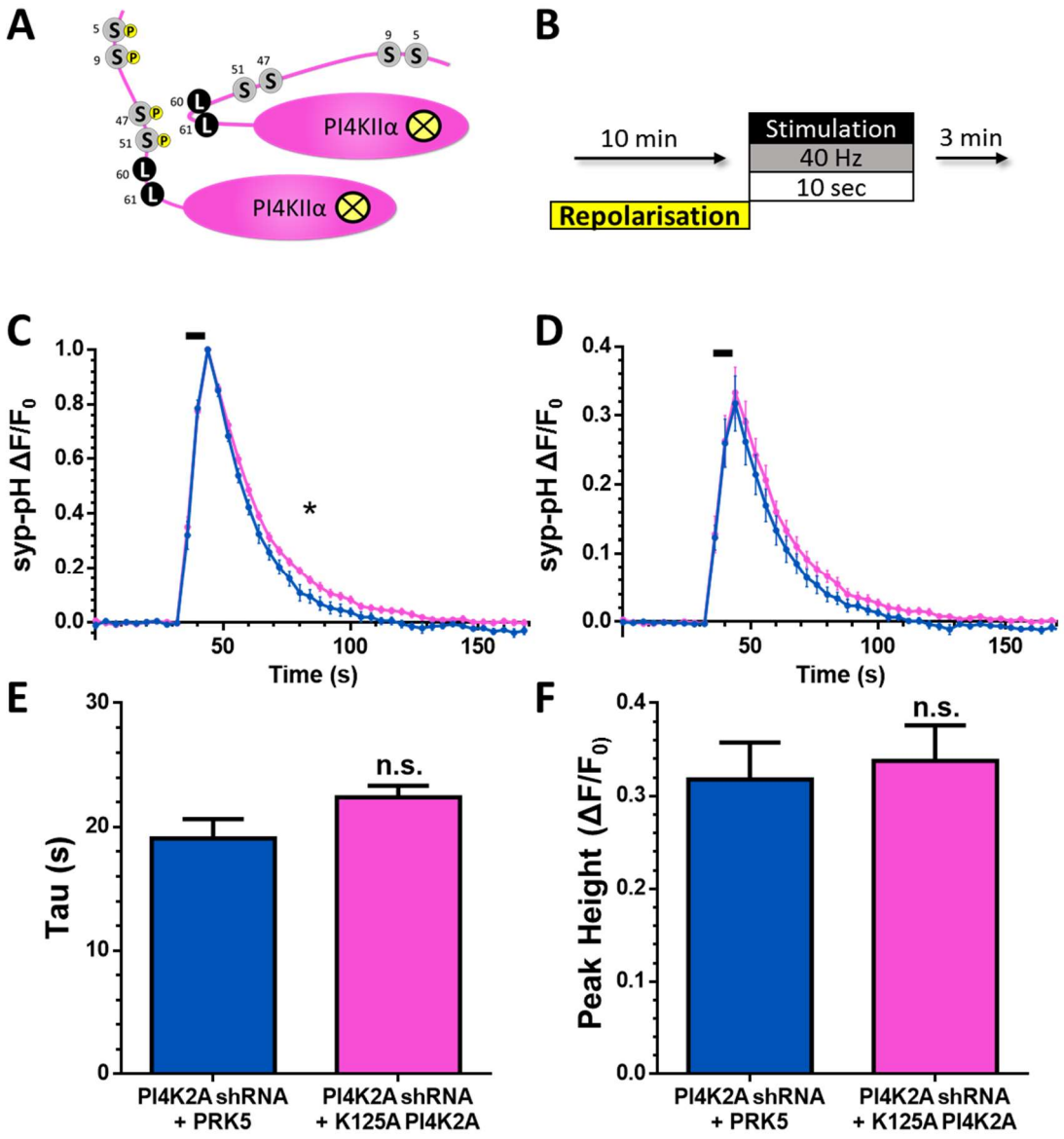

Figure 4.15 shRNA-Resistant K152A PI4KIIα does not Rescue Accelerated CME Knockdown Phenotype

CGNs were triple-transfected with PI4KIIα shRNA, synaptophysin-pHluorin (syp-pH) and either a PRK5 empty vector or a shRNA-resistant K152A PI4KIIα (A). B) Cells were incubated with imaging buffer for 10 minutes prior to stimulation and then continuously onwards. Cells were stimulated with a HFS train (400 AP, 40 Hz). C and D) PI4KIIα shRNA + PRK5 (blue) or + K152A PI4KIIα (pink). C) Average time trace ± SEM normalised to peak fluorescence is displayed with stimulation indicated by black bar. D) Average time trace ± SEM normalised to maximum ammonia pulse fluorescence is displayed with stimulation indicated by black bar E) Average endocytic kinetics of each condition (tau) + SEM. F) Average peak heights of each condition (F/F_0) + SEM. PI4KIIα shRNA + PRK5 n=9, PI4KIIα shRNA + K152A PI4KIIα n=12. Time traces: *=$p<0.05$, Two-way ANOVA, Bonferroni post-test. Bar charts: n.s., Student's t-test.

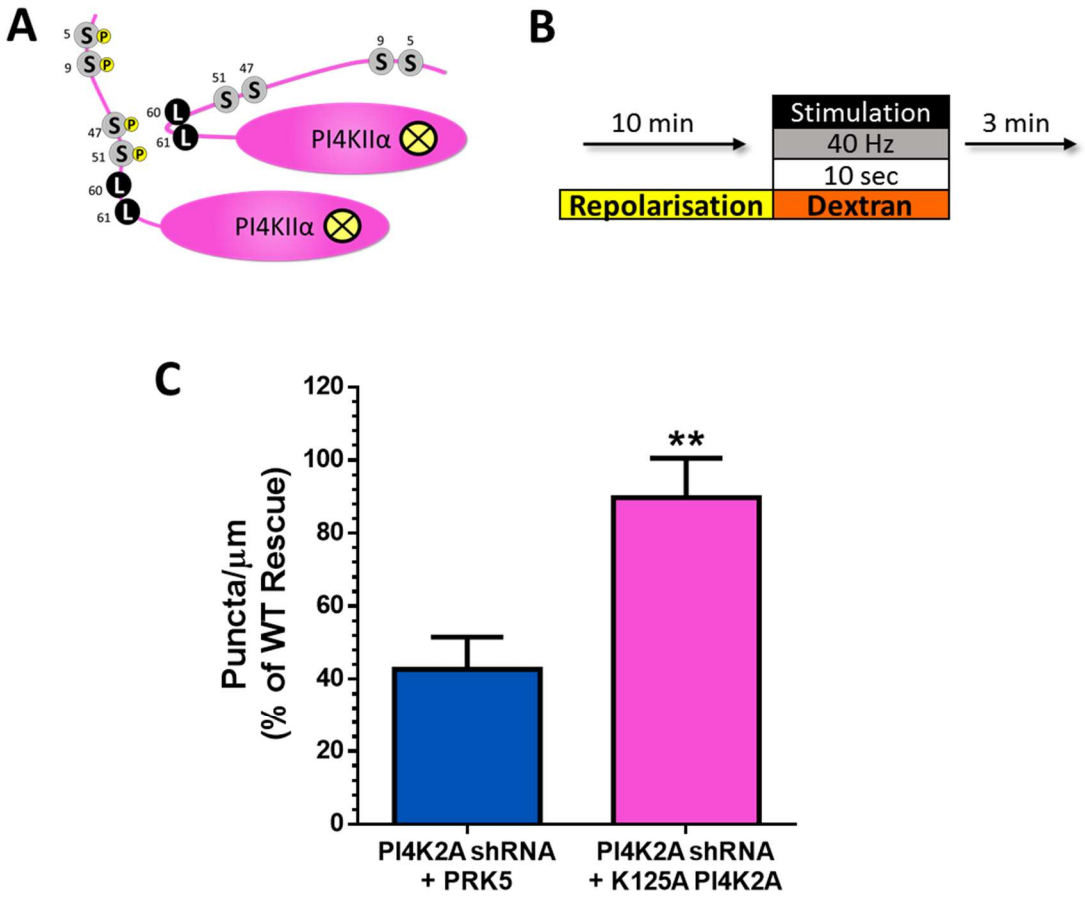

Figure 4.16 shRNA-Resistant K152A PI4KIIα Successfully Rescues Inhibited ADBE Knockdown Phenotype

CGNs were triple-transfected with PI4KIIα shRNA, an empty mCer vector and either an PRK5 empty vector or shRNA-resistant K152A PI4KIIα (A). B) Cells were repolarised in imaging buffer for 10 minutes. Cells were stimulated with a HFS train (400 AP, 40 Hz) in the presence of 50 µM dextran. C) Average number of dextran puncta per µm of axon expressed as a proportion of WT rescue + SEM. PI4KIIα shRNA + PRK5 n=32, PI4KIIα shRNA + K152A PI4KIIα n=30. **=p<0.01, Student's t-test.

4.2.3 Overexpression of Mutant PI4KIIα Reveals Differential Mechanisms for PI4KIIα Influence on Exocytosis, CME and ADBE

4.2.3.1 Overexpression Wild-Type PI4KIIα Causes Increased Exocytosis During HFS

When examining the ability of the shRNA-resistant wild-type PI4KIIα protein to rescue the phenotypes caused by silencing PI4KIIα a new role for PI4KIIα was revealed. Expression of WT PI4KIIα into a knockdown background caused an increase in peak height when compared to knockdown. This was interesting as no effect on peak height was seen with depleted PI4KIIα. The increase in the rate of CME means it is unlikely that an inhibitory effect on exocytosis was masked by a decrease in concurrent endocytosis and as such it can be stated with confidence that there was no effect on exocytosis with PI4KIIα depletion.

It is possible that this increase in exocytosis was caused by the relative overexpression of WT PI4KIIα in this rescue system when compared to endogenous PI4KIIα as measured in scrambled shRNA transfected cells (see Figure 4.6). If this is the case it would be assumed that this increase in exocytosis on HFS would be observable in CGNs overexpressing WT PI4KIIα without a concurrent knockdown of endogenous PI4KIIα.

To test this hypothesis, CGNs triple-transfected with syp-pH PI4KIIα KD, were compared to CGNs triple transfected with syp-pH, scrambled shRNA and either

PRK5 empty vector (syp-pH Control) or WT PI4KIIα (syp-pH WT Overexpression) (Figure 4.17 A). Cells were then subjected to a single HFS (Figure 4.17 B).

As well as investigating exocytosis, this experiment also allowed the opportunity to investigate and impact of PI4KIIα overexpression on endocytic rate. As knockdown of PI4KIIα increases the rate of CME it is possible that the overexpression of PI4KIIα could cause an opposite effect, slowing CME kinetics. When normalised to the peak of syp-pH fluorescence no difference in retrieval of syp-pH after stimulation was seen between syp-pH control and overexpression of WT PI4KIIα (Figure 4.17 C). When the tau values were quantified it was clear that no significant difference was seen between control and syp-pH WT overexpression whereas knockdown of PI4KIIα resulted in a comparable, reduced tau value as seen in previous HFS experiments (Figure 4.17 E).

To distinguish any change in exocytosis, the amount of syp-pH fluorescence increase upon stimulation was studied in relation to the total presence of syp-pH (as revealed by an ammonia buffer pulse at the end of each experiment). Using this method, a highly significant increase was seen in exocytosis during HFS for syp-pH WT overexpression when compared to syp-pH control time trace (Figure 4.17 D). It can be stated confidently that this increase in peak height is due to an increase in exocytosis as tau analysis shows that WT PI4KIIα does not cause modulation of CME. This reasoning can be further strengthened as the duration of the stimulus in the above protocol is sufficiently short that one would not expect to see an effect on peak height due purely to an endocytic defect. When peak heights were quantified this increase is still pronounced, however the values were not significant when

subjected to a one-way ANOVA (Figure 4.17 F). Despite this, analysis of the time trace itself testifies to a significant increase in exocytosis in the presence of WT PI4KIIα overexpression.

4.2.3.2 Overexpression of Quadruple Phospho-Mimetic PI4KIIα Causes Increased Exocytosis on HFS

I next examined any effects of overexpressing the quadruple phospho-mimetic QUAD-D PI4KIIα mutant which was previously used for rescue experiments. The nature of these mutations causes a change in the structure of the protein (see Figure 4.5) allowing consistent access for AP-3 whereas the wild-type PI4KIIα must undergo phosphorylation via GSK3 to gain this structural configuration. QUAD-D PI4KIIα was unable to rescue the accelerated CME phenotype caused by knockdown of PI4KIIα possibly due to its quick removal from the cytoplasm after expression.

CGNs were triple-transfected with syp-pH Control, syp-pH PI4KIIα KD or syp-pH, scrambled shRNA and QUAD-D PI4KIIα (syp-pH QUAD-D Overexpression) (Figure 4.18 A). Cells were subjected to a single HFS (Figure 4.18 B) and syp-pH fluorescence was monitored over time.

No significant difference between syp-pH Control and syp-pH QUAD-D Overexpression was seen in the rate of syp-pH retrieval after HFS when visualising the fluorescence traces normalised to peak height (Figure 4.18 C). When tau values were quantified it was also clear that the overexpression does not affect endocytic kinetics compared to control whereas PI4KIIα knockdown resulted in decreased tau values consistent with previous HFS experiments (Figure 4.18 E).

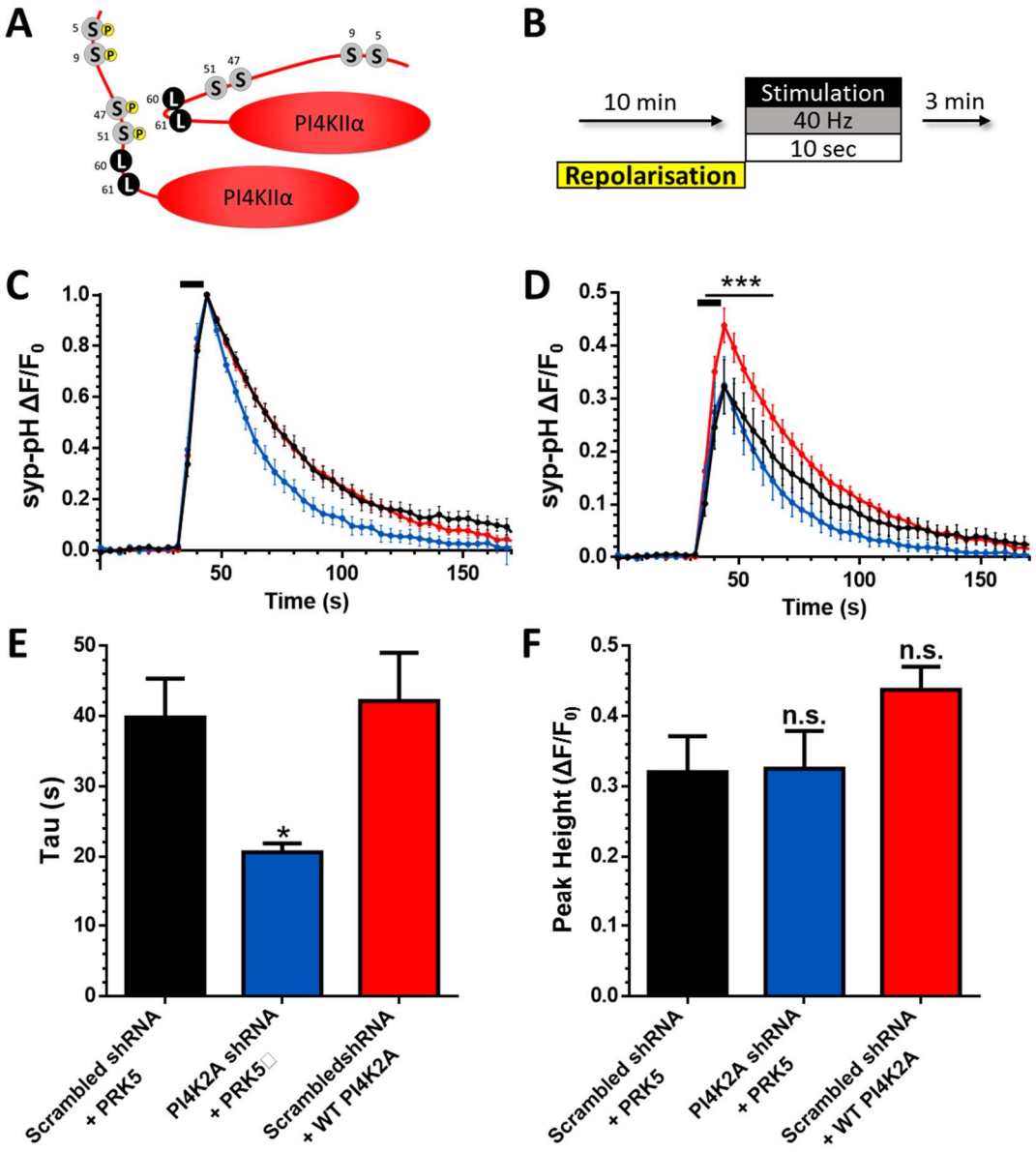

Figure 4.17 Overexpression of WT PI4KIIα Affects Peak Height But Not Endocytic Rate

CGNs were triple-transfected synaptophysin-pHluorin (syp-pH), scrambled shRNA with either an empty PRK5 vector or WT PI4KIIα (A) or PI4KIIα shRNA with PRK5. B) Cells were incubated with imaging buffer for 10 minutes prior to stimulation and then continuously onwards. Cells were stimulated with a HFS train (400 AP, 40 Hz). C and D) Scrambled shRNA + PRK5 (black), PI4KIIα shRNA + PRK5 (blue) or Scrambled shRNA + WT PI4KIIα (red). C) Average time trace ± SEM normalised to peak fluorescence with stimulation indicated by black bar. D) Average time trace ± SEM normalised to maximum ammonia pulse fluorescence with stimulation indicated by black bar E) Average endocytic kinetics of each condition (tau) + SEM. F) Average peak heights of each condition (F/F_0) + SEM. Scrambled shRNA + PRK5 n=8, PI4KIIα shRNA + PRK5 n=5, Scrambled shRNA + WT PI4KIIα n=7. Time traces: ***=p<0.001, Two-way ANOVA, Bonferroni post-test. Bar charts: *=p<0.05, One-way ANOVA to Scrambled PRK5.

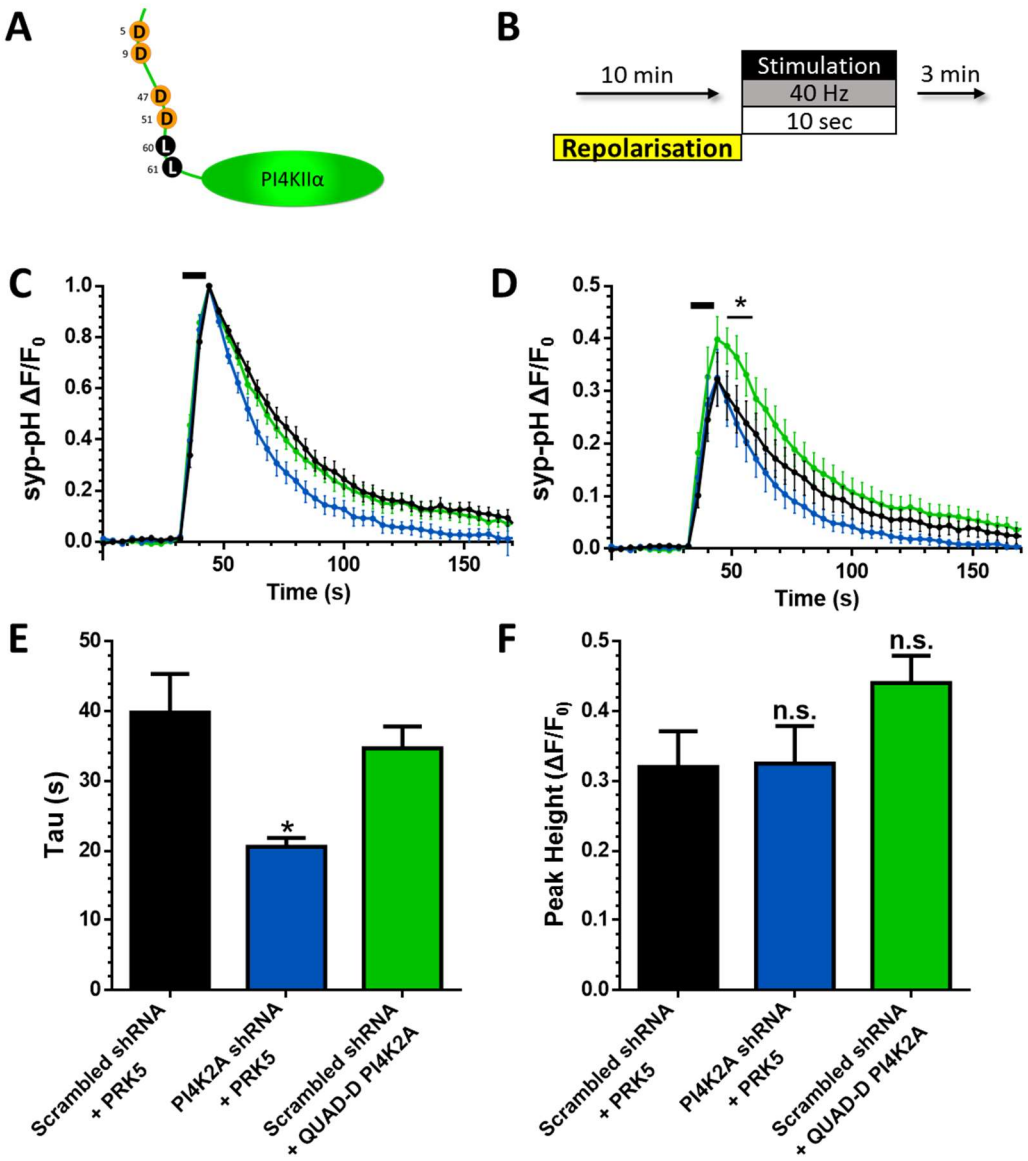

Figure 4.18 Overexpression of QUAD-D PI4KIIα Has a Mild Effect on Peak Height but not on Endocytic Rate

CGNs triple-transfected synaptophysin-pHluorin (syp-pH), scrambled shRNA with either an empty PRK5 vector or QUAD-D PI4KIIα (A) or PI4KIIα shRNA with PRK5. B) Cells were incubated with imaging buffer for 10 minutes prior to stimulation and then continuously onwards. Cells were stimulated with a HFS train (400 AP, 40 Hz). C and D) Scrambled shRNA + PRK5 (black), PI4KIIα shRNA + PRK5 (blue) or Scrambled shRNA + QUAD-D PI4KIIα (green). C) Average time trace ± SEM normalised to peak height with stimulation indicated by black bar. D) Average time trace ± SEM normalised to maximum ammonia pulse fluorescence with stimulation indicated by black bar E) Average endocytic kinetics of each condition (tau) + SEM. F) Average peak heights of each condition (F/F_0) + SEM. Scrambled shRNA + PRK5 n=8, PI4KIIα shRNA + PRK5 n=5, Scrambled shRNA (same data as seen in 4.17) + QUAD-D PI4KIIα n=9. Time traces: *=$p<0.05$, Two-way ANOVA, Bonferroni post-test. Bar charts: *=$p<0.05$, One-way ANOVA to Scrambled PRK5.

To examine any effect on exocytosis caused by syp-pH QUAD-D Overexpression traces were instead normalised to total syp-pH fluorescence elicited by an ammonia buffer pulse at the end of each experiment. A significant increase in evoked syp-pH fluorescence was seen after HFS in syp-pH QUAD-D Overexpression CGNs (Figure 4.18 D) in a similar manner to that seen in syp-pH WT Overexpression cells. Again, this increase in evoked fluorescence can be attributed to increased exocytosis as the rate of CME was unaffected by QUAD-D overexpression. When peak heights were analysed separately however this difference in peak height does not retain significance although the trend is clear (Figure 4.18 F). This result was unexpected as this increase in exocytosis was not observed when expressing QUAD-D in a PI4KIIα -depleted background.

4.2.3.3 Overexpression of S9/51A PI4KIIα Does Not Affect Either CME or Exocytosis

I next investigated any effect of overexpressing S9/51A PI4KIIα. This protein is constitutively closed in structure and has inhibited binding with AP-3 (Robinson et al. 2014).

When S9/51A PI4KIIα was expressed in a PI4KIIα knockdown background the rate of CME was increased to be significantly faster than the increased rate caused by the PI4KIIα knockdown. To determine if this phenotype was purely a consequence of S9/51A PI4KIIα being the dominant form of PI4KIIα in the cell or if this mutated PI4KIIα would exert the same effects on the rate of CME in a cell without PI4KIIα

depletion, the same experiment was performed without the knockdown of endogenous PI4KIIα.

CGNs were triple-transfected with syp-pH Control, syp-pH PI4KIIα KD or syp-pH, scrambled shRNA and S9/51A PI4KIIα (syp-pH S9/51A Overexpression) (Figure 4.19 A). Cells were subjected to a single HFS (Figure 4.19 B) and syp-pH fluorescence was monitored over time.

No significant effect was seen in the rate of CME either via observing the individual time traces (Figure 4.19 C) or via comparison of calculated tau values (Figure 4.19 E) between syp-pH Control and syp-pH S9/51A Overexpression. This shows that the S9/51A PI4KIIα does not have the ability to affect the kinetics of CME in the presence of endogenous PI4KIIα. The lack of effect on endocytic rate when S9/51A PI4KIIα is expressed in a cell which also contains endogenous PI4KIIα would suggest that this mutation does not lead to a gain-of-function with dominant-negative capabilities.

No effect of S9/51A PI4KIIα overexpression was seen on exocytosis when comparing syp-pH fluorescence traces (Figure 4.19 D), this is recapitulated when peak heights are calculated (Figure 4.19 F). This shows that the S9/51A mutation inhibits the ability of PI4KIIα to increase exocytosis with overexpression.

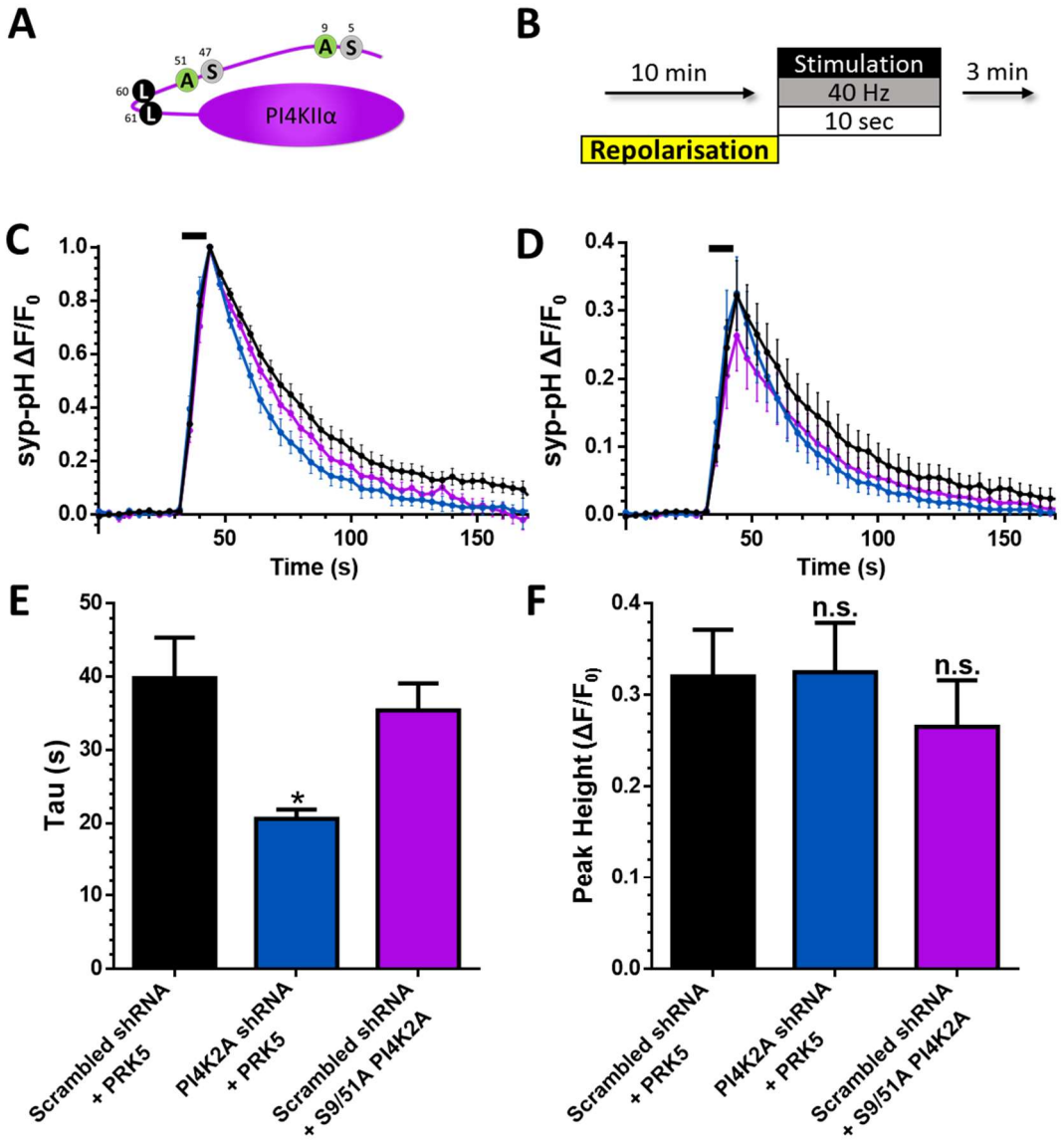

Figure 4.19 Overexpression of S9/51A PI4KIIα Does Not Affect Either Peak Height or Endocytic Rate

CGNs were triple-transfected synaptophysin-pHluorin (syp-pH), scrambled shRNA with either an empty PRK5 vector or S9/51A PI4KIIα (A) or PI4KIIα shRNA with PRK5. B) Cells were incubated with imaging buffer for 10 minutes prior to stimulation and then continuously onwards. Cells were stimulated with a HFS train (400 AP, 40 Hz). C and D) Scrambled shRNA + PRK5 (black), PI4KIIα shRNA + PRK5 (blue) or Scrambled shRNA + S9/51A PI4KIIα (purple). C) Average time trace ± SEM normalised to peak fluorescence with stimulation indicated by black bar. D) Average time trace ± SEM normalised to maximum ammonia pulse fluorescence with stimulation indicated by black bar E) Average endocytic kinetics of each condition (tau) + SEM. F) Average peak heights of each condition (F/F_0) + SEM. Scrambled shRNA + PRK5 n=8, PI4KIIα shRNA + PRK5 n=5, Scrambled shRNA + S9/51A PI4KIIα n=11. Bar charts: *=p<0.05, One-way ANOVA to

4.2.3.4 Overexpression of L60/61A PI4KIIα Does Not Affect Either CME or Exocytosis

I next investigated the effect of overexpressing the AP-3 binding mutant L60/61A PI4KIIα on the exocytosis and retrieval of syp-pH. Similar to S9/51A, L60/61A PI4KIIα expression in a PI4KIIα knockdown background increased the rate of CME to a rate which was significantly quicker than that observed in the PI4KIIα knockdown. As these two affected syp-pH retrieval similarly in the knockdown background and as both mutants contain mutations which inhibit AP-3 binding I would predict that both S9/51A and L60/61A would exert similar effects (or a lack thereof) on syp-pH response when overexpressed.

CGNs were triple-transfected with syp-pH Control, syp-pH PI4KIIα KD or syp-pH scrambled shRNA and L60/61A PI4KIIα (syp-pH L60/61A Overexpression) (Figure 4.20 A). Cells were subjected to a single HFS (Figure 4.20 B) and syp-pH fluorescence was monitored over time.

No significant effect was seen in the rate of CME either via observing the time traces (Figure 4.20 C) or via comparison of calculated tau values (Figure 4.20 E) between syp-pH Control and syp-pH L60/61A Overexpression. This is in line with what was observed with S9/51A PI4KIIα and shows that the overexpression of L60/61A PI4KIIα does not influence the kinetics of CME in the presence of endogenous PI4KIIα as might have been expected from additional quickening seen when L60/61A PI4KIIα is expressed in a knockdown background.

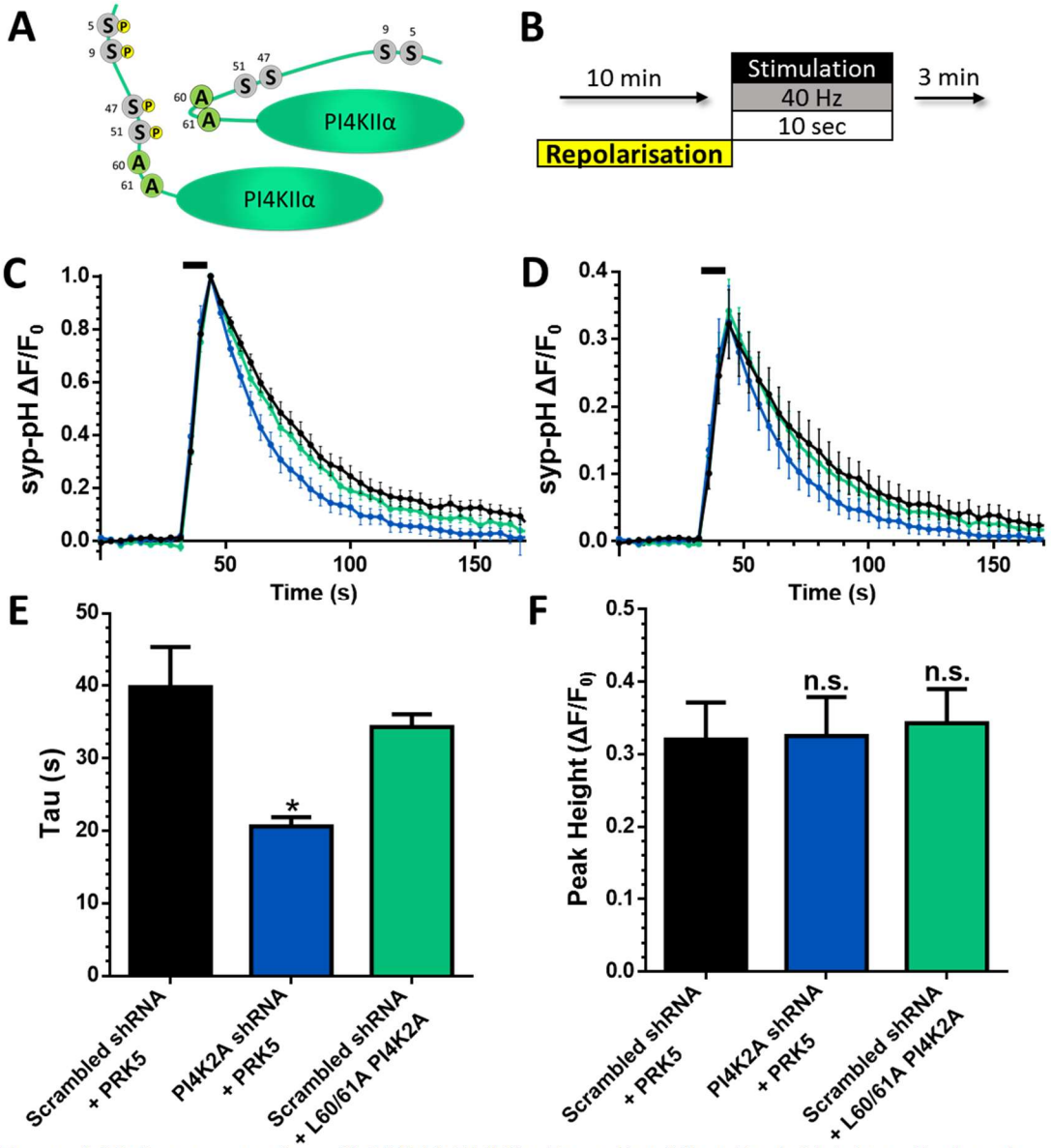

Figure 4.20 Overexpression of L60/61A PI4KIIα Does Not Affect Peak Height or Endocytic Rate

CGNs were triple-transfected synaptophysin-pHluorin (syp-pH), scrambled shRNA with either an empty PRK5 vector or L60/61A PI4KIIα (A) or PI4KIIα shRNA with PRK5. B) Cells were incubated with imaging buffer for 10 minutes prior to stimulation and then continuously onwards. Cells were stimulated with a HFS train (400 AP, 40 Hz). C and D) Scrambled shRNA + PRK5 (black), PI4KIIα shRNA + PRK5 (blue) or Scrambled shRNA + L60/61A PI4KIIα (turquoise). C) Average time trace ± SEM normalised to peak fluorescence with stimulation indicated by black bar. D) Average time trace ± SEM normalised to maximum ammonia pulse fluorescencewith stimulation indicated by black bar E) Average endocytic kinetics of each condition (tau) + SEM. F) Average peak heights of each condition (F/F_0) + SEM. Scrambled shRNA + PRK5 n=8, PI4KIIα shRNA + PRK5 n=5, Scrambled shRNA + L60/61A PI4KIIα n=8. Bar charts: *=$p<0.05$, One-way ANOVA to Scrambled PRK5.

No effect was seen on amount of exocytosis with overexpression of L60/61A PI4KIIα in comparison to control (Figure 4.20 D and F). This is in accordance with the results seen with the overexpression of S9/51A PI4KIIα, it is possible that AP-3 binding plays a role in the ability of PI4KIIα to increase exocytosis.

4.2.4 Overexpression of a Kinase-dead PI4KIIα has Dominant Negative Effects on Vesicle Recycling

The kinase-dead PI4KIIα was one of only two mutant forms of the protein which failed to cause any effect on the phenotype of knocking down PI4KIIα. If the effect of PI4KIIα knockdown on CME was due to a depletion in phosphorylated products of PI4KIIα (as could be assumed by a lack of rescue by a kinase-dead mutant) then one would assume overexpression of this kinase-dead mutant would have no effect on the endocytic kinetics of syp-pH after HFS.

CGNs were triple-transfected with syp-pH Control, syp-pH PI4KIIα KD or syp-pH, scrambled shRNA and K152A PI4KIIα (syp-pH K152A Overexpression) (Figure 4.21 A). Cells were subjected to a single HFS (Figure 4.21 B) and syp-pH fluorescence was monitored over time.

When observing the fluorescence time course, syp-pH K152A overexpression cells exhibit noticeably faster syp-pH endocytosis than syp-pH Control (Figure 4.21 C) resulting in a significant difference between the two traces. When taus were calculated, it becomes clear that overexpressing K152A causes a significant increase in the rate of CME when compared to syp-pH Control (Figure 4.21 E), resulting in similar kinetics to that seen in syp-pH PI4KIIα KD cells.

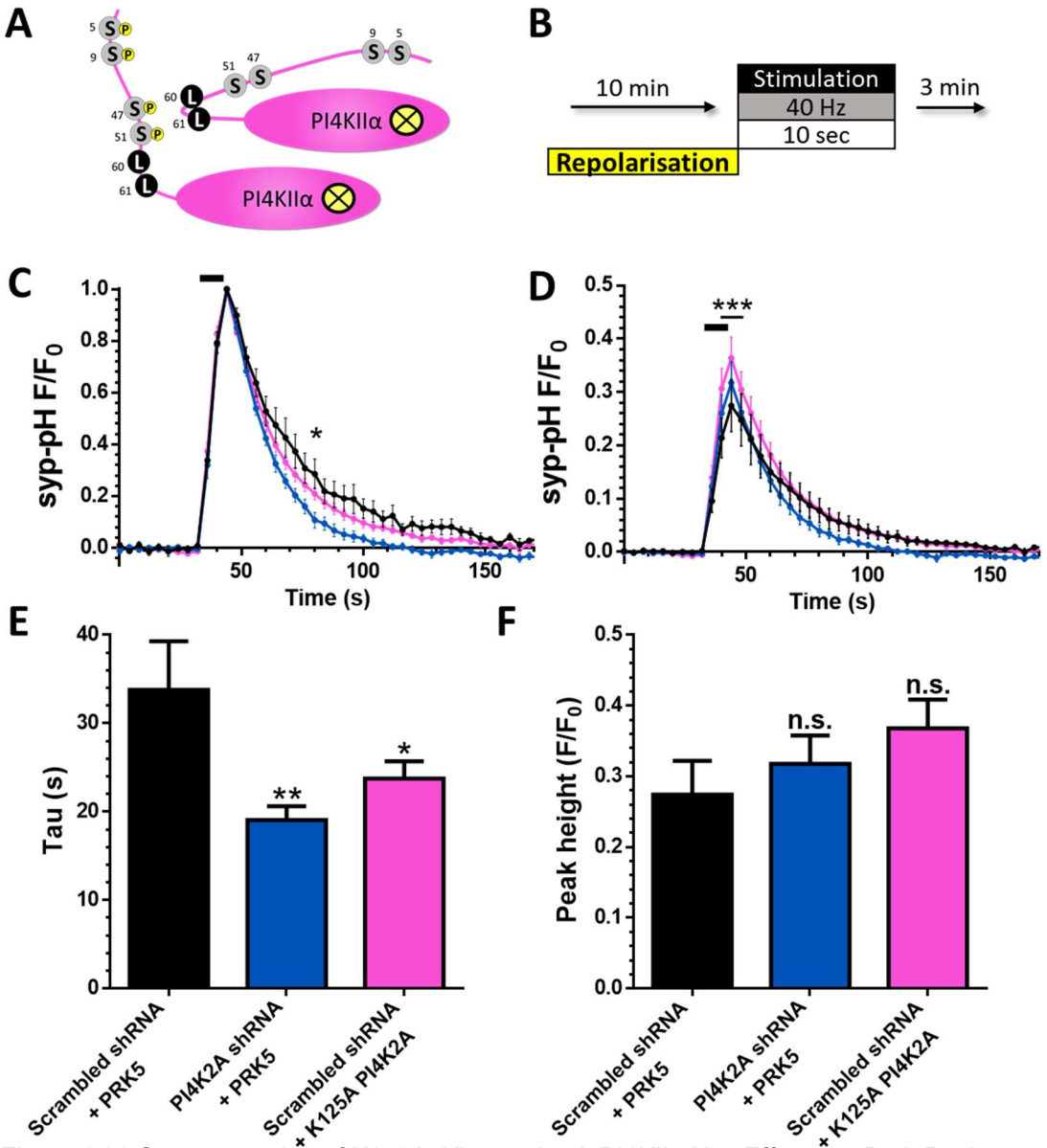

Figure 4.21 Overexpression of K152A, Kinase-dead, PI4KIIα Has Effects on Both Peak Height and Endocytic Rate

CGNs were triple-transfected synaptophysin-pHluorin (syp-pH), scrambled shRNA with either an empty PRK5 vector or K152A PI4KIIα (A) or PI4KIIα shRNA with PRK5. B) Cells were incubated with imaging buffer for 10 minutes prior to stimulation and then continuously onwards. Cells were stimulated with a HFS train (400 AP, 40 Hz). C and D) Scrambled shRNA + PRK5 (black), PI4KIIα shRNA + PRK5 (blue) or Scrambled shRNA + K152A PI4KIIα (pink). B) Average time trace ± SEM normalised to peak height is displayed with stimulation indicated by black bar. D) Average time trace ± SEM normalised to maximum ammonia pulse fluorescence is displayed with stimulation indicated by black bar E) Average endocytic kinetics of each condition (tau) + SEM. F) Average peak heights of each condition (F/F_0) + SEM. Scrambled shRNA + PRK5 n=8, PI4KIIα shRNA + PRK5 n=5, Scrambled shRNA + K152A PI4KIIα n=12. Time traces: ***=p<0.001, Two-way ANOVA, Bonferroni post-test. Bar charts:**=P<0.01, *=p<0.05, One-way ANOVA to Scrambled PRK5.

Another interesting phenotype caused by the overexpression of K152A PI4KIIα is a significant increase in evoked syp-pH fluorescence upon stimulation in comparison to syp-pH Control (Figure 4.21 D). This significant increase is again lost when peak heights of all 3 conditions are compared though the trend remains evident (Figure 4.21 F). Despite this it is clear from the fluorescence time traces that there is an increase syp-pH fluorescence upon stimulation which cannot be attributed to decreased endocytosis as it has been ascertained that the rate of CME is increased with this overexpression.

4.2.4.1 Overexpression of PI4KIIα Does Not Affect ADBE

As it is clear that the overexpression of PI4KIIα can have effects on the physiology of a nerve terminal, overexpression of each shRNA-resistant PI4KIIα was conducted in conjunction with an ADBE assay.

CGNS were triple-transfected with mCer empty vector, Scrambled shRNA and either a PRK5 empty vector (mCer Control) or WT (mCer WT Overexpression), QUAD-D (mCer QUAD-D Overexpression), S9/51A (mCer S9/51A Overexpression), L60/61A (mCer L60/61A Overexpression) or K152A (mCer K152A Overexpression) PI4KIIα. Cells were subjected to a single HFS in the presence of dextran (50 μM) (Figure 4.22 A).

Overexpression of different PI4KIIα mutants did not cause an increase in the number of synapses undergoing ADBE (Figure 4.22 B). However, I have shown that PI4KIIα activity is essential for ADBE. These results may suggest that once PI4KIIα

abundance is at a certain level it reaches a threshold and can have no further impact on ADBE.

In conclusion, utilising a series of manipulations including knockdowns, rescues and overexpressions I have ascertained roles for PI4KIIα expression and/or activity in CME, ADBE and exocytosis. Rescues and overexpression have shown different properties of the protein to be relevant to each phenotype, revealing multiple methods of action of this one kinase which affect all three processes (see Table 4.1).

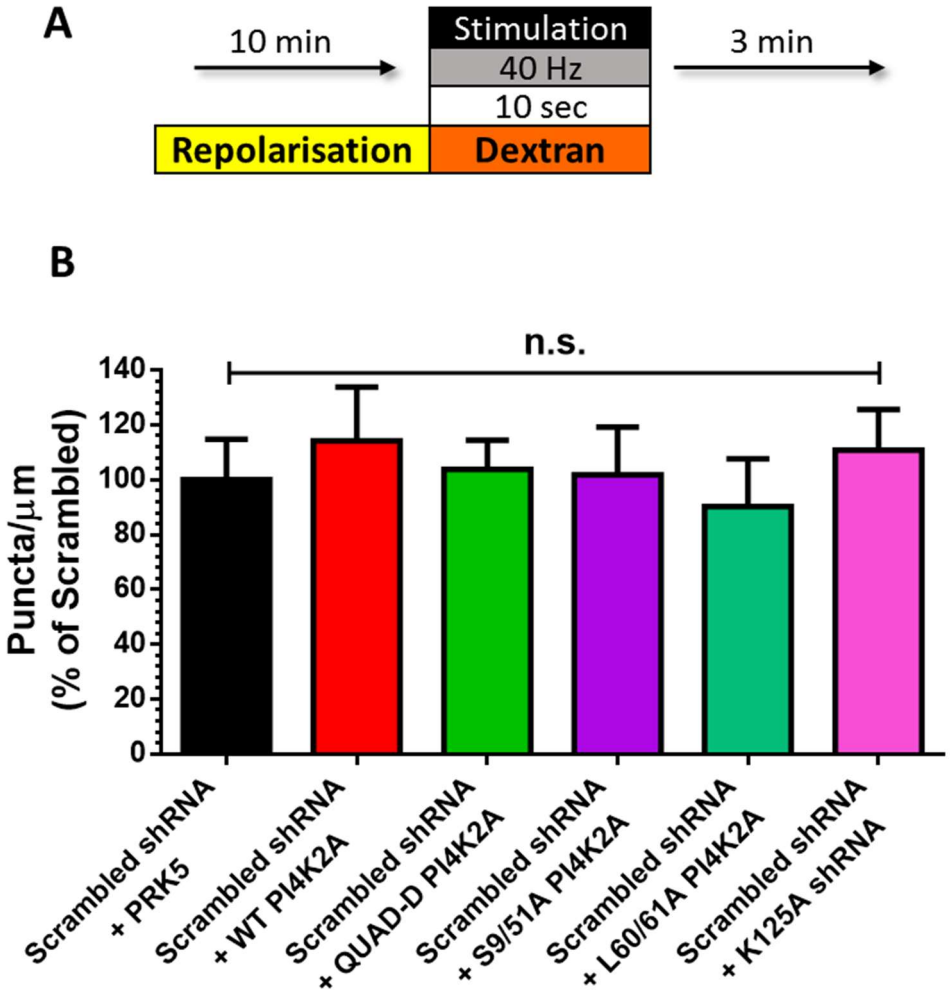

Figure 4.22 Overexpression of PI4KIIα Does Not Affect Dextran Uptake

CGNs were triple-transfected with an empty mCer vector, Scrambled shRNA and either an PRK5 empty vector or shRNA-resistant WT, QUAD-D, S9/51A, L60/61A or K125A PI4KIIα. (A) Cells were repolarised in imaging buffer for 10 minutes. Cells were stimulated with a HFS train (400 AP, 40 Hz) in the presence of 50 µM dextran. B) Average number of dextran puncta per µm of axon expressed as a proportion of scrambled shRNA + PRK5 + SEM. Scrambled shRNA + PRK5 n=25, Scrambled shRNA + WT PI4KIIα n=20, Scrambled shRNA + QUAD-D PI4KIIα n=20, Scrambled shRNA + S9/51A PI4KIIα n=18, Scrambled shRNA + L60/61A PI4KIIα n=19, Scrambled shRNA + L60/61A PI4KIIα n=19 . n.s. , One-way ANOVA to scrambled shRNA + PRK5 with Bonferroni post-test.

PI4KIIα	Effect	CME	ADBE	Exocytosis
KD	Depletion of PI4KIIα	Increased Rate	Inhibited	No Effect

PI4KIIα	Effect of Mutation	In KD Background (Rescue)			Overexpression		
		CME	ADBE	Exocytosis	CME	ADBE	Exocytosis
WT	None	Rescue	Rescue	Increased	No Effect	No Effect	Increased
QUAD-D	Permanently "Open" for AP-3 binding	No Rescue	No Rescue	No Effect	No Effect	No Effect	Increased
S9/51A	Permanently "Closed", no AP-3 binding	Further Increased Rate	Rescue	No Effect	No Effect	No Effect	No Effect
L60/61A	AP-3 Binding Site Ablated	Further Increased Rate	Rescue	No Effect	No Effect	No Effect	No Effect
K152A	Kinase-dead, Possible AP-3 Binding Deficit	No Rescue	Rescue	No Effect	Increased Rate	No Effect	Increased

Table 4.1 PI4KIIα Expression and Effects on Endo- and Exocytosis

4.3 Discussion

4.3.1 PI4KIIα Knockdown and its Consequences for SV Recycling

4.3.1.1 PI4KIIα Knockdown Inhibits ADBE

Above I have shown that ADBE is inhibited with the down-regulation of PI4KIIα (see Figure 4.4). PI4KIIα abundance is regulated via phosphorylation by GSK3, which is most active during basal conditions (Woodgett 1990). As such, one could interpret these results to mean that during extended periods of low activity, when GSK3-mediated PI4KIIα degradation is increased, a threshold for ADBE is raised. These results could also be interpreted conversely: in a chronically depolarised environment in which GSK3 is inhibited, the abundance of PI4KIIα increases due to a lack of degradation. This increase in PI4KIIα abundance causes an increased potential of the cell to perform ADBE which is needed during intense stimulation. This could show a method of chronic regulation of ADBE incidence through GSK3 activity.

4.3.1.2 PI4KIIα Knockdown Accelerates CME

As ADBE is decreased with a knockdown of PI4KIIα one might expect any inhibition of syp-pH retrieval to be attributable to this inhibition. However, as the rate of syp-pH retrieval during HFS is actually increased it is apparent that there is no inhibition on syp-pH uptake with inhibition of ADBE. Therefore, the increase in the

rate of syp-pH endocytosis must be assumed to be indicative of an increase in the rate of CME.

The effect on CME kinetics is only apparent at stimulation intensities in which ADBE would normally be activated. I hypothesised that the increased rate of CME is somehow coupled to the inhibition of ADBE. As the data shows the amount of exocytosis is unaffected with PI4KIIα knockdown it can be logically assumed that a cell in which PI4KIIα expression has been silenced experiences the same amount of inserted SV membrane. The most efficient method to compensate for this is to increase the rate of the other main form of endocytosis.

4.3.1.3 Protein-Specific Effects of PI4KIIα Knockdown

To assess the means through which PI4KIIα knockdown causes the phenotypes observed in both CME and ADBE one must consider all possible effects on the cell with the removal of PI4KIIα.

4.3.1.3.1 PI4KIIα Substrates and Further Metabolites

The depletion of PI4KIIα will have several effects. Firstly, as PI4KIIα is the only active PI4K isoform found on SVs (Guo et al. 2003) the amount of PI4P produced and residing on SVs will be decreased. This may cause an additional effect on the levels of other phosphoinositides for which PI4P is a precursor - $PI(4,5)P_2$ and $PI(3,4,5)P_3$. If the abundance of these two metabolites is not decreased however, it would mean a shift in the ratio of the three phosphoinositides within synapse.

Previous work has been done showing a necessity for certain phosphoinositides in the normal recycling of SVs and bulk endosomes. One study observed both syp-pH retrieval and ADBE incidence in PIPKIγ knockout mice. PIPKIγ is the main PI5K responsible for $PI(4,5)P_2$ production in synapses (Wenk et al. 2001). Without PIPKIγ there was a significant decrease in abundance of $PI(4,5)P_2$ in the brain (Di Paolo et al. 2004).

Cultured neurons from the PIPKIγ knockout mice exhibited a decreased rate of syp-pH endocytosis (Di Paolo et al. 2004). This shows that a decrease in $PI(4,5)P_2$ causes an effect in direct opposition to that caused by decreased PI4P such as would occur in PI4KIIα knockdown synapses. However, unlike my findings this slowing of endocytic kinetics was seen during mild stimulation. The retrieval of syp-pH during HFS was not investigated though the decrease in the rate of syp-pH endocytosis was conserved with prolonged stimulation.

PIPKIγ knockout mice also exhibited an increased number of bulk endosomes after stimulation as measured by HRP uptake (Di Paolo et al. 2004). Interestingly, the decreased abundance of $PI(4,5)P_2$ again results in an opposite phenotype to that seen with a decrease in PI4P as should be caused with knockdown of PI4KIIα.

These results could lead one to the conclusion that these phenotypes are purely caused by PI4P abundance: one might expect PIPKIγ knockout to result in a build-up of PI4P due to decreased conversion into $PI(4,5)P_2$. However, PIPKIγ knockout mice showed no alteration in PI4P abundance (Di Paolo et al. 2004).

It has previously been shown that silencing of PI4KIIα results in a decrease in PI4P abundance which was not recapitulated in $PI(4,5)P_2$ as one may expect (Ketel et al. 2016). These results could indicate that it may not be the overall abundance of these molecules but the proportions in which PI4P and $PI(4,5)P_2$ (and possibly $PI(3,4,5)P_3$) exist which can affect both CME and ADBE. It is possible that the opposition in proportions of these two phosphoinositide forms is what is in fact causing the observed phenotypes in both PI4KIIα knockdown (decreased PI4P and unaffected $PI(4,5)P_2$) and PIPKIγ knockout (decreased $PI(4,5)P_2$ but unaffected PI4P) systems. More work will be needed to investigate the effect of PI4KIIα knockdown on the abundance of all of these phosphoinositide forms in the cells used here.

It should also be noted that levels of PI itself could be the cause of phenotypic alterations seen with PI4KIIα knockdown. DGKθ is responsible for converting the signalling lipid dicylglycerol (DAG) into phosphotatidic acid (PtdOH) which serves as a precursor for PI. Recent work has shown that diacylglycerol kinase θ (DGKθ) knockout mice show a large depletion in PtdOH production in the brain. Neurons from these knockout mice displayed a dramatic slowing of CME (Goldschmidt et al. 2015). It is possible that the decrease in PI production caused by the decrease in PtdOH is responsible for the slowing in CME kinetics. This could correlate with the finding of increased rate in CME kinetics caused by a relative increase in PI on SVs caused by the removal of one of its main kinases on SVs: PI4KIIα.

4.3.1.3.2 AP-3 Binding and Localisation

A further effect of PI4KIIα knockdown is on the localisation of the adaptor protein AP-3. Previous work has shown a dependence on AP-3- PI4KIIα binding in localisation of both PI4KIIα and AP-3 to the early endosome, with a knockdown of PI4KIIα resulting in a higher cytosolic presence of AP-3 (Craige et al. 2008). Though this study was performed in HEK cells there is sufficient evidence to suggest the presence of early endosomes in nerve terminals (de Hoop et al. 1994; Wucherpfennig et al. 2003; Hoopmann et al. 2010) and as such this is a relevant observation when considering a role PI4KIIα in the presynapse. GSK3-mediated AP-3- PI4KIIα binding has also been shown to facilitate trafficking of PI4KIIα out of the synapse to the lysosome for degradation (Robinson et al. 2014). It is possible that in CGN terminals the knockdown of PI4KIIα facilitates an increased AP-3 abundance in the cytosol of the presynapse due to a disturbance in AP-3 trafficking to both early endosomes within and lysosomes without the nerve terminal.

Further work could be done to determine any role increased cytosolic AP-3 may play in either CME or ADBE. To date, no specific role for AP-3 has been found in CME. Investigations of the mocha mouse have shown a varied reliance of SV proteins in their recycling (Kantheti et al. 1998) with certain subpopulations of synaptic vesicles being depleted in these AP-3 deficient mice (Kantheti et al. 2003). These results have been attributed to an AP-3-dependent compensatory endocytosis and separate from CME (Voglmaier et al. 2006). However, in depth investigations using overexpression of AP-3 have not been conducted to study SV recycling and may elucidate whether

the increased cytosolic fraction of AP-3 caused by silencing PI4KIIα expression is implementing the observed acceleration of syp-pH retrieval during HFS.

This experiment would not reveal whether this retrieval is via classic CME or through another, AP-3-specific route. However, inhibition of CME-specific interactions via pharmacological means such as interrupting clathrin cage formation via Pitstop2-AM (Von Kleist et al. 2011) or genetic means such as silencing the expression of CME machinery such as clathrin heavy chain may reveal through what means any accelerated retrieval of SV proteins was occurring.

AP-3 has been shown to have a role in the budding of SVs from bulk endosomes but knockdown of AP-3 did not show any effect on ADBE as measured by dextran uptake (Cheung & Cousin 2012). The data acquired so far however, may suggest an effect of the increased abundance of AP-3 on ADBE. As such it may be pertinent to perform ADBE measuring assays such as HRP uptake in CGNs overexpressing AP-3. Equally as important could be the investigation into ADBE budding in PI4KIIα KD cells. If the theory of increased AP-3 abundance is correct, it is possible that this system will exhibit potentiated ADBE budding.

4.3.2 Wild-type and Mutant Versions PI4KIIα and What They Reveal About PI4KIIα Function

As it seems that the effects of PI4KIIα knockdown on CME and ADBE may have their roots in different properties of the protein, it is possible that each of these phenotypes is in fact being caused via separate mechanisms. Each form of PI4KIIα expression revealed varied roles for different functions of the protein (see Table 4.1). The effects of PI4KIIα manipulation were considered in context of both major effects of PI4KIIα knockdown in an attempt to form explanations of the effects seen with both rescue and overexpression of each of the PI4KIIα forms.

4.3.2.1 CME Kinetics Are Only Rescued by expression of WT PI4KIIα

In CGNs, CME is accelerated with a depletion of PI4KIIα (Figure 4.3). To investigate which specific property of PI4KIIα is essential for the role played in modulating CME a series of shRNA-resistant PI4KIIα proteins were expressed into both a knockdown background (rescue) and a background containing normal levels of PI4KIIα (overexpression).

4.3.2.2 Wild-Type PI4KIIα and CME Kinetics

Wild-type PI4KIIα was successful in rescuing the endocytic kinetics after CME. This shows a specificity in the action of PI4KIIα shRNA used. What was also interesting was that, despite an absence of PI4KIIα causing an acceleration of CME, an effective overexpression (see Figure 4.6) in this knockdown background did not cause an

inhibition in CME kinetics. Overexpression of this wild-type PI4KIIα in an endogenous PI4KIIα background also resulted in no effect on the retrieval kinetics of syp-pH. This could imply that the role of PI4KIIα in CME is not related to the kinase activity of the protein. One would assume that if a decrease of PI4P results in an acceleration of CME than an increase in PI4P would result in a deceleration, as this is not observed it is possible that PI4P is not integral to the role of PI4KIIα in CME. However, it is unknown if the overexpression of PI42KA would affect PI4P abundance in relation to that of $PI(4,5)P_2$ or $PI(3,4,5)P_3$ and as such the proportions of these molecules may be unaffected, resulting in a lack of phenotype.

These results could allow the explanation of CME being modulated by AP-3 abundance and localisation. CGNs are cultured in a depolarising medium, in which GSK3 is chronically inhibited. As such, it can be assumed that in control conditions PI4KIIα abundance is high as a result of an environment without much GSK3-mediated degradation. It is possible that if there is an upper-threshold of PI4KIIα abundance (or lower-threshold for AP-3 cytosolic abundance) to modulate CME that it has been reached within the chronically depolarised CGNs and as such experiments with overexpression may not result in further effects on the physiology of endocytosis. One potential method to explore this possibility would be to remove CGNs which have been transfected with overexpression constructs as well as the relevant control from their depolarising medium for a 24-hour period prior to experiments. This may have a modulating effect on PI4KIIα levels due to increased GSK3 activity. Differences observed between CME rates between control and overexpression conditions here may reveal the existence of an upper threshold of PI4KIIα abundance for the modulation of endocytosis.

4.3.2.3 Phospho-Mimetic PI4KIIα and CME Kinetics

Quadruple phospho-mimetic (QUAD-D) PI4KIIα is mutated to mimic PI4KIIα which has undergone phosphorylation by GSK3 and is thought to have a conformational change allowing access to AP-3 binding sites (Robinson et al. 2014). Expression of QUAD-D PI4KIIα into a P PI4KIIα knockdown background did not result in a reversal of the acceleration of CME kinetics.

The explanation as to the inability of QUAD-D PI4KIIα to rescue CME kinetics is difficult. This protein is able to bind AP-3 and as such should reverse any cytosolic increase caused by PI4KIIα knockdown. As such, this would raise questions as to the validity of the AP-3 argument for the function of PI4KIIα in CME.

However, it should be considered that endogenous PI4KIIα can exist in both GSK-phosphorylated or non-phosphorylated forms and therefore not all PI4KIIα proteins are accessible for AP-3 binding at any one time. However, QUAD-D PI4KIIα is innately accessible to AP-3. As AP-3 binding of PI4KIIα causes its relocation it is possible that QUAD-D is not located substantially on SVs in order to perform its kinase function and/or whatever modulating function it normally provides.

Unfortunately, it is unknown if the phosphorylation of PI4KIIα by GSK3 (or the mutation to mimic its phosphorylation) affects the kinase ability of the enzyme. The nature of the experimental medium would make the quantification of different phosphoinositide abundance impossible. This could be quantified if lentivirus vectors were used to infect whole cultures of CGNs and thin layer chromatography-blotting or autoradiography was implemented to measure the amount of incorporation of

radioactive phosphate groups. The ability to produce PI4P as well as its metabolites of each of the mutant forms of PI4KIIα used here is of vital importance to fully understand the implications of their effects on endocytosis and is something that will be explored in future.

Overall these results imply that phosphorylation of PI4KIIα on these sites, normally performed by GSK3, inactivates PI4KIIα in relation to its capacity in regulating CME. However, the mechanism by which this inactivation occurs is currently unclear.

4.3.2.4 Phospho-Null PI4KIIα and CME Kinetics

Two phospho-null mutants were utilised in rescue experiments – S9/51A and L60/61A. Both mutations interrupt the binding of AP-3 via two separate mechanisms. S9/51A contains a mutation of the serine priming sites on the N-terminal domain of PI4KIIα which allow GSK3 to phosphorylate serines 5 and 47. This inhibition of GSK3 phosphorylation means the N-terminal will not undergo its conformational change, opening its hairpin shape and allowing access to a di-leucine AP-3 binding motif. This mutation inhibits AP-3 binding. L60/61A contains mutations to the two residues making up this binding motif, preventing AP-3 binding.

Expression of both AP-3 binding deficient PI4KIIα versions into a knockdown background actually accelerates CME further than the knockdown in isolation (Figure 4.11 and Figure 4.12). It is unclear as to why expression of a mutated form of PI4KIIα would exacerbate a phenotype caused by its removal.

As both mutated forms PI4KIIα do not experience normal AP-3 binding it should be considered that this is the primary cause of this exacerbated phenotype rather than increased abundance of PI4KIIα itself as this accelerating phenotype is not seen with the "over-rescue" of PI4KIIα levels with the other shRNA-resistant forms of PI4KIIα when compared to endogenous levels. This is given further credence when one considers that overexpression of both of these mutated phenotypes does not cause the same acceleration of CME as seen in CGNs overexpressing S9/51A or L60/61A behave identically to scrambled controls (Figure 4.19 and Figure 4.20). This would not be the case if an increased abundance of these PI4KIIα forms in the nerve terminal alone was the cause of the effects seen with rescue.

It has been noted that when PI4KIIα with ablated AP-3 binding is expressed into a PI4KIIα knockdown background the cytosolic presence of AP-3 is increased (Craige et al. 2008). This is seemingly due to a necessity for this binding to relocate PI4KIIα and AP-3 to early endosomes and lysosomes (Craige et al. 2008; Robinson et al. 2014). When these AP-3 binding-deficient forms are expressed in the presence of endogenous PI4KIIα, normal binding of AP-3 would continue and therefore the increase in cytosolic AP-3 would not occur. This could explain the differences seen in syp-pH retrieval between rescue and overexpression with these phospho-null PI4KIIα mutants.

To further investigate the role of AP-3 abundance in the modulation of CME kinetics, further work could be performed utilising AP-3 overexpression or knockdown in conjunction with syp-pH retrieval. High resolution microscopy with immunofluorescence could also be performed on transfected cells to see if PI4KIIα

knockdown causes an increase in cytosolic versus membrane-bound AP-3 in a manner that is then exacerbated by a rescue with these phospho-null mutant forms of PI4KIIα.

Again, it is currently unclear as to whether these mutations hinder the kinase activity of PI4KIIα. Clarification of this matter in the future will allow a better understanding of the role PI levels may play in CME regulation.

4.3.2.5 Kinase-Dead PI4KIIα and CME Kinetics

Expression of a kinase-dead PI4KIIα (K152A) was incapable of rescuing the accelerated endocytosis phenotype seen in a knockdown background (Figure 4.15). This result is in accordance with the hypothesis that the rate of CME is somehow effected by the proportions of different phosphoinositides in the presynapse. A decrease in PI4P abundance or a shift in the ratio of PI4P to $PI(4,5)P_2$ could be causing the observed acceleration of CME in PI4KIIα knockdown cells which kinase-dead PI4KIIα is unable to rectify.

Overexpression of this kinase-dead mutant PI4KIIα also had an effect on the rate of CME (Figure 4.21). It is possible that this dominant-negative effect is caused by a K152A PI4KIIα competing with endogenous PI4KIIα for PI binding, inhibiting its action indirectly and causing a decrease in PI4P. As the acceleration of CME observed with overexpression of K152A PI4KIIα was not as dramatic as is observed with a knockdown it is apparent that any competitive inhibition caused by overexpressing K152A PI4KIIα is not entire and endogenous PI4KIIα is still capable of performing at least a portion of its function.

The AP-3 explanation could also fit these results. It has been shown that AP-3 binding is primarily modulated by the sorting motif on the N-terminal domain PI4KIIα. However, it is also regulated by its kinase function downstream of this domain (Craige et al. 2008). Therefore, it is possible that the lack of rescue observed with K152A expression in a knockdown background is actually due to a decreased binding probability with AP-3, resulting in an increased cytosolic AP-3 abundance in a similar but less dramatic manner than that observed with the other AP-3 binding deficient PI4KIIα forms (S9/51A and L60/61A).

The dominant negative effect of K152A overexpression is more complicated. In the same study mentioned above, a kinase-dead mutant form of PI4KIIα was used (D308A PI4KIIα) as well as mutant-specific PI4KIIα antibodies. The efficiency of cross-linking with AP-3 was analysed in comparison to WT PI4KIIα in rescue or wild-type backgrounds. In both backgrounds the D308A mutant lacking kinase function formed a cross-linkable complex with AP-3 with half the efficiency displayed with WT PI4KIIα (Craige et al. 2008). This paper did not however examine the localisation of AP-3 to early endosomes with this overexpression of kinase-dead PI4KIIα. It is possible that the dominant negative effect seen here with K152A PI4KIIα is due to a similar AP-3 binding effect. If K152A PI4KIIα binds 50% of AP-3 but is then not relocated to the endosome, it may mean that AP-3 is accumulating in the cytosol as is seen with PI4KIIα knockdowns.

4.3.2.6 Exocytosis is Increased with overexpression of PI4KIIα Able to Bind AP-3

The rescue of PI4KIIα with a shRNA-resistant form of wild-type PI4KIIα resulted in an increase in syp-pH exocytosis (Figure 4.7). The same effect was seen with an overexpression of wild-type PI4KIIα (Figure 4.17). It is unclear why overexpression of WT PI4KIIα would cause an increased peak height, especially as a knockdown of PI4KIIα had no effect on this variable (Figure 4.3). It is possible that this exocytic effect is symptomatic of this increase in PI4KIIα abundance and/or the products of the kinase activity of PI4KIIα in the nerve terminal in a manner that is not bidirectional.

As mentioned previously, it has been shown that the knockdown of PI4KIIα in one cell type causes a decrease in PI4P levels but does not result in a decreased abundance of $PI(4,5)P_2$ (Ketel et al. 2016). It is unknown if overexpression of PI4KIIα causes an increase in the levels of $PI(4,5)P_2$ though it is a possibility as an increased abundance of PI4KIIα would most likely lead to an increased production of its precursor PI4P. As it has previously been shown that a reduction in $PI(4,5)P_2$ production can lead to a smaller RRP (Di Paolo et al. 2004), it is possible that the converse is true and that in increasing the production of $PI(4,5)P_2$ somehow increases the number of SVs in the RRP, resulting in a larger release of syp-pH upon stimulation. It would tally that a decrease in syp-pH exocytosis was not seen within the knockdown system if it is the case that removal of PI4KIIα does not affect $PI(4,5)P_2$ production.

However, overexpression of kinase-dead PI4KIIα also caused an increase in syp-pH peak height during stimulation (Figure 4.21) making this explanation unlikely.

It is possible that this overexpression effect is somehow related to the relationship of PI4KIIα with AP-3. However, it is unclear how this effect would cause an exocytic effect in only one direction. Knockdown of PI4KIIα causes an increase in cytosolic AP-3 and it is possible that overexpression would cause an increase in AP-3 trafficking to both the endosome and lysosome, decreasing its presence in the cytosol. If the effect on exocytosis was in fact due to a relationship with AP-3 one would expect that a knockdown would cause a relative decrease in peak height. However, it is possible that there is a threshold of AP-3 which is required to modulate exocytosis and overexpression of PI4KIIα decreases cytosolic AP-3 to surpass this threshold. The fact that only the overexpression of forms of PI4KIIα able to bind AP-3, including kinase-dead PI4KIIα which experiences only partially ablated AP-3 binding (Craige et al. 2008), cause this phenotype makes this a more likely explanation for this increase in syp-pH exocytosis.

4.3.2.7 Inhibition of ADBE Is Successfully Rescued by All But Phospho-Mimetic Mutant

The role for PI4KIIα in the formation of bulk endosomes during HFS is harder to theorise. Wild-type, phospho-null and kinase-dead versions of PI4KIIα were all capable of rescuing the inhibition of ADBE caused by knockdown of PI4KIIα (Figure 4.8,-11,-13,-15 and -17). Only QUAD-D was incapable of restoring normal dextran uptake.

From these results, it can be inferred that the kinase function of PI4KIIα is not essential in the normal function of ADBE. Nor is AP-3 binding/abundance. Together with data collected using syp-pH it can also be deduced that the effects of PI4KIIα knockdown on both ADBE and CME are not functionally coupled. This is demonstrated by phospho-null PI4KIIα rescue causing an exacerbation of the CME phenotype (Figure 4.11 and Figure 4.12) but a full rescue of ADBE (Figure 4.13 and Figure 4.14). The overexpression of K152A PI4KIIα in cells expressing endogenous PI4KIIα also had no observable effect on the amount of dextran uptake in comparison to control (Figure 4.22), showing a lack of a dominant-negative action of kinase-dead PI4KIIα on ADBE unlike that seen on CME.

The phospho-mimetic form of PI4KIIα was somehow incapacitated with regards to its role in ADBE. This indicates that GSK3 phosphorylation somehow inactivates PI4KIIα. As this effect is not tied in with the kinase or AP-3 binding properties of the protein, the theories of this mutation connected to altered AP-3 abundance and PI4P production are not relevant to ADBE. However, one property of QUAD-D PI4KIIα which could impact on its function in ADBE is its location. As discussed earlier, it is likely that QUAD-D PI4KIIα is more quickly and more efficiently bound by AP-3 than its wild-type counterpart. If this is true it is more quickly and efficiently trafficked away from SVs. This would mean not only a decrease in PI4KIIα on SVs but also a decrease in PI4P production on SVs. However, as the kinase-dead form of PI4KIIα rescues ADBE it is unlikely that PI4P is the critical component for functional ADBE. It is possible that PI4KIIα must simply be present for the normal formation of bulk endosomes. This may mean that PI4KIIα is a marker for yet-to-be

identified ADBE-specific cargo or adaptor proteins to initiate invagination upon HFS.

Overexpression of all forms of PI4KIIα had no effect on the incidence of ADBE as measured by dextran uptake. This would imply that, although a knockdown of PI4KIIα causes an inhibition of ADBE, overexpression of PI4KIIα has no effect on ADBE incidence. However, this conclusion has two caveats: firstly, the cell type used in these experiments may be prone to physiologically high PI4KIIα abundance due to its depolarised culture conditions and as such any effect of PI4KIIα on ADBE in control conditions may already be saturated. Performing these experiments in cell types cultured in a non-depolarising medium with a lower innate PI4KIIα abundance may reveal a bi-directional effect of PI4KIIα abundance. Secondly, dextran is not a measure of the amount of ADBE occurring in each nerve terminal but a measure of how many synapses in a given length of axon are undergoing ADBE. To measure the number of bulk endosomes per synapse the use of a lentiviral vector would again be needed to induce a culture-wide infection of relevant DNA. Once this was attained an HRP-uptake assay could be performed and imaged using electron microscopy. In lieu of a more accurate, live-cell assay this would be the most accurate method to quantify bulk endosome formation per synapse in CGNs with manipulated PI4KIIα expression.

Much more work is needed to identify the specific nature of the role of PI4KIIα in ADBE. One area of focus should be the interaction of PI4KIIα with endocytic machinery and the effects of each of the mutations used here on those interactions. Interactions between PI4KIIα and many endocytic proteins such as endophilin,

SNX9, SNX18 and SGIP1 are inhibited via ubiquitination of PI4KIIα (Mössinger et al. 2012). Interestingly, the site of ubiquitination is within 10 residues of one site for GSK3 phosphorylation (Ser 5/9). As such it is a possibility that phosphorylation by GSK3 (or mutations such as QUAD-D) could also cause this block in normal interactions possibly inactivating PI4KIIα with regards to its role in endocytosis. Performing GST-pull downs on WT PI4KIIα alongside each of the available mutant forms may give a clearer picture as to the role of GSK phosphorylation in PI4KIIα function with regards to endocytosis. It may also offer an explanation as to the failure of QUAD-D to rescue both CME and ADBE phenotypes.

In conclusion, a role for PI4KIIα has been revealed in both CME and ADBE in CGNs during HFS. I have also found that different properties of the PI4KIIα protein are responsible for its action in both of these although the precise nature of its method of action is still unidentified. Future work will focus on phosphoinositide effects through PI4KIIα manipulation. AP-3 abundance and localisation will also warrant further investigation as to roles in the recycling of synaptic vesicle proteins via CME. A detailed analysis of phospho-dependent interactions between PI4KIIα and presynaptic proteins may reveal important information about PI4KIIα function, especially in the context of ADBE.

A Variety of pHluorins Preferentially

Report CME

5. A Variety of pHluorins Preferentially Report CME

5.1 Introduction

In the previous chapter the knock-down of PI4KIIα resulted in an inhibition of ADBE along with an acceleration of CME. These results raised questions as to the possible coupling between CME and ADBE. One hypothesis is that the absence of PI4KIIα was only directly affecting one of these endocytic modes and the other was merely compensating for that change. Therefore, it is possible that ADBE was decreased due to increased CME capacity or vice versa. Further experimentation however seemed to show a functional separation of these two endocytic modes, with ADBE inhibition being rescued by mutant forms of the protein which did not rescue, and actually exacerbated, the accelerated CME phenotype (see Figure 4.11, Figure 4.12, Figure 4.13 and Figure 4.14).

In light of these results, further experiments were required to investigate the bi-directionality of inhibition or facilitation of one endocytic mode due to an effect on the other. It is important to investigate this problem more precisely, manipulating those proteins directly involved with either CME or ADBE as it is possible that the expression of mutant PI4KIIα disturbed this natural coupling between endocytic modes.

Previous work has examined the effect of manipulating CME-specific machinery such as Clathrin Heavy Chain (CHC) or adaptor-protein 2 (AP-2) on the recycling of synaptotagmin-pHluorin (Kononenko et al. 2014) and found a slowing in the retrieval of this SV protein only during mild stimulation. Work utilising the acute

relocation of a FKBP-tagged protein (re-routing) (M. S. Robinson et al. 2010), has shown a dependence on clathrin and stonin-2 for endocytosis of synaptophysin-pHluorin (syp-pH) (Willox & Royle 2012). However, these experiments did not explore the effects on pHluorin recycling caused by manipulating of ADBE in isolation from CME. Therefore, a series of experiments were conducted to systematically approach the issue investigating the roles of both forms of endocytosis in the recycling of a variety of SV proteins.

Effects of specifically blocking either CME or ADBE on the recycling of a variety of tagged SV proteins were investigated using a selection of genetic or pharmacological manipulation. Genetically encoded versions of the most abundant SV proteins, tagged with pHluorin molecules, were used; synaptobrevin II-pHluorin (sybII-pH) and syp-pH, synaptotagmin 1-pHluorin (tagmin-pH) and vGLUT 1-pHluorin (vGlut-pH).

A further rationale for these experiments was to assess the role of ADBE in the recycling of these SV cargoes. It is currently unknown what role ADBE has in reclaiming SV cargo inserted into the PM upon exocytosis and whether it performs this role with any specificity. For example, does ADBE have its own adaptor proteins which specifically recognise SV cargo or does it simply invaginate SV cargo along with the large portion of membrane without selection? It was hoped that the individual manipulation of these endocytic routes could identify any proportion of SV cargo retrieved via ADBE compared to CME.

5.2 Results

5.2.1 Pharmacological Inhibition of ADBE has no Effect on the Recycling of Several pHluorins

5.2.1.1 CGNs Display no Significant Trafficking of Synaptophysin-pHluorin via ADBE During HFS

The rate of endocytosis can be revealed using pHluorins. After cessation of stimulation, exocytosis has stopped and the fluorescence of a transfected cell decreases as those pHluorin molecules which have been exposed to the extracellular space via exocytosis undergo endocytosis and their new vesicles/endosomes acidify. However, the rate of fluorescence decrease after stimulation is technically a function of the rate of both acidification and of endocytosis. The process of CME acidification using pHluorins similar to those used in this thesis was estimated as 4-5 seconds (Sankaranarayanan & Ryan 2000; Atluri & Ryan 2006). With acidification occurring so rapidly after endocytosis, one can use the kinetics and extent of the quenching of fluorescence of pHluorins to equate the rate and extent of CME.

During mild stimulation the dominant form of endocytosis is CME (Granseth et al. 2006; Zhu et al. 2009), therefore the observed endocytosis of pHluorin is due to internalisation via this endocytic mode. However, during HFS CME reaches its maximum capacity (Sankaranarayanan & Ryan 2000) and another form of membrane retrieval is required. During these stimulation conditions both CME and ADBE occur in the presynapse, with ADBE being the dominant mode of membrane retrieval under these conditions (Royle & Lagnado 2003; Wu et al. 2007; Clayton et al. 2008).

It is currently unknown what role ADBE plays in the specific retrieval of SV cargo and, by extension, what portion of the observed endocytosis of a population of pHluorin molecules can be attributed to ADBE.

To isolate what, if any, fraction of pHluorin-tagged SV protein syp-pH is internalised via ADBE during HFS a stimulation protocol was designed wherein two sequential and identical stimulations "S1" and "S2" were delivered to a syp-pH transfected CGN in the presence of the GSK3 and Cdk5 inhibitors CT99021 (CT, 2 μM) and roscovitine (10 μM) respectively (Figure 5.2 A).

CT and roscovitine do not interfere with ADBE during a priming HFS "S1" (400AP, 40 Hz) as it does not affect dynamin I dephosphorylation by calcineurin (Clayton et al. 2010). However these drugs prevent GSK3 and Cdk5 from rephosphorylating dynamin I, an action which is required to allow ADBE in a second HFS "S2" (Clayton et al. 2010). The effect on ADBE via GSK3/Cdk5 inhibition can be visualised via the uptake of dextran during S2 with/without CT or roscovitine respectively (Figure 5.1). The mechanism of action for these compounds allows the comparison of an HFS-evoked syp-pH response with the contribution of ADBE during S1 to that in the absence of ADBE during S2 (Figure 5.2 A).

Peak heights and endocytic time constants (tau – τ) were taken from time-lapse traces of pHluorin fluorescence of all conditions (see 2.2.5.1.4.1): control, CT, roscovitine and CT plus roscovitine (Figure 5.2 B, C, D and E respectively). Ratios of peak heights (S1/S2) and taus (S1/S2) (Figure 5.2 G) from individual syp- pH responses were compared between all conditions to visualise differences in response during S2 due to the removal of ADBE.

There were no significant differences observed either in the S1/S2 peak height ratio (Figure 5.2 F) or tau ratio (Figure 5.2 G) during inhibition of either GSK3 by CT or Cdk5 by roscovitine or by the two in combination when compared to control. This implies that inhibition of ADBE does not impact on either the amount of exocytosis or the kinetics of endocytosis (depicted by peak height and tau values respectively) meaning that ADBE may not play a significant role in the recycling of syp-pH during HFS.

To assess if ADBE's lack of contribution to SV cargo recycling is limited to syp-pH, a series of further experiments utilising other commonly used pHluorins were performed.

Using the same "S1 S2" protocol the role of ADBE was assessed in the recycling of vGlut-pH, tagmin-pH and sybII-pH (Figure 5.3 A, Figure 5.4 A and Figure 5.5 A). Ratios of peak heights (S1/S2) and tau values (S1/S2) of the response of each pHluorin was compared between control and CT conditions (Figure 5.3, Figure 5.4 and Figure 5.5 B and C respectively). No significant differences were seen with the inhibition of ADBE by CT either in peak height or tau ratio for any of these

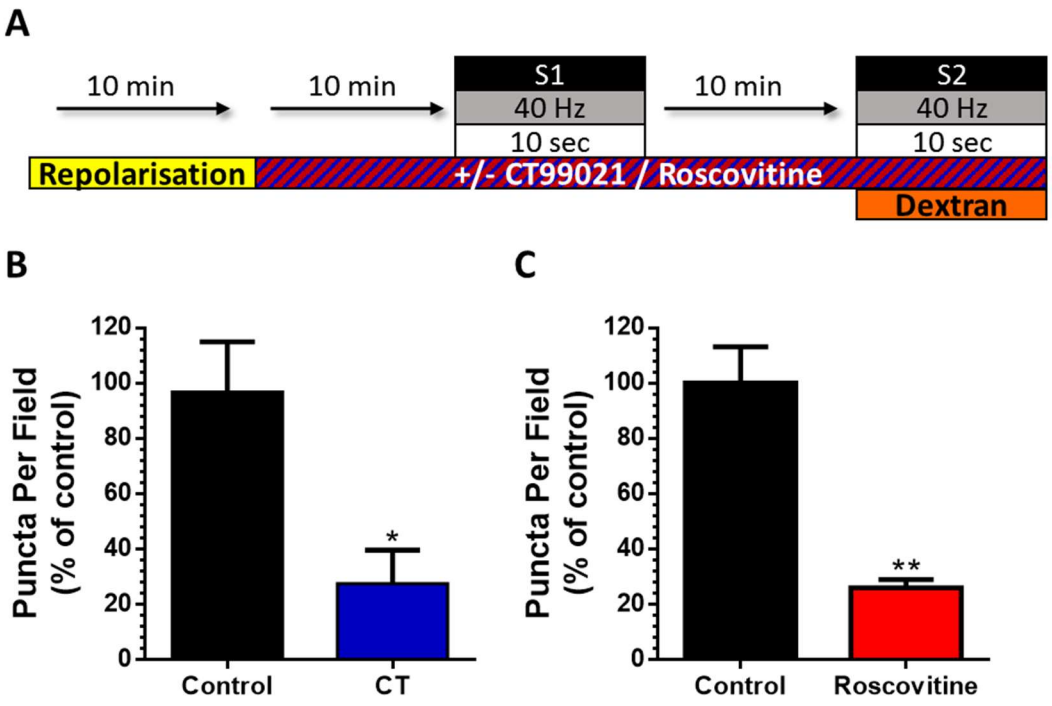

Figure 5.1 CT and Roscovitine effectively Inhibit ADBE

A) CGNs were repolarised in imaging buffer for 10 minutes prior to incubation with imaging buffer alone (Control) or supplemented with 2μM CT99021 (CT) or 10 μM Roscovitine for 10 minutes. Cells were stimulated with a HFS train (400 AP, 40 Hz) (S1) and allowed to recover for 10 minutes. Cells were then stimulated with a second HFS train (S2) in the presence of 50 μM dextran. B) and C) Average dextran puncta per field + SEM for Control Vs. CT (B) or Control Vs, Roscovitine (C). Control n=4, CT n=5 (B). Control n=3, Roscovitine n=3 (C). *=$p<0.05$, **=$p<0.01$. Student's t-test.

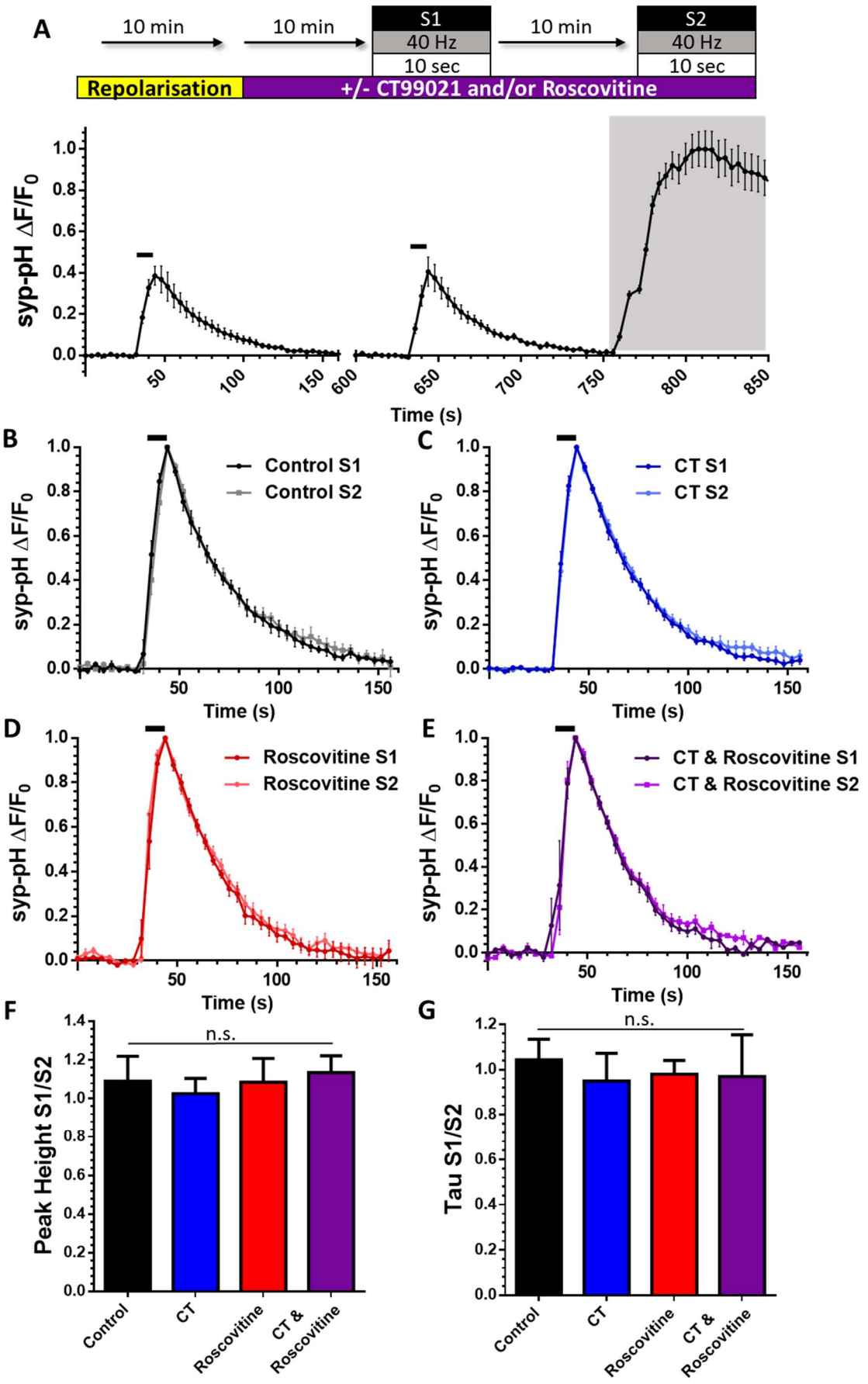
A
10 min
10 min
S1
40 Hz
10 sec
10 min
S2
40 Hz
10 sec
Repolarisation
+/- CT99021 and/or Roscovitine
syp-pH ΔF/F0
Time (s)
B
Control S1
Control S2
C
CT S1
CT S2
D
Roscovitine S1
Roscovitine S2
E
CT & Roscovitine S1
CT & Roscovitine S2
F
Peak Height S1/S2
n.s.
Control
CT
Roscovitine
CT & Roscovitine
G
Tau S1/S2
n.s.
Control
CT
Roscovitine
CT & Roscovitine

Figure 5.2 Pharmacological Inhibition of ADBE has no Effect on Synaptophysin-pHluorin Recycling.

A) Protocol (top) and representative control trace (bottom) of experiment: Repolarised CGNs transfected with synaptophysin-pHluorin (syp-pH) were incubated with imaging buffer (control) supplemented with either 2 µM CT99021 (CT), 10 µM roscovitine or both 10 minutes and then continuously onwards. Cells were challenged with 2 sequential HFS trains (400 AP, 40 Hz) (S1 and S2) 10 minutes apart and then challenged with 50 mM NH_4Cl (shaded region). B-E) Average time course ($\Delta F/F_0$) $\pm$ SEM of S1 overlaid with S2 for control, CT, roscovitine and CT plus roscovitine respectively. All stimulations were normalised to the evoked peak height. Black bars represent stimulation. F) Average ratios of peak height ($\Delta F/F_0$) S1/S2 + SEM G) Average ratios of tau values (s) S1/S2 + SEM. Control n=6, CT n=5, Roscovitine n=6, CT/Roscovitine n=4. n.s., one-way ANOVA with Bonferroni post-test.

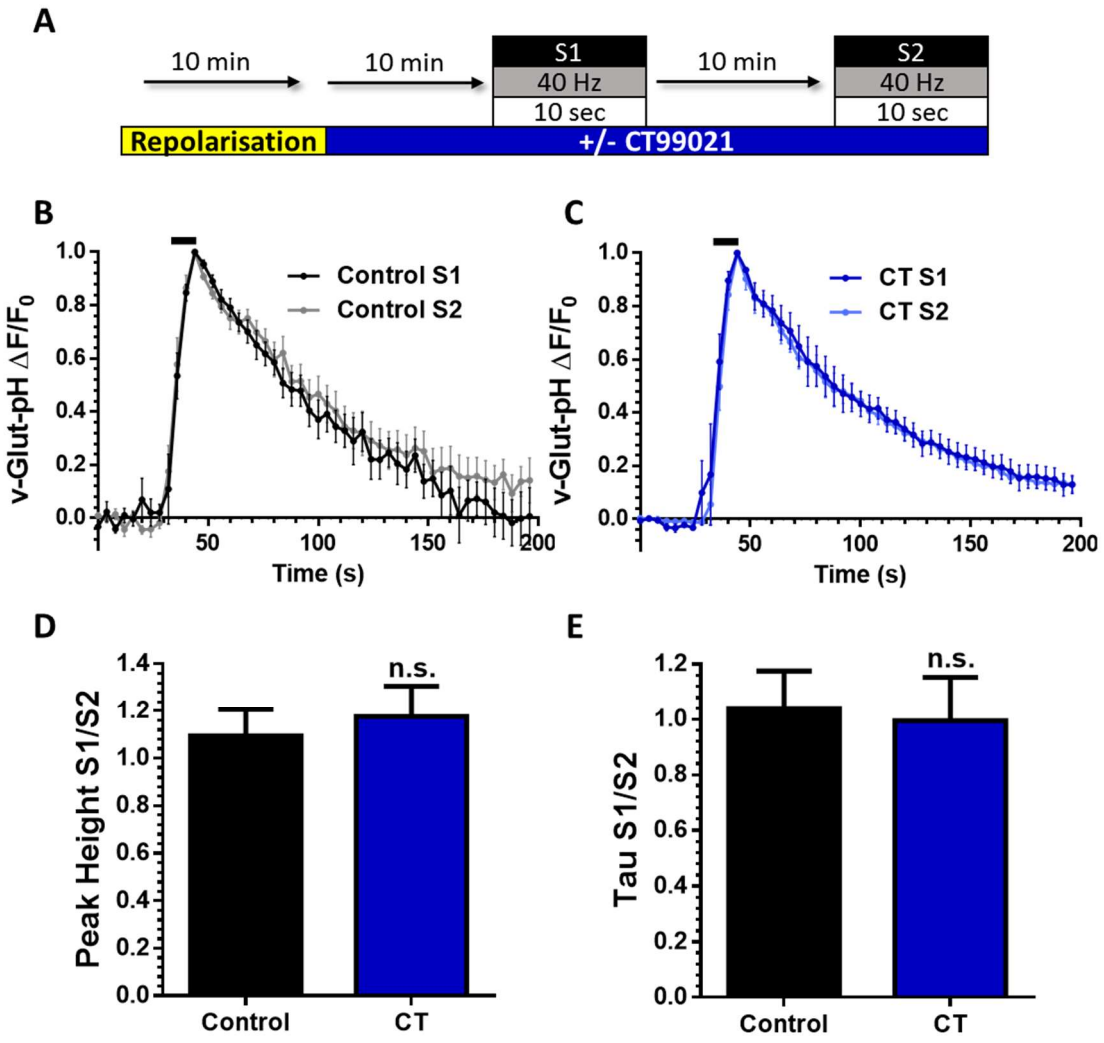

Figure 5.3 Pharmacological Inhibition of ADBE does not Affect on vGlut-pHuorin Recycling

A) “S1 S2” experiment. CGNs co-transfected with mCer and vGlut-pHluorin (vGlut-pH) were incubated with imaging buffer for 10 minutes before being incubated in imaging buffer alone (control) or supplemented with 2 μM CT99021 (CT) for 10 minutes prior to S1 and then continuously onwards. Cells were challenged with 2 sequential HFS trains (400 AP, 40 Hz) (S1 and S2) 10 minutes apart. B and C) Average time traces ± SEM of S1 overlaid with S2 for control and CT respectively. D) Average ratio value of peak height (F/F_0) S1 over peak height S2 + SEM. E) Average ratio of tau (s) S1 over S2 + SEM. Control n=6, CT n=5. n.s., Student’s t-test.

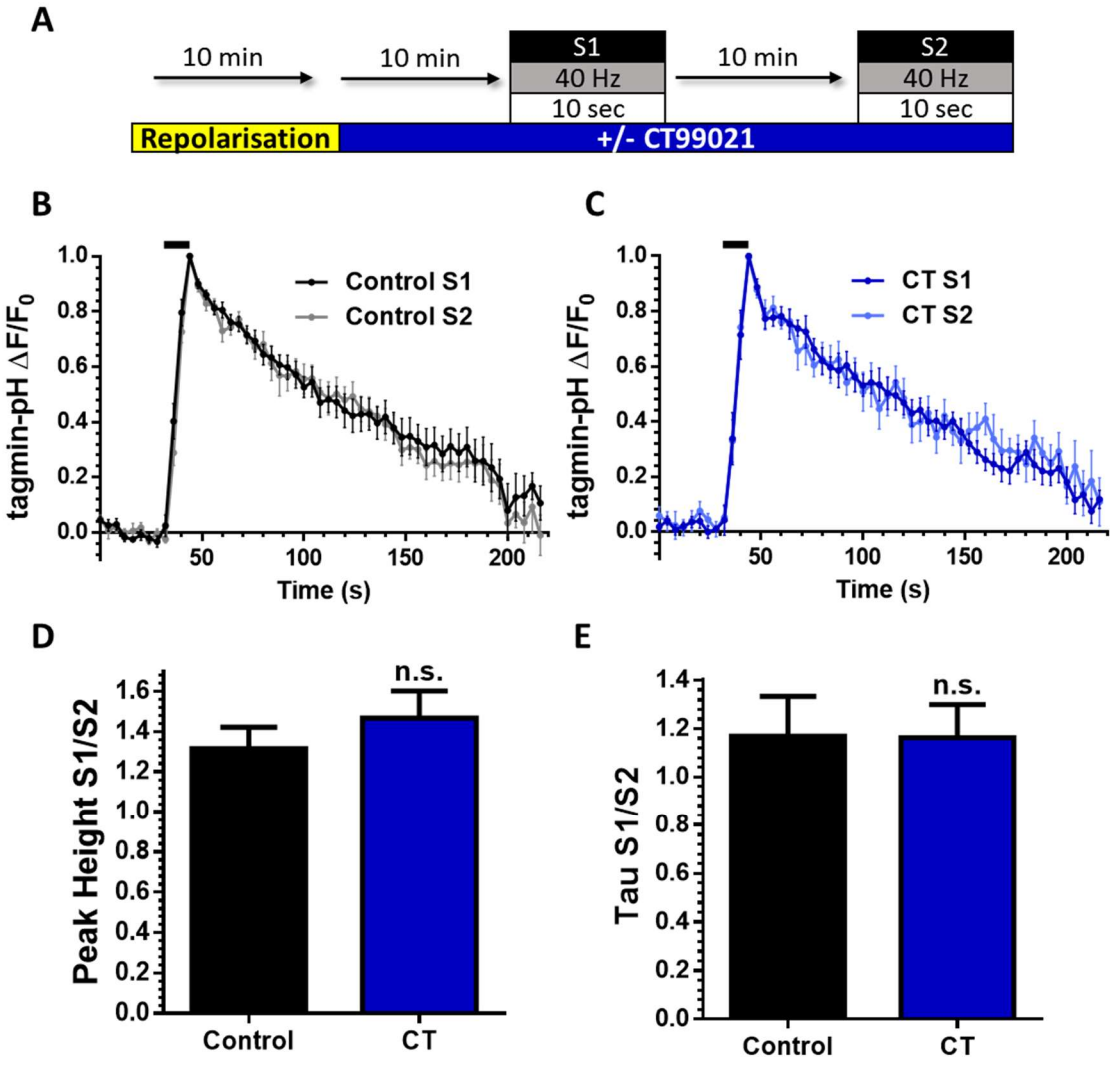

Figure 5.4 Pharmacological Inhibition of ADBE does not Affect Synaptotagmin-pHluorin Recycling

A) Protocol of "S1 S2" experiment. CGNs co-transfected with mCer and synaptotagmin-pHluorin (tagmin-pH) were incubated with imaging buffer for 10 min before being incubated in imaging buffer alone (control) or supplemented with 2 μM CT99021 (CT) for 10 minutes prior to S1 and then continuously onwards. Cells were challenged with 2 sequential HFS trains (400 AP, 40 Hz) (S1 and S2) 10 minutes apart. B and C) Average time traces ± SEM of S1 overlaid with S2 for control and CT respectively. D) Average ratio value of peak height (F/F_0) S1 over peak height S2 + SEM. E) Average ratio of tau (s) S1 over S2 + SEM. Control n=9, CT n=10. n.s.,Student's t-test.

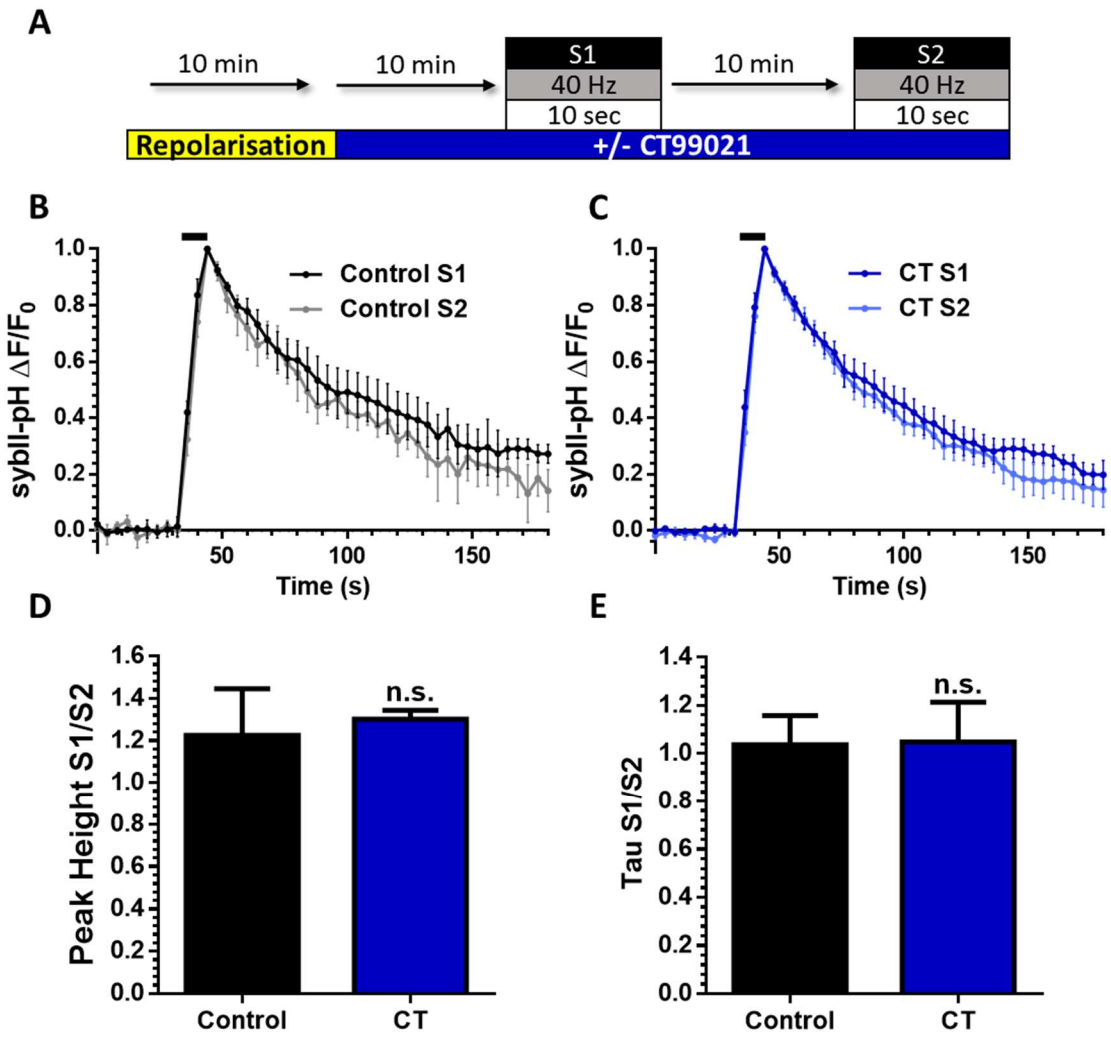

Figure 5.5 Pharmacological Inhibition of ADBE does not Affect Synaptobrevin II-pHluorin Recycling

A) Protocol of "S1 S2" experiment. CGNs co-transfected with mCer and synaptobrevin II-pHluorin (sybII-pH) were incubated in imaging buffer for 10 min before being incubated with imaging buffer alone (control) or supplemented with 2 μM CT99021 (CT) for 10 minutes prior to S1 and then continuously onwards. Cells were challenged with 2 sequential HFS trains (400 AP, 40 Hz) (S1 and S2) 10 minutes apart. B and C) Average time traces ± SEM of S1 overlaid with S2 for control and CT respectively. D) Average ratio of peak height (F/F_0) S1 over peak height S2 + SEM. E) Average ratio of tau (s) S1 over S2 + SEM. Control n=4, CT n=6. n.s., Student's t-test.

pHluorins (Figure 5.3, Figure 5.4 and Figure 5.5 D and E respectively) indicating that ADBE does not significantly contribute to the recycling of vGlut-pH, tagmin-pH or sybII-pH during HFS. Taken together these results suggest that a wide range of commonly used pHluorins do not traffic via ADBE.

5.2.1.2 Hippocampal Neurons Display no Significant Trafficking of Synaptophysin-pHluorin via ADBE During HFS

So far these experiments have indicated that in CGNs exogenously expressed SV proteins tagged with a pH-sensitive marker are trafficked independently of the dominant form of endocytosis, ADBE, during HFS.

To assess if this finding is specific to CGNs or if it common to most neuronal subtypes, hippocampal neurons expressing syp-pH were utilised in an identical "S1 S2" protocol, inhibiting ADBE only on the second stimulation (Figure 5.6 A-C).

No significant difference was found in peak height ratio between control and CT conditions (Figure 5.6 D) showing that the inhibition of ADBE did not affect the amount of exocytosis occurring on S2. No significant difference was found between tau ratios of control or CT conditions (Figure 5.6 E) showing no effect of ADBE inhibition on the rate of endocytosis. However, in hippocampal neurons a slowing of endocytic kinetics on S2 was observed leading to a smaller ratio value. This was consistent across both control and CT conditions however and as such is not pertinent to the manipulation of ADBE.

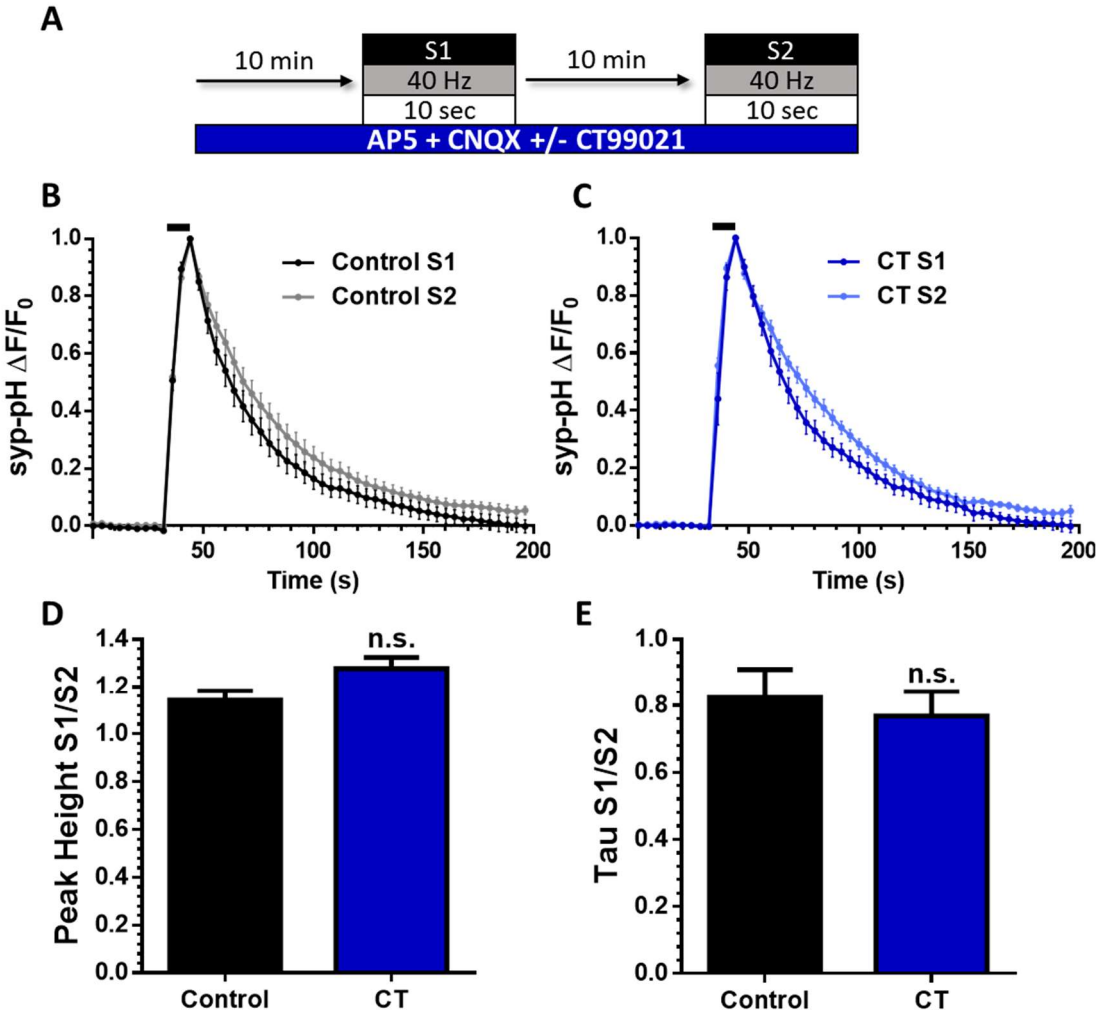

Figure 5.6 Pharmacological Inhibition of ADBE Does Not Effect Synaptophysin-pHluorin Retrieval in Hippocampal Neurons During HFS

A) Protocol of "S1 S2" experiment. Hippocampal neurons transfected with synaptophysin-pHluorin (syp-pH) were incubated with hippocampal imaging buffer (control) or supplemented with 2 μM CT99021 (CT) for 10 minutes prior to S1 and then continuously onwards. Cells were challenged with 2 sequential HFS trains (400 AP, 40 Hz) (S1 and S2) 10 minutes apart. B and C) Average time traces ± SEM, S1 overlaid with S2 for control and CT respectively. D) Average ratio of peak height (F/F_0) S1 over peak height S2 + SEM. E) Average ratio of tau (s) S1 over S2 + SEM. Control n=5, CT n=6. n.s., Student's t-test.

`

5.2.2 Genetic Inhibition of ADBE has no Effect on the Recycling of Synaptophysin-pHluorin

Previous experiments discussed here have shown that pHluorins are predominantly recycled via an alternative endocytic route to ADBE. Pharmacological approaches however can be troublesome due to non-specific effects as well as the possibility of their degradation during prolonged exposure to either light or temperature. To further strengthen my hypothesis, the same question was approached using a genetic manipulation.

Syndapin I is an essential molecule for ADBE (Clayton et al. 2009). During HFS dynamin I is dephosphorylated on two serine residues (Ser774 and 778) facilitating an interaction with syndapin I (Clayton et al. 2009). This interaction is needed for ADBE as shown by phospho-null mutant forms of dynamin I resulting in a lack of ADBE in CGNs (Clayton et al. 2009). By knocking down syndapin I ADBE is also significantly inhibited (Clayton et al. 2009) as visualised by the inhibition of dextran uptake in syndapin I-depleted cells (Figure 5.7). This established syndapin I knock down system was utilised to visualise syp-pH recycling during a "Single HFS" experiment in comparison to a control condition.

CGNs co-expressing syp-pH and either syndapin shRNA or an empty vector (pSuper neo) were stimulated with a train of 400 AP at 40 Hz (HFS) (Figure 5.8 A). Fluorescence was plotted over time and compared between conditions (Figure 5.8 B). No significant difference was found either in amount of exocytosis as evidenced by peak height (Figure 5.8 C) or the time constant of endocytosis (tau) (Figure 5.8 D).

Therefore, the genetic ablation of ADBE had no effect on syp-pH recycling, giving further evidence that syp-pH is not significantly recycled via ADBE during HFS.

5.2.3 No Evidence of Synaptophysin-pHluorin Being Sequestered by ADBE During High Frequency Stimulation

The rate of decrease in pHluorin fluorescence after an action potential train is a function of both vesicle/endosome acidification and endocytosis. When referring to CME, SV acidification occurs rapidly (4-5 sec) and as such the rate of decrease of pHluorin fluorescence after stimulation can be considered an approximation of the rate of endocytosis (Sankaranarayanan & Ryan 2000; Atluri & Ryan 2006).

This issue becomes more complicated however when monitoring ADBE, as a bulk endosome has a larger internal volume than a SV (approximately 50 fold larger assuming an endosome of 150 nm diameter (Cheung & Cousin 2013)). This larger volume should mean a significantly longer period of time to acidify and therefore quench any pHluorin cargo fluorescence especially when one considers the availability of V-type ATPase responsible for vesicle acidification is extremely limited in nerve terminals (Takamori, Holt, Stenius, Edward A Lemke, et al. 2006) with only 1 or 2 copies per SV.

It therefore follows that pHluorins internalised via ADBE would remain fluorescent for a significant time period after their uptake. To search for evidence of pHluorin molecules sequestered into a neutral environment away from the PM (a bulk endosome which is still acidifying) after a HFS, an experimental protocol to track endosome acidification was used.

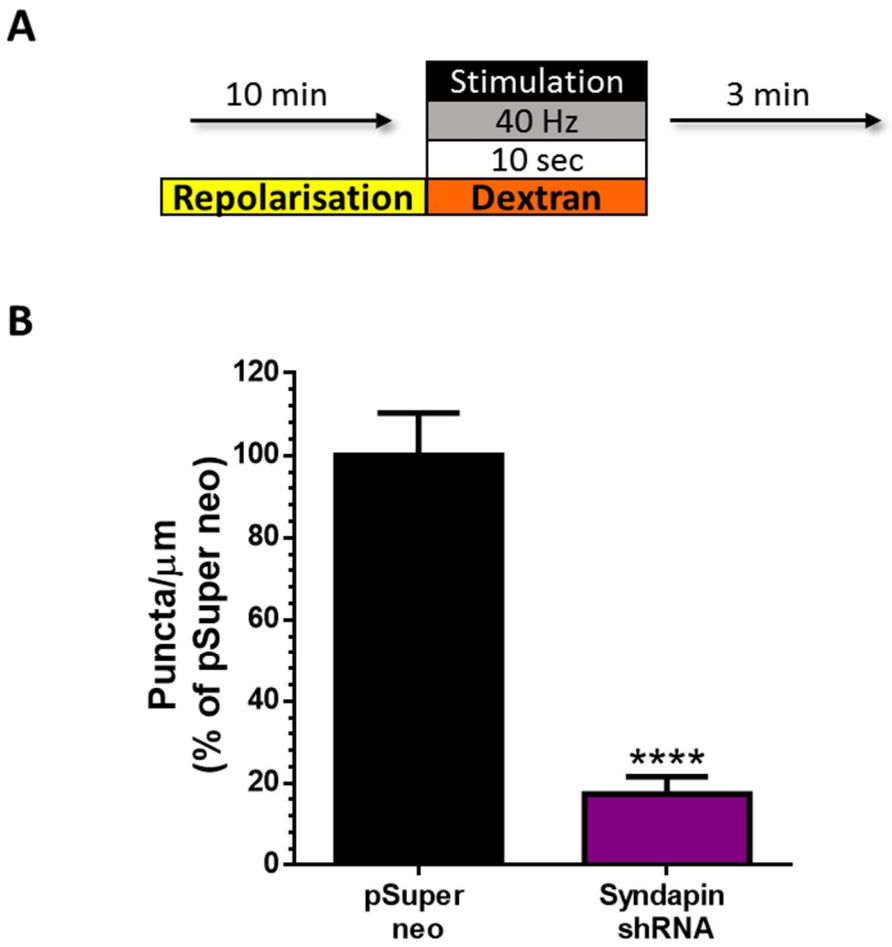

Figure 5.7 Silencing Syndapin I Expression Effectively Inhibits ADBE

A) CGNs transfected with empty vector pSuper neo or Syndapin I shRNA were repolarised in imaging buffer for 10 minutes. Cells were stimulated with a HFS train (400 AP, 40 Hz) in the presence of 50 µM dextran. B) Average number of dextran puncta per µm of axon expressed as a proportion of empty pSuper neo + SEM. pSuper n=33, Syndapin shRNA n=40. ****=p<0.0001. Student's t-test.

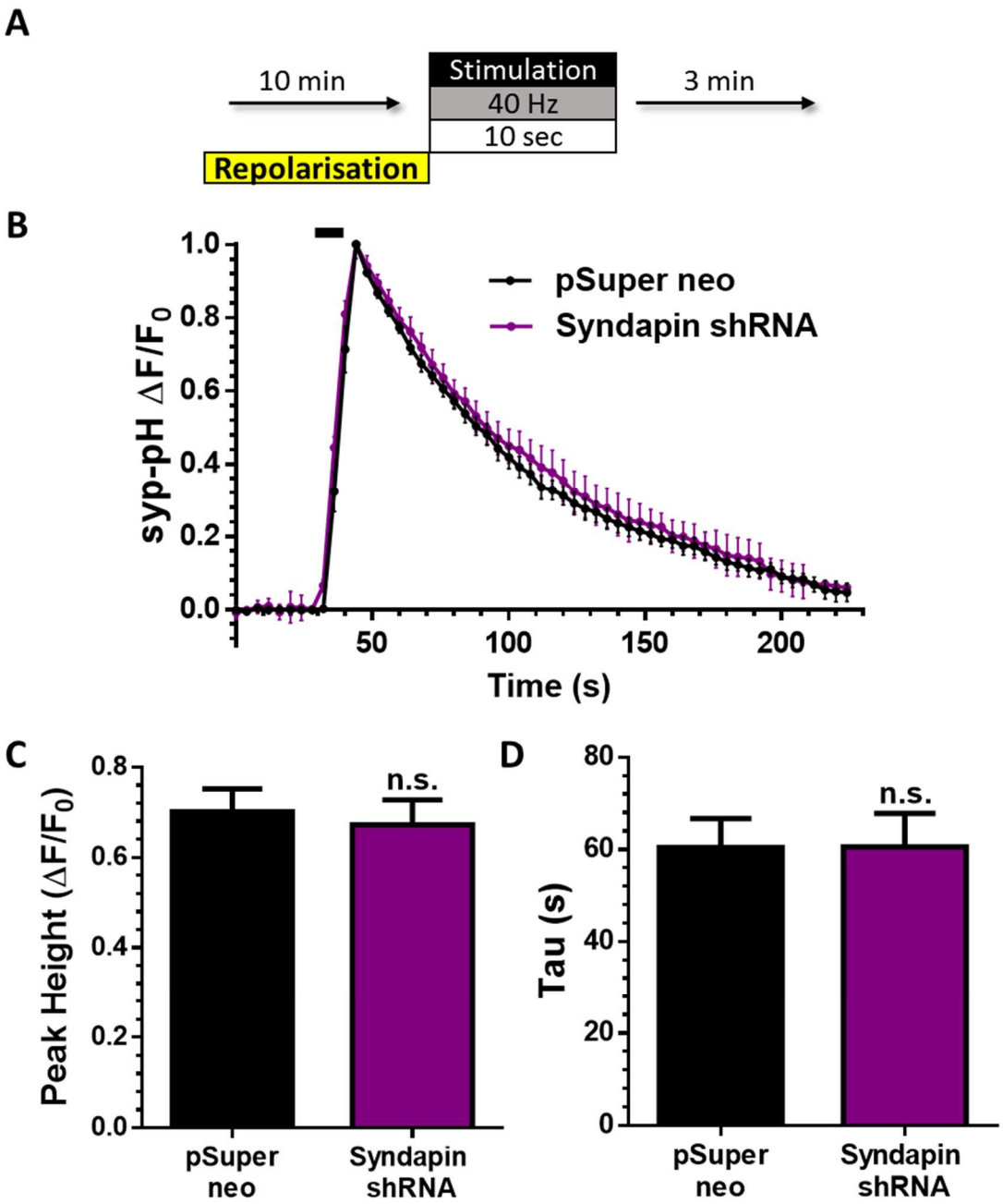

Figure 5.8 Genetic Inhibition of ADBE Does not Effect Synaptophysin-pHluorin Retrieval During HFS

A) CGNs co-transfected with either mCer empty vector (pSuper neo) or syndapin shRNA (Syndapin KD) and synaptophysin-pHluorin (syp-pH) were incubated with imaging buffer for 10 minutes prior to stimulation and then continuously onwards. Cells were stimulated with HFS train (400 AP, 40 Hz). B) Average time trace ± SEM is displayed with stimulation indicated by black bar. C) Average peak heights of each condition (F/F_0) + SEM. D) Average endocytosis kinetics (tau) + SEM. Syndapin KD n=8 Control n=5. n.s., Student's t-test.

An impermeant, weak acidic buffer was pulsed over syp-pH transfected cells before and after stimulation, comparing the “quenchable” portion of pHluorin molecules in a cell pre- and post-stimulation (Figure 5.9 A and B). Before stimulation this fraction represents those pHluorin molecules residing on the PM “the surface fraction”. The quenching of this fraction should mean all pHluorins are in an acidic environment and therefore non-fluorescent.

Any difference between the quenchable portion of fluorescence pre- and post-stimulation could indicate pHluorin-tagged SV cargo having been sequestered into a neutral environment away from the membrane. A third acid pulse was also performed a minute later to assess, if pHluorin molecules were sequestered into a bulk endosome structure, at what rate that endosome was acidifying (Figure 5.9 A and B).

No significant difference was seen between the “quenchable” portions of syp-pH fluorescence pre-stimulation or at either post-stimulation acid wash (Figure 5.9 C). This indicates that newly endocytosed syp-pH is either rapidly acidified and therefore is not being retrieved via ADBE or that bulk endosomes acidify at the same rate as SVs. Syp-pH response during HFS is unaffected by two independent methods of ADBE inhibition, this would therefore suggest that the former of these possibilities is correct.

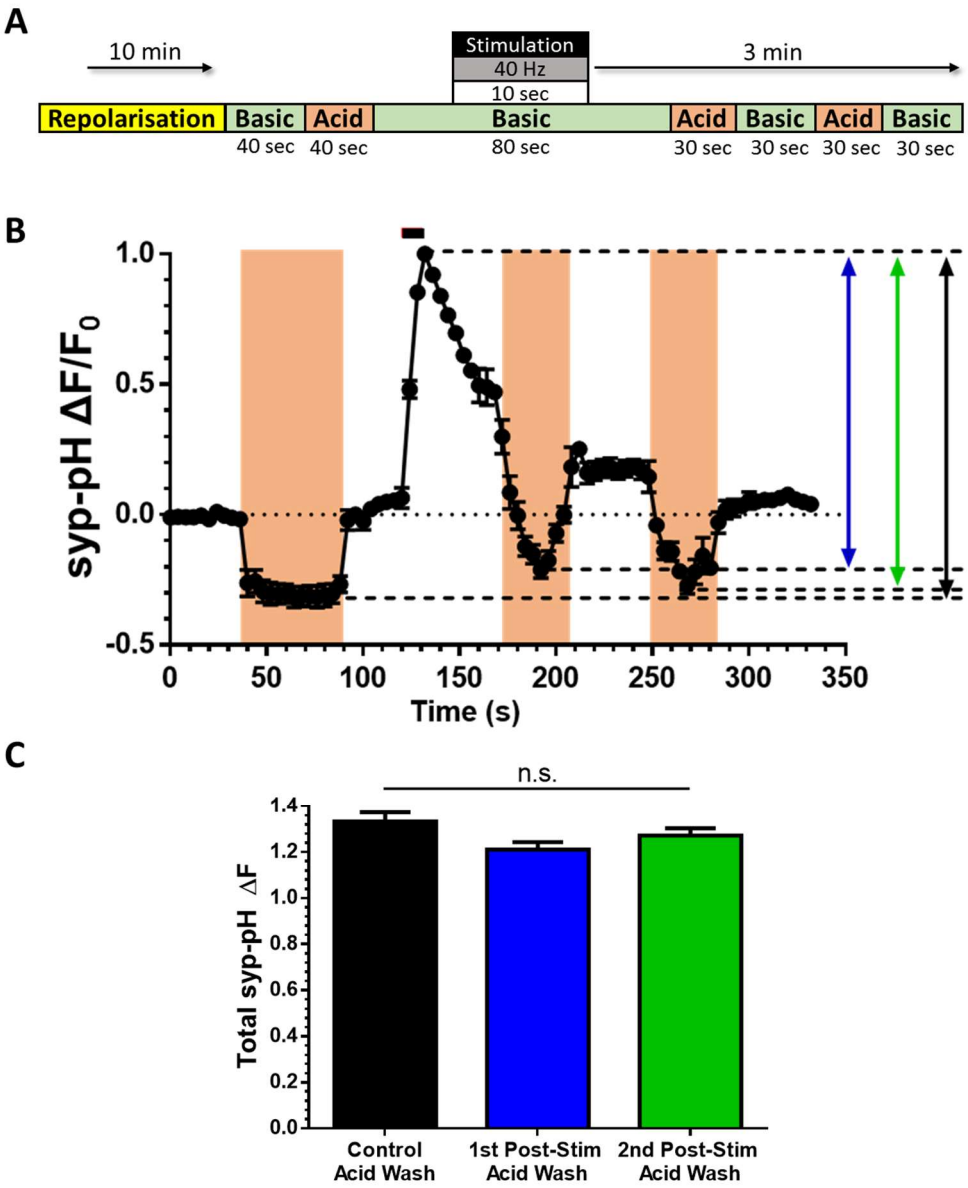

Figure 5.9 There is no Evidence of Sequestered Synaptophysin-pHluorin After *HFS*

A) Protocol of experiment: CGNs transfected with synaptophysin-pHluorin (syp-pH) were repolarised before a control acid wash (peach bars), isolating fluorescence of surface bound syp-pH. Cells were then stimulated with HFS train (400 AP, 40 Hz) and two more acid washes performed at 30 seconds (1st Post-Stim) and 90 seconds (2nd Post-stim) post-stimulation. B) Average time trace F/F_0 ± SEM with stimulation indicated by black back bar, traces were normalised to stimulation peak height and difference between peak height and acid wash fluorescence calculated for control (black arrow), 1st Post-stim (blue arrow) and 2nd Post-stim (green arrow) washes ($\Delta F/F_0$), C) Average $\Delta F/F_0$ values + SEM. n=12. n.s. One-way ANOVA with Bonferroni post-test.

5.2.4 Pharmacological Inhibition of CME Severely Disrupts Synaptophysin-pHluorin Retrieval

The experiments thus far have indicated that many typical pHluorins are not recycled via ADBE. However, it has not yet been shown which endocytic mode is responsible for recovering SV cargo after HFS. The most obvious candidate for SV cargo recycling is CME. To test this hypothesis CME was inhibited in CGNs using the clathrin inhibitor Pitstop2-AM (Von Kleist et al. 2011).

To be sure of a CME-specific effect of Pitstop-2 on endocytosis an experiment was performed, assessing any possible effect on ADBE. Pitstop-2 was used acutely just prior to a HFS in the presence of dextran in CGNs (Figure 5.10 A). No significant effect was seen on ADBE in the presence of Pistop-2 in CGNs in comparison to cells stimulated with HFS in the presence of dextran without Pitstop (Figure 5.10 B).

CGNs transfected with syp-pH were stimulated using the same "S1 S2" protocol as described previously (5.2.1.1). Pitstop-2 was included just prior to S2 inhibit CME (Figure 5.11 A). Fluorescence was plotted over time for both conditions with S1 and S2 overlaid for both control and Pitstop-2 (Figure 5.11 B and C respectively). A significant difference was seen between S1 and S2 when average traces were compared which was not present between S1 and S2 of control.

Efficiency of syp-pH retrieval was measured by comparing the fluorescence drop after stimulation as a percentage of fluorescence increase on stimulation, this is the proportion of pHluorin molecules retrieved post-stimulation as a percentage of those deposited into the PM on stimulation.

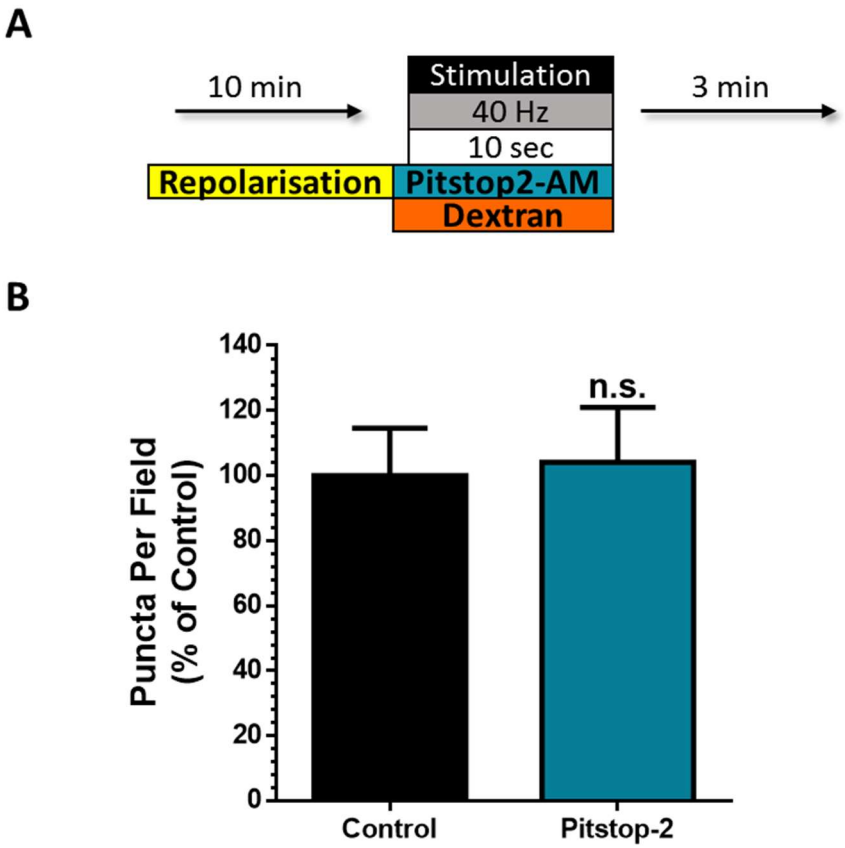

Figure 5.10 Acutely Inhibiting CME Does Not Inhibit ADBE

A) CGNs were repolarised in imaging buffer for 10 minutes prior to incubation with imaging buffer with 50 µM dextran alone (Control) or supplemented with 15µM Pitstop-2 for 10 seconds. Cells were stimulated with a HFS train (400 AP, 40 Hz). B) Average dextran puncta per field + SEM for Control Vs. Pitstop-2. Control n=7, Pitstop-2 n=7. n.s. Student's t-test.

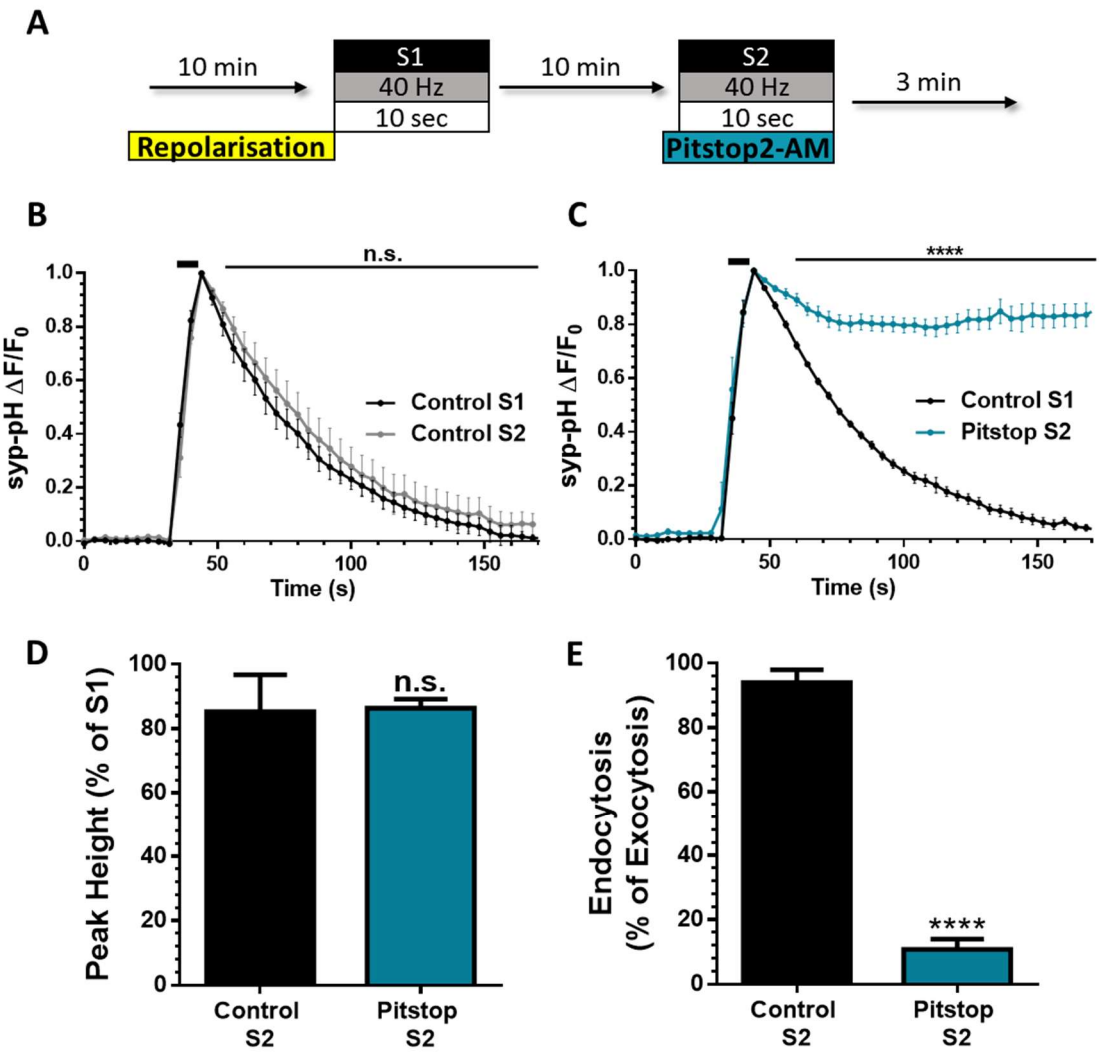

Figure 5.11 Pharmacological Inhibition of CME Effectively Ablates Syp-pH Retrieval During HFS

A) CGNs transfected with synaptophysin-pHluorin (syp-pH) were incubated with imaging buffer for 10 minutes prior to stimulation and then continuously onwards. Cells were challenged with 2 sequential action potential trains of 400 AP at 40 Hz separated by 10 minutes. Cells were supplemented with 15 μM PItstop-2 8-12 seconds prior to S2 (Pitstop) or nothing (control). B) Average time course of control S1 overlaid with S2 C) Average time course of Pitstop S1 overlaid with S2. Each trace is normalised to baseline and peak fluorescence on stimulation. Black bars indicate location and duration of stimulation. D) Average value of peak height evoked on S2 as a proportion of S1 +SEM. E) Average value of endocytosis as a percentage of fluorescence decrease after increase on S2. Control n=5, Pitstop n=6. Error bars are equal to SEM. Time course: ****= p<0.0001 two-way ANOVA, Bar chart: ****= p<0.0001 Student's t-test.

No significant effect was seen on exocytosis (Figure 5.11 D) however retrieval of syp-pH was inhibited by nearly 90% at a time point by which control cells had retrieved all exocytosed syp-pH (Figure 5.11 E). As ADBE is unaffected by this drug treatment (see Figure 5.10) this demonstrates that, even during a stimulation protocol in which CME is not the dominant form of endocytosis, SV cargo is being retrieved almost exclusively via CME.

5.2.4.1 Pitstop-2 does not Affect Acidification of SVs During the Experimental Timeframe.

Previous work has suggested an impact of Pitstop-2 on vesicle acidification (Hua et al. 2013). As such it is possible that the lack of fluorescence drop seen with the application of pitstop-2 could be attributed to an off-target effect. To examine the effect of Pitstop-2 on vesicle pH during the time-frame of the previous experiment, a protocol was designed to track the baseline fluorescence of vesicles over time with and without the presence of pitstop-2 (Figure 5.12 A).

Syp-pH transfected cells were imaged for a minute to acquire a baseline fluorescence; this is the fluorescence of surface-bound pHluorin molecules exposed to the neutral pH of the extracellular media. An ammonium chloride solution was then pulsed over the culture for a further minute; this has the effect of de-acidifying all synaptic vesicles thereby allowing the maximal fluorescence of all pHluorin molecules within the transfected cell. After these preliminary baseline measurements imaging buffer alone (control) or supplemented with Pitstop-2 was pulsed over the cultures. This solution was continuously perfused over the culture for a period

consistent with previous experiments using Pitstop-2. If Pitstop-2 had an effect on vesicle pH during this time period, it would be observable as an increase in baseline fluorescence over time. No significant difference in baseline fluorescence, and therefore the pH of the population of SVs between control and Pitstop-2-treated conditions was observed over this time-frame.

However, when this solution was left on cultures for a further 5 minutes a significant increase in baseline fluorescence (corresponding to an increase in vesicle pH) was observed in Pitstop-2-treated cells when compared to controls (Figure 5.12 B).

This indicates that Pitstop-2 does have off-target effects on SV pH over a longer period of time, however it does not affect the pH of vesicles within the time-frame of the experiments conducted here. This also means that the drastic inhibition of the syp-pH fluorescence decrease after stimulation in the presence of Pitstop-2 cannot be attributed to its effects on vesicle pH and must, therefore, be due to its effects on syp-pH retrieval via the inhibition of CME.

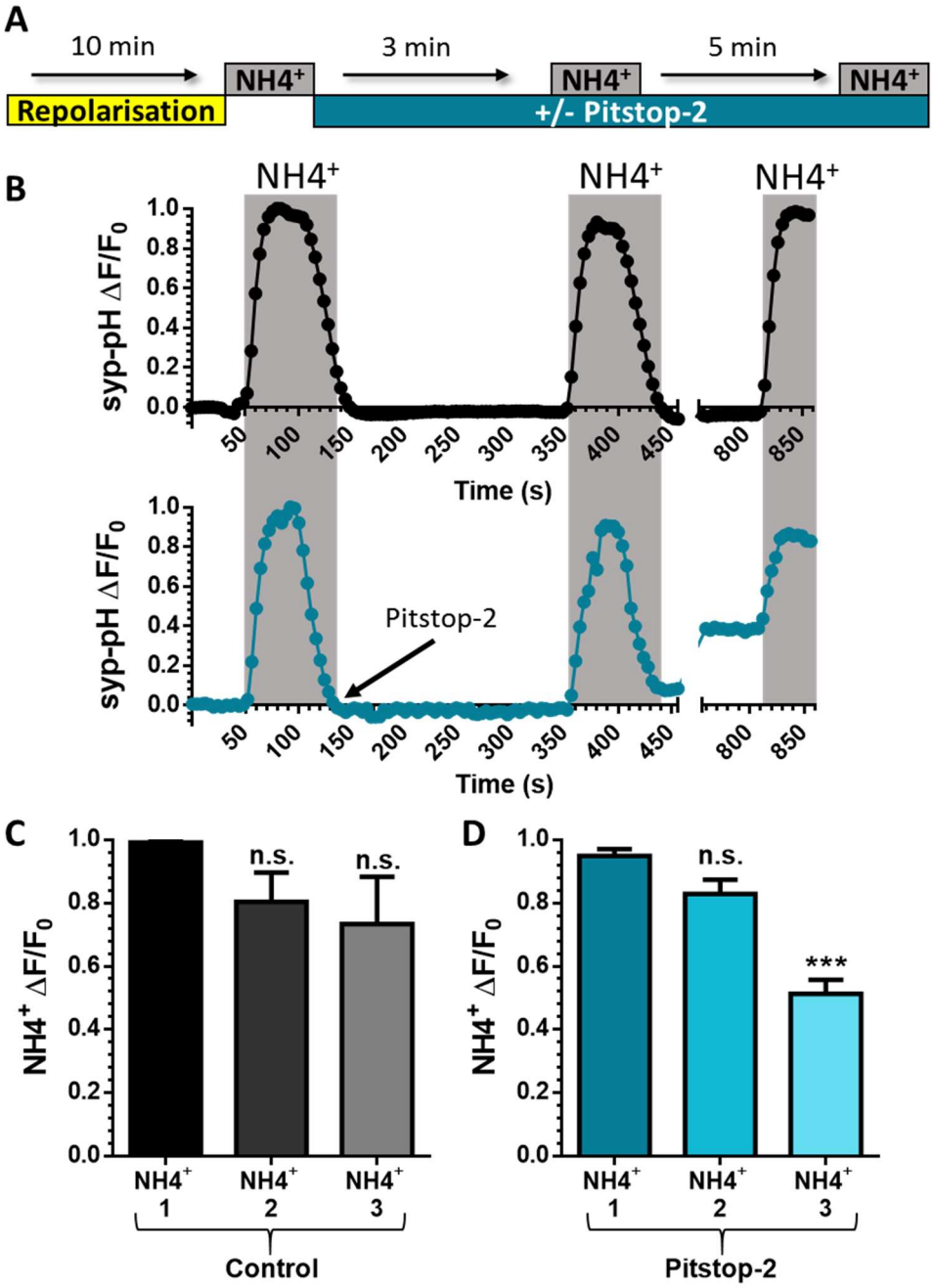

Figure 5.12 Pitstop- 2 Does not Affect Vesicle Acidity During Experimental Time Frame

A) CGNs transfected with synaptophysin-pHluorin (syp-pH) were incubated with imaging buffer for 10 minutes prior to an ammonium buffer (NH^+- grey bands) for one minute before being replaced with imaging buffer (control) supplemented with 15 μM Pitstop-2. After 3 minutes cells were given a second NH^+ pulse and then washed with the relevant buffer. After 5 minutes a third NH^+ pulse was applied. B) Example time courses of control (above) and Pitstop-treated (below) conditions normalised to initial baseline and highest fluorescence (0 and1 respectively). Pitstop n=3 Control n=3.

5.2.5 Genetic Inhibition of CME Severely Affects Synaptophysin-pHluorin Retrieval

5.2.5.1 CGNs Exhibit Severe Inhibition of Synaptophysin-pHluorin Retrieval with Silenced CHC Expression

5.2.5.1.1 Silencing of CHC Expression Causes Severe Inhibition of Synaptophysin-pHluorin Retrieval During Low Frequency Stimulation

A genetic method was used to interfere with clathrin-coated vesicle formation and investigate any effects on syp-pH recycling due to the possibility of off-target effects inherent with the use of pharmacological interventions. A CHC shRNA vector, previously shown to significantly reduce the expression of CHC (Royle et al. 2005) was used. CHC levels were measured in CGNs expressing CHC shRNA or its scrambled control by overlaying images of transfected CGNs with CHC antibody staining. Fluorescence measurements were taken from both transfected and non-transfected synapses (Figure 5.13 A and B) and compared. CHC shRNA transfected cells displayed a 75% decrease in CHC after 3 days when compared to non-transfected cells in the same region (Figure 5.13 B and C). A scrambled vector showed no difference in CHC levels (Figure 5.13 A and C). This demonstrates the high efficacy of the CHC shRNA used.

CGNs were co-transfected with syp-pH and either CHC shRNA or its scrambled vector. Cultures were then stimulated at a low frequency (10 Hz 30 sec, LFS) which

is known to activate CME but not ADBE (Granseth et al. 2006; Clayton et al. 2008; Clayton & Cousin 2009).

Using this protocol (Figure 5.14 A) CGNs displayed a significant difference in syp-pH retrieval (Figure 5.14 B and D). CHC-depleted cells retained over 50% of exocytosed syp-pH on the PM after a time point when control cells had re-internalised all exocytosed syp-pH (Figure 5.14 D). The amount of exocytosed syp-pH (as measured by fluorescence increase on stimulation – peak height) was unaffected by this CHC-knockdown (Figure 5.14 C), therefore this CHC-dependent effect on syp-pH recycling was limited to endocytic and not exocytic mechanisms.

5.2.5.1.2 Silencing of CHC Expression Causes Sever Inhibition of Synaptophysin-pHluorin Retrieval During High Frequency Stimulation

This experiment was repeated using HFS to investigate whether inhibiting CME via CHC knockdown would affect syp-pH retrieval when CME is not the dominant form of endocytosis. CGNs transfected with the same CHC shRNA/ scrambled vector and syp-pH were stimulated using the same HFS protocol as previously described (40 Hz 10 sec) (Figure 5.15 A).

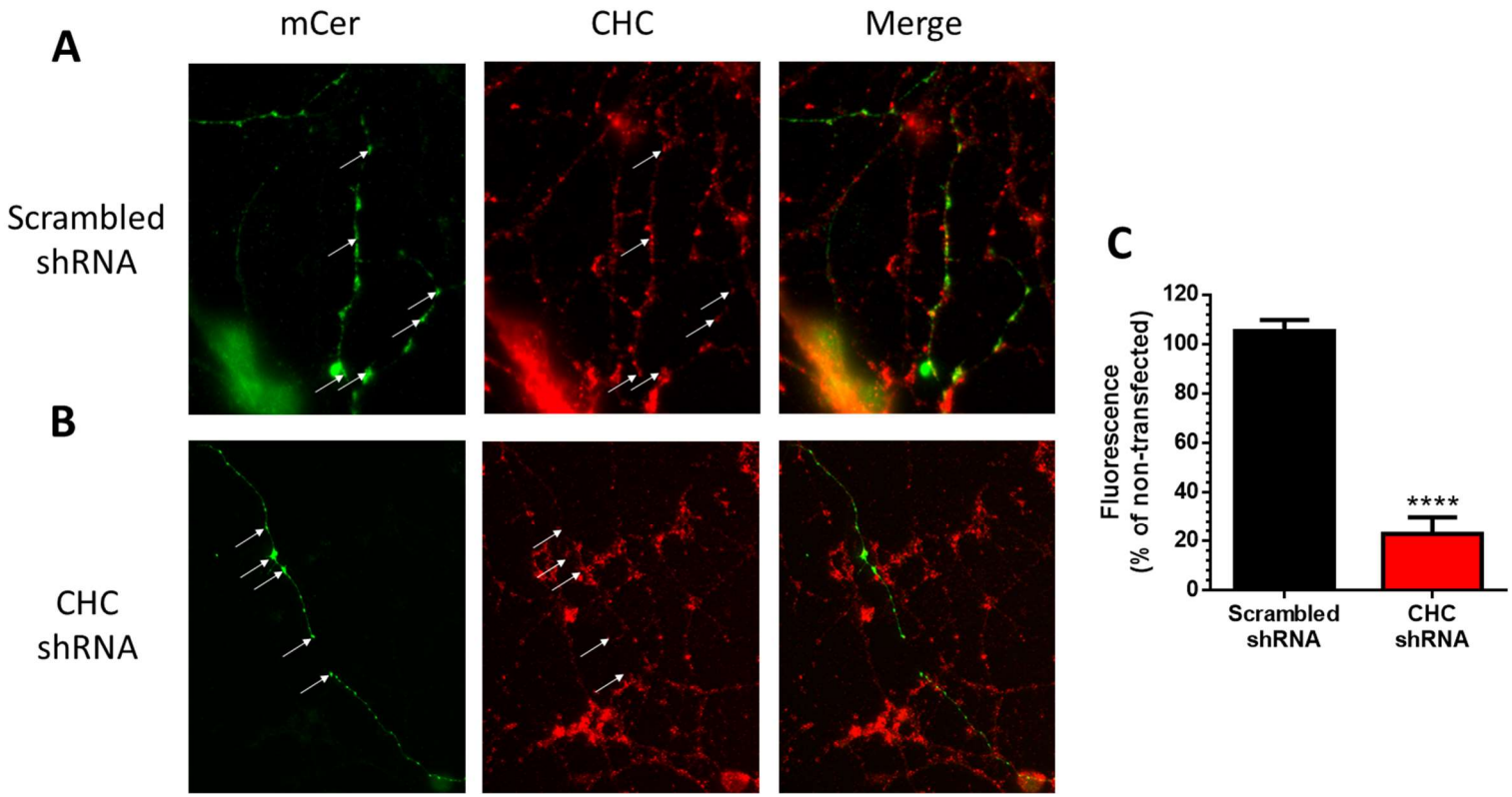

Figure 5.13 CHC shRNA Significantly Reduces CHC Levels in CGNs

Images of CGNs transfected with A) Scrambled shRNA or B) CHC shRNA. The whole CGN culture was labelled with GFP Ab (left) and a CHC Ab (middle), when overlaid one can see that the synapses of the transfected cell (white arrows) do not exhibit CHC labelling in the presence of CHC shRNA. Average fluorescence of Scrambled shRNA or CHC shRNA transfected CGN synapses as a percentage of fluorescence nearby non-transfected synapses of similar size + SEM. Scrambled shRNA n=12, CHC shRNA n=16. ****= $p<0.0001$. Student's t-test.

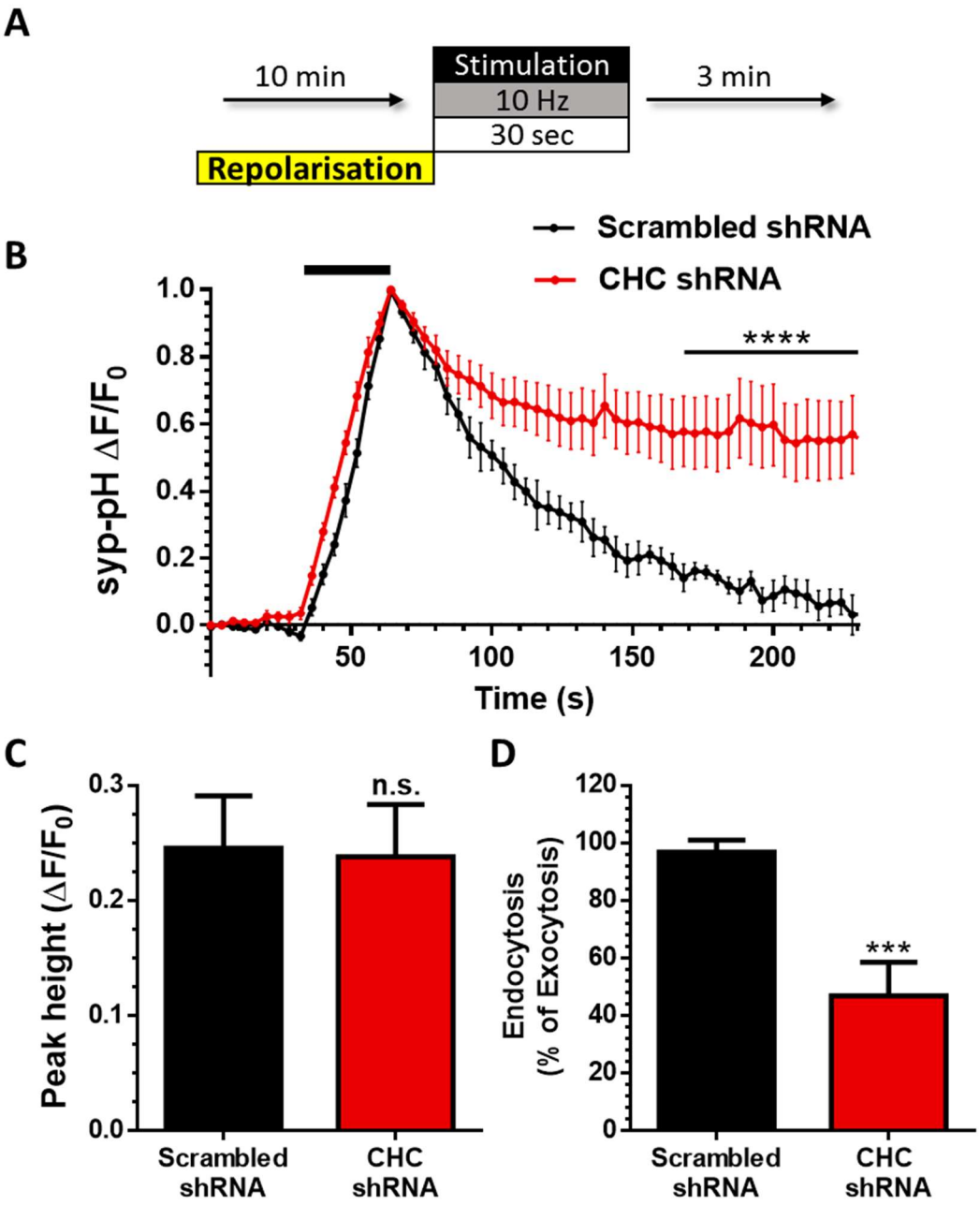

Figure 5.14 Genetic Inhibition of CME Significantly Reduces Synaptophysin-pHluorin Retrieval During LFS in CGNs.

A) CGNs co-transfected with either control scrambled shRNA vector (Scrambled shRNA) or CHC shRNA and synaptophysin-pHluorin (syp-pH) were incubated with imaging buffer for 10 minutes prior to stimulation and then continuously onwards. Cells were stimulated with a LFS train (300 AP, 10 Hz). B) Average time trace ± SEM is displayed with stimulation indicated by black bar. C) Average peak heights of each condition (F/F_0) + SEM. D) Average extent of syp-pH retrieval (endocytosis) measured as a percentage of exocytosis F/F_0 + SEM. Scrambled shRNA n=5, CHC shRNA n=8. Time trace: ****=P<0.0001, Two-way ANOVA, Bonferroni post-test. Bar charts: ***=p<0.001, Student's t-test.

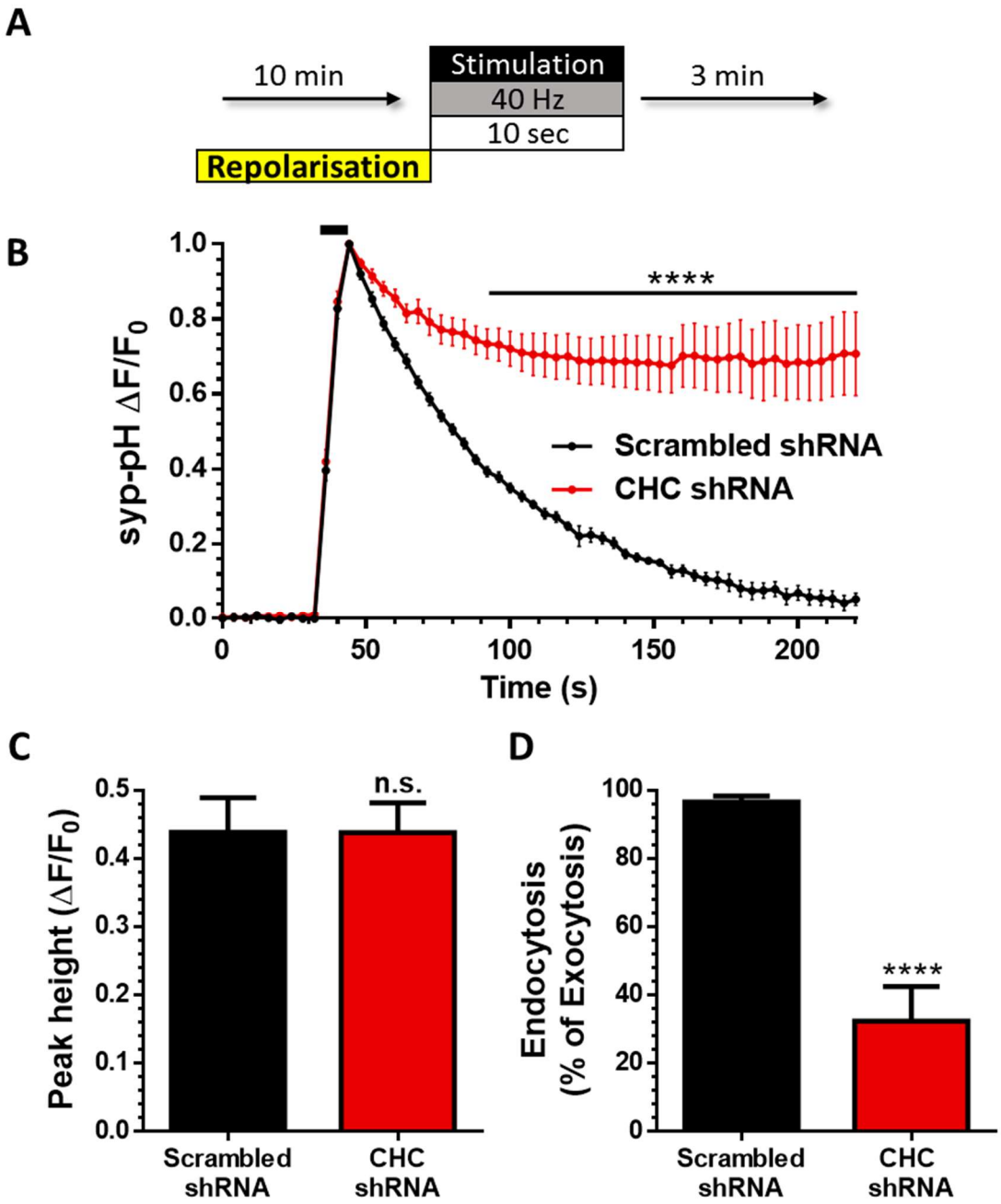

Figure 5.15 Genetic Inhibition of CME Significantly Reduces Retrieval of Synaptophysin-pHluorin During HFS in CGNs

A) CGNs co-transfected with either control scrambled shRNA vector (Scrambled shRNA) or CHC shRNA and synaptophysin-pHluorin (syp-pH) were incubated with imaging buffer for 10 minutes prior to stimulation and then continuously onwards. Cells were stimulated with a HFS train (400 AP, 40 Hz). B) Average time trace ± SEM is displayed with stimulation indicated by black bar. C) Average peak heights of each condition (F/F_0) + SEM. D) Average extent of syp-pH retrieval (endocytosis) measured as a percentage of exocytosis F/F_0 + SEM. Scrambled shRNA n=7, CHC shRNA n=8. Time trace: ****=P<0.0001, Two-way ANOVA. Bar charts: ****=p<0.0001, Student's t-test.

A significant difference in the recycling of syp-pH was seen between control and CHC-depleted cells after HFS (Figure 5.15 B). CHC-depleted cells retained almost 70% of exocytosed syp-pH on their PM at a time point where scrambled shRNA-transfected cells had re-internalised all exocytosed syp-pH (Figure 5.15 D). The amount of exocytosed syp-pH (peak height) was unaffected by CHC-depletion (Figure 5.15 C) showing that CHC knockdown affected only the retrieval of syp-pH and not SV fusion.

Syp-pH uptake is inhibited via this genetic approach even during stimulation intensities when the dominant form of endocytosis is the clathrin-independent ADBE. This is further proof that this SV cargo is being primarily recycled via clathrin-dependent mechanisms i.e. CME, and not via ADBE.

To investigate any effects of CHC knockdown on ADBE, CGNs transfected with CHC shRNA and its scrambled control were stimulated with a HFS train (400 AP, 40 Hz) in the presence of dextran (50 µM) (Figure 5.16 A). CGNs transfected with CHC shRNA showed a significant inhibition ADBE as measured by dextran puncta/µm transfected axon in comparison to controls (Figure 5.16 B).

As ADBE is thought to be clathrin-independent this was an unexpected result and as such this experimental paradigm was repeated in hippocampal neurons (Figure 5.16 C). Interestingly, hippocampal neurons showed no effect on ADBE in the presence of CHC shRNA.

CGNs and hippocampal neurons display nearly identical levels of CHC expression in the presence of CHC shRNA (CHC shRNA transfected cells displayed an 80 %

decrease in CHC after 7 days when compared to non-transfected cells in the same region – Figure 5.17) and as such it is unclear as to why this difference in ADBE inhibition may occur. However, as hippocampal neurons display unaffected ADBE it was important to assess if the lack of syp-pH retrieval in CGNs is in any part due to the inhibition of ADBE by CHC knockdown.

5.2.5.2 Hippocampal Neurons Exhibit Severe Inhibition of Synaptophysin-pHluorin Retrieval with Silenced CHC Expression

To ensure that this clathrin-dependent dominance of syp-pH trafficking was not specific to CGNs (in which ADBE was also inhibited), the experiments described previously were conducted in hippocampal cultures. Identical stimulation protocols to those on CGNs were performed on hippocampal cultures (Figure 5.18 A and Figure 5.19 A).

Comparable inhibition of syp-pH retrieval was seen in hippocampal neurons as that which was seen in CGNs in CHC-depleted cells compared to scrambled controls (Figure 5.18 B and Figure 5.19 B). Peak height was unaffected by knockdown of CHC for both LFS and HFS (Figure 5.18 C and Figure 5.19 C). LFS and HFS resulted in similar percentages of stranded syp-pH after stimulation as that seen in CGNs (Figure 5.18 D and Figure 5.19 D), at a time point when control cells had entirely retrieved deposited syp-pH.

This would indicate that the dominant contribution of CME in the retrieval of exocytosed syp-pH post-stimulation is true for both mild and intense stimulation in hippocampal neurons. The fact that the inhibition of ADBE in CGNs does not have

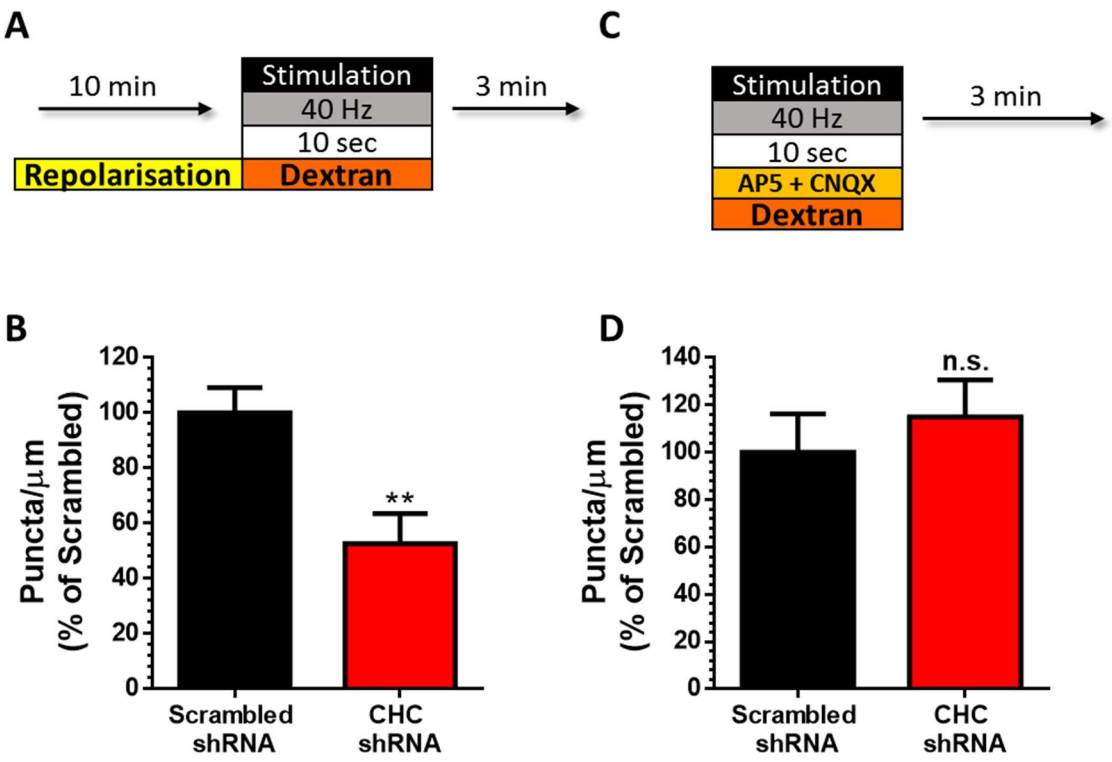

Figure 5.16 Chronic Inhibition of CME Affects ADBE in CGNs but not Hippocampal Neurons

A and C) CGNs or Hippocampal neurons respectively transfected with either Scrambled shRNA or CHC shRNA. A only) were repolarised in imaging buffer for 10 minutes. A and C) Cells were stimulated with a HFS train (400 AP, 40 Hz) in the presence of 50 µM dextran. B and D) Average puncta per µm + SEM of transfected axon of CGN or hippocampal cells respectively. CGNs: Scrambled shRNA n=28, CHC shRNA n=30. Hippocampal neurons: Scrambled shRNA n=20, CHC shRNA n=17. **=p<0.01. Student's t-test

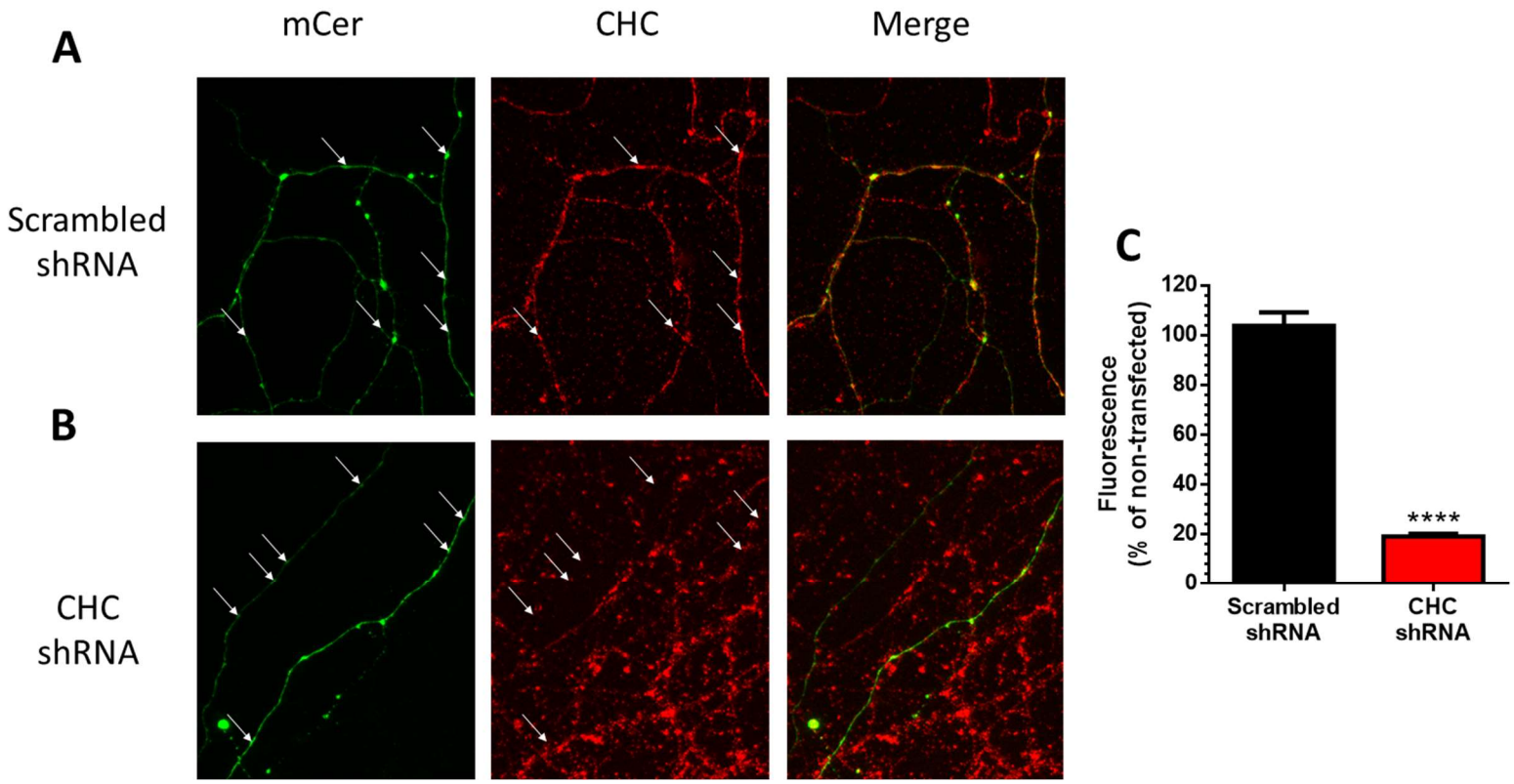

Figure 5.17 CHC shRNA Significantly Reduces CHC Levels in Hippocampal Neurons

Images of Hippocampal neurons transfected with A) Scrambled shRNA or B) CHC shRNA. The whole hippocampal cell culture was labelled with GFP Ab (left) and a CHC Ab (middle), when overlaid one can see that the synapses of the transfected cell (white arrows) do not exhibit CHC labelling in the presence of CHC shRNA. Average fluorescence of Scrambled shRNA or CHC shRNA transfected Hippocampal synapses as a percentage of fluorescence nearby non-transfected synapses of similar size.+ SEM. Scrambled shRNA n=16, CHC shRNA n=15. ****= $p<0.0001$. Student's t-test.

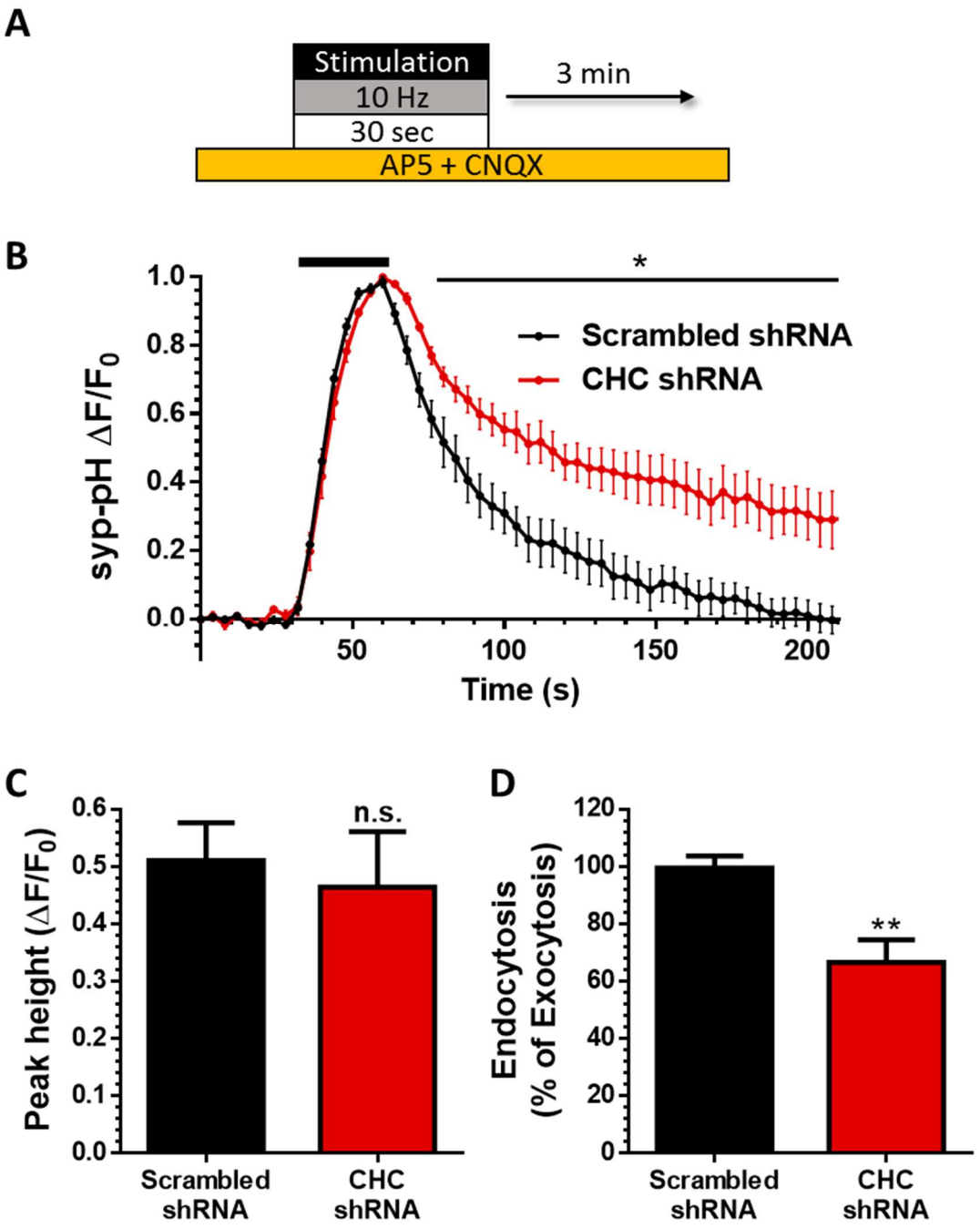

Figure 5.18 Genetic Inhibition of CME Significantly Reduces Synaptophysin Retrieval in Hippocampal Neurons During LFS

A) Hippocampal neurons co-transfected with either control scrambled shRNA vector (Scrambled shRNA) or CHC shRNA and synaptophysin-pHluorin (syp-pH) were incubated with hippocampal imaging buffer continuously. Cells were stimulated with a LFS train (300 AP, 10 Hz). B) Average time trace ± SEM is displayed with stimulation indicated by black bar. C) Average peak heights of each condition (F/F_0) + SEM. D) Average extent of syp-pH retrieval (endocytosis) measured as a percentage of exocytosis F/F_0 + SEM. Scrambled shRNA n=5, CHC shRNA n=5. Time trace: *=P<0.05, Two-way ANOVA. Bar charts: **=p<0.01, Student's t-test.

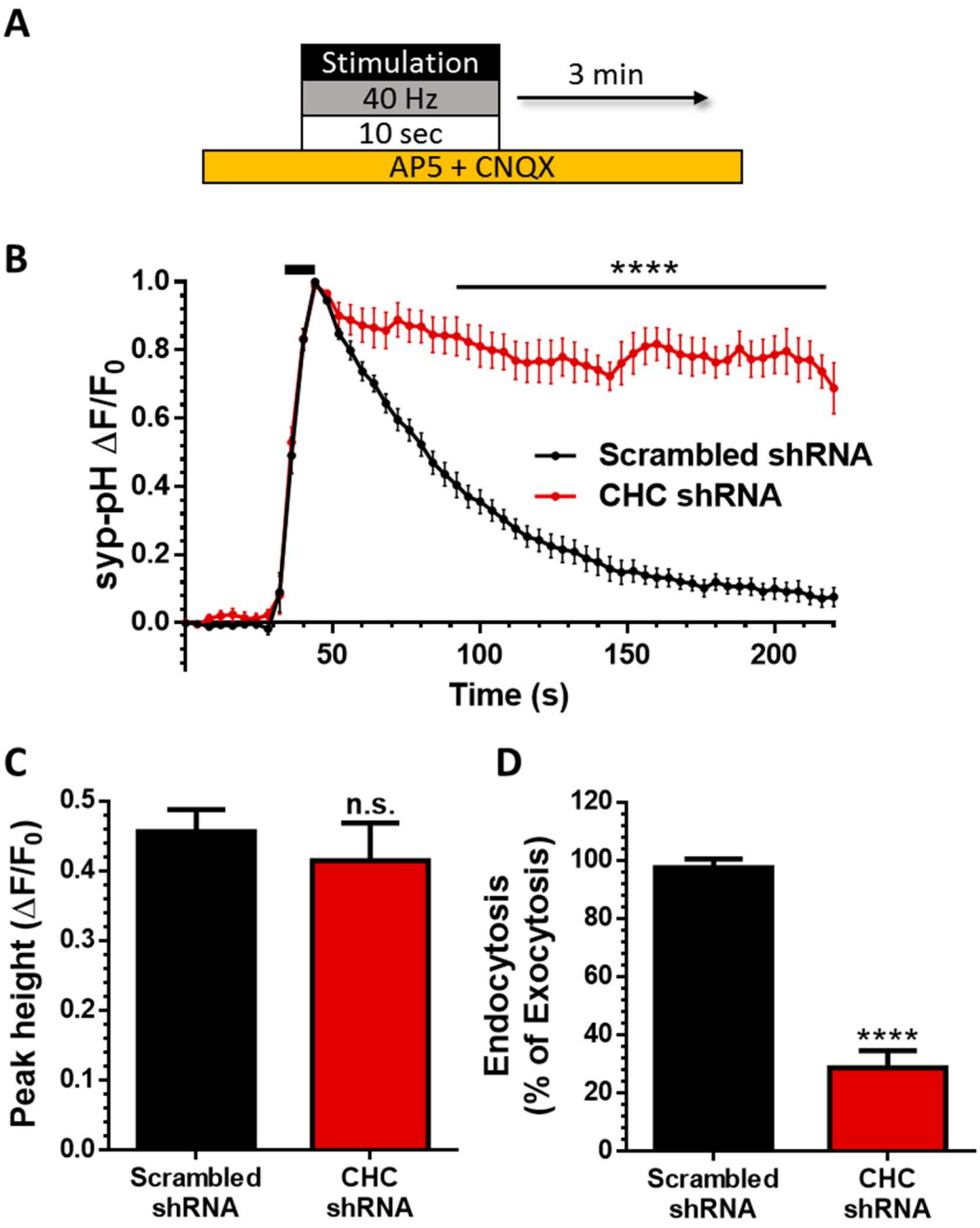

Figure 5.19 Genetic Inhibition of CME Significantly Reduces Synaptophysin-pHluorin Retrieval in Hippocampal Neurons During HFS

A) Hippocampal neurons co-transfected with either control scrambled shRNA vector (Scrambled shRNA) or CHC shRNA and synaptophysin-pHluorin (syp-pH) were incubated with hippocampal imaging buffer continuously. Cells were stimulated with a HFS train (400 AP, 40 Hz). B) Average time trace ± SEM is displayed with stimulation indicated by black bar. C) Average peak heights of each condition (F/F_0) + SEM. D) Average extent of syp-pH retrieval (endocytosis) measured as a percentage of exocytosis F/F_0 + SEM. Scrambled shRNA n=9, CHC shRNA n=6. Time trace: ****=P<0.0001, Two-way ANOVA. Bar charts: ****=p<0.0001, Student's t-test.

an additive effect on the inhibition of syp-pH retrieval is further evidence that ADBE does not contribute to the retrieval of syp-pH during HFS.

5.2.5.2.1 Genetic Inhibition of CME Severely Inhibits Synaptotagmin I-pHluorin Retrieval after Intense Stimulation

To address the possibility that the dominance of clathrin-dependent trafficking of SV cargo across stimulations is unique to syp-pH, the pHluorin tagged SV protein Synaptotagmin I-pHluorin (tagmin-pH) was used.

It has previously been claimed that CHC knockdown has an effect on retrieval of pHluorin tagged SV cargo only during mild stimulation and that this effect is absent at higher frequencies (Kononenko et al. 2014). As this is direct contradiction to the results compiled so far the stimulation protocol used in this publication was replicated (40 Hz 5 sec) as opposed to the standard HFS (40 Hz 10 sec) predominantly used for this work, to assess the possibility that this inconsistency could cause the discrepancies between both findings (Figure 5.20 A).

Despite this however, a significant difference was seen between CHC shRNA transfected and scrambled controls in the retrieval of tagmin-pH (Figure 5.20 B) with an average of 45% of exocytosed tagmin-pH remaining stranded on the PM at a time point when control cells had successfully retrieved all previously deposited reporter (Figure 5.20 D). In other words, a robust inhibition of tagmin-pH was seen using identical stimulation conditions to the previous study, suggesting CME does retrieve SV cargo during HFS.

One additional difference is the method of shRNA delivery, with the other group using a lentiviral vector. Since lentivirus preferentially infects excitatory neurones (Nathanson et al. 2009), a silencing of CHC expression may reduce glutamatergic transmission, while keeping GABAergic transmission intact. This may lead to decreased spontaneous activity, effectively silencing the culture.

To test if this effect could be causing the differences between this work and that reported in Kononenko et al 2014 tetrodotoxin (TTX) (100 nM) was applied for 48 hours to hippocampal cultures co-transfected with CHC shRNA and syp-pH before conducting a single HFS experiment (Figure 5.21 A). The removal of spontaneous activity during culture via TTX did not affect the ability of CHC knockdown to inhibit syp-pH retrieval during HFS (Figure 5.21 B-D). As such the causes of the differences between the results here and in other work is undetermined.

Together this data clearly demonstrates that a variety of common SV cargoes (syp-pH, vGlut-pH, tagmin-pH and sybII-pH) are not being significantly trafficked via ADBE. Instead, it has been revealed that these pHluorins are being largely retrieved via a clathrin-dependent process during stimulation intensities in which ADBE is dominant in both CGNs and hippocampal cells.

5.2.6 Clathrin Has a Role in Recycling at Physiological Temperatures

Recently questions have been raised as to which endocytic modes are active at physiological temperatures as opposed to room temperature, at which many studies characterising these endocytic routes have been performed (Watanabe et al. 2014). To date all of the studies in this thesis have been performed at room temperature

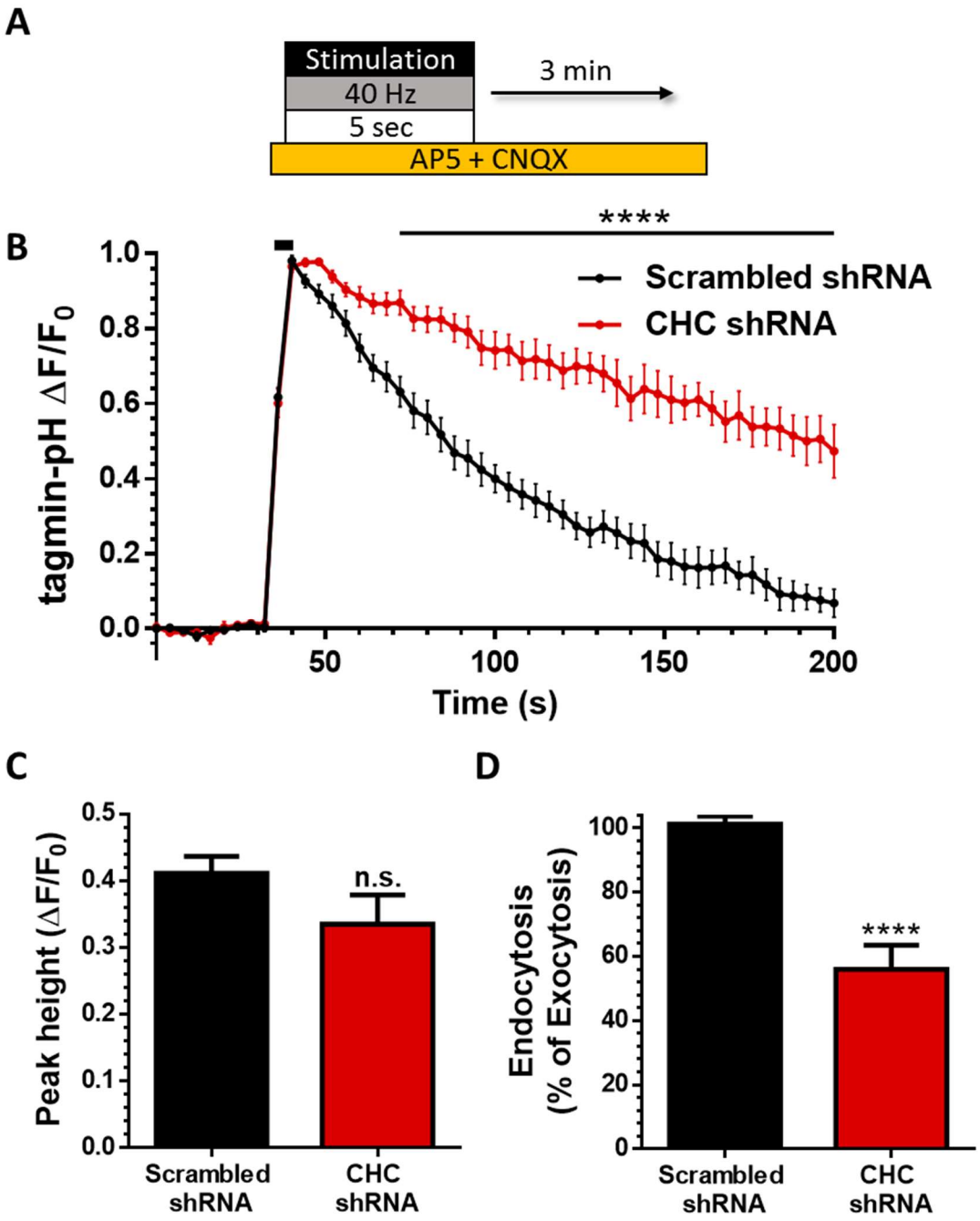

Figure 5.20 Genetic Inhibition of CME Significantly Reduces Synaptotagmin-pHluorin Retrieval in Hippocampal Neurons During HFS

A) Hippocampal neurons co-transfected with either control scrambled shRNA vector (Scrambled shRNA) or CHC shRNA and synaptotagmin-pHluorin (tagmin-pH) were incubated with hippocampal imaging buffer continuously. Cells were stimulated with a HFS train (400 AP, 40 Hz). B) Average time trace ± SEM is displayed with stimulation indicated by black bar. C) Average peak heights of each condition (F/F_0) + SEM. D) Average extent of tagmin-pH retrieval (endocytosis) measured as a percentage of exocytosis F/F_0 + SEM. Scrambled shRNA n=10, CHC shRNA n=9. Time trace: ****=P<0.0001, Two-way ANOVA Bonferroni post-test. Bar charts: ****=p<0.0001, Student's t-test.

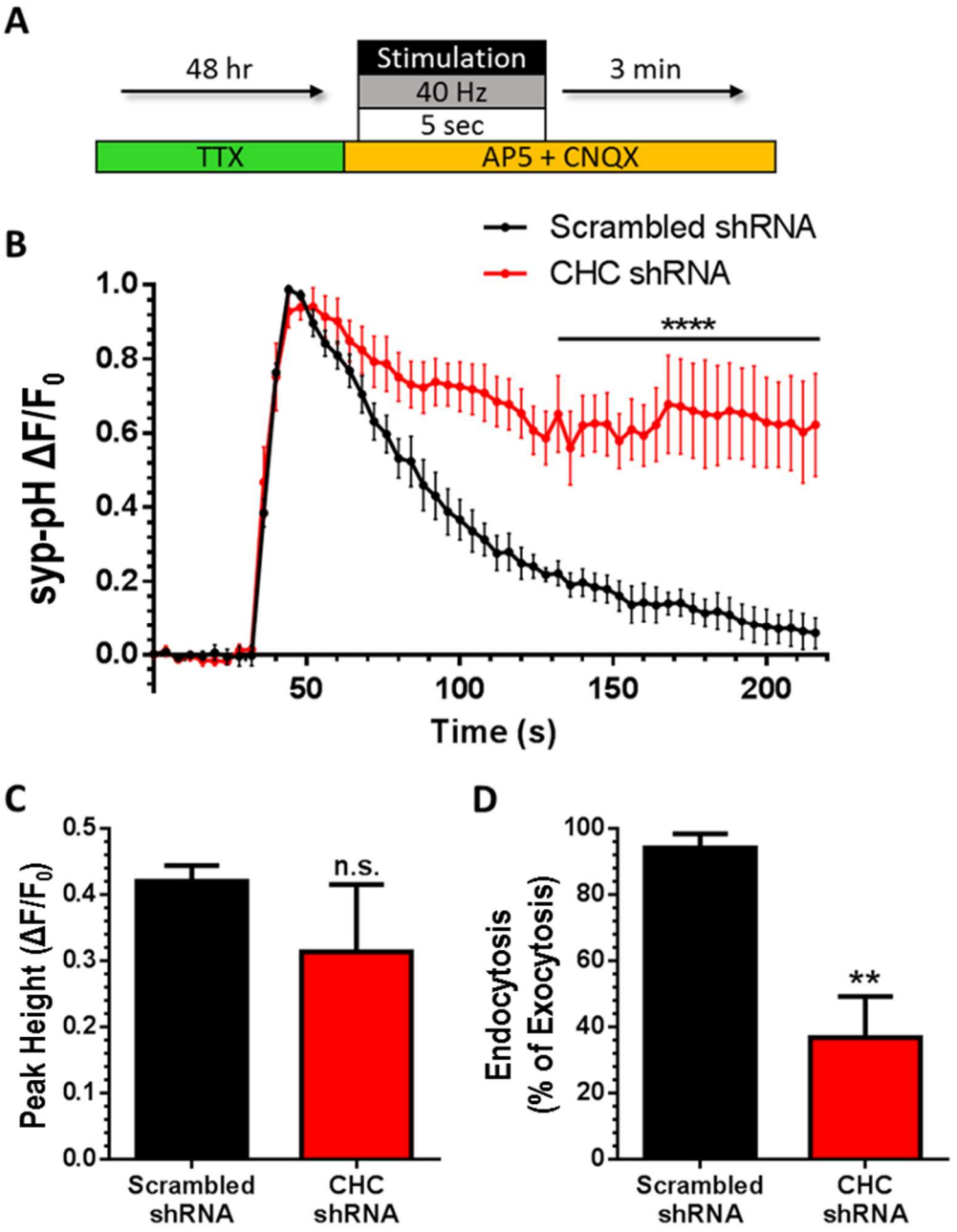

Figure 5.21 Silencing Network Activity Does Not Ameliorate Effect of CHC Knock Down on Synaptophysin-pHluorin Retrieval

A) Hippocampal neurons co-transfected with either control scrambled shRNA vector (Scrambled shRNA) or CHC shRNA and synaptophysin-pHluorin (syp-pH) had incubation medium supplemented with 100 nM TTX for 48 hr previous to experiment. Hippocampal imaging buffer was perfused continuously throughout experiment. Cells were stimulated with a HFS train (400 AP, 40 Hz). B) Average time trace ± SEM with stimulation indicated by black bar. C) Average peak heights of each condition (F/F_0) + SEM. D) Average extent of syp-pH retrieval (endocytosis) measured as a percentage of exocytosis F/F_0 + SEM. Scrambled shRNA n=5, CHC shRNA n=4. Time trace: ****=P<0.0001, Two-way ANOVA Bonferroni post-test. Bar charts: **=p<0.01, Student's t-test

where CME is dominant at low frequencies and ADBE is dominant at high frequencies.

To investigate how physiological temperatures impact on the trafficking of SV cargo via CME, clathrin-cage formation during a HFS at 37 ºC was inhibited using Pitstop-2. CGNs transfected with syp-pH were perfused with imaging buffer heated to a constant temperature of 37 ºC, which was supplemented with or without Pitstop-2 8-12 seconds before stimulation (Figure 5.22 A).

Pitstop-2 exposure resulted in an average of 33% of exocytosed syp-pH remaining in a neutral environment at a time point where control cells had fully retrieved all exocytosed syp-pH (Figure 5.22 B and D). This results shows a clathrin-dependent mechanism in the recycling of syp-pH even at physiological temperatures.

To further test the role of clathrin in syp-pH recycling at physiological temperatures a CHC shRNA vector was used. Hippocampal cells were chosen for this experiment as it has been noted that CHC knockdown in CGNs, but not hippocampal neurons, causes an inhibition of ADBE (see Figure 5.16). Hippocampal neurons co-transfected with syp-pH and either CHC shRNA or its scrambled control were then perfused with hippocampal imaging buffer at a constant temperature of 37 ºC and an otherwise standard “single HFS” experiment was performed (Figure 5.23 A).

Clathrin-depleted cells showed a significantly different fluorescent response to HFS when compared to scrambled controls (Figure 5.23 B). The presence of CHC shRNA resulted in 70% of all exocytosed syp-pH remaining in a neutral environment (Figure 5.23 D) at a time point when scrambled control had fully retrieved all exocytosed

syp-pH. These results together show an integral role for clathrin in the recycling of syp-pH at physiological temperatures at levels comparable to those seen at room temperature. This shows that clathrin-independent ADBE does not acquire a role in pHluorin recycling during the altered endocytic profile seen at physiological temperatures.

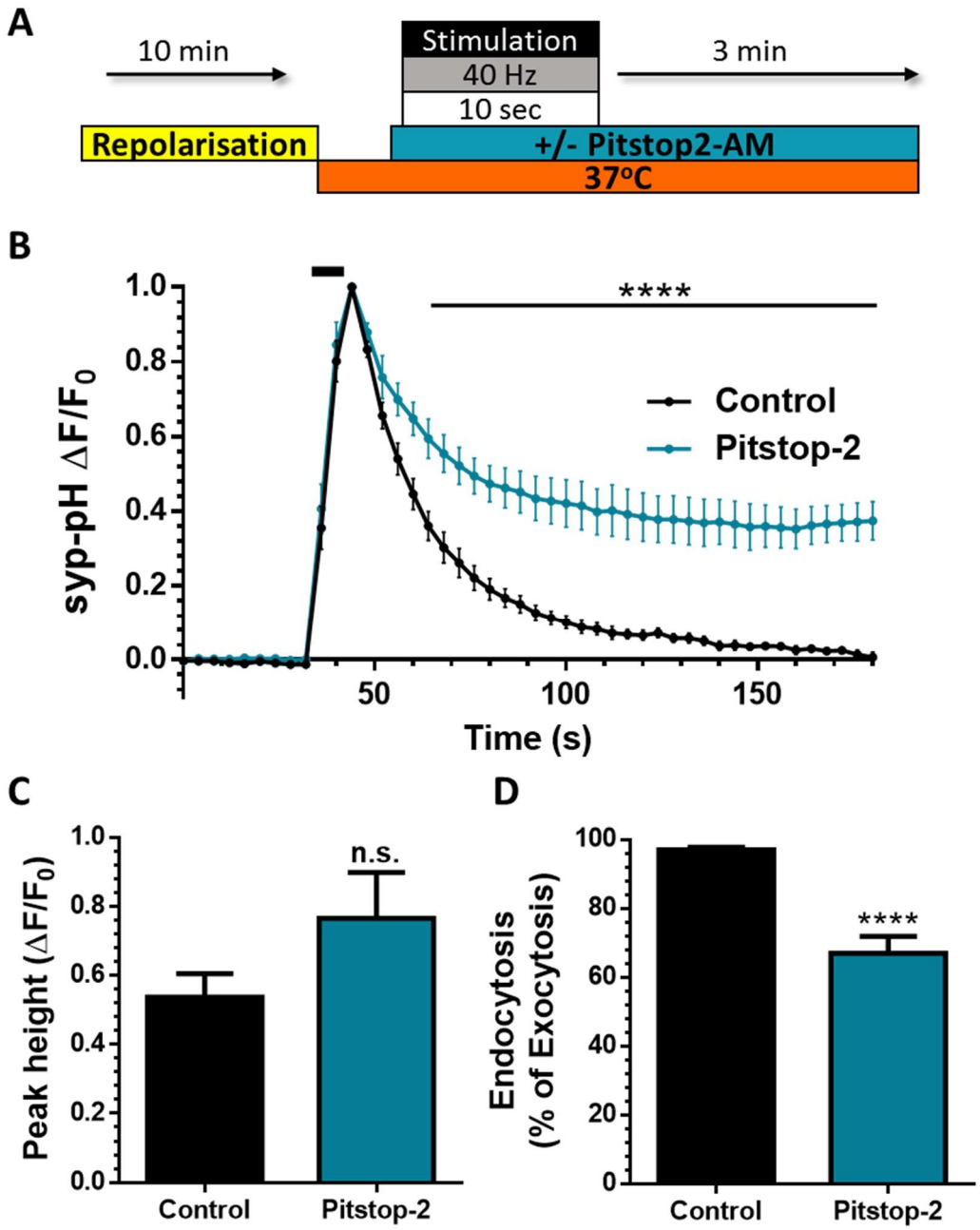

Figure 5.22 Pharmacological Inhibition Shows a Role for Clathrin in CGNs at Physiological Temperatures

A) CGNs transfected with synaptophysin-pHluorin (syp-pH) were incubated with imaging buffer for 10 minutes prior to stimulation and perfused with imaging buffer heated continuously to 37 ˚C onwards (control) supplemented with Pitstop-2 8-12 seconds before stimulation (Pitstop-2). Cells were stimulated with a HFS train (400 AP, 40 Hz). B) Average time trace ± SEM is displayed with stimulation indicated by black bar. C) Average peak heights of each condition (F/F_0) + SEM. D) Average extent of syp-pH retrieval (endocytosis) measured as a percentage of exocytosis F/F_0 + SEM. Control n=7, Pitstop-2 n=8. Time trace: ****=P<0.0001, Two-way ANOVA. Bar charts: ****=p<0.0001, Student's t-test.

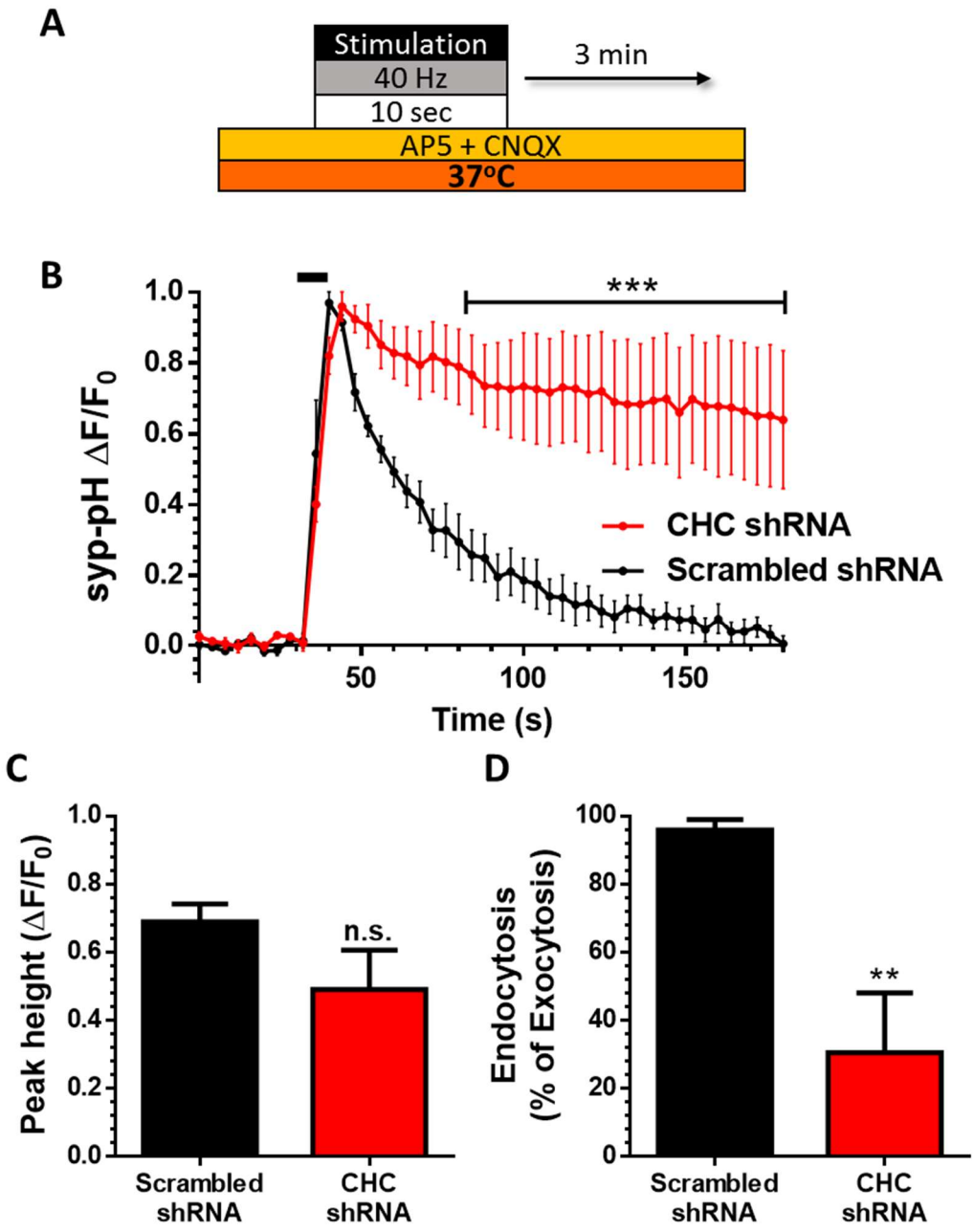

Figure 5.23 Genetic Inhibition Shows a Role for Clathrin in Hippocampal Neurons at Physiological Temperatures

A) Hippocampal neurons co-transfected a control scrambled shRNA (Scrambled shRNA) or CHC shRNA and synaptophysin-pHluorin (syp-pH) were perfused with hippocampal imaging buffer heated continuously to 37 ºC. Cells were stimulated with a HFS train (400 AP, 40 Hz). B) Average time trace ± SEM is displayed with stimulation indicated by black bar. C) Average peak heights of each condition (F/F_0) + SEM. D) Average extent of syp-pH retrieval (endocytosis) measured as a percentage of exocytosis F/F_0 + SEM. Scrambled shRNA n=5, CHC shRNA n=4. Time trace: ***=p<0.001, Two-way ANOVA. Bar charts: **=p<0.01, Student's t-test.

5.3 Discussion

The maintenance of neurotransmission is reliant on the specific and efficient retrieval of deposited SV cargo with the correct stoichiometry, forming fusion-competent SVs for future rounds of exo- and endocytosis. This is performed via a complex set of relationships between adaptor proteins and their cargo, recruiting and sorting the correct constituents from the active zone. These presynaptic adaptor-cargo relationships have so far been specifically identified in the context of CME. There is currently very little known about the specificity of ADBE in retrieving SV cargo during HFS.

It has been proposed that cargo sorting onto SVs occurs predominantly on the endosome after scission (Clayton & Cousin 2009). This is due to the rapid nature of ADBE as well as the requirement for both AP-1 and AP-3 at the budding stage. The need for adaptor proteins may suggest that SV protein uptake is fairly non-selective during ADBE itself and that cargo sorting predominantly occurs on the endosome during this process (Cheung & Cousin 2012).

Using several approaches, it has been shown here that pHluorin-tagged versions of many SV proteins, currently widely used to investigate the recycling of their endogenous counterparts, are not being recycled via ADBE after HFS.

5.3.1 Inhibition of ADBE Does Not Result in Altered Trafficking of a Variety of pHluorins in Different Cell Types

The effect of acute inhibition of ADBE on the recycling of syp-pH during HFS was assessed utilising the necessity for the rephosphorylation of dynamin I for consecutive rounds of ADBE (Tan et al. 2003). CT99021 and roscovitine inhibit this rephosphorylation, causing inhibition of ADBE on a second HFS (Clayton et al. 2010).

Effects on the priming stimulus as a result of drug exposure were noted, the application of CT caused a decreased syp-pH peak height to the S1 (control: 0.41 $\pm$ 0.06, CT: 0.24 $\pm$ 0.04), this reduction was consistent across both stimulations (S2 – control: 0.41 $\pm$ 0.07, CT 0.26 $\pm$ 0.02). The lack of difference in peak height between S1 and S2 implies that this difference is not associated with an effect of CT on ADBE and is due to off-target effects. The resultant ratio of peak heights was consistent with all other conditions (Figure 5.2 F). This effect was not seen with other pHluorins used.

Our results would suggest that ADBE has no significant contribution to the recycling of syp-pH, sybII-pH, tagmin-pH and vGlut-pH. As these pHluorins utilise the same adaptor proteins as their endogenously expressed counterparts it could therefore be concluded that the same is true for the endogenous SV proteins.

The knockdown of syndapin I and chronic inhibition of ADBE had no effect on either release or retrieval of syp-pH during HFS. Further implying that ADBE does not play a role in the retrieval of synaptophysin-pHluorin during HFS.

Another approach to this study would be through the use of a syndapin I "knocksideways" experiment. Rapamycin is used to form a heterodimer between an exogenously expressed protein of interest tagged with an FKBP domain and a mitochondrial marker containing a complimentary FRB domain, rapidly re-routing the protein of interest. If this is done in a cell which has also been depleted of its endogenous protein of interest this is termed "knocksideways" (Robinson et al. 2010) and allows one to visualise the effect of an almost instantaneous knockdown. This has advantages over the procedures used here as it precludes the possibility of any confounding off-target drug effects cause by pharmacological intervention or compensatory mechanisms caused by a chronic knockdown. However, an FKBP-tagged protein which is re-routed may also carry with it any proteins with which it is bound. Therefore, any functional effect seen upon rapamycin exposure may also be due to a re-routing of these binding partners.

However, I achieved consistent results between acute pharmacological and chronic knockdown inhibition of ADBE and the knockdown used here did not result in a phenotype that would suggest injury to transfected cells. As such, I am confident in these results.

5.3.2 No disparity is Seen Between Acid-Accessible pHluorin Pre- and Post-Stimulation

The rate of CME as measured by quenching of fluorescence of internalised pHluorin has been measured as being rapid (4-5 sec) (Sankaranarayanan & Ryan 2000; Atluri & Ryan 2006). Although it has been suggested a slower acidification rate of 15

seconds (Egashira et al. 2015), this was only detectable utilising SV proteins tagged to mOrange.

The probes mOrange and pHluorin differ in pKa (the pH at which half of the probes molecules are protonated), with values of 6.5 (Shaner et al. 2008) and 7.1 (Sankaranarayanan & Ryan 2000) respectively. This means that mOrange is a more accurate tool to measure the later stages of vesicle acidification. However, mOrange is not entirely quenched inside a fully acidified vesicle SV, meaning it would not be an appropriate tool for some of the experiments here such as the acid-wash assays.

It is known that the fluorescence of pHluorins used in this thesis are rapidly quenched when internalised via CME. As pHluorin is used for each experiment discussed in this thesis, and an attempt to infer information as to the time taken until full acidification of a structure after endocytosis was not made, it is a suitable tool for these experiments.

Using acidic washes and HFS I found no evidence of syp-pH retrieving via any structure which it is not immediately acidified. These results are in concordance with previous data acquired at lower frequencies (Sankaranarayanan & Ryan 2000) in which conditions ADBE is not active.

The lack of evidence for sequestered syp-pH after HFS would indicate no role for ADBE in the retrieval of syp-pH in conditions when it is the dominant form of endocytosis.

5.3.3 Inhibition of CME Results in Massive Deficits in syp-pH Retrieval

The effects of inhibiting CME was investigated through different means. Firstly via Pitstop-2 which inhibits the interaction between clathrin and adaptor protein-2 (AP-2) (Von Kleist et al. 2011) effectively inhibiting the formation of a clathrin-coated pit leading to inhibition of CME.

Inhibiting CME pharmacologically resulted in a dramatic inhibition of syp-pH retrieval during a stimulation protocol in which CME is not the dominant form of endocytosis.

In a recent paper it was suggested that pHluorins should not be utilised in conjunction with pitstop-2 due to an undefined effect on vesicle acidity (Hua et al. 2013). However, I have shown that this caution was not relevant here; the innate fluorescence of a pHluorin-transfected cell does increase after exposure to pitstop-2, but only after the period of time in which the other experiments using this drug were completed.

Another concern with the use of pitstop-2 is due to its “non-specificity” (Willox et al. 2014). It has been noted that the inhibition of CME caused by exposure to pitstop-2 is not purely a result of its action on the N-terminal domain of clathrin heavy-chain as was previously believed. As such, no assumptions should be drawn about this domain from experiments with pitstop-2. However, as pitstop-2 is a potent inhibitor of CME and as I was not probing for functions of specific domains within the clathrin complex, pitstop-2 is a suitable tool for these purposes.

A knockdown of CHC was also utilised to investigate the effects of inhibiting CME on pHluorin retrieval. Using the same shRNA and scrambled controls a knockdown of 75% (CGNs) or 80% (hippocampal neurons) of CHC was seen in comparison to non-transfected controls. Using this shRNA, a significant inhibition of syp-pH retrieval was seen in both CGNs and hippocampal cells for LFS (300 AP, 10 Hz) and HFS (400 AP, 40 Hz) showing that whether CME is the dominant form of endocytosis or not, it has a major role in the trafficking of syp-pH across different cell types.

An unusual finding within this dataset was that the knockdown of CHC causes an inhibition of ADBE as measured by dextran in CGNs but not hippocampal neurons. Although it is not certain why this may be, one possibility is that it is due to the different culture conditions of the two cell types. CGNs are unusual in that they are cultured in permanently depolarising conditions (Burgoyne & Cambray-Deakin 1988). This means ADBE is active throughout the period of culture for CGNs, whereas it is not in hippocampal neurons. Since CHC is also necessary for the budding of SVs from bulk endosomes (Heerssen et al. 2008; Kasprowicz et al. 2008; Kononenko et al. 2014) it is possible that with a knockdown of CHC in CGNs there is a build-up of un-budded endosomes. Any proteins essential for ADBE may remain sequestered on these endosomes, leading to an inability to form new endosomes from the PM upon stimulation. In support of this theory, the inhibition of CME acutely via pitstop-2 does not cause an inhibition of ADBE in CGNs as measured by dextran uptake.

Previous work focussing on the role of clathrin or CME in pHluorin retrieval have yielded varied results. Granseth et al. used CHC siRNA to reveal the role for CME in syp-pH retrieval. Their group found significant inhibition in syp-pH retrieval in a CHC-depleted cell in comparable levels to work shown here with both 4 and 40 AP at 20 Hz stimulation (Granseth et al. 2006). This is in agreement with my findings.

However, another study using CHC shRNA showed an effect of CHC-depletion on tagmin-pH retrieval only during mild stimulation (200 AP, 5 Hz) and a lack of any inhibition on the retrieval of tagmin-pH during a high frequency stimulus train (200 AP, 40 Hz) (Kononenko et al. 2014). To address this anomalous result these experiments were recreated here, using tagmin-pH as opposed to syp-pH and the slightly different stimulation protocol used by Kononenko et al. of 200 AP, 40 Hz. In these experiments, a significant inhibition in tagmin-pH was seen using this experimental paradigm.

The reasons for the conflicting findings in this area are undetermined. The cell type and stimulation profile used is identical, although the buffers utilised for imaging are different. The resultant levels of CHC after knockdown were also comparable, although the method of shRNA delivery was different. Kononenko et al. utilised a lentiviral vector which preferentially infects excitatory neurons (Nathanson et al. 2009). It is possible that a culture-wide infection of excitatory neurons with CHC shRNA would reduce glutamatergic transmission, leading to a decrease in spontaneous activity within the culture. To control for this possible discrepancy, hippocampal neurons co-transfected with CHC shRNA or its scrambled control and syp-pH were exposed to tetrodotoxin for 48 hours, silencing the culture prior to the

same stimulation. Using this protocol, a comparable level of inhibition in syp-pH retrieval was seen to that in previous experiments with CHC shRNA, contradicting those seen by Kononenko et al..

Further work could be done to identify the causes for these inconsistent results. A recent paper has noted a large variability of CHC knockdown efficacy even within cells exposed to the same shRNA (López-Murcia et al. 2014). This could be an explanation as to inconsistent results found between different laboratories. This work also found a correlation between resultant level of CHC after knockdown and its functional effect in autaptic synapses.

Other CME-essential machinery has been examined in previous studies as to their role in SV protein retrieval. Knockdowns of subunits of AP-2 have shown marked effects on the kinetics of endocytosis of a multitude of pHluorin-tagged SV proteins during mild stimulation (Kim & Ryan 2009; Kononenko et al. 2014). Effects on retrieval during HFS has been less intensively examined. One study observed an effect of AP-2 knockdown on tagmin-pH retrieval at low frequencies which was lost at high frequencies (Kononenko et al. 2014). However, another found endocytic slowing of vGlut-pH retrieval at higher frequencies (Foss et al. 2013).

Knockdowns are not an ideal system to test for the role of a protein. This is due to the possibility of compensatory effects or, in the case of CHC, injury to the cells especially after a 7-day transfection such as is utilised for hippocampal neurons. A loss of CHC over a prolonged period may affect the health of a neuron due to the loss of spontaneous activity.

An observably unhealthy cell or nerve terminal would usually be excluded from a data-set. This is accomplished due to its characteristic lack of pHluorin retrieval after stimulation. Any nerve terminals exhibiting these traces are routinely screened out during data analysis. However, as this characteristic is the resultant phenotype of CHC knockdown, the same screening protocols could not be conducted on both conditions in these experiments. To ensure there was no bias in the analysis of these results a separate analysis was performed including all nerve terminals which responded to stimulation with an increase in fluorescence. This was performed in both conditions, regardless of whether this fluorescence then decreased. The results were consistent. Although the control condition average traces no longer appeared to retrieve as quickly or efficiently due to the inclusion of these "unhealthy" traces, there was still a significant difference between fluorescent traces from control and CHC knockdown neurons, in which syp-pH retrieval was severely impaired after HFS (data not shown).

Unhealthy cells are symptomatic of a chronic removal of an essential protein. However, due to the high level of reproducibility between cell types, stimulation intensities and means of CME intervention (both chronic and acute), as well as corroborative results from another, independent team I am confident that the inhibition seen here with the knockdown of CHC is due to a real effect on the retrieval of pHluorins caused by the inhibition of CME during HFS.

5.3.4 ADBE Does Not Gain New Roles in pHluorin Recycling at Physiological Temperatures

Recent work using the extremely rapid “flash and freeze” fixation process has shown that single AP stimulation elicits an entirely different endocytic mode exclusively at physiological temperatures (34-37 ºC): ultrafast endocytosis.

Ultrafast endocytosis forms large vesicles (60-80 nm diameter) from the PM by means of actin polymerisation which can be seen fully formed in the synapse as little as 50 ms after a single action potential (Watanabe, Rost, et al. 2013). Although ultrafast endocytosis is clathrin-independent, the large endocytic vesicles created bud into SVs via a clathrin-dependent mechanism after around 3 seconds (Watanabe et al. 2014).

The molecular physiology of a large endocytic vesicle formed via ultrafast endocytosis has not been studied and as such it is not known which, if any, SV cargo proteins are retrieved via this mechanism. Although, since it appears that CME does not occur during these stimulation conditions (Watanabe et al. 2014) one would assume that ultrafast endocytosis would be responsible for recycling deposited SV proteins. However, studies have not yet investigated whether action potential trains would evoke ultrafast endocytosis at physiological temperatures or if CME activation would then be required for the retrieval of SV cargo.

To assess the function of clathrin at physiological temperatures pitstop-2 was used. It was found that the inhibition of syp-pH retrieval in the presence of pitstop-2 was not as pronounced at physiological temperatures as at room temperature. One reason for

this could be the pitstop-2 itself; it is stable at room temperature for a period of hours but it is not known what happens to the compound when heated to 37 ºC. It is possible that in these conditions the drug has started to degrade by the time it reaches the culture leading to a lower efficiency, as such these results should be treated with caution.

It is also possible that at physiological temperature, syp-pH retrieval is less reliant on CME as another, high capacity form of clathrin-independent endocytosis has been activated: ultrafast endocytosis.

However, experiments utilising the same CHC shRNA as previously conducted at this new temperature resulted in a comparable inhibition of syp-pH retrieval as that seen at room temperature. This implies that the muted effect on syp-pH retrieval seen at physiological temperatures using pitstop-2 is more likely due to a deactivation of the compound due to its heating prior to exposure to the cell.

The inhibition of clathrin function in these conditions, either through pharmacological intervention or through CHC knockdown, will cause not only the inhibition of CME from the PM but also the budding of SVs from any large ultrafast vesicles. Both of these processes would occur within the timeframe of the experiments described. As it is unknown whether ultrafast large vesicles acidify before or after budding it should be remembered that what is being visualised here in the retrieval of syp-pH is the role of clathrin and not specifically of CME. However, the differences in diameter between these two structures would mean an acidification time around twice as long for an ultrafast vesicle as a SV.

In summary, I have shown through various manipulations of both CME and ADBE that a variety of SV cargoes are predominantly retrieved via clathrin-dependent endocytosis, with no evidence of its internalisation via ADBE.

VAMP4 is a Specific and Necessary Cargo for ADBE

6. VAMP4 is a Specific and Necessary Cargo for ADBE

6.1 Introduction

The formation of functional, fusion-competent SVs requires the incorporation of the correct protein cargo with the appropriate stoichiometry (Ashby et al. 2006). CME efficiently retrieves SV cargo deposited into the PM during exocytosis via a clathrin coat and a series of different adaptor proteins (Rao et al. 2012; Kelly & Owen 2011).

Bulk endosome formation is a rapid, high capacity means of retrieving membrane during intense stimulation (Clayton et al. 2008). However, results acquired and detailed in the previous chapter would suggest that ADBE does not retrieve a substantial proportion of many SV cargoes.

ADBE is thought to be clathrin-independent as inactivation or knockdown of clathrin does not affect the formation of bulk endosomes as measured by FM-dye uptake (Heerssen et al. 2008; Kasprowicz et al. 2008) or electron microscopy (Kononenko et al. 2014) (but see Figure 5.16) in neurons. It is unknown if any adaptor proteins or SV cargo are involved with specificity for ADBE or ultrafast endocytosis at the PM.

SVs formed via ADBE repopulate the reserve pool, a population of SVs which are only mobilised during intense stimulation and after the synchronous release of the RRP (Richards et al. 2003; Cheung et al. 2010). This would imply that they possess a specific molecular identity allowing them to be recognised and shuttled to the appropriate pool. This also implies that SVs formed from bulk endosomes gain the necessary cargo proteins to be fusion-competent. However, as was shown in the previous chapter, this does not occur via retrieval from the PM. One possibility is

that these SVs are shuttled through an endosomal intermediate, equipping them with the SV proteins required to allow future exocytosis.

I aimed to determine if any cargo proteins were retrieved from the PM via ADBE. If so, I also aimed to identify any adaptor proteins which may facilitate this retrieval. The existence of such would allow ADBE-derived SVs a specific protein composition, allowing their recognition and appropriate shuttling to vesicle pools or endosomal intermediates.

To examine this possibility, a candidate ADBE-retrieved SV protein was needed. The SV protein VAMP4 was chosen as VAMP4-pHluorin (VAMP4-pH) exhibits an unusual fluorescence change upon stimulation at higher frequencies in hippocampal cells (Raingo et al. 2012). On such HFS VAMP4-pH reports an activity-dependent decrease in fluorescence. This is the opposite to the majority of pHluorins which show a dramatic increase in fluorescence during such stimuli. It is possible that this activity-dependent decrease in fluorescence could denote a retrieval of VAMP4-pH via ADBE.

It is possible ADBE is responsible for generating SVs that mediate asynchronous release making VAMP4 of particular interest as a potential ADBE cargo due to its role in mediating asynchronous neurotransmitter release (Raingo et al. 2012). Up- or downregulation of VAMP4 expression in mouse hippocampal cells caused a correlative effect on the amount of asynchronous release. AP-3b2 knock out mice have a decreased capacity for asynchronous release (Evstratova et al. 2014) and AP-3 is known to be essential for the budding of SVs from a bulk endosome (Cheung & Cousin 2012).

It has been proposed that the ratio of synaptobrevin II to VAMP4 dictates in which pool an SV resides (Raingo et al. 2012). The model proposed is thus: SVs containing a high abundance of synaptobrevin II and a lower abundance of VAMP4 are directed for synchronous release, whereas SVs with a higher abundance of VAMP4 compared to synaptobrevin II are utilised to sustain asynchronous release. As bulk endosomes show a de-enrichment of synaptobrevin II (Nicholson-Fish et al. 2015) it is possible that uptake of VAMP4 via ADBE forms SVs with a distinct molecular signature, directing them to maintain a SV pool responsible for mediating asynchronous release.

I aimed to investigate the possibility that SVs with a higher proportion of VAMP4 molecules are formed via ADBE. The retrieval of the pHluorin-tagged VAMP4 protein was tracked under different stimulation conditions.

6.2 Results

6.2.1 The VAMP4-pHluorin Response Differs Between High and Low Frequency Stimulation

VAMP4-pH has been identified as a potential reporter of ADBE due to its unusual fluorescence change upon HFS (Raingo et al. 2012). However, in this study the response of VAMP4-pH to milder stimulation was not examined. This is important as ADBE does not occur during mild stimulation and any differences observed in the response of VAMP4-pH between high and low frequency stimulation could reveal differential trafficking that should be characteristic of an ADBE cargo protein.

Firstly, VAMP4-pH retrieval in CGNs at different stimulation intensities was investigated. Co-transfection of mCer with VAMP4-pH allowed identification of transfected neurites as VAMP4-pH has a low basal fluorescence. The VAMP4-pH fluorescence of transfected cells was recorded as they were stimulated with a train of 300 AP at 10 Hz (LFS) to selectively stimulate CME, or 400 AP at 40 Hz (HFS) to initiate both CME and ADBE (Figure 6.1 A).

The fluorescence of individual nerve terminals expressing VAMP4-pH was plotted over time (Figure 6.1 B and C). After a LFS, nerve terminals predominantly displayed an increase in fluorescence after stimulation (Figure 6.1 B). This resulted in an average trace which has a small but steady increase in fluorescence over time. This is in agreement with Raingo et al. as this is potentially the reporting of asynchronous release of SVs containing VAMP4-pH. These responses have been termed “upstrokes” as they continue to increase after stimulation terminates.

After HFS, a large proportion of synapses exhibited a decrease in fluorescence below baseline after stimulation terminated (termed “downstrokes”) as well as a smaller proportion still exhibiting upstrokes. This results in an average trace which remains relatively stable during and after stimulation (Figure 6.1 C). When proportions of synapses exhibiting either upstrokes or downstrokes are compared between LFS and HFS, there are significantly more nerve terminals exhibiting downstrokes in fluorescence during HFS (Figure 6.1 D). This suggests that during HFS VAMP4-pH is being internalised through an endocytic mode which does not occur during or after LFS. It is possible that these slow downstrokes represent a slowly acidifying endosome.

To determine whether this activity-dependent response profile was specific to CGNs or common across multiple cell types, the same experiments were conducted in hippocampal neurons (Figure 6.2 A). After LFS, VAMP4-pH transfected hippocampal cells displayed an average fluorescence trace which increased over time (Figure 6.2 B) in concordance with VAMP4-pH response in CGNs.

Hippocampal cells exposed to HFS, unlike CGNs, exhibited an immediate decrease in fluorescence. The rapid nature of this downstroke may suggest something other than bulk endosome acidification and may be due to an increased rate of CME during HFS. This immediate decrease was then followed by either slow increases or decreases in fluorescence after stimulation, in a similar manner and magnitude to that observed in CGNs (Figure 6.2 C). These slower changes are defined as upstrokes and downstrokes for hippocampal neurons. When comparing the proportions of synapses exhibiting upstrokes versus downstrokes in fluorescence, there is a significant

increase in the proportion of downstrokes in cells during HFS compared to LFS (Figure 6.2 D).

The initial decrease followed by either an upstroke or downstroke in fluorescence described can also be directly observed when viewing time-lapse images. Focussing on individual nerve terminals one can see that, upon stimulation, the fluorescence of a responsive nerve terminal sharply decreases, followed by a bidirectional change in fluorescence over a longer period of time (Figure 6.3).

Hippocampal neurons and CGNs both display a significant increase in the number of nerve terminals displaying downstrokes in fluorescence after HFS. CGNs show an average proportion of around 60% of synapses displaying downstrokes. In agreement, previous work has identified that only a subpopulation of CGN nerve terminals undergo ADBE during intense stimulation as measured by dextran uptake (Clayton & Cousin 2009). This was also the case with hippocampal nerve terminals, however this subpopulation was found to be smaller than present in CGNs (Wenzel et al. 2012). In agreement, the experiments conducted here revealed that the proportion of hippocampal cell nerve terminals displaying downstrokes was smaller than in CGNs, around 40%.

The different response profiles between HFS and LFS in both hippocampal neurons and CGNs would suggest that this pHluorin is being trafficked via different endocytic modes in an activity-dependent manner. ADBE is the dominant form of endocytosis during HFS. As such, it is possible that the downstrokes in VAMP4-pH fluorescence observed almost entirely during HFS are in fact nerve terminals in which VAMP4-pH has been internalised via ADBE. The slow decrease in

fluorescence that persists after HFS could therefore be an indicator of the slow acidification kinetics of a bulk endosome.

In addition to the hypothesis presented above, there are other potential explanations for the appearance of VAMP4-pH downstrokes during HFS. One possibility is that the decrease in fluorescence is not due to an acidification, but due to relocation of VAMP4-pH from the area of the allocated ROI used to measure fluorescence intensity. To test this, a dataset from a previous experiment using hippocampal neurons transfected with VAMP4-pH (Figure 6.4 A) was re-analysed. Firstly, standard 3x3 pixel ROIs were placed over synapses (Figure 6.4 B) and fluorescence within these ROIs was monitored over time. These ROIs were then increased in diameter to form 6x6 pixel ROIs (Figure 6.4 C) and again fluorescence within these ROIs was measured over time.

When traces from both ROI sets were averaged and overlaid there was no difference observed (Figure 6.4 D) and the same characteristics were seen; an immediate downstroke followed by a diversity of upstrokes or downstrokes. This shows the immediate decrease and any changes after this were not due to an escape of VAMP4-pH from the nerve terminal.

6.2.2 Pharmacological Inhibition of ADBE Inhibits VAMP4-pHluorin Downstrokes

So far experiments using VAMP4-pH in both hippocampal neurons and CGNs have indicated a difference in its fluorescent response between HFS and LFS, with a large population of synapses exhibiting a slow decrease in fluorescence after HFS only.

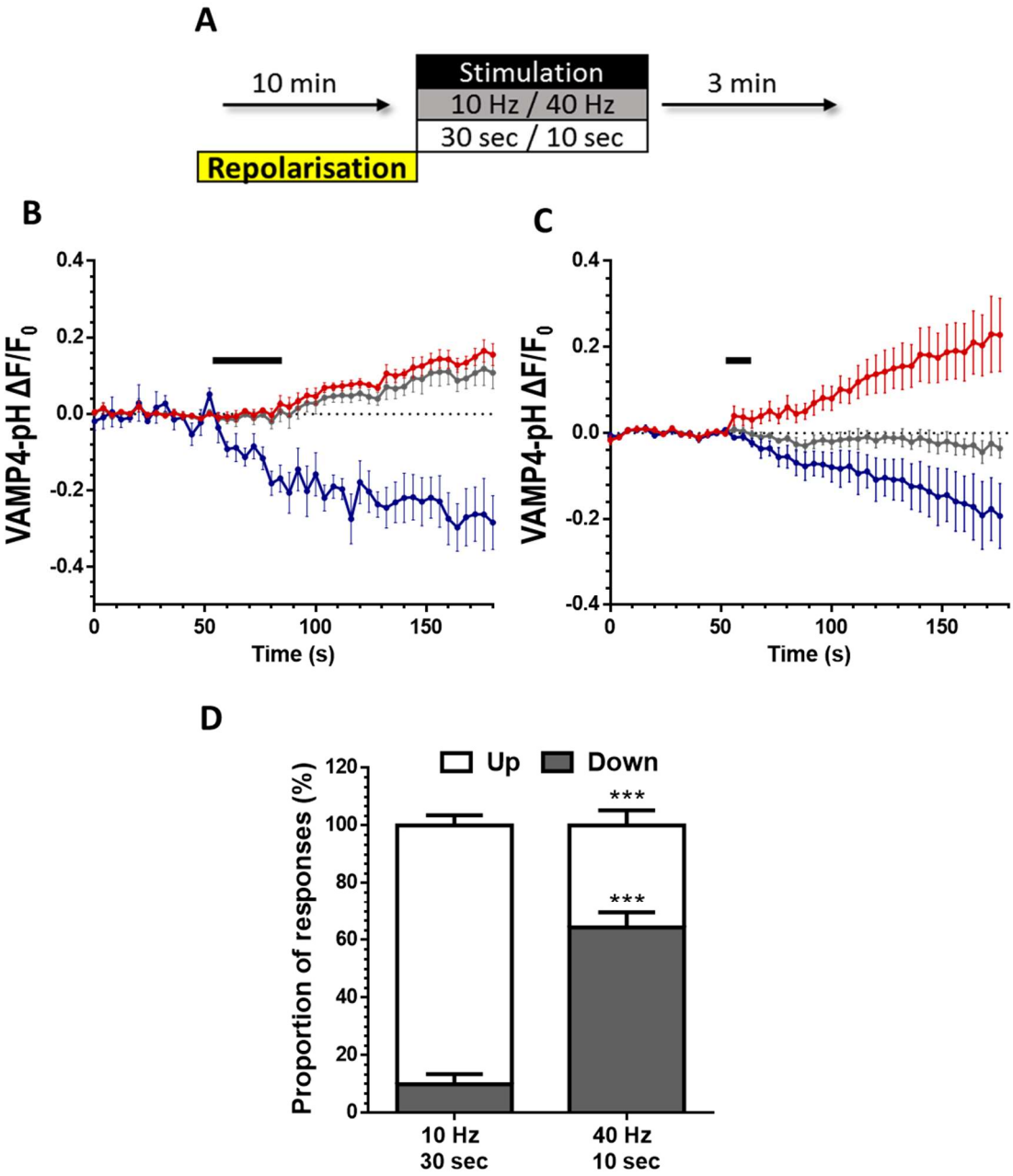

Figure 6.1 VAMP4-pHluorin Responds Differently between Stimulation Intensities in CGNs

A) CGNs co-transfected empty mCer vector and VAMP4-pHluorin (VAMP-pH) were incubated in imaging buffer for 10 mins prior to stimulation and then continuously onwards. Cells were stimulated with a LFS or HFS train (300 AP, 10 Hz or 400 AP, 40 Hz respectively). B and C) Representative averages (grey) LFS and HFS time trace respectively with separated populations of increasing (Up, red) and decreasing (Down, blue) fluorescence ± SEM with stimulation indicated by black bar. D) Average proportions of synapses within a transfected cell increasing (Up) or decreasing (Down) in VAMP4-pH fluorescence after stimulation + SEM. 10 Hz 30 sec n=5, 40 Hz 10 n=7. ***=p<0.001. Student's t-test between conditions.

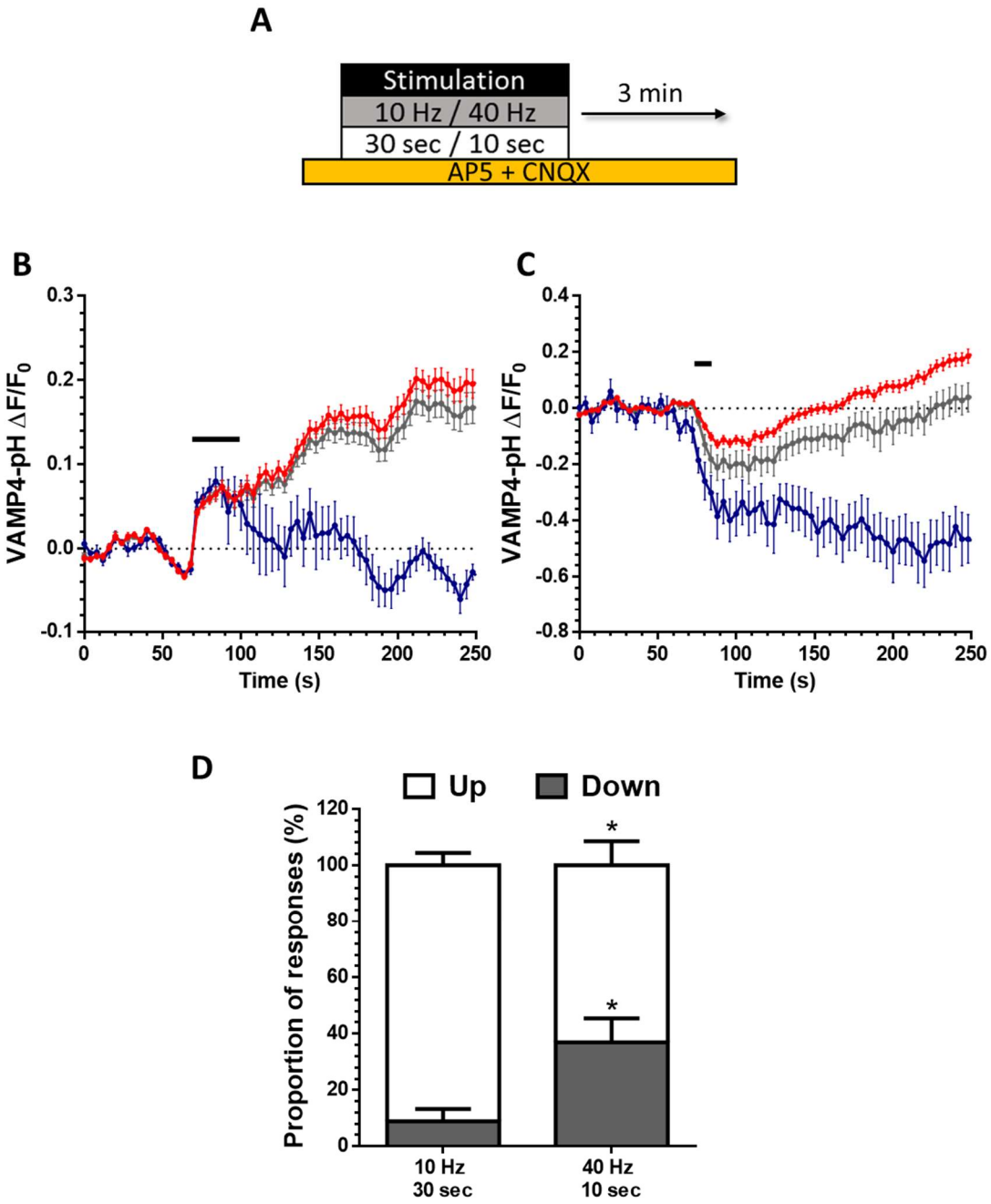

Figure 6.2 VAMP4-pHluorin Responds Differently between Stimulation Intensities in Hippocampal Neurons

A) Hippocampal neurons co-transfected empty mCer vector and VAMP4-pHluorin (VAMP-pH) were perfused with continuously. Cells were stimulated with a LFS or HFS train (300 AP, 10 Hz or 400 AP, 40 Hz respectively). B and C) Representative averages (grey) LFS and HFS time trace respectively with separated populations of increasing (Up, red) and decreasing (Down, blue) fluorescence ± SEM with stimulation indicated by black bar. D) Average proportions of synapses within a transfected cell increasing (Up) or decreasing (Down) in VAMP4-pH fluorescence after stimulation + SEM. 10 Hz 30 sec n=3, 40 Hz 10 n=4. *=$p<0.05$. Student's t-test between conditions.

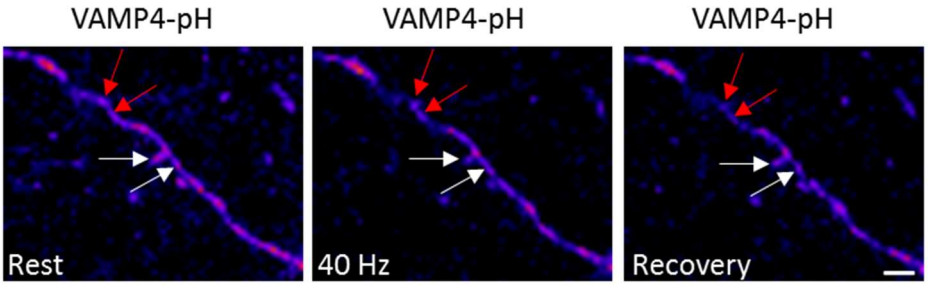

Figure 6.3 Bi-Directional Changes in VAMP4-pH Fluorescence are Directly Visible During Image Acquisition

Hippocampal neurons transfected with VAMP4-pH before (left) during (middle) and after (right) HFS (400 AP, 40 Hz). All arrows indicate responsive synapses, which decrease in fluorescence during stimulation. After stimulation has cease, each responsive synapse continues to either increase in fluorescence (“upstrokes”, white arrows) or decrease in fluorescence (“downstrokes”, red arrows). Scale bar, 10 μm.

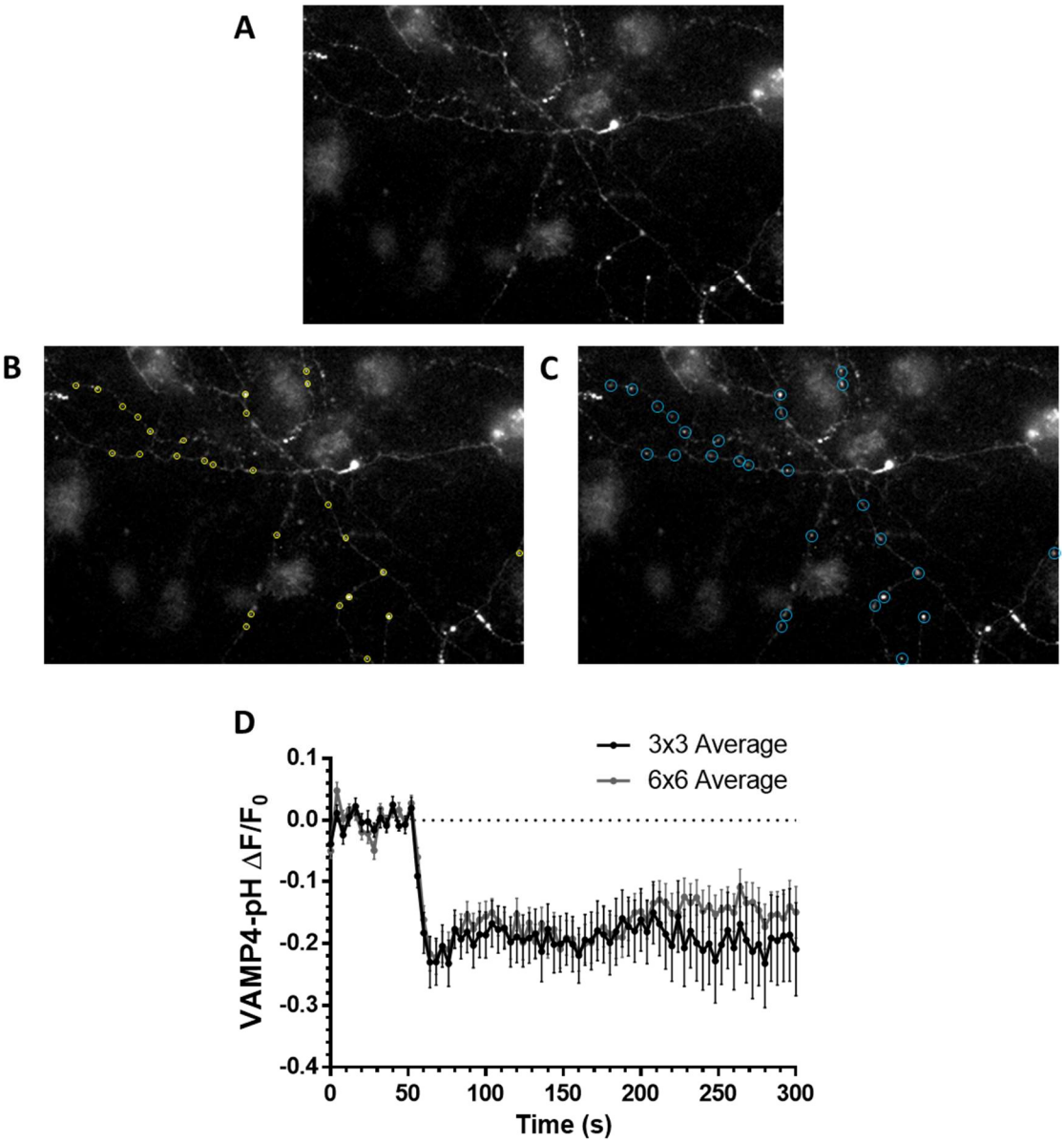

Figure 6.4 Evoked Decrease in VAMP4-pH Fluorescence is not due to its Escape from the Nerve Terminal

A) Hippocampal neurons transfected with VAMP4-pH were perfused continuously with hippocampal imaging buffer. Cells were stimulated with a HFS train (400 AP, 40 Hz). B) 3x3 pixel ROIs were placed over synapses as revealed by an ammonia imaging buffer pulse and fluorescence monitored over time. C) These ROIs were then increased in diameter to 6x6 pixels and fluorescence monitored over time. D) Time traces of VAMP-pH fluorescence ± SEM from 3x3 pixel ROIs (black) and 6x6 pixel ROIs (grey) overlaid.

I next tested the hypothesis that observed downstrokes in VAMP4-pH fluorescence during HFS represent VAMP4-pH internalised in a slowly acidifying bulk endosome. This was done via the pharmacological inhibition of ADBE. CGNs co-transfected with VAMP4-pH and an empty mCer vector were stimulated with 2 HFS trains 10 minutes apart, with or without the GSK3 inhibitor CT99021 (CT, 10 μM) (Figure 6.5 A) in an identical "S1 S2" protocol to that performed previously on cells expressing syp-pH, vGlut-pH, tagmin-pH and sybII-pH (see Figure 5.2, Figure 5.3, Figure 5.4 and Figure 5.5 respectively). This protocol allows visualisation of effects on VAMP4-pH trafficking during an acute inhibition of ADBE at S2.

For control conditions, both S1 and S2 exhibited the same proportion of each type of response as seen with a single HFS (Figure 6.5 B), however there was little uniformity of response per nerve terminal between S1 and S2 i.e. a typical nerve terminal exhibiting an upstroke during S1 could exhibit either an up- or downstroke during S2 and vice versa (Figure 6.6). The resultant diversity of responses led to four classifications of responsive nerve terminals:

- S1 Upstroke, S2 Upstroke
- S1 Upstroke, S2 Downstroke
- S1 Downstroke, S2 Upstroke
- S1 Downstroke, S2 Downstroke

These were then grouped based on the response of a nerve terminal per stimulation e.g. the "S1 Up" group included nerve terminals that exhibited an upstroke after S1 regardless of which response occurred on S2 (Table 6.1).

Stimulation	S1	Grouping	S2	Grouping
Direction	Upstroke	S1 "Up"	Upstroke	S2 "Up"
	Upstroke	S1 "Up"	Downstroke	S2 "Down"
	Downstroke	S1 "Down"	Upstroke	S2 "Up"
	Downstroke	S1 "Down"	Downstroke	S2 "Down"

Table 6.1 Grouping of VAMP4-pH transfected Synapses by Fluorescence Response after Stimulation

Control cells showed the same proportion of upstrokes and downstrokes over both S1 and S2. In the presence of CT, the same proportions of upstrokes and downstrokes were seen during the S1 as in control cells (Figure 6.5 C), this indicates there is no effect of CT exposure on the retrieval of VAMP4-pH during the priming stimulus. However, in the presence of CT there was a significant reduction in the proportion of synapses exhibiting a downstroke after S2 (in which ADBE had been inhibited) (Figure 6.5 C).

These results support the hypothesis that the slow downstrokes in VAMP4-pH fluorescence after HFS represent VAMP4-pH molecules that have been retrieved via ADBE and are contained within a slowly acidifying bulk endosome.

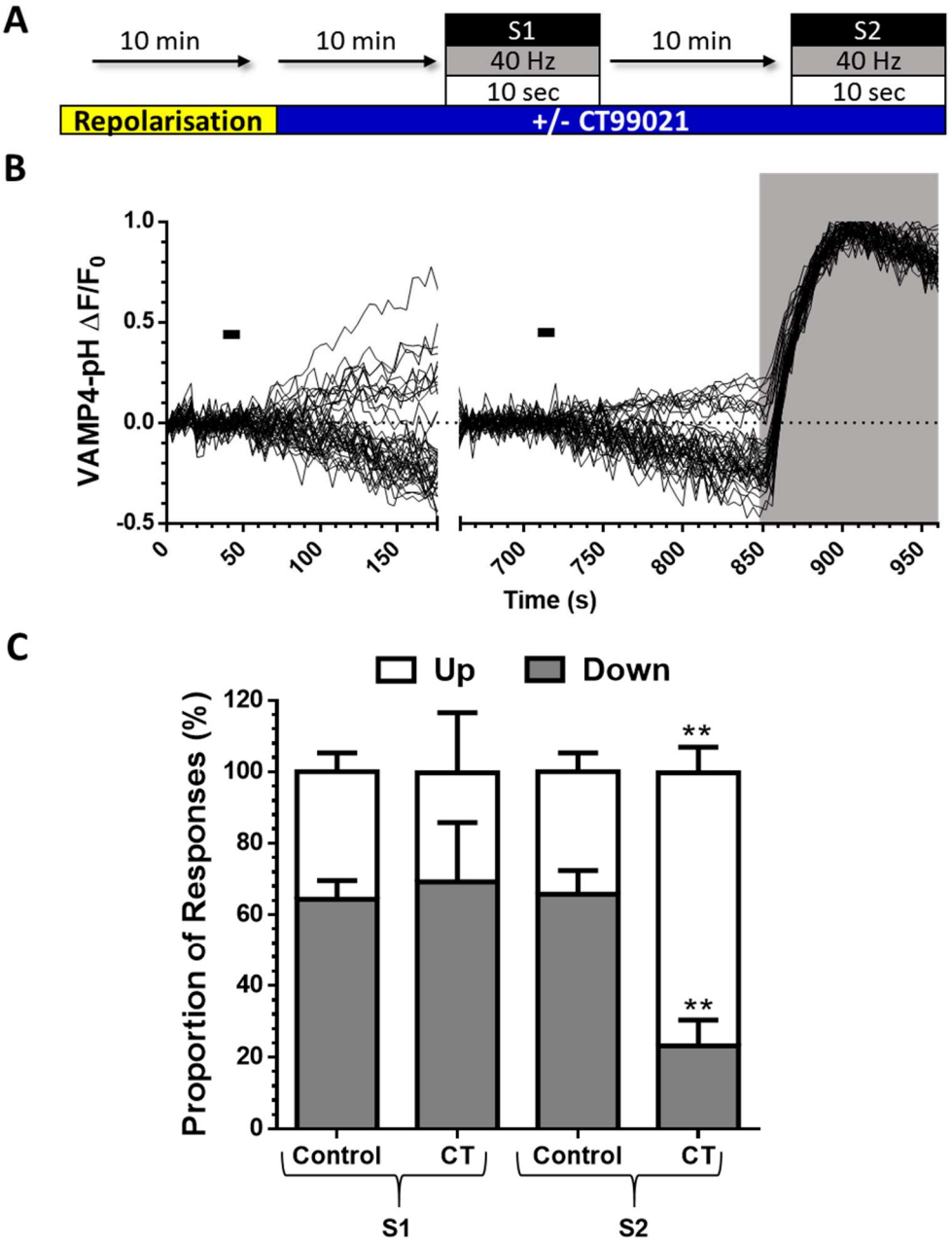

Figure 6.5 Pharmacological Inhibition of ADBE Inhibits VAMP4-pHluorin Downstrokes

A) CGNs co-transfected empty mCer vector and VAMP4-pHluorin (VAMP-pH) were incubated in imaging buffer for 10 mins before being incubated in imaging buffer alone (control) or supplemented with 2 μM CT99021 (CT) for 10 minutes prior to S1 and then continuously onwards. Cells were challenged with 2 sequential HFS trains (400 AP, 40 Hz) (S1 and S2) 10 minutes apart. B) Representative control time course depicting decay corrected responses of all responding synapses on one transfected cell normalised to NH+ pulse (grey band). C) Average proportions of synapses within a transfected cell increasing (Up) or decreasing (Down) in VAMP4-pH fluorescence after S1 and S2 + SEM. Control n=5, CT n=7. **=p<0.01. Student's t-test Control Vs CT S1 and S2.

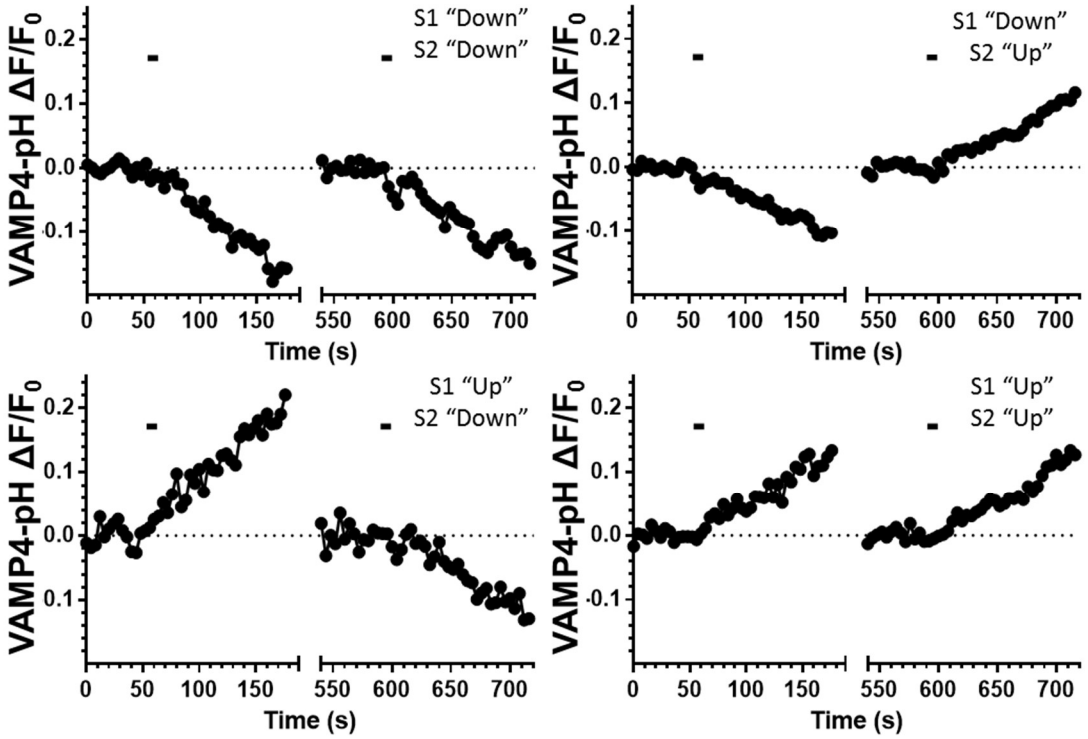

Figure 6.6 Example of Diversity of Responses Within VAMP4-pH "S1 S2" Experiment

Representative VAMP4-pH fluorescence traces from individual nerve terminals of one transfected CGN. Each of the four classifications of responses is represented: S1 “Down” S2 “Down” (top left), S1 “Down” S2 “Up” (top right), S1 “Up” S2 “Down” (bottom left), S1 “Up” S2 “Up” (bottom right). Black bars represent stimulation.

Interestingly, the proportions of upstrokes and downstrokes were consistent across S1 and S2 for control cells even though the identity of those nerve terminals displaying a downstroke differs between the two stimulations. Thus transfected cells display a consistent proportion of nerve terminals undergoing ADBE across sequential stimuli, even though the subpopulation of nerve terminals undergoing ADBE is altered between stimulations (Figure 6.6).

6.2.3 Genetic Inhibition of ADBE Inhibits Downstrokes of VAMP4-pHluorin After HFS

VAMP4-pH is unique amongst the SV proteins tested here in that the inhibition of ADBE has a pronounced effect on its retrieval profile when compared to a control stimulus.

A separate manoeuvre was used to confirm that VAMP4-pH fluorescence downstrokes represent the quenching of pHluorin molecules which have been internalised by ADBE. Syndapin I shRNA was utilised to inhibit ADBE in an identical protocol as used previously with syp-pH (see 5.2.2).

CGNs co-expressing VAMP4-pH and either an empty mCer-pSuper vector or mCer-pSuper vector expressing syndapin shRNA were subjected to a single HFS (Figure 6.7 A).

CGNs expressing the control pSuper vector exhibited the same, stable average fluorescence trace as seen previously, appearing relatively flat due to individual boutons exhibiting either an increase or decrease in fluorescence. In contrast, the

average response of CGNs expressing syndapin I shRNA noticeably increased in fluorescence after stimulation (Figure 6.7 B). This suggests an alteration in the number of nerve terminals displaying slow downstrokes. When the number of nerve terminals displaying upstrokes and downstrokes was quantified and compared, it was apparent that CGNs expressing the control pSuper vector showed consistent proportions of upstrokes and downstrokes as observed in previous CGN HFS experiments. This is in contrast to CGNs expressing syndapin I shRNA which exhibited a dramatic reduction in the proportion of nerve terminals exhibiting downstrokes (Figure 6.7 C). This results in the overall increase in fluorescence over time when compared to controls.

These results show that VAMP4-pH retrieval is significantly affected by the inhibition of ADBE, whether it be via pharmacological or genetic means. This adds weight to the hypothesis that slow downstrokes could represent the quenching of VAMP4-pH fluorescence in acidifying bulk endosomes. This is an effect not seen with any other pHluorins tested here and as such it appears that VAMP4-pH alone amongst said other pHluorins is recycled via ADBE.

6.2.4 VAMP4-pHluorin is Sequestered into a Slowly Acidifying Environment After High but not Low Frequency Stimulation.

The absence of downstrokes in VAMP4-pHluorin fluorescence after LFS as well as after HFS with the inhibition of ADBE, collectively suggests that VAMP4-pH is being recovered via ADBE. If this is the case, a proportion of VAMP4-pH should be retrieved into a slowly acidifying compartment, with its fluorescent response

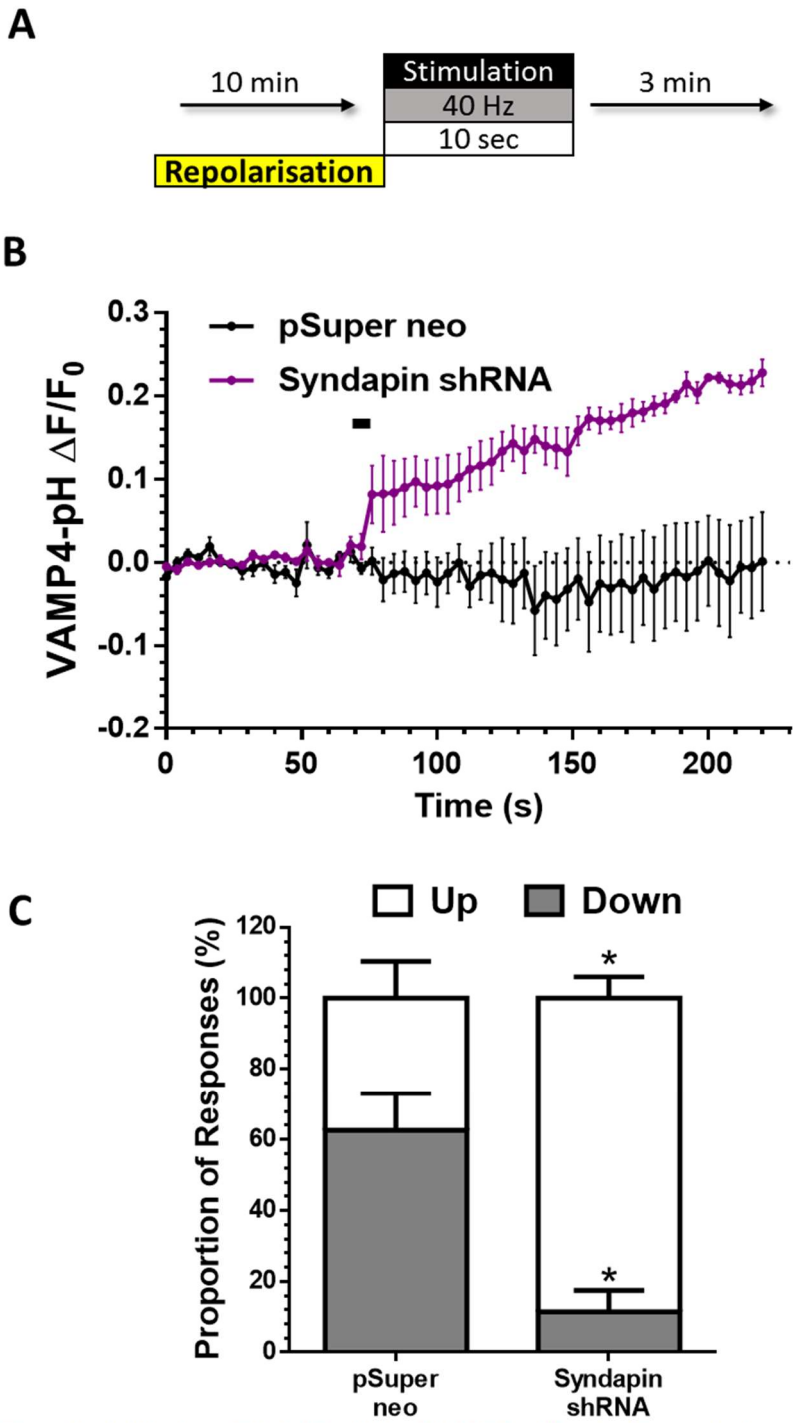

Figure 6.7 Genetic Inhibition of ADBE Inhibits VAMP4-pHluorin Downstrokes

A) CGNs co-transfected with empty mCer-tagged pSuper vector (pSuper neo) or syndapin shRNA and VAMP4-pHluorin (VAMP4-pH) were incubated in imaging buffer for 10 mins prior to stimulation and then continuously onwards. Cells were stimulated with a HFS train (400 AP, 40 Hz respectively). B) Average time traces of fluorescence $\pm$ SEM with stimulation indicated by black bar. C) Average proportions of synapses within a transfected cell increasing (Up) or decreasing (Down) in VAMP4-pH fluorescence after stimulation + SEM. pSuper neo n=5, Syndapin shRNA n=7. *=$p<0.05$. Student's t-test between conditions.

protected from application of an impermeant weak acid to the exterior of the cell. To test this hypothesis, a protocol was employed very similar to that previously designed to determine if syp-pH was sequestered into a slowly acidifying compartment after HFS (see Figure 5.9).

CGNs co-expressing VAMP4-pH and an empty mCer vector were pulsed with impermeant acidic imaging buffer to evaluate the surface or "quenchable" fraction of the VAMP4-pH fluorescence at rest. This fraction was then compared to the "quenchable" portion after a LFS (300 AP, 10 Hz) or HFS (400 AP, 40 Hz) when the cells were quickly subjected to a second acidic imaging buffer pulse (Figure 6.8 A). Any difference observed between the quenchable portions of VAMP4-pH acquired pre- and post-stimulation could indicate molecules which have been taken up via ADBE and are therefore still in a neutral pH environment. One would not expect to identify any difference after a LFS as ADBE does not occur during these stimulation conditions.

When stimulated with a LFS, the quenchable portion of VAMP4-pH fluorescence post-stimulation was almost identical to that before stimulation (Figure 6.8 B). When measured as a percentage of the pre-stimulation portion, 95% of VAMP4-pH previously quenched by an acid wash was still accessible to acid (Figure 6.8 C). Therefore, in CGNs there is no evidence of any sequestered VAMP4-pH after LFS. This is in agreement with the absence of ADBE during this stimulation protocol.

When stimulated with a HFS the quenchable portion of VAMP4-pH is noticeably different post-stimulation to that seen with a LFS (Figure 6.8 B). Around 42% of VAMP4-pH that was quenchable pre-stimulation was inaccessible to acid after HFS

(Figure 6.8 C). This indicates that this subpopulation of pHluorin molecules has been internalised into a neutral pH, for example a bulk endosome.

To determine whether this result was common to other neuronal cell types, the same experimental protocols were repeated in cultured hippocampal neurons (Figure 6.9 A). As seen with CGNs, VAMP4-pH showed no evidence of sequestered pHluorin in an environment of neutral pH after a LFS (Figure 6.9 B and C). This is in contrast to the results found with HFS, where approximately 32% of previously surface-bound pHluorin has been sequestered away from the membrane into a slowly acidifying compartment after stimulation (Figure 6.9 C).

These results further indicate that both CGNs and hippocampal neurons retrieve VAMP4-pH differently in response to either LFS or HFS. During LFS, VAMP4-pH would appear either to not be retrieved or is being retrieved via an endocytic mode that undergoes rapid acidification after scission from the membrane such as CME. During HFS, a large portion of VAMP4-pH appears to be internalised via a structure which takes a significantly longer period of time to acidify, such as a bulk endosome formed via ADBE.

6.2.5 Pharmacological Inhibition of CME does not Alter VAMP4-pHluorin Retrieval

Now that it is apparent that VAMP4-pH is recovered via ADBE, it is important to assess what role, if any, CME plays in the retrieval of VAMP4-pH. This was firstly addressed using the clathrin-cage inhibitor pitstop-2 which inhibits clathrin – AP-2 interactions (Von Kleist et al. 2011).

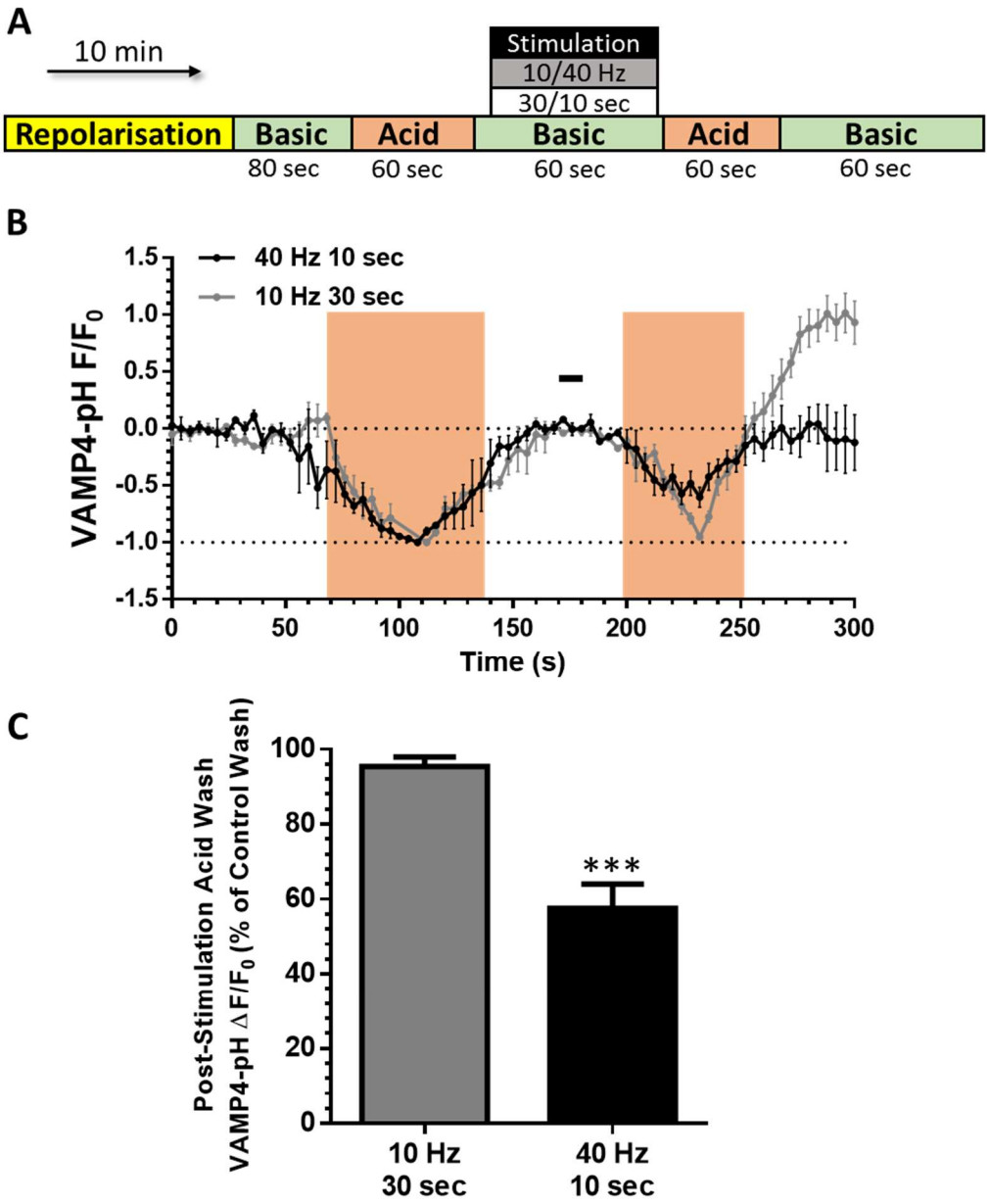

Figure 6.8 VAMP4-pHluorin is Sequestered after HFS but not LFS in CGNs

A) CGNs co-transfected with VAMP4-pHluorin (VAMP4-pH) and mCer were repolarised before a control acid wash (peach bars), isolating fluorescence of surface bound VAMP4-pH. Cells were then stimulated with a LFS/HFS train (300 AP. 10 Hz or 400 AP, 40 Hz respectively) and one more acid wash performed immediately post-stimulation. B) Average time trace F/F_0 ± SEM, traces were normalised to basal fluorescence (0) and the lowest point of the pre-stimulation acid wash (-1). The black bar indicates location of 40 Hz 10 sec stimulation. C) The average difference in fluorescence drop of the post-stimulation acid wash as a percentage of the pre-stimulation acid wash ($\Delta F/F_0$) for 10 Hz 30 sec (grey) and 40 Hz 10 sec (black) + SEM. 10 Hz n=5, 40 Hz n=3. ***= $p<0.001$. Student's t-test.

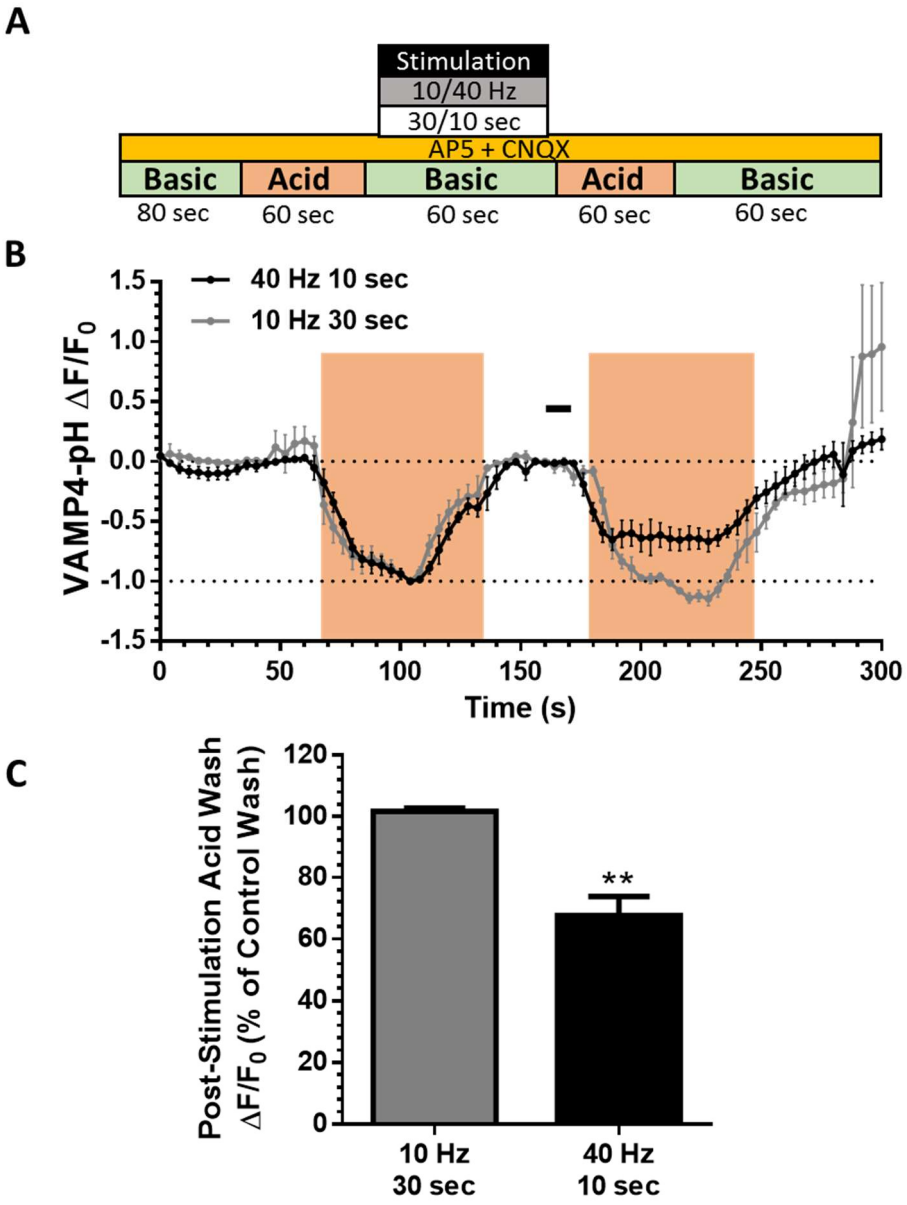

Figure 6.9 VAMP4-pHluorin is Sequestered after HFS but not LFS in Hippocampal Neurons

A) Hippocampal neurons co-transfected with VAMP4-pHluorin (VAMP4-pH) and mCer were given a control acid wash (peach bars), isolating fluorescence of surface bound VAMP4-pH. Cells were then stimulated with a LFS/HFS train (300 AP. 10 Hz or 400 AP, 40 Hz respectively) and one more acid wash performed immediately post-stimulation. B) Average time trace F/F_0 ± SEM, traces were normalised to basal fluorescence (0) and the lowest point of the pre-stimulation acid wash (-1). The black bar indicates location of 40 Hz 10 sec stimulation. C) The average difference in fluorescence drop of the post-stimulation acid wash as a percentage of the pre-stimulation acid wash ($\Delta F/F_0$) for 10 Hz 30 sec (grey) and 40 Hz 10 sec (black) + SEM. 10 Hz n=3, 40 Hz n=4 **= $p<0.01$. Student's t-test.

The role of CME during LFS was assessed using a single LFS train. CGNs transfected with VAMP4-pH and an empty mCer vector were subjected to a stimulus train of 300 AP at 10 Hz. For control conditions, imaging buffer was perfused over the culture continuously. For pitstop-2 conditions, this imaging buffer was supplemented with 15 μM pitstop-2 8-12 seconds before stimulation (Figure 6.10 A).

A significant difference was seen during stimulation when comparing fluorescence traces for both conditions (Figure 6.10 B). Controls cells exhibited a comparable response to those CGNs previously transfected with VAMP4-pH and subjected to a LFS train; the average trace remains fairly stable during stimulation and then exhibits a slow and steady increase after stimulation cessation. CGNs exposed to pitstop-2 however exhibited an increase in fluorescence upon stimulation not usually seen in control cells. This significance disappears after stimulation as control cells continue to increase in fluorescence to a comparable level seen during stimulation in pitstop-2-treated cells. This would imply that CME has a role in the retrieval of VAMP4-pH into SVs during LFS.

The role of CME during HFS was assessed using a "S1 S2" protocol. In this protocol CGNs co-expressing VAMP4-pH and an empty mCer vector were subjected to 2 HFS trains separated by 10 minutes. The second stimulation (S2) was performed in the presence of pitstop-2 (15 μM) (Figure 6.11 A).

The HFS train at S1 evoked a typical VAMP4-pH response, with the average trace displaying little deviation from the baseline. In the absence of CME at S2, the VAMP4-pH fluorescence time course exhibits an initial, small but significant peak in fluorescence. After cessation of stimulation this significant difference is lost as a

slow decrease is seen across all nerve terminals (Figure 6.11 B). The decrease in fluorescence was exhibited in all nerve terminals as opposed to a subpopulation within each cell, resulting in a further significant deviation from the control stimulation fluorescence trace after stimulation.

These results indicate that during both LFS and HFS, CME does have a role in the retrieval of VAMP4-pH. However, the characteristic slow retrieval of VAMP4-pH from the PM after HFS is not clathrin-dependent as this is preserved and even accentuated with the inhibition of CME.

The fluorescent response of VAMP4-pH in hippocampal neurons has a very different profile than that seen in CGNs during HFS (see Figure 6.1 C and Figure 6.2 C). CGNs display no fluorescence change upon stimulation followed by either an upstroke or downstroke in fluorescence, whereas hippocampal neurons display an immediate and sharp decrease in fluorescence (shown not to be due to relocation of VAMP4-pH – see Figure 6.4), which is then followed by either an upstroke or downstroke. To assess if any of these characteristics could be attributed to CME, a single HFS protocol was used in VAMP4-pH-expressing hippocampal neurons with or without 15 μM pitstop-2 (Figure 6.12 A).

Control hippocampal neurons displayed a fluorescence trace comparable to previous control conditions when subjected to HFS. However, in the presence of pitstop-2 and therefore in the absence of CME, the immediate drop in fluorescence seen upon stimulation has been significantly attenuated (Figure 6.12 B). This significant difference disappears after stimulation ends.

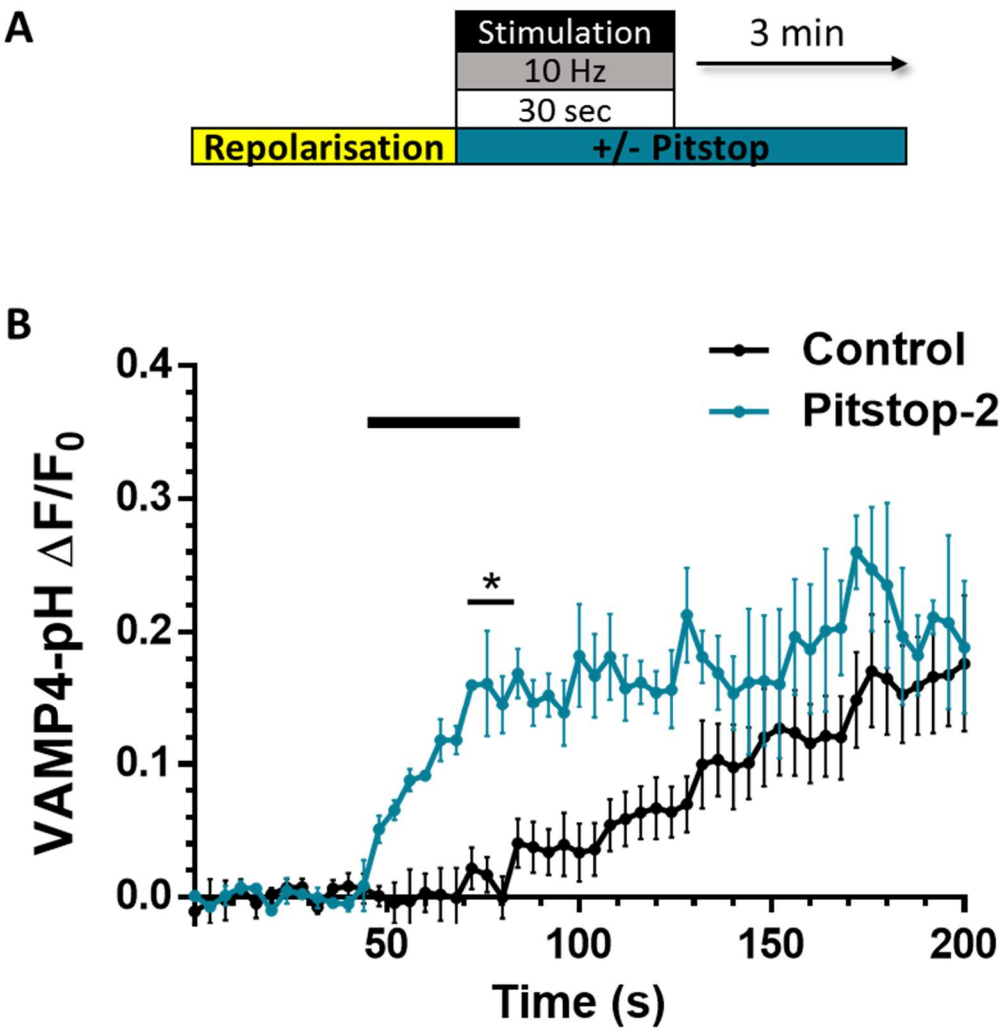

Figure 6.10 Pharmacological Inhibition of CME Does Not Affect VAMP4-pH Response After Stimulation

A) CGNs co-transfected empty mCer vector and VAMP4-pHluorin (VAMP4-pH) were incubated in imaging buffer for 10 mins prior to stimulation and then continuously onwards. Cells were challenged with a LFS trains (300 AP, 10 Hz) with or without Pistop-2 supplemented to the imaging buffer 8-12 seconds before stimulation. B) Average time traces of control (black) overlaid withPistop-2 (blue) $\pm$ SEM with stimulation depicted by black bar. Control n=5, Pitstop n=3. *=$p<0.05$. Two-way ANOVA with Bonferroni post-test.

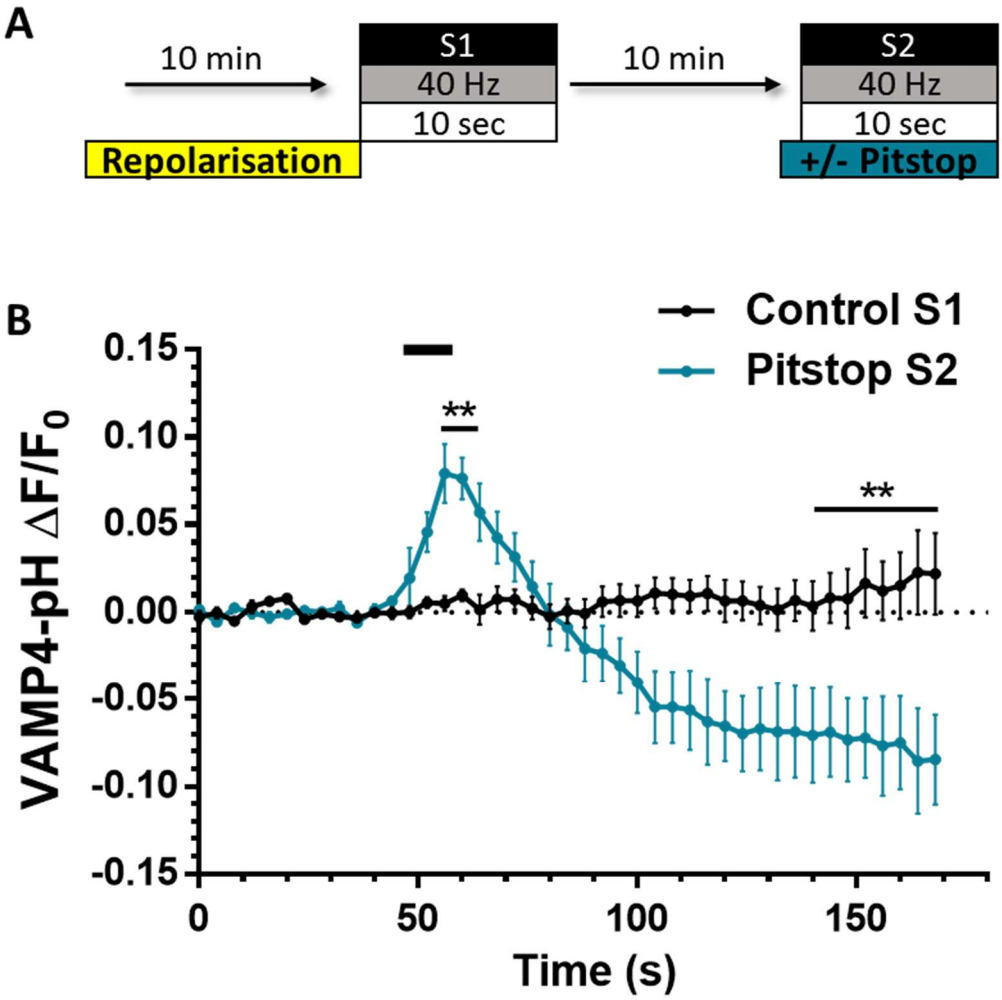

Figure 6.11 Pharmacological Inhibition of CME Does Not Arrest VAMP4-pHluorin Retrieval After HFS in CGNs

A) CGNs co-transfected with empty mCer vector and VAMP4-pHluorin (VAMP4-pH) were incubated in imaging buffer for 10 mins prior to S1 and then continuously onwards. Cells were challenged with 2 sequential HFS trains (400 AP, 40 Hz) (S1 and S2) 10 minutes apart. Pitstop-2 was supplemented to the imaging buffer 8-12 seconds before S2. B) Average time traces of S1 (control, black) overlaid with S2 (Ptistop-2, blue) ± SEM with stimulation depicted by black bar. n=3. **=p<0.01. Two-way ANOVA with Bonferroni post-test.

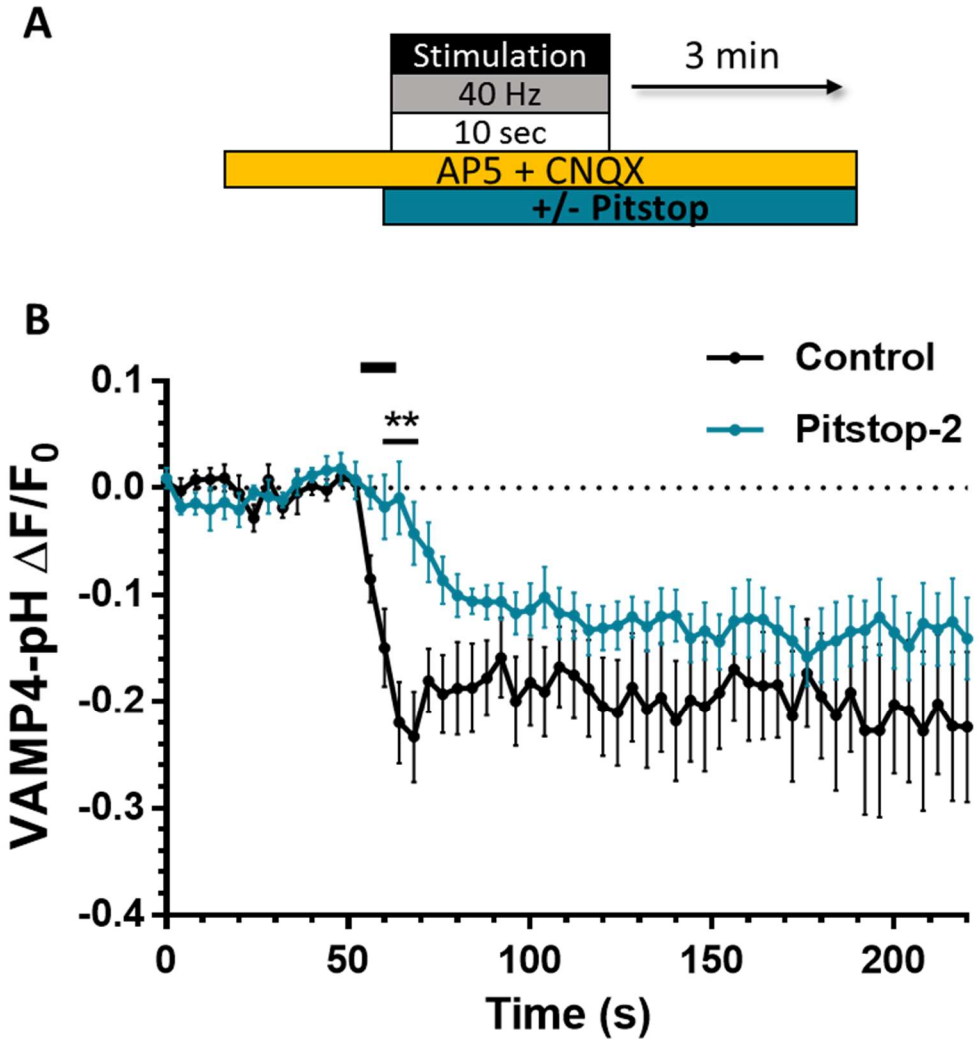

Figure 6.12 Pharmacological Inhibition of CME Does Not Arrest VAMP4-pHluorin Retrieval During HFS in Hippocampal Neurons

A) Hippocampal Neurons co-transfected with empty mCer vector and VAMP4-pHluorin (VAMP4-pH) perfused with hippocampal imaging buffer continuously. Cells were challenged with a HFS trains (400 AP, 40 Hz) with or without Pitstop-2 supplemented to the imaging buffer 8-12 seconds before stimulation. B) Average time traces of control (black) overlaid with Pitstop-2 (blue) ± SEM with stimulation depicted by black bar. Control n=5, Pitstop n=3. *=p<0.05. Two-way ANOVA with Bonferroni post-test.

These results indicate that CME plays a role in the retrieval of VAMP4-pH during both LFS and HFS. However, it would appear that this role does not extend far beyond the timeframe of stimulation, as control and pistop-2-treated conditions re-converge and significant difference is lost after this. It would also appear that the slow decreases that are seen after HFS are not an artefact of internalisation of VAMP4-pH by any clathrin-mediated form of endocytosis.

6.2.6 Genetic Inhibition of CME does not Affect VAMP4-pHluorin Downstrokes

To confirm the lack of a role for CME in the slow downstrokes of VAMP4-pH, CME was inhibited by expressing CHC shRNA (as used previously, see 5.2.5). To address this problem entirely it was decided that both LFS and HFS protocols should be conducted, thus allowing the visualisation of the role of CME in VAMP4-pH retrieval during LFS, when it is the dominant form of endocytosis, as well as during HFS when ADBE becomes dominant but CME is still active.

CGNs co-expressing VAMP4-pH and CHC shRNA, or its scrambled shRNA control were challenged with a LFS and fluorescence was monitored over time (Figure 6.13 A). No significant difference was observed between the average fluorescence traces after LFS between CHC shRNA or scrambled shRNA (Figure 6.13 B). There was also no alteration in the proportion of synapses exhibiting upstrokes or downstrokes (Figure 6.13 C). These results suggest that although CME may play a small role in the recycling of VAMP4-pH in CGNs (as seen when inhibited acutely, see Figure 6.11), its absence can be compensated for when inhibited chronically.

It is also possible that CHC shRNA is not as effective a method of inhibiting CME at LFS as pitstop-2. During LFS, less clathrin is required to compensate for the membrane inserted via SV exocytosis. It is possible that the 20% of CHC still expressed in the KD system is sufficient to perform CME at a sufficient rate to allow the continued internalisation of a small proportion of VAMP4-pH via CME.

To investigate the contribution of CME to VAMP4-pH retrieval during HFS (when ADBE is dominant), CGNs co-transfected with VAMP4-pH and CHC shRNA or a scrambled control were challenged with a single HFS (Figure 6.14 A).

CGNs expressing CHC shRNA exhibit the same, small peak in VAMP4-pH fluorescence as observed with pitstop-2 treatment. However, in this experiment the characteristic slow decrease after this peak was not observed (Figure 6.14 B). This fluorescent phenotype was caused by a significant decrease in the proportion of nerve terminals displaying a downstroke in fluorescence after stimulation (Figure 6.14 C). This might suggest that, in this system, CHC knockdown is causing an inhibition of ADBE. In agreement, CHC shRNA does significantly inhibit dextran uptake in CGNs as noted previously (Figure 5.16 B). Thus, it is difficult to interpret the impact of CHC depletion on the VAMP4-pH response during HFS in CGNs, since there is also a confounding effect of this manoeuvre on ADBE.

Silencing CHC expression in hippocampal neurons does not have this inhibitory effect on ADBE (Figure 5.16 C). This cell type therefore is a more suitable model to test the role of a CME on the recycling of a pHluorin which seems to traffic through both ADBE and CME.

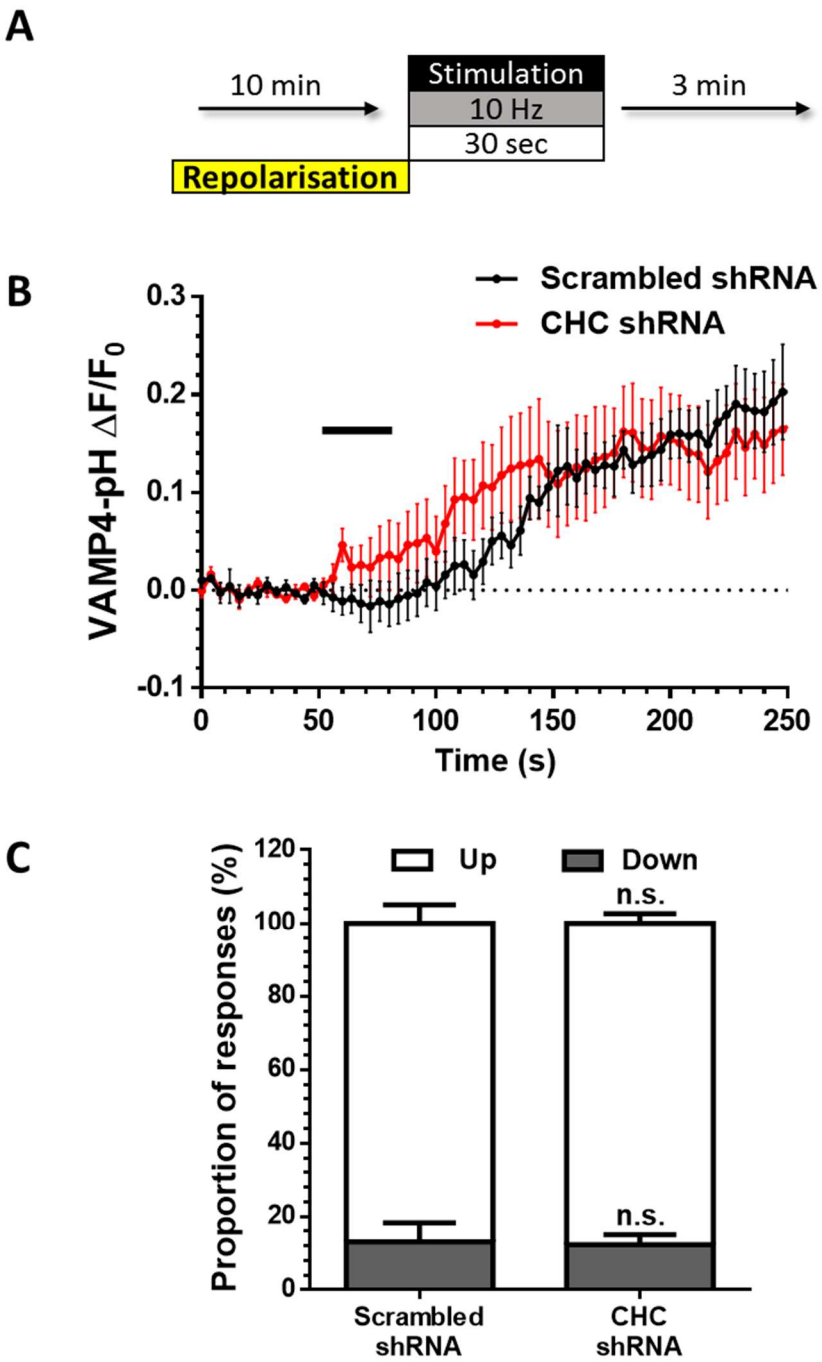

Figure 6.13 Silencing CHC Expression does not Affect the VAMP4-pHluorin Response After LFS.

A) CGNs co-transfected empty mCer vector and VAMP4-pHluorin (VAMP4-pH) were incubated in imaging buffer for 10 mins prior to stimulation and then continuously onwards. Cells were stimulated with a LFS train (300 AP, 10 Hz). B) Average time traces of scrambled shRNA (black) and CHC shRNA (red) ± SEM with stimulation depicted by black bar. C) Average proportions of synapses within a transfected cell increasing (Up) or decreasing (Down) in VAMP4-pH fluorescence after stimulation + SEM. Scrambled sRNA n=5, CHC shRNA n=6. n.s. Student's t-test between conditions.

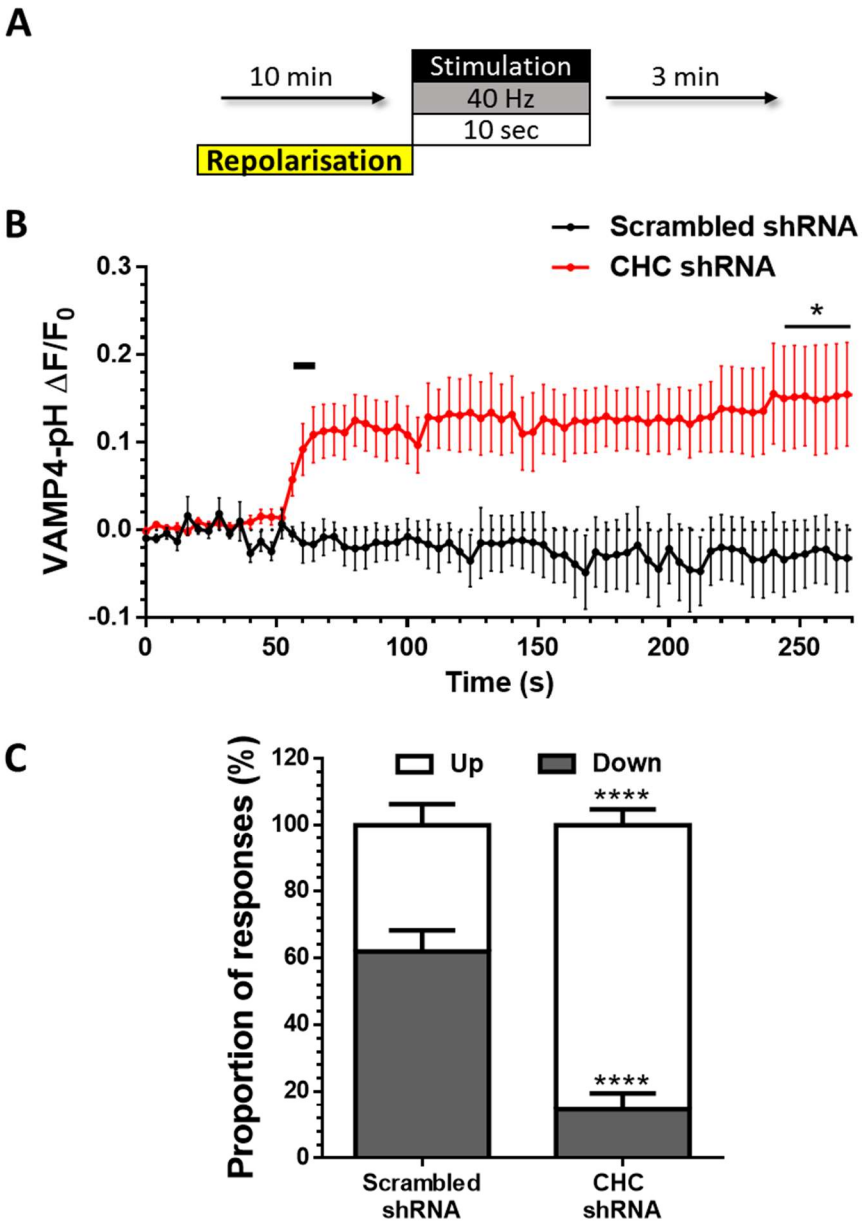

Figure 6.14 Silencing CHC Expression Affects VAMP4-pHluorin Retrieval During HFS.

A) CGNs co-transfected with a scrambled shRNA vector (black) or CHC shRNA (red) and VAMP4-pHluorin (VAMP4-pH) were incubated in imaging buffer for 10 mins prior to stimulation and then continuously onwards. Cells were stimulated with a HFS train (400 AP, 40 Hz). B) Average time traces of fluorescence ± SEM with stimulation indicated by black bar. C) Average proportions of synapses within a transfected cell increasing (Up) or decreasing (Down) in VAMP4-pH fluorescence after stimulation + SEM Scrambled shRNA n=7, CHC shRNA n=6. *=$p<0.05$. Two-way ANOVA, Bonferroni post-test. Bar chart: ****=$p<0.0001$, Student's t-test between conditions

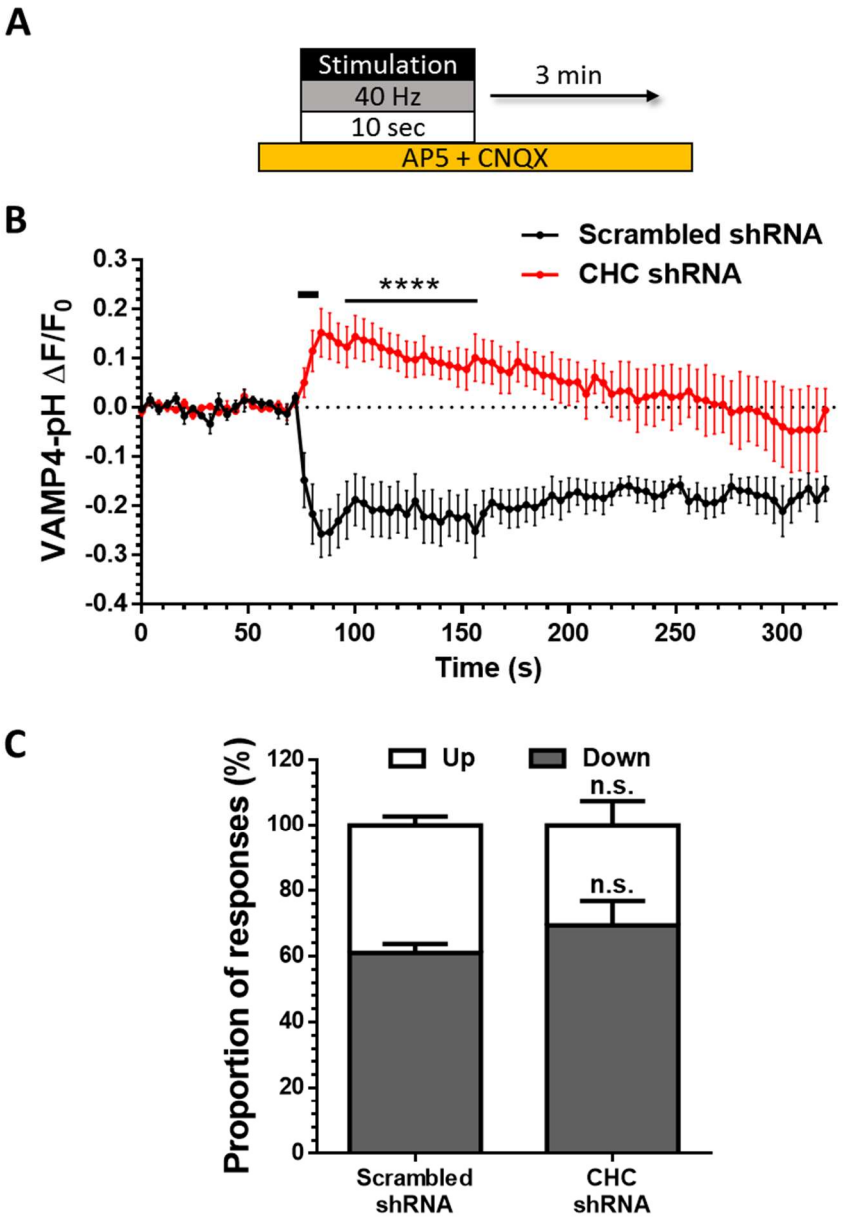

Figure 6.15 Silencing CHC Expression Does Not Affect VAMP4-pHluorin Retrieval or ADBE in Hippocampal Neurons

A) Hippocampal neurons were co-transfected with a scrambled shRNA vector (black) or CHC shRNA (red) and VAMP4-pHluorin (VAMP-pH). Cells were then stimulated with a HFS train (400 AP, 40 Hz) and perfused continuously with hippocampal imaging buffer. B) Average time traces of fluorescence ± SEM with stimulation indicated by black bar. C) Average proportions of synapses within a transfected cell increasing (Up) or decreasing (Down) in VAMP4-pH fluorescence after stimulation + SEM Scrambled shRNA n=5, CHC shRNA n=4.Time trace: ****=p<0.0001. Two-way ANOVA, Bonferroni post-test. Bar chart: n.s. Student's t-test between conditions.

Hippocampal neurons were co-transfected with VAMP4-pH and either CHC shRNA or its scrambled control and challenged with a single HFS (Figure 6.15 A). Hippocampal neurons transfected with the control shRNA exhibited a typical average fluorescence trace: an immediate decrease on stimulation followed by a diversity of upstrokes or downstrokes, in comparable proportions to those seen with control conditions in previous HFS experiments (Figure 6.15 B and C). In the absence of CHC in hippocampal cells, VAMP4-pH displayed a similar fluorescence trace to that seen when CME is inhibited acutely with pitstop-2 in CGNs (Figure 6.15 B, see Figure 6.11): upon stimulation VAMP4-pH exhibits a small peak followed by a slow decrease in fluorescence. The proportion of nerve terminal displaying a downstroke in fluorescence after HFS was not affected by the silencing of CHC expression (Figure 6.15 C).

These results indicate that when CME is inhibited in a system in which ADBE is unaffected, VAMP4-pH is still efficiently retrieved. Therefore, the slow downstrokes in VAMP4-pH fluorescence are not clathrin-dependent. VAMP4-pH is selectively retrieved via ADBE and is the first identified genetically-encoded reporter of ADBE.

6.2.7 Silencing VAMP4 expression Affects ADBE but not CME

The work discussed so far has shown that VAMP4-pH is being internalised via ADBE during HFS. The question remains as to whether this uptake is selective or whether this uptake is due to the location and abundance of VAMP4-pH (and endogenous VAMP4) on the PM.

To test for function of VAMP4 on both forms of endocytosis, VAMP4 shRNA was used to silence endogenous VAMP4 expression in CGNs. This shRNA was successful in reducing VAMP4 to less than 40% of its endogenous levels (Figure 6.16).

To investigate any role of VAMP4 in CME, a single HFS protocol utilising syp-pH was conducted. The rationale for this was that it has been established that, even during HFS, syp-pH is predominantly retrieved via CME. As such, investigations performed utilising syp-pH will only report alterations in CME and not ADBE. CGNs co-expressing syp-pH with VAMP4 shRNA and its scrambled control were subjected to a standard single HFS (400 AP, 40 Hz) (Figure 6.17 A) with their fluorescence monitored over time (Figure 6.17 B).

CGNs expressing control scrambled shRNA, exhibited an evoked fluorescence increase and tau values consistent with the control conditions of previous CGN experiments. CGNs expressing VAMP4 shRNA, showed no significant difference in fluorescence increase upon stimulation (Figure 6.17 C), showing no effect on the exocytosis of SVs labelled with syp-pH. There was also no significant effect on endocytosis kinetics after stimulation (Figure 6.17 D). As syp-pH is being predominantly recycled via CME even during HFS, it can be concluded from this result that the depletion of VAMP4 has no effect on CME.

As I had ascertained that VAMP4 depletion has no effect on either SV exocytosis or CME, I now aimed to determine the effect of this knockdown on ADBE. In this protocol, CGNs expressing VAMP4 shRNA or its scrambled control were subjected to HFS in the presence of dextran (50 μM) (Figure 6.18 A). The comparative number

of synapses undergoing ADBE was estimated by calculating the number of dextran puncta/ length of axon.

CGNs expressing the scrambled shRNA vector exhibited a similar number of puncta/μm of axon to previous control conditions, whereas the silencing of VAMP4 expression resulted in a significantly reduced amount of dextran uptake per μm of axon (Figure 6.18 B). This indicates a significant inhibition of ADBE in neurons where VAMP4 is depleted.

These results would indicate that, although VAMP4 does not appear to have a role in the process of CME, its retrieval via ADBE is not a passive occurrence as its presence is essential for the function of ADBE.

Although no significant effect was seen on syp-pH trafficking when VAMP4-expression was silenced, the essential requirement for VAMP4 for ADBE provides an opportunity to investigate the effects of ablating this endocytic mode on presynaptic function during a train of intense and sustained activity. One would expect that the removal of ADBE from a synapse would have effects on SV turnover. It is possible that these effects would become apparent over a series of high frequency stimuli, revealing the role for ADBE-derived SVs in presynaptic performance during sustained HFS.

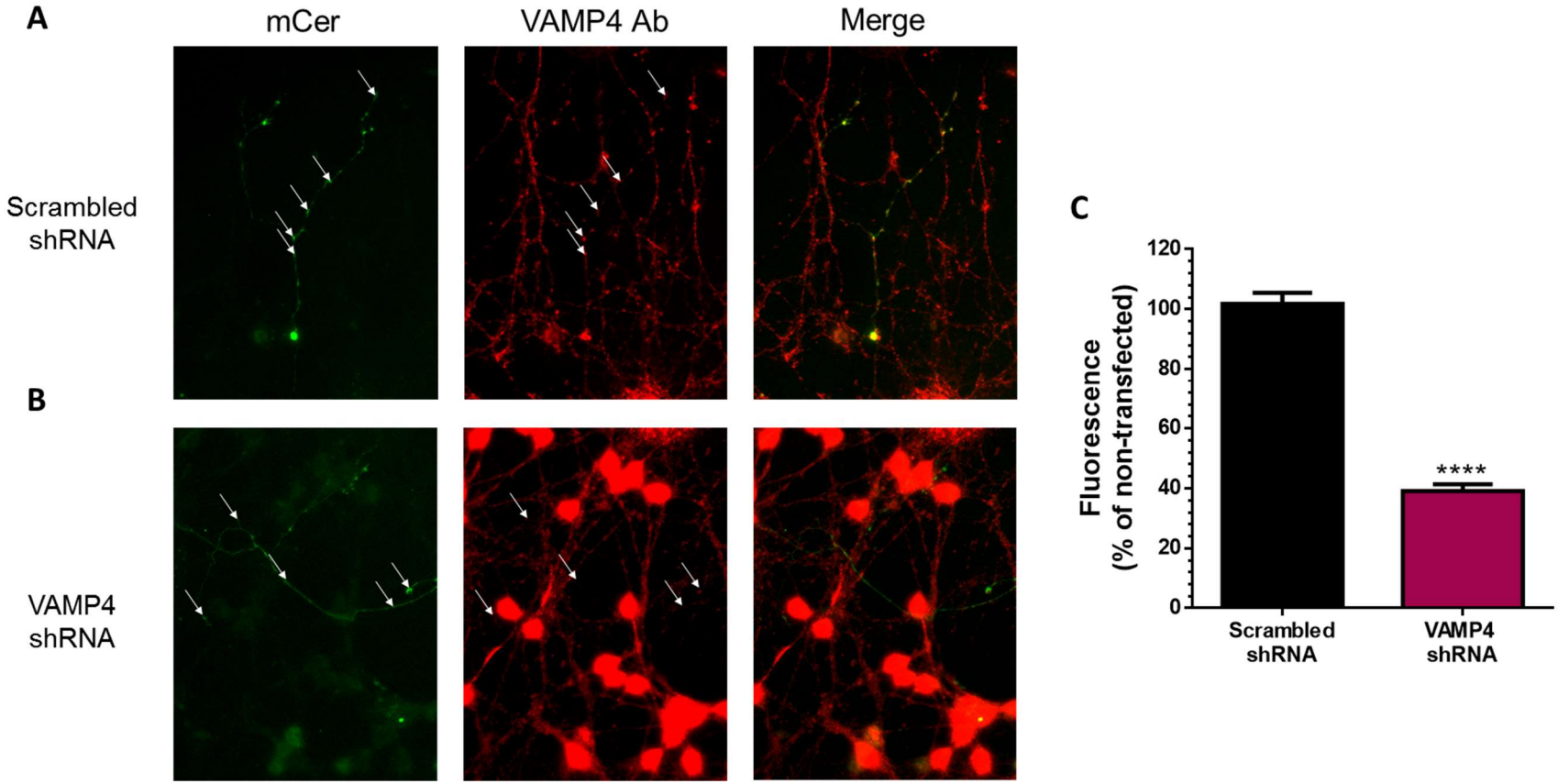

Figure 6.16 VAMP4 shRNA Effectively Reduces VAMP4 Expression in CGNs

Images of CGNs transfected with A) Scrambled shRNA or B) VAMP4 shRNA. The culture was labelled with GFP Ab (left) and VAMP4 Ab (middle). These images were overlaid (right) to visualise intensity of VAMP4 Ab labelling in the nerve terminals of the transfected cell (white arrows). Average fluorescence of VAMP4 Ab for Scrambled shRNA or VAMP4 shRNA transfected CGN synapses as a percentage of fluorescence nearby non-transfected synapses of similar size + SEM. Scrambled shRNA n=12, VAMP4 shRNA n=16. ****= $p<0.0001$. Student's t-test.

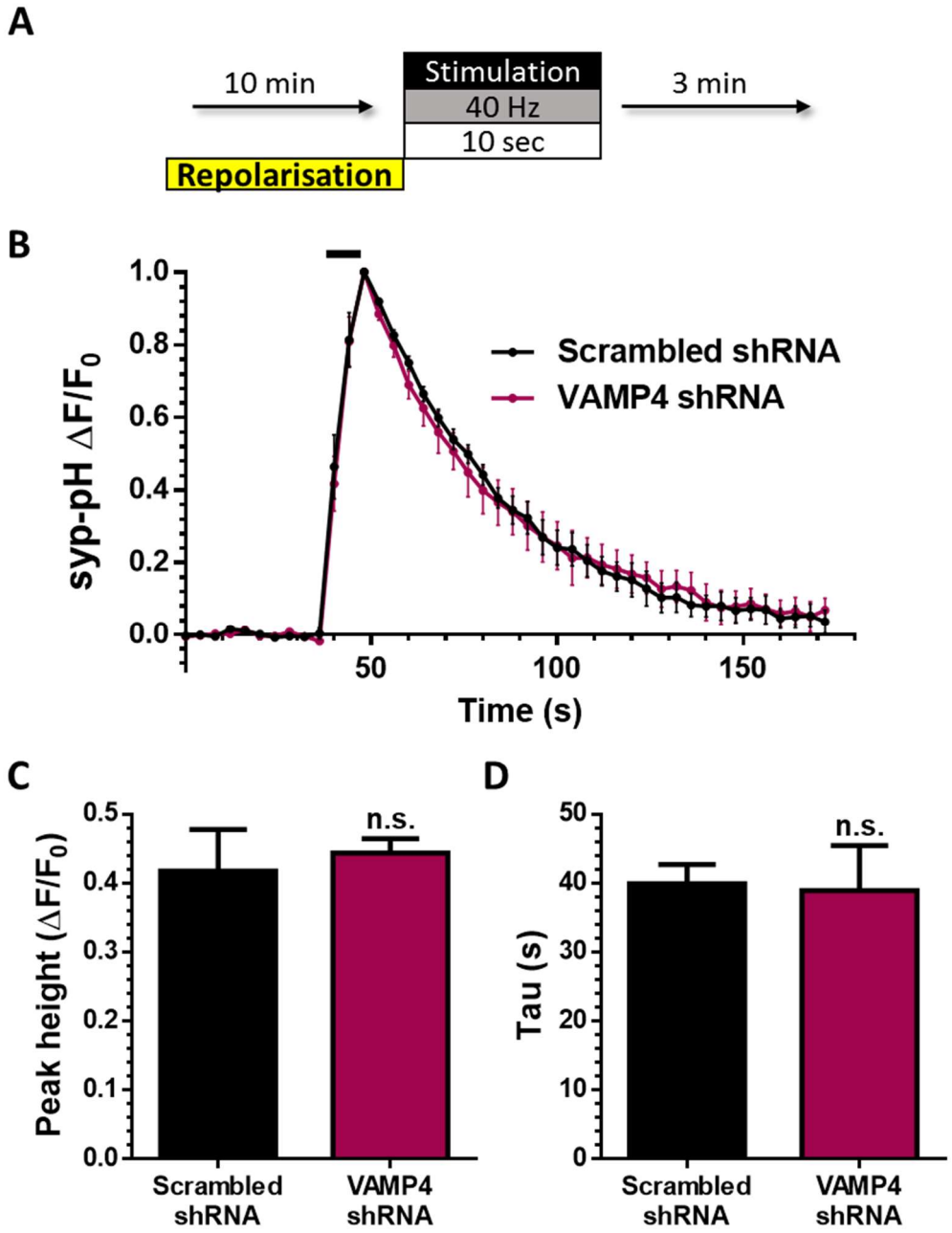

Figure 6.17 Silencing VAMP4 Expression Does not Affect Synaptophysin-pHluorin Retrieval During HFS

A) CGNs co-transfected a control scrambled shRNA or VAMP4 shRNA and synaptophysin-pHluorin (syp-pH) were perfused with repolarised for 10 minutes in imaging buffer and then continuously onwards. Cells were stimulated with a HFS train (400 AP, 40 Hz). B) Average time trace ± SEM is displayed with stimulation indicated by black bar. C) Average peak eights of each condition (F/F_0) + SEM. D) Average endocytic kinetics (tau) of syp-pH retrieval (seconds) + SEM. Scrambled shRNA n=8, VAMP4 shRNA n=6. n.s., Student's t-test

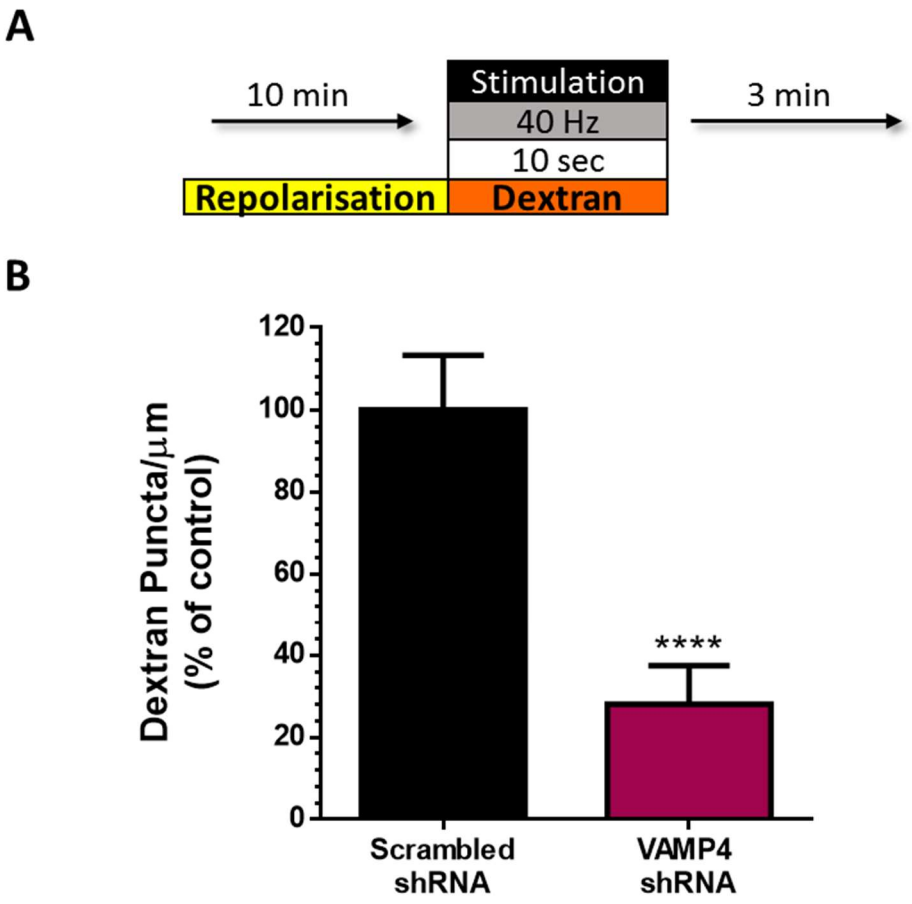

Figure 6.18 Silencing VAMP4 Expression Inhibits ADBE During HFS

A) CGNs transfected with either Scrambled shRNA or VAMP4 shRNA were repolarised in imaging buffer for 10 minutes. Cells were stimulated with a HFS train (400 AP, 40 Hz) in the presence of 50 µM dextran. B) Average puncta per µm of transfected axon + SEM expressed as a percentage of Scrambled shRNA condition Scrambled shRNA n=28, CHC shRNA n=30. Hippocampal cells: Scrambled shRNA n=49, VAMP4 shRNA n=53. ****=p<0.0001. Student's t-test

An experimental protocol was designed to probe for the possible effects of ADBE inhibition on presynaptic performance during repeated trains of HFS. In this protocol hippocampal neurons were transfected with syp-pH and either VAMP4 shRNA or its scrambled control and challenged with four HFS trains each separated by 10 minutes (Figure 6.19 A)

In control cells, bulk endosomes formed on the first stimulation should have budded and donated SVs to the recycling pool within the time frame of the experiment (Cheung et al. 2010). It is possible that the lack of SVs donated via budding from bulk endosomes would cause a depletion of releasable vesicles over time.

The syp-pH response of hippocampal neurons expressing the control scrambled shRNA was highly reproducible. Neurons responded to each HFS with a progressive reduction in evoked peak fluorescence with each consecutive stimulation, with the second stimulation 62% of the first followed by 40% and 32% for the third and fourth stimulations respectively (Figure 6.19 C). There was a significant difference between control and VAMP4-depleted cells in syp-pH fluorescence over time from the second stimulation onwards (Figure 6.19 B).

VAMP4-depleted cells exhibited an exaggerated decrease in peak fluorescence. A peak height of 47% was seen on the second stimulation when compared to the first, followed by 25% and 17% for the third and fourth stimulations respectively. A significant difference between these values is seen from the third stimulation onwards (Figure 6.19 C). The endocytic rate (tau) however does not exhibit any significant differences between control and VAMP4-depleted neurons (Figure 6.19 D) showing that the decreased peak height is not due to modulated CME.

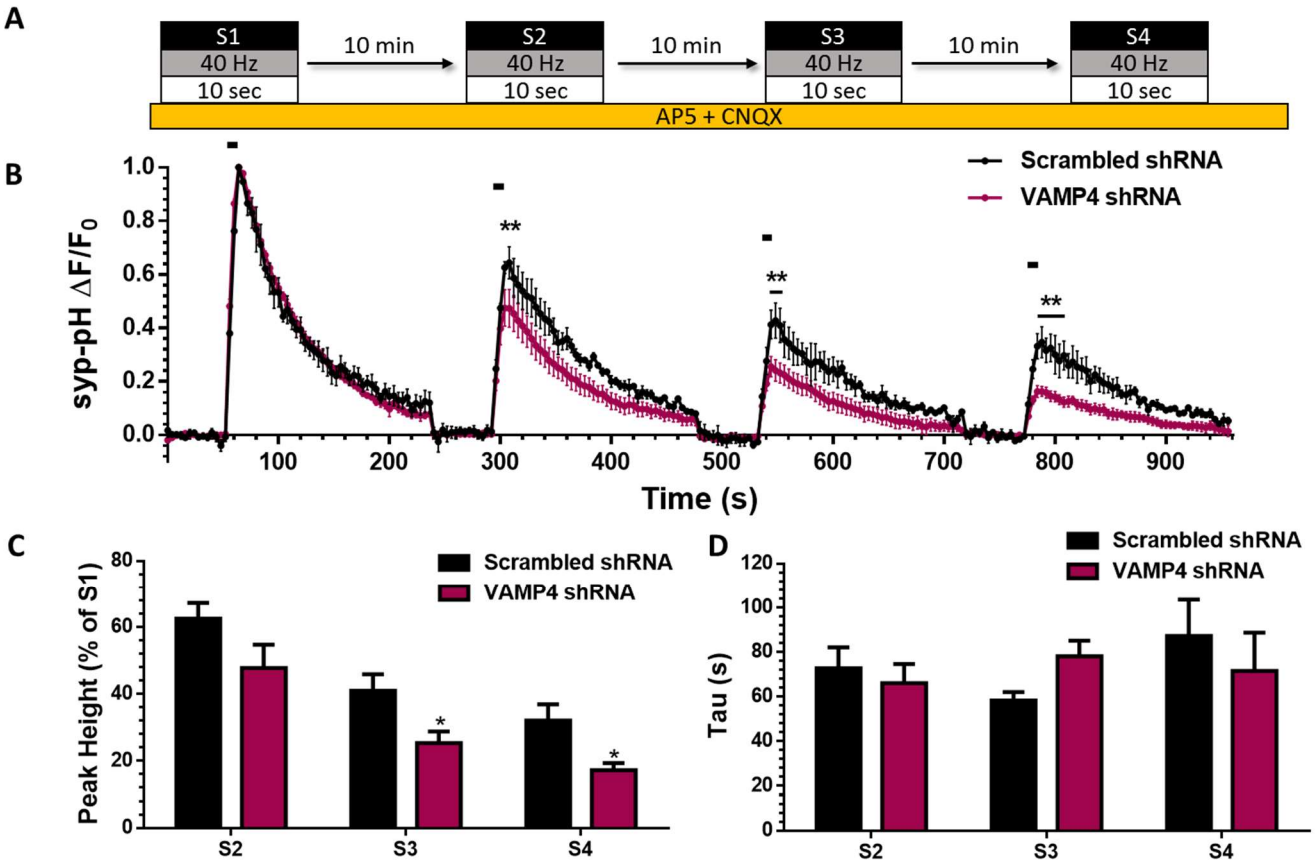

Figure 6.19 Silencing VAMP4 Expression Affects Presynaptic Performance during Sustained HFS

A) Hippocampal neurons co-transfected with either scrambled shRNA or VAMP4 shRNA and syp-pH were perfused continuously with hippocampal imaging buffer and stimulated with 4 HFS trains each separated by 10 minutes. B) Average time trace of fluorescence ($\Delta F/F_0$) $\pm$ SEM normalised to the first stimulation peak. C) Average Peak heights S2 onwards + SEM as a percentage of S1. D) Average tau of S2 onwards (seconds) + SEM. Time trace: **=p<0.01, Two-way ANOVA, Bonferroni post-test. Bar charts: *=p<0.05, Student's t-test per stimulation between conditions.

These results indicate that the removal of ADBE leads to a depleted stock of fusion-ready SVs. This effect is only revealed over several HFS, suggesting ADBE-derived SVs contribute to synaptic transmission during times of intense neuronal activity.

6.2.8 A Di-leucine Motif on VAMP4 is Essential for ADBE

I next investigated which protein interaction mediates the necessity for VAMP4 in ADBE. VAMP4 contains a di-leucine motif at residues 25 and 26 in its cytoplasmic N-terminal domain which facilitates interactions with AP-1 (Peden et al. 2001) (Figure 6.20 A). To assess if the essential role of VAMP4 in ADBE is mediated via its interaction with AP-1, a VAMP4-pH with the first leucine residue of the di-leucine motif mutated to an alanine (VAMP4-pH L25A) (Figure 6.20 B) was used. This mutation inhibits AP-1 binding (Peden et al. 2001), thereby allowing one to visualise the importance of this interaction in the trafficking of VAMP4-pH.

6.2.8.1 Retrieval of VAMP4-pH is Disrupted with the Mutation of an Adaptor-Binding Di-leucine Motif

To determine the importance of AP-1 interaction in the integral role of VAMP4 during ADBE, CGNs co-transfected with either wild-type VAMP4-pH (VAMP4-pH WT) or mutant VAMP4-pH (VAMP4-pH L25A) and an empty mCer vector were stimulated with HFS (400 AP, 40 Hz) (Figure 6.21 A).

Nerve terminals expressing VAMP4-pH L25A exhibited a significantly different fluorescence trace than those expressing VAMP4-pH WT (Figure 6.21 B). CGNs expressing VAMP4-pH WT produced the typical stable average fluorescence during

and after HFS caused by its component upstrokes and downstrokes. However, nerve terminals expressing VAMP4-pH L25A exhibit an average fluorescence which increases quickly upon stimulation and then remains constant in fluorescence with very few of the downstrokes below baseline characteristic of WT VAMP4-pH (Figure 6.21 C).

The fluorescence trace produced by these neurons exhibits similar characteristics to that of CGNs whose expression of syndapin I has been silenced, inhibiting ADBE (see Figure 6.7).

The same protocol was repeated in hippocampal neurons (Figure 6.22 A) and a very similar average fluorescence profile was seen for the L25A mutant, with an immediate upstroke on stimulation followed by a small and steady increase over time (Figure 6.22 B). Again, very few downstrokes below baseline were observed after stimulation for this VAMP4 mutant (Figure 6.22 C).

These results indicate that the adaptor protein binding site (residing at Leu 25 and Leu 26) is required for the internalisation of VAMP4 via ADBE as the characteristic downstrokes, seen in synapses in which ADBE is operating normally, are significantly reduced when adaptor binding has been abolished. It would also imply that the immediate internalisation of VAMP4-pH, which is normally apparent in hippocampal cells, is also mediated by an adaptor protein interaction.

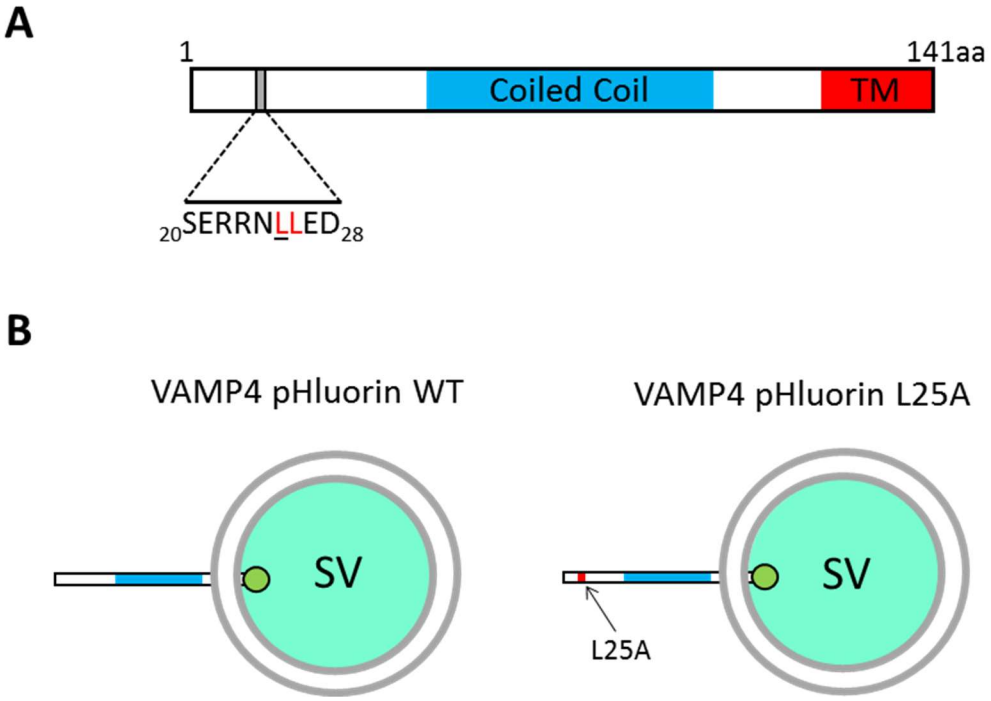

Figure 6.20 VAMP4-pH with Mutated Adaptor Protein Binding Site

A) WT VAMP4 contains a di-leucine motif in it cytoplasmic domain (blue and white) at residues Leu 25 and Leu 26 (red letters). This motif was mutated at residue Leu 25 (underlined). B) WT VAMP4 fused to pHluorin on its luminal domain (green circle) was used in previous experiments. This WT VAMP4 was mutated at Leu 25 to an alanine (Ala25), forming L25A (red segment) to create VAMP4-pHluorin L25A

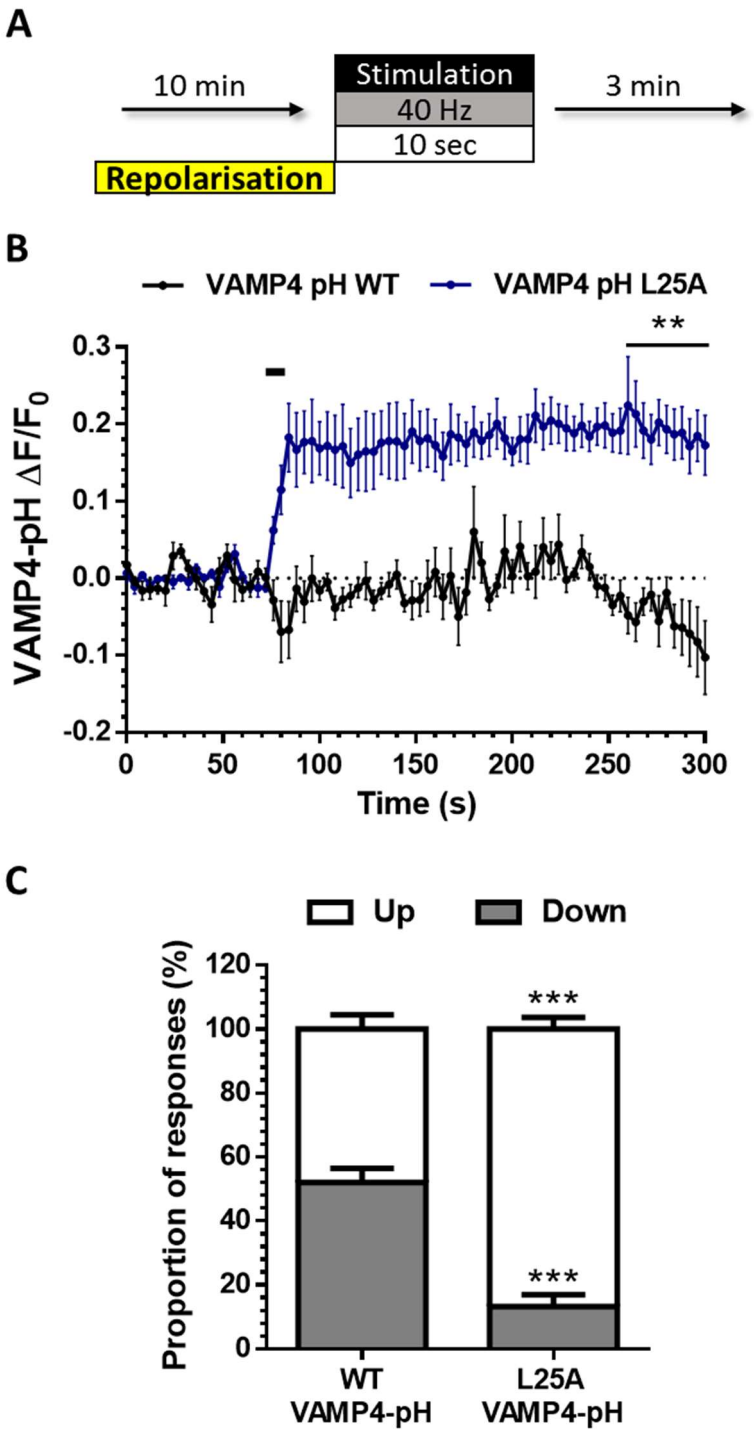

Figure 6.21 VAMP4-pH L25A Does not Display Characteristic Slow Retrieval in CGNs

A) CGNs co-transfected with either Wild-type VAMP4-pHluorin (VAMP4-pH WT) or mutated L25A VAMP4-pHluorin (VAMP4-pH L25A) were incubated with imaging buffer for 10 minutes before stimulation and then continuously onwards. Cells were stimulated with a HFS train (400 AP, 40 Hz). B) Average time trace ± SEM is displayed with stimulation indicated by black bar. C) Average proportions of synapses within a transfected cell increasing (Up) or decreasing (Down) in VAMP4-pH fluorescence after stimulation + SEM. VAMP4-pH WT n=5, VAMP4-pH L25A n=5. Time trace: **=P<0.01, Two-way ANOVA Bonferroni post-test. Bar chart: ***=p<0.001, Student's t-test between conditions.

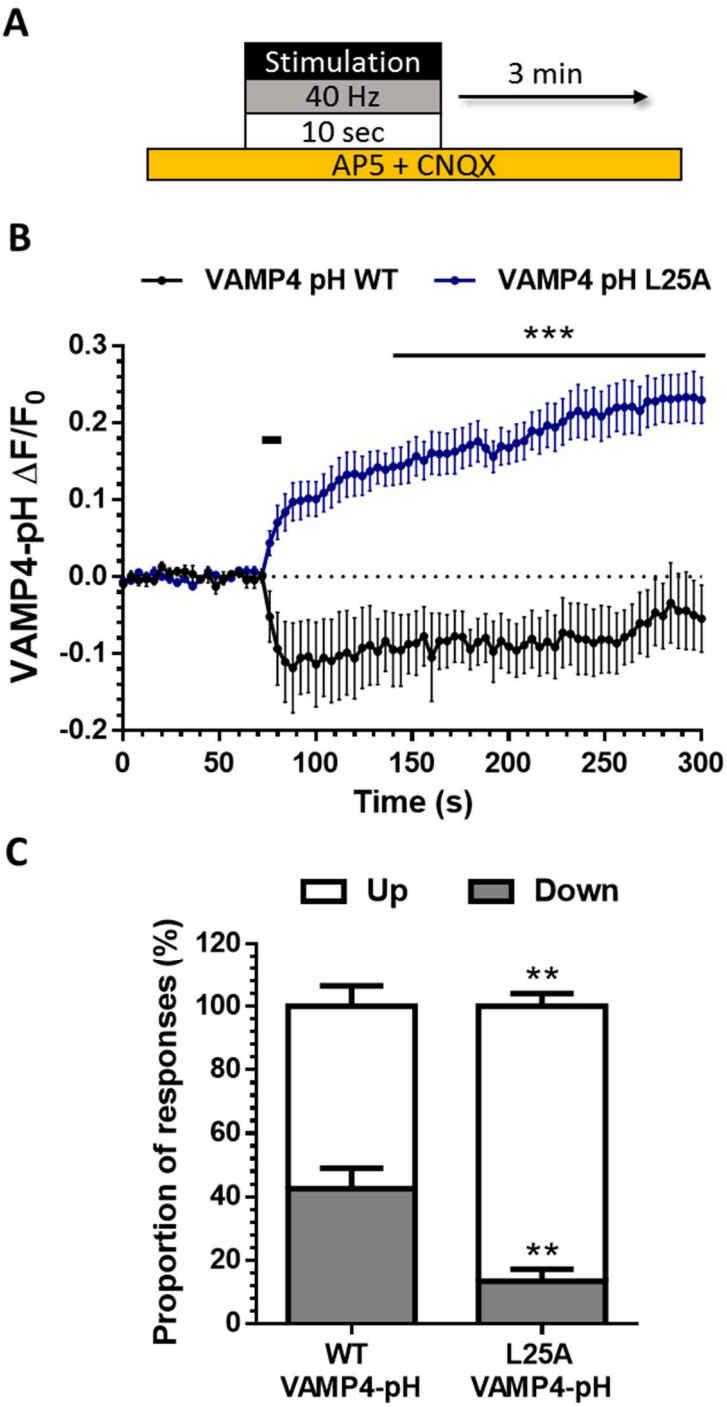

Figure 6.22 VAMP4-pH L25A Does not Display Characteristic Slow Retrieval in Hippocampal Neurons

A) Hippocampal neurons co-transfected with either Wild-type VAMP4-pHluorin (VAMP4-pH WT) or mutated L25A VAMP4-pHluorin (VAMP4-pH L25A) were incubated with hippocampal imaging buffer continuously. Cells were stimulated with a HFS train (400 AP, 40 Hz). B) Average time trace ± SEM is displayed with stimulation indicated by black bar. C) Average proportions of synapses within a transfected cell increasing (Up) or decreasing (Down) in VAMP4-pH fluorescence after stimulation + SEM. VAMP4-pH WT n=6, VAMP4-pH L25A n=7. Time trace: ***=P<0.001, Two-way ANOVA, Bonferroni post-test. Bar chart: **=p<0.01, Student's t-test between conditions.

6.2.8.2 VAMP4 Overexpression Does Not Affect ADBE

I have concluded, based on the lack of downstrokes seen when tracking VAMP4-pH L25A after HFS, that VAMP4 uptake into bulk endosomes is mediated via its interaction with adaptor proteins. It is possible however, that the lack of downstrokes seen when expressing VAMP4-pH L25A is due to a dominant negative effect on ADBE caused by the overexpression of a mutant VAMP4 protein.

To assess this possibility, the following protocol was designed; overexpressing either VAMP4-pH WT or the mutant VAMP4-pH L25A in CGNs and evaluating any effect on ADBE in comparison to a GFP empty vector (to control for the expression of the modified GFP molecule - pHluorin). This experiment would also reveal any effect of overexpression VAMP4-pH WT on prevalence of ADBE. This is important as, to date, VAMP4-pH is the only pHluorin seen to be trafficking via ADBE. As its now apparent that VAMP4 is essential for ADBE, the possibility that overexpressing a pHluorin-tagged VAMP4 protein increases the occurrence of ADBE needs to be addressed.

CGNs triple-transfected with mCer empty vector, scrambled shRNA and either VAMP4-pH WT, VAMP4-pH L25A or an empty GFP vector were challenged with a HFS (400AP, 40 Hz) in the presence of dextran (50 μM) (Figure 6.23 A).

Overexpressing VAMP4-pH WT caused no increase in the number of synapses undergoing ADBE as measured by number of puncta/μm of axon when compared to the GFP control (Figure 6.23 B). This is an important result as it shows that the

VAMP4-pH assay used throughout this project is not enhancing the ability of the presynapse to undergo ADBE.

The overexpression of VAMP4-pH L25A similarly had no significant effect on the number of synapses undergoing ADBE (Figure 6.23 B). From this it can be concluded that the decreased number of downstrokes seen in VAMP4-pH L25A trafficking is not due to a decreased incidence of ADBE, but instead due to an inability of this mutant L25A VAMP4 to be recruited into bulk endosomes. This would indicate a requirement for adaptor proteins in VAMP4 recruitment into bulk endosomes during HFS and further highlights that the retrieval of VAMP4 via ADBE is a specific process and not merely due to its location or abundance.

6.2.8.3 Inhibition of ADBE via VAMP4 Knockdown is not Rescued by Mutated VAMP4 Which is Incapable of Binding Adaptor Proteins

VAMP4 is essential for ADBE (see Figure 6.18), and its interaction with adaptor proteins is essential for its retrieval during ADBE (see Figure 6.21 and Figure 6.22). However, it has not been determined whether the interaction of VAMP4 with adaptor proteins is in itself essential for ADBE to proceed. To determine this, the ability of both VAMP4-pH WT and the mutant VAMP4-pH L25A (both shRNA-resistant) to rescue ADBE was tested with the simultaneous knockdown of endogenous VAMP4 via shRNA.

CGNs co-transfected with VAMP4 shRNA and either VAMP4-pH WT, VAMP4-pH L25A or an empty GFP vector were challenged with a HFS train (400AP, 40 Hz) in the presence of dextran (50 μM) (Figure 6.23 A). Puncta per μm of axon were quantified and compared against control cells co-transfected with scrambled shRNA plus a GFP empty vector.

The expression of VAMP4-pH WT resulted in a full rescue of ADBE back to control levels (Figure 6.23 B, Figure 6.24), showing that the effect on ADBE caused by silencing endogenous VAMP4 expression is fully reversible by replacing it with a functional exogenous form of the protein. Again this is important, since it confirms that the inhibition of ADBE was due to VAMP4 depletion and not off targets effects of the shRNA

When endogenous VAMP4 is replaced with the L25A mutant form, ADBE is not restored (Figure 6.23 B, Figure 6.24). These results confirm that VAMP4 is essential for ADBE and that its interaction with adaptor proteins is an essential step in the progression of ADBE.

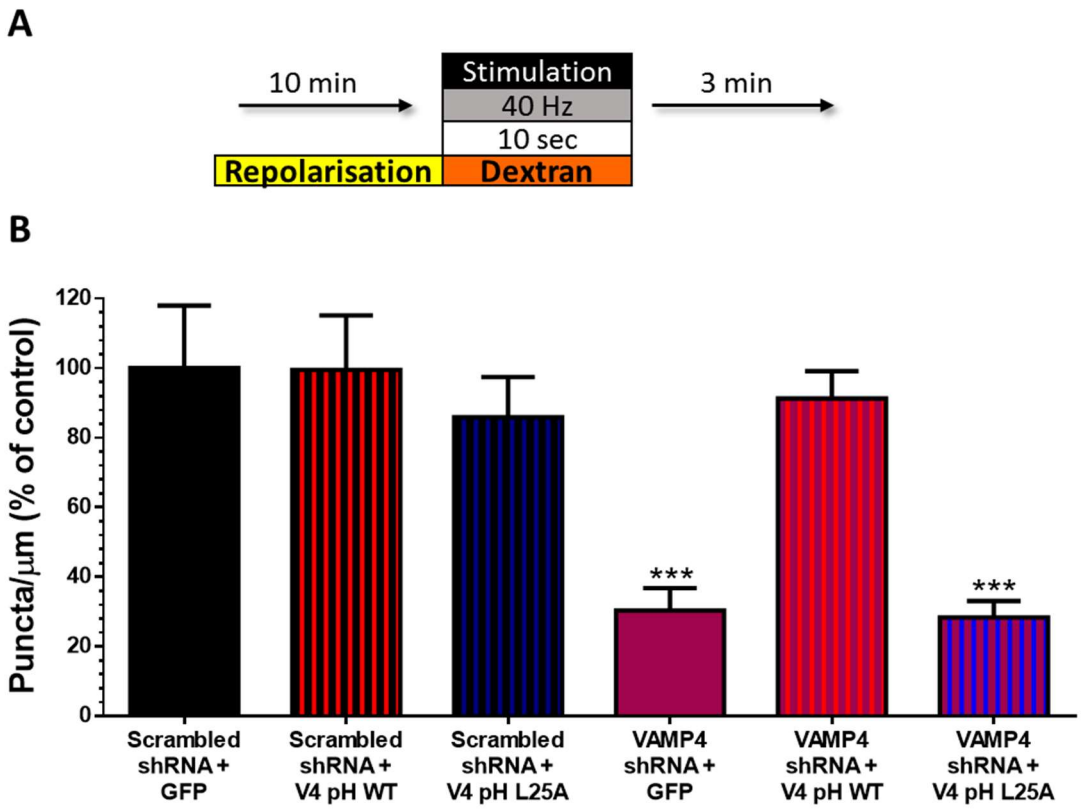

Figure 6.23 ADBE is not Rescued by Expression of Mutated AP-1 Binding-Deficient VAMP4

A) CGNs co-transfected with either VAMP4 shRNA or its scrambled control and either VAMP4 WT pHluorin, VAMP4 L25A pHluorin or an empty GFP-tagged vector were incubated with imaging buffer for 10 minutes prior to stimulation with a HFS train (400 AP, 40 Hz) in the presence of 50 µM dextran. B) Average puncta per µm of axon + SEM for each condition as a percentage of the control condition (Scrambled shRNA + GFP). Scrambled shRNA + GFP n=23, Scrambled shRNA + VAMP4-pH WT n=24, Scrambled shRNA + VAMP4-pH L25A n=25, VAMP shRNA + GFP n=21, VAMP4 shRNA + VAMP4-pH WT n=23, VAMP4 shRNA + VAMP4-pH L25A n=26. ***=P<0.001, One-way ANOVA comparison to Control (Scrambled shRNA + GFP).

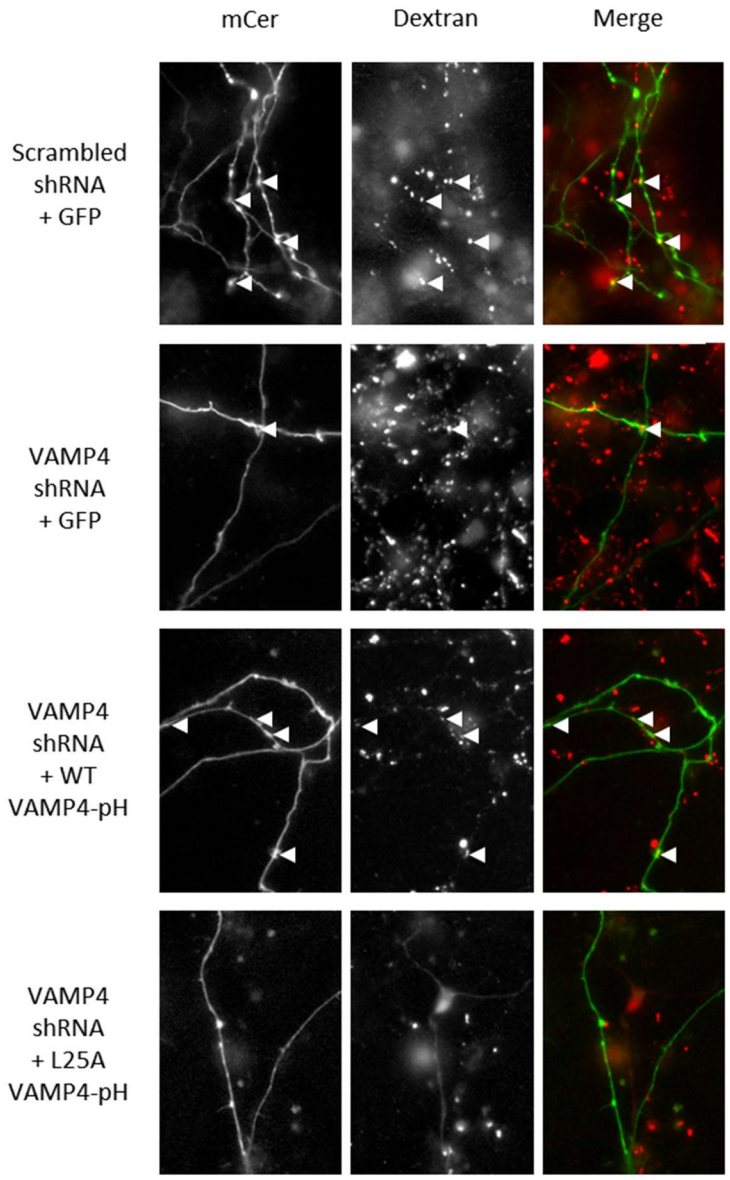

Figure 6.24 VAMP4 with Mutated Protein with Interrupted Adaptor Protein Binging Does not Rescue ADBE

CGNs transfected with an mCer empty vector, VAMP4 shRNA and either a GFP empty vector, WT VAMP4-pH or L25A VAMP4-pH. Cells were repolarised for 10 minutes in imaging buffer and then exposed to HFS (400 AP, 40 Hz) in the presence of 50 μM dextran. Images were acquired of mCer (left) and dextran (middle) and then overlaid (right) to identify dextran puncta localised within transfected neurons (white arrows).

6.3 Discussion

During intense neuronal activity, exocytosis causes a transient accumulation of SV cargo as well as membrane in the PM of central nerve terminals. Under these conditions, ADBE becomes the dominant form of endocytosis.

It is known that this endocytic mode has a high capacity, as it retrieves much larger sections of membrane than a single SV. However, the capacity of this mode for the retrieval of SV cargo from the PM is unknown. Clathrin and adaptor proteins have both been shown to be necessary for the formation of functional SVs from bulk endosomes (Heerssen et al. 2008; Kasprowicz et al. 2008; Cheung & Cousin 2012; Kononenko et al. 2014), but are not required for the formation and scission of endosomes from the PM (Heerssen et al. 2008; Kasprowicz et al. 2008; Cheung & Cousin 2012; Kononenko et al. 2014), suggesting a lack of SV cargo sorting into these invaginating structures. Work discussed in the previous chapter also indicates a lack of retrieval of a variety of SV cargoes via ADBE.

I investigated another, less commonly used pHluorin molecule; VAMP4-pH with a hope to understand its unique response to more intense stimuli. Using several approaches, I have shown here that VAMP4-pH is selectively retrieved via ADBE unlike other pHluorins examined. I have also found a necessity for VAMP4 for ADBE and isolated the location of its functional binding site.

6.3.1 VAMP4-pH Responds Differently Between LFS and HFS

Our experiments revealed that mild and intense stimulation elicited a differential effect on the fluorescent response of VAMP4-pH. During HFS both CGNs and hippocampal cells exhibited a subpopulation of nerve terminals in which the fluorescence of VAMP4-pH would undergo a slow decrease in fluorescence over time. Inhibiting ADBE in CGNs via pharmacological and genetic means showed that this endocytic mode was essential for the presence of these downstrokes.

Independent manipulations of both CME and ADBE revealed that these downstrokes were indicative of an invaginated bulk endosome slowly acidifying over time. All manipulations were conducted using either pharmacological interventions or knockdown systems, both of which have potential pitfalls. One such pitfall was demonstrated in the knockdown of clathrin heavy chain (CHC) in CGNs. Knockdown of this protein caused differential effects between hippocampal cells and CGNs and actually resulted in an inhibition of ADBE, a process for which CHC is not an essential molecule. However, the juxtaposition of VAMP4-pH response between the two cell types actually strengthened my existing hypothesis; when one considers that in a system in which CHC knockdown causes an inhibition of both CME and ADBE (CGNs see Figure 6.14) there is no slow retrieval after HFS, it can be concluded that the downstrokes seen after HFS in another CHC knockdown system in which ADBE is not inhibited are in fact reporting the uptake and acidification of VAMP4-pH within bulk endosomes.

To ensure that no other side effects of the manipulations discussed here have gone unnoticed, further experiments could be conducted using alternative technologies such as the acute relocation via knocksideways of a protein-of-interest such as syndapin I to achieve acute inhibition of ADBE.

6.3.2 VAMP4-pH is Retrieved Differently Between CGNs and Hippocampal Cells

6.3.2.1 A Higher Proportion of CGN Versus Hippocampal Cell Nerve Terminals Undergo ADBE

When quantified, it became clear that VAMP4-pH transfected CGNs contained a larger proportion of nerve terminals displaying downstrokes than hippocampal cells. Previous studies utilising dextran found that only 35% of CGN nerve terminals exhibited uptake of dextran when exposed to high potassium (Clayton & Cousin 2009), compared to a maximum of 20% of nerve terminals in hippocampal cultures with high frequency stimulations (Wenzel et al. 2012). Interestingly, this disparity in participating nerve terminals between cell types in conserved between the two measures of ADBE. This observation is further supported by the greater percentage of sequestered VAMP4-pH in CGNs than in hippocampal cells after HFS (see Figure 6.8 and Figure 6.9).

However, the information gathered utilising VAMP4-pH would suggest higher proportions of nerve terminals undergoing ADBE in both cell types (60-65% of CGN versus 40% of hippocampal cell nerve terminals). These results could indicate that

VAMP4-pH is a more sensitive reporter of ADBE than dextran uptake. This is possibly due to the non-directed manner of fluid phase marker uptake, making it possible that all not all nerve terminals undergoing ADBE actually accumulate dextran.

Another conclusion that could be drawn from this information is that certain nerve terminals are not capable of undergoing ADBE. This hypothesis appears incorrect however as during two HFS, even though the proportions of nerve terminals undergoing ADBE between stimulations are equivalent in percentage, it is not the same populations of nerve terminals undergoing ADBE between stimulations. This is evidenced by the existence of traces displaying a downstroke after one stimulus but not after the other.

To assess the proportion of nerve terminals which undergo ADBE during at least one of the two rounds of intense stimuli, existing data from CGN "S1 S2" experiments were re-analysed. Each nerve terminal was grouped based on the criterion of whether the response it exhibited after at least one stimulation was a downstroke. This identifies all nerve terminals which underwent ADBE in response to either stimulus during the experiment (this includes all nerve terminals included under the titles: S1 Up S2 Down, S1 Down S2 Down and S1 Down S2 Up). This analysis showed that 90% of all CGN nerve terminals will undergo ADBE during two rounds of HFS (data not shown).

This finding bears significance in two ways; firstly, it appears that nearly all if not all CGN nerve terminals retain the capacity to undergo ADBE during HFS. Secondly, this endocytic mode is not uniformly triggered during every intense stimulation in

nerve terminals. Although the reasons for non-uniformity of ADBE initiation are not yet determined, these are never-the-less important observations as they demonstrate the ability of each nerve terminal to produce VAMP4-positive SVs which go on to mediate asynchronous release, independent of whether a specific nerve terminal is undergoing ADBE during any one stimulation.

The difference in incidence of ADBE between hippocampal cells and CGNs is interesting in itself. The reason for this is unknown, however it has been observed n other studies (Clayton & Cousin 2009; Wenzel et al. 2012). One possibility is that CGNs are "hardwired" to undergo ADBE. CGNs can experience unusually high frequency, firing via mossy fibre input *in vivo* of up to 300 Hz (Linne & Jalonen 2003) and cultures must be incubated in elevated K^+ to avoid apoptosis (Burgoyne & Cambray-Deakin 1988). This environment may lead to a specialisation of CGNs to more efficiently activate ADBE under HFS.

Another possibility is that the heterogeneity of hippocampal cultures causes a confounding of results. CGNs can be cultured to greater than 95% homogeneity (Burgoyne & Cambray-Deakin 1988) whereas hippocampal cultures contain around 35:65% of GABAergic : non-GABAergic boutons (Wenzel et al. 2012). GABAergic boutons belong to inhibitory interneurons, a cell type which is characterised by high rates of activity (Bartos et al. 2007) and which are more prone to ADBE as measured by dextran uptake (Wenzel et al. 2012). This increase in incidence of ADBE in the cell type accustomed to higher frequency firing is in agreement with the hypothesis that CGNs are more prone to ADBE due to their high firing rate *in vivo*. The majority of hippocampal cultures are non-GABAergic and less prone to ADBE, possibly

resulting in the lower incidence of ADBE in hippocampal cultures than in CGN cultures.

Future investigations should be focussed on why a nerve terminal will undergo ADBE during one HFS and not the next, or vice versa. It is possible that the initiation of ADBE is affected by previous experienced stimulation, SV pool size or input from post-synaptic partners. Manipulation of these factors may offer insight into the factors increasing or decreasing likelihood of ADBE in a nerve terminal during a given stimulation. For example, sequential stimulation experiments in hippocampal cells or CGNs expressing VAMP4-pH may reveal a change in probability of ADBE events based on the number or frequency of previous stimulations.

It is also possible that each nerve terminal may undergo both asynchronous release and ADBE during each stimulation but to different extents. As these two processes would result in a slow increase or decrease in VAMP4-pH fluorescence respectively, it is possible that the observed VAMP4-pH response in any given nerve terminal is a report of the balance of both of these processes. i.e. in a nerve terminal undergoing a higher incidence of bulk endosome formation, the net effect on VAMP4-pH fluorescence would be a downstroke, as it is effectively cancelling out and overshadowing the effect of asynchronous release on the overall fluorescence of VAMP4-pH in that specific nerve terminal. It is very possible that all nerve terminals undergo asynchronous release after HFS, however this is only observable in nerve terminals undergoing little or no ADBE during that stimulus. This hypothesis is

supported by the almost uniform increase in VAMP4-pH during HFS with inhibition of ADBE through silencing syndapin I expression (see Figure 6.7).

6.3.2.2 Hippocampal Cell Nerve Terminals Exhibit an Acute Response to Stimulation Not Seen in CGNs

Another interesting difference between CGNs and hippocampal cells is the immediate response of VAMP4-pH to a HFS. CGNs exhibit no obvious response upon stimulation, with changes in fluorescence occurring slowly and only after cessation of stimulation. Hippocampal cells exhibit a distinct and dramatic decrease of fluorescence during the HFS itself. The most obvious possible cause for this effect was examined first; an artefact of the restrictive size of the acquisition area. However, upon doubling the size of said area to include neighbouring axonal regions, this characteristic drop in fluorescence was still observed.

A logical explanation for this activity-dependent drop in fluorescence is the internalisation of VAMP4-pH upon HFS into a rapidly-acidifying environment. This is unlikely to be a bulk endosome as one would expect to see a much slower quenching of pHluorin internalised via this route, in line with its rate of acidification. It is possible that VAMP4-pH is retrieved via endocytosis and the structure in which it is contained then immediately fuses with an acidified endosome (possibly a bulk endosome formed via a previous stimulation). However, if this is the case it is unknown why this would be more prevalent in hippocampal cells than in CGNs.

This immediate drop observed in VAMP4-pH in hippocampal cells appears to be dependent upon clathrin and may, therefore, be reporting VAMP4-pH internalised

via CME. When clathrin cage assembly is inhibited by pitstop-2 application, there is a significant slowing of the fluorescence drop (Figure 6.12) and knockdown of clathrin heavy-chain completely abolishes it, instead there is a peak in fluorescence upon stimulation (see Figure 6.15). The different results between these two interventions could be explained by relative efficiency of these methods to inhibit CME. It is possible, as pitstop-2 prevents the formation of a clathrin coat, that any pre-formed coat residing at the clathrin-coated pit is sufficient to allow some CME to occur.

When CME is inhibited via pitstop-2 in CGNs, VAMP4-pH exhibits a peak in fluorescence followed by a decrease below baseline (see Figure 6.11). The reason this occurs in CGNs and not hippocampal cells is not clear. Interestingly, when the endocytic kinetic (tau) is calculated for the post-stimulation decrease in VAMP4-pH fluorescence in the presence of pitstop-2 a value of 31 $\pm$ 2 seconds is achieved. This is almost identical to the time constant of the post-stimulation decrease in VAMP4-pH after stimulation in CGNs in the presence of pitstop-2, which is 32 seconds $\pm$ 2. This would imply that, although the two traces have differing characteristics, the same process is being reported. It is also of note that this time course is an order of magnitude slower than that of SV acidification (Atluri & Ryan 2006; Egashira et al. 2015) and is consistent with the acidification rate of the larger internal volume of a bulk endosome. This is extremely indicative that, in the absence of CME, VAMP4-pH is retrieved predominantly via ADBE in both CGNs and hippocampal cells.

CGNs recapitulate this peak in VAMP4-pH fluorescence upon stimulation in neurons where CHC has been knocked down (see Figure 6.14). This supports the hypothesis

that some VAMP4-pH is being endocytosed via CME in both CGNs and hippocampal cells. If this is true, it is possible that the activity-dependent drop in fluorescence seen in hippocampal cells (see Figure 6.2) is due to more VAMP4-pH being internalised via this route in hippocampal cells, possibly due to the lower incidence of ADBE in this cell type.

Another possible explanation for the dramatic differences in VAMP4-pH response during HFS between CGNs and hippocampal cells, is a difference in the amount of VAMP4-pH on readily-releasable vesicles. If SVs residing in the RRP of a CGN nerve terminal contain a greater copy number of VAMP4-pH molecules than hippocampal cells, CGNs would exhibit a higher evoked fluorescence increase of VAMP4-pH on stimulation than hippocampal cells. If the fluorescence change initiated via internalisation of VAMP4-pH via CME and externalisation of VAMP4-pH (via exocytosis) are equal in magnitude in CGNs but not hippocampal cells, this could account for the lack of a net fluorescence change upon stimulation in CGNs in comparison to the dramatic drop in VAMP4-pH seen in hippocampal cells. i.e. the amount of VAMP4-pH retrieved via CME is around equal to the amount being exocytosed upon stimulation in CGNs, whereas in hippocampal cells far more is being retrieved during stimulation than released.

This explanation would also account for the effect of pitstop-2 on VAMP4-pH in CGNs and not hippocampal cells (see Figure *6.12* and Figure 6.11 respectively). Inhibiting CME results in an evoked increase in fluorescence which is otherwise unseen. This would suggest that VAMP4-pH is normally retrieved via CME in CGNs, however this is usually masked by that being externalised. Pitstop-2 does not

have as marked an effect on VAMP4-pH fluorescence upon HFS in hippocampal cells as there is not as large a fluorescence increase to reveal by removing confounding fluorescence decrease (VAMP4-pH internalisation via CME).

6.3.2.3 VAMP4 is Essential for ADBE and its Internalisation is Dependent on Adaptor Proteins

VAMP4 does not appear to bind with AP-2, instead its sorting is dependent on AP-1 (Hinners et al. 2003) and as such it should not be clustered at the active zone in the same fashion as other SV proteins. Clustering of SV proteins may force VAMP4 into the peri-active zone, the site of ADBE. If this is true it could be argued that the uptake of VAMP4 into bulk endosomes is purely due to its relative abundance and location on the presynaptic membrane. This would not appear to be the case however. Experiments performed using acidic imaging buffer for this project indicate a surface-bound fraction of VAMP4-pH of 23 $\pm$ 4% in resting CGNs, or 36 $\pm$ 7% in resting hippocampal nerve terminals. Other published work has found comparable surface-bound fractions of tagmin-pH and sybII-pH to be 26.5 $\pm$ 3 and 19.7 $\pm$ 2.6 respectively (Pan et al. 2015) in hippocampal synapses. Despite this, these pHluorins do not show evidence of retrieval via ADBE (see Figure 5.4 and Figure 5.5). Therefore, a high abundance on the PM does not seem to be a deciding factor in retrieval via this endocytic mode.

Further evidence against this argument for non-specific uptake was provided by demonstrating the necessity for normal VAMP4 expression for the function of

ADBE in CGNs. A knockdown of VAMP4 showed a significant inhibition in ADBE as measured by dextran uptake.

The need for VAMP4 (and by logical extension ADBE) in the maintenance of neurotransmission over sequential HFS was also demonstrated. The inhibition of ADBE via VAMP4 knockdown resulted in a significant decrease in evoked fluorescence peak height of syp-pH over a series of four HFS compared to control. Further work could be done to determine if this run-down effect is in fact due to a run-down of vesicles caused by a lack of SVs formed from bulk endosomes as my hypothesis states. A recapitulation of these results when inhibiting ADBE via other mechanisms such as sustained CT92001 incubation or syndapin I knockdown would give confirmation. As would the visualisation of the RRP in transfected nerve terminals after stimulation.

I have also elucidated a mechanism of the action of VAMP4 in ADBE using VAMP4 L25A. This form of VAMP4 has been mutated to eliminate binding with adaptor protein partners, specifically AP-1 (Peden et al. 2001). The loss of this binding site renders the protein incapable of rescuing the inhibition of ADBE caused by VAMP4 knockdown, unlike its wild-type counterpart. This shows a necessity for interaction of VAMP4 with adaptor proteins for normal functioning ADBE. VAMP4-pH L25A also showed an almost complete lack of slow downstrokes after stimulation, indicating that it is not internalised via ADBE. This is not due to a dominant negative effect of VAMP4-pH L25A on the occurrence of ADBE as demonstrated through dextran uptake assays. This would imply that this adaptor protein binding site is essential for the internalisation of VAMP4 via ADBE. It would be interesting to

express this VAMP4 mutant into a knockdown background and repeat the sequential HFS experiment discussed above. This experiment would re-introduce a VAMP4 protein which is incapable of rescuing ADBE but is otherwise unaltered. This would allow the observer to test the requirement of VAMP4 versus the necessity for functioning ADBE in the maintenance of neurotransmission over sequential HFS.

The internalisation of VAMP4 upon stimulation also appears to be dependent on binding with adaptor proteins. The immediate response of VAMP4-pH L25A is very different to VAMP4-pH WT in both CGNs and hippocampal cells. Upon stimulation, an immediate peak is seen in both CGNs and hippocampal cells, the lack of an immediate downstroke in hippocampal shows that this rapid internalisation usually observed is adaptor protein-dependent. It should be noted that the average fluorescence trace acquired using VAMP4-pH L25A greatly resembles that of wildtype VAMP4-pH expressed in CGNs depleted of syndapin I, inhibiting ADBE. This could also imply that this immediate drop is in somehow linked with ADBE. Further work is needed to investigate the provenance of this immediate fluorescence drop in hippocampal cells; performing the same syndapin I knockdown with wild-type VAMP4-pH could answer the question of whether the internalisation of VAMP4-pH observed upon stimulation is facilitated via CME or ADBE.

The L25A mutation disrupts binding of AP-1 (Peden et al. 2001) and no evidence has been found for the interaction of VAMP4 with AP-2 and AP-3. Further experiments, such as looking at effects of VAMP4-pH response with the knockdown of AP-1, are needed to prove which adaptor-protein interaction is in fact responsible for VAMP4 uptake in ADBE.

AP-3 plays a joint role with AP-1 in SV formation from bulk endosomes (Cheung & Cousin 2012) and the inhibition of this budding in AP-3 KO mice has shown a reduction in vesicles supporting asynchronous release (Evstratova et al. 2014) thought to be derived from bulk endosomes.

The information compiled here could indicate that VAMP4 is the initial marker for AP-1 binding, causing the invagination of a bulk endosome. AP-3 is then responsible for the budding of VAMP4-rich SVs which are directed to fill the pool of SVs responsible for asynchronous release. However, previous work has shown no requirement for the AP-1γ subunit in ADBE (Cheung & Cousin 2012) although this study utilised dextran uptake as a measure of ADBE. This protocol is an indicator of how many nerve terminals have experienced ADBE and not the amount of ADBE within each nerve terminal. This AP-1 knockdown did result in a decrease in reserve pool size, a phenotype which could be caused by either a decrease in the number of invaginated bulk endosomes or of SV budding and as such, a role for AP-1 in the formation of bulk endosomes may warrant further investigation.

6.3.3 VAMP4 is Enriched in Endosomal Membranes

All work described so far has been utilising exogenous versions of endogenous SV proteins. To investigate the validity of my observations with regards to endogenous SV proteins, experiments were performed within the laboratory utilising an optimised fractionation protocol; CGNs were stimulated with high KCl, lysed via mechanical disruption and then fractionated utilising a non-ionic density gradient medium (Nycodenz) (Barysch et al. 2010). Lysates from the SV and bulk endosome

fraction were submitted to Western blotting (Nicholson-Fish et al. 2015). The abundance of proteins was converted into an endosome/SV ratio. vGlut1 and synaptobrevin-II were both found to be highly enriched in SVs when compared to endosomes with ratios of less than 0.5. Synaptotagmin and synaptophysin had ratios of between 1 and 1.5. As ADBE is the dominant form of endocytosis during intense stimulation, the bulk endosome fraction would contain far more membrane. As such a value of 1-1.5 could be considered to show less uptake via ADBE than CME. VAMP4 was found to be significantly enriched in the endosome fraction, with a resultant endosome/SV ratio of over 2 (Nicholson-Fish et al. 2015).

This data could suggest that other endogenous SV cargo investigated in the previous chapter is being retrieved via ADBE (although not in a proportionate manner to CME). Unfortunately, the nature of this experiment makes controlling for amount of membrane difficult. Another interpretation of this data would be that, as I have shown that there is a lack of uptake via ADBE of these SV proteins, their presence in endosomes is due to the fusion of SVs formed via CME which are rich with these proteins having fused with endosomes post-invagination. However, it is apparent that VAMP4 is being retrieved more selectively via ADBE.

In conclusion, I have identified an SV protein which is unique in that it is selectively and preferentially retrieved via ADBE. I have also determined a necessity for this SV protein, including its functional domain to allow ADBE to proceed. This discovery should allow the advancement of investigations of both the initiation and progression of ADBE, which have heretofore been hindered by a lack of reliable tools.

Final Discussion

7. Final Discussion

The efficient recycling of SVs is essential to maintain synaptic transmission. This system is tightly regulated and involves cascades of protein-protein and -lipid interactions, facilitated by a plethora of kinases and phosphatases, which together ensure the temporal and spatial co-ordination of exo- and endocytosis. There are two main forms of endocytosis; CME, which forms individual SVs and is dominant during mild stimulation and ADBE, a higher capacitance mode which retrieves larger surfaces of membrane to be formed into SVs later. The work contained in this thesis has focussed on the essential components of ADBE.

7.1 PI3K Activity and Localised Calcium Concentration are Essential Akt/GSK3 Phosphorylation

During HFS a signalling cascade is initiated, causing phosphorylation and activation of Akt. Akt then phosphorylates GSK3, causing inhibition of its kinase activity. This cascade is essential for the continuation of ADBE (Clayton et al. 2010). Dynamin I dephosphorylation is essential for ADBE to occur, active GSK3 rephosphorylates dynamin I after stimulation, thereby allowing it to be used for further rounds of ADBE. The inactivation of GSK3 by phosphorylation during HFS allows maximal dephosphorylation of dynamin I during stimulation. The essential factors responsible for the initiation of this signalling cascade were not defined.

The activity-dependent nature of this signalling cascade implied a role for calcium and my initial experiments focussed on the manipulation of intracellular Ca^{2+}. Allowing entry of Ca^{2+} independent of stimulation caused both Akt and GSK3

phosphorylation and showed that Ca^{2+} entry was sufficient for Akt/GSK3 phosphorylation (Figure 3.2). The buffering of intracellular Ca^{2+} during HFS showed that Ca^{2+} was also necessary. The use of Ca^{2+} buffers with differing abilities to deplete microdomain of Ca^{2+} at the active zone during stimulation also showed that a microdomain of Ca^{2+} was required to allow activation of the cascade, whereas buffering cytosolic Ca^{2+} had no effect on Akt/GSK3 phosphorylation (Figure 3.5). The use of a VGCC inhibitor demonstrated that entry via these Ca^{2+} channels is required for the phosphorylation of both Akt and GSK3 (Figure 3.4).

Our investigations as to the upstream components of this cascade brought me to examine PI3K, a known component of BDNF-stimulated Akt/GSK3 phosphorylation (Smillie et al. 2013). The presence of two different inhibitors of PI3K caused an ablation of Akt/GSK3 phosphorylation during HFS (Figure 3.6) showing a role for this kinase upstream of Akt activation.

In the search for the Ca^{2+}-sensitive initiator of this cascade I examined the PI3K-activator calmodulin. Although calmodulin did appear to play a role in Ca^{2+}-activated Akt/GSK3 phosphorylation independent of stimulation, its inhibition did not show any effect on the signalling cascade during HFS (Figure 3.7) and therefore it is not an upstream component of this activity-dependent signalling cascade.

The identity of this upstream catalyst is of importance, as its discovery offers another avenue for the manipulation of ADBE in central nerve terminals. Several Ca^{2+}-sensitive possibilities, such as Ras-GRF and PI3K-C2α, have the potential to be involved in the initiation of this cascade, but neither fit the current data optimally. Ras-GRF is thought to be activated via calmodulin (Farnsworth et al. 1995; Bähler &

Rhoads 2002) the inhibition of which did not affect Akt/GSK3 phosphorylation. Also, the effect seen on the cascade via PI3K inhibition with both wortmannin and LY294002 would eliminate PI3K-C2α as it is insensitive to both drugs at the levels used here. Further candidates suffer similar contradictions (see 3.3) and more work is required to identify the activator of PI3K within this signalling cascade.

One possibility is that the Akt/GSK3 phosphorylation is caused purely due to a secretion of BDNF in neurons during HFS (Matsuda et al. 2009), which has already been shown to act through PI3K (Smillie et al. 2013). This would mean that Akt/GSK3 phosphorylation is an indirect result of local Ca^{2+} increases. PI3K can activate PDK1 or the mTORC2 complex via growth factor receptors (Oh & Jacinto 2011) and inhibition of these may lead to further insight as to the progression of PI3K activation through to Akt/GSK3 phosphorylation and provide a clue as to the activator of PI3K. If BDNF excretion is in fact the initial activator of PI3K during HFS, then those manipulations resulting in inhibited Akt/GSK3 phosphorylation should exhibit a concurrent decrease in BDNF secretion during HFS. BDNF sequestering agents could also be applied to cultures during HFS to investigate any effect on Akt and GSK3 phosphorylation and this is one area that would be of great interest for further work.

It is possible that PI3K not only has a role in the formation, but that it also plays a role in the budding of bulk endosomes. PI3K is responsible for the production of $PI(3,4,5)P_3$ (Hao et al. 1997) as well as PI(3)P (Patki et al. 1997) which bind the budding-essential adaptor protein, AP-3 and early endosome antigen 1 (EEA1) respectively. Early endosome fusion is dependent on PI3K activity (Jones & Clague

1995) and treatment with wortmannin results in an inhibition of the recycling of FM-dye taken up via ADBE (Richards et al. 2004). These factors together may lead one to the view that PI3K has a primary function in the fusion of a bulk endosome, or an intermediate, fusing with an early endosome via a PI3K-dependent mechanism. PI3K inhibition after stimulation via LY294002 or wortmannin in conjunction with either the FM unloading protocol or the HRP budding assay (see 1.3.2.3.4) could reveal any effect on the budding of bulk endosomes in the absence of its activity.

7.2 PI4KIIα is an Essential Protein for ADBE

PI4KIIα is enriched in synapses, being responsible for all PI4K activity on SVs (Guo et al. 2003), and is also regulated by GSK3 activity. Phosphorylation by GSK3 causes the translocation and degradation of PI4KIIα (Robinson et al. 2014). In conjunction, these facts made PI4KIIα an interesting candidate for a possible role in SV recycling or, more specifically, in ADBE.

The knockdown of PI4KIIα caused two concomitant phenotypes across the two major endocytic routes. Firstly, PI4KIIα -depleted CGNs showed an increased rate in the retrieval of syp-pH (an indicator of endocytic rate) (Figure 4.3). Secondly, PI4KIIα -depleted cells displayed a significant inhibition in dextran uptake (an indicator of successful ADBE) (Figure 4.4). Together these phenotypes were suggestive of a compensatory mechanism, although the question remained as to whether decreased PI4KIIα caused an increased rate of CME which in turn caused an inhibition of ADBE or vice versa.

GSK3 phosphorylates PI4KIIα on two serine residues which is thought to cause a conformational shift of the protein, allowing access of AP-3 to a di-leucine binding site (Robinson et al. 2014) and allowing transport of PI4KIIα for degradation.

Mutations of these phosphorylation sites revealed their necessity in the role of PI4KIIα in SV recycling; a mutant which mimics GSK3 phosphorylation of PI4KIIα was unable to rescue either CME kinetics or ADBE inhibition during knockdown of the endogenous protein (Figure 4.9 and 4.10), whereas a phospho-null mutant exacerbated the accelerated syp-pH retrieval rate but successfully rescued ADBE Figure 4.11 and 4.13). This trend was mimicked by a mutant version of the protein with a mutated di-leucine motif which does not interact with AP-3 (Figure 4.12 and 4.14).

This separation of phenotypes by the two latter mutants suggested that the endocytic effects seen with a PI4KIIα knockdown were not causally linked as previously thought and that PI4KIIα actually plays distinct roles in either mode of retrieval. A mutant version of the PI4KIIα, which did not possess the kinase activity of its wild-type counterpart, was successful in rescuing ADBE showing that the kinase function of the enzyme is not essential for its role in this endocytic mode (Figure 4.16). The kinase-dead mutant did partially rescue the accelerated syp-pH retrieval (Figure 4.15) but also displayed a dominant-negative effect on syp-pH retrieval in CGNs expressing endogenous PI4KIIα (Figure 4.21). This indicates that the kinase activity of PI4KIIα is important in its function in CME.

Further work is required to determine the implications of the differential effects of each of these mutant forms of PI4KIIα. The execution of GST-pull downs using each

mutated form of PI4KIIα could reveal a difference in binding partners in line with the phosphorylation status of these particular sites, as well as any effects of binding in the presence or absence of the kinase activity of the protein. Any modifications of interactions with CME- or ADBE-specific proteins could reveal a mechanism for the role of PI4KIIα in each endocytic mode.

It is still unknown if the phosphorylation status of PI4KIIα is changed within a HFS. GSK3 undergoes rapid inactivation under such conditions which may mean that PI4KIIα is dephosphorylated within a similar time period. Western blot analysis using existing phospho-specific antibodies (Robinson et al. 2014) could be performed on cell lysates before, immediately after or at set intervals after HFS. This would allow visualisation of the time course of PI4KIIα dephosphorylation, as well as its rephosphorylation and may allow further insight into its function in ADBE during HFS.

The role of GSK3 in the stability of PI4KIIα could imply a chronic activity-dependent regulation for PI4KIIα in cell types such as CGNs which experience long periods of intense stimulation. In these conditions there would be less degradation of PI4KIIα when compared to cells which experience milder stimulation, possibly facilitating a higher occurrence of ADBE. If so, this should also be true for the cultured hippocampal cells and CGNs, as their incubation media mimic these conditions. A comparison of the levels of PI4KIIα between both chronically depolarised CGNs and hippocampal cells may lend insight into this hypothesis. A comparison could also be made between CGNs direct from high K^+ medium and CGNs which have been placed into a basic sodium solution and allowed to

repolarise. This could be performed as a time course experiment, allowing the observer to determine if GSK3 is able to affect a clearance of PI4KIIα in a relatively fast manner.

The use of an HRP uptake assay in conjunction with a lentiviral infection of different PI4KIIα constructs resulting in their overexpression could also reveal, with more fidelity, whether the level of PI4KIIα expression affects ADBE in two directions. The dextran experiments performed here are only a measure of how many synapses performed ADBE and not how many endosomes were being formed. If overexpression of PI4KIIα does in fact cause a larger number of endosomes formed per HFS, this could be useful information with regards to the aim to find methods of modulating ADBE.

Although the knockdown of PI4KIIα results in a decrease of the phosphoinositide PI4P (Mössinger et al. 2012) (especially on SVs), the effects on the levels of other PIs may be more complicated. It is possible that the depletion of one PI is not the only cause of phenotypes seen, but actually the result in the shift of a ratio of one or more different PIs. In order to investigate if it is in fact a disturbance in the creation of the phosphoinositides causing the physiological effects of PI4KIIα there are a number of further experiments which could be conducted utilising overexpression or knockdown of other kinases such as phosphaditylinositol-4-phosphate 5 kinase (PI5K), PIKfyve.

Proportions of PI4P to $PI(4,5)P_2$ and $PI(3,4,5)P_3$ are regulated not only by PI3Ks and PI5Ks but also by phosphatases like synaptojanins I and II (Cremona et al. 1999; Berman et al. 2008; Chang-Ileto et al. 2011; McPherson et al. 1996; Woscholski et

al. 1998) or oculocerebrorenal syndrome of Lowe (OCRL) (Attree et al. 1992) by their removal of phosphate groups on the D5 position of PI(4,5)P2 and PI(3,4,5)P3 (see Figure 1.5).

Previous work has shown an increase in PI(4,5)P_2 levels along with a decrease in PI4P and PI levels in synaptojanin I deficient mice (Cremona et al. 1999). Work with this mouse model or other forms of synaptojanin I manipulation with those CME and ADBE-monitoring protocols available may reveal more information as to the importance of the proportions of these phosphoinositides in the presynapse for normal endocytosis.

7.3 Most pHluorin-tagged Synaptic Vesicle Proteins Are Not Recycled via ADBE

My initial theory explaining the effects of PI4KIIα knockdown included a coupling mechanism between the two major forms of endocytosis, allowing compensation of one mode when the other is altered. This was disproved when the two phenotypes were separated in one experiment. ADBE was rescued by one mutant form of the protein but the rate of retrieval of syp-pH was further accelerated. This raised questions as to the ability of ADBE to retrieve SV proteins. If ADBE function is restored, how is more SV protein still being retrieved via CME? What is the normal proportion of SV protein retrieved via ADBE compared to CME? To answer these questions a series of experiments were designed and performed; using syp-pH and an acid wash protocol the proportion of syp-pH which had been internalised into a neutral compartment such as an endosome was revealed to be insignificant. The

pharmacological inhibition of ADBE resulted in no change in the kinetics or efficiency of syp-pH, vGlut-pH, tagmin-pH or sybII-pH compared to a control stimulus. These results would all indicate that a wide selection of pHluorin-tagged SV proteins, are not significantly retrieved via ADBE.

To determine what form of endocytosis is responsible for the internalisation of these probes, a series of experiments were performed manipulating the well-defined cargo-specific mode of CME. Inhibitions, both genetic and pharmacological, of CME showed a near ablation of syp-pH retrieval after HFS showing that this is the primary route for syp-pH internalisation, even when this is not the dominant form of PM retrieval. This remained true even when CME was inhibited at physiological temperatures. This showed that ADBE does not gain function in the retrieval of cargo at physiological temperatures. It also demonstrated that, although it would appear from recent work that other forms of endocytosis are present in a nerve terminal at physiological temperatures, these are not the dominant method for SV cargo retrieval during HFS.

Combined, this data suggests that the variety of pHluorin-tagged SV proteins which are used widely in research to monitor changes in endocytosis, are in fact predominantly retrieved via (and therefore reporting) CME and not ADBE.

Further work is needed to guarantee the effects on pHluorin retrieval after inhibition of CME is not a side effect of an unhealthy cell due to a prolonged knockdown of an essential protein. Although the effect on syp-pH retrieval was also seen using pharmacological methods, there is always a question of non-specific action or, specifically for pitstop-2, an effect on the acidification of vesicles (although this

particular issue was addressed. See Figure 5.12). One acute and specific method of CME inhibition would be to utilise a re-routing of clathrin from the PM and monitor the effect on pHluorin retrieval in comparison to a control stimulus (Willox & Royle 2012). This experiment does have its own shortcomings in that clathrin will not be rerouted in isolation, but will be connected to many of its binding partners which form the machinery for CME. However, as these interactions will largely be specific for CME, the experiment should still have the desired CME-specific effect in relation to SV cargo retrieval from the PM.

Other questions still remain as to the discrepancies between the results obtained from my work and those published by other groups, in which a clathrin depleted cell showed inhibition of pHluorin-tagged SV protein retrieval only during mild and not more intense stimulation. A method of identifying the level of knockdown of clathrin in each cell used for live cell retrieval experiments could allow insight into the hypothesis that individual cells within one population exposed to the same siRNA can have a large disparity in the efficacy of clathrin knockdown. It is possible that this variation is of vital importance in the severity of the phenotype observed (López-Murcia et al. 2014).

7.4 VAMP4 is Specifically Trafficked via and is Essential for ADBE

Work with a battery of pHluorin-tagged SV proteins showed that very little, if any, of their population was being retrieved via ADBE during HFS. If this was the case, and one believes the abundant evidence that SVs formed via ADBE are recycled differently than those formed via CME (Richards et al. 2000; Sara et al. 2002; Richards et al. 2004; Clayton & Cousin 2009; Cheung et al. 2010), one must ask the

question of how these SVs are recognised by their shuttling machinery. I determined that it was likely that there was a specific SV protein which marks these SVs to allow correct trafficking.

Previous work with VAMP4-pHluorin showed a distinct fluorescence change upon intense stimulation over mild stimulation in that the fluorescence of a synapse actually decreases (Raingo et al. 2012). This is highly unusual for a pHluorin-tagged SV protein and indicative of a mass internalisation which seemingly only occurs during intense stimulation. These results led me to believe that VAMP4 may be significantly internalised via ADBE.

To test this hypothesis, experiments were performed in two cell types in which cells transfected with VAMP4-pHluorin were exposed to both LFS and HFS. I discovered that individual fluorescence traces from transfected synaptic boutons could be separated into two populations with regards to their net change in fluorescence over time. In the case of CGNs, HFS led to a population of boutons which exhibited a slow increase in fluorescence and another exhibiting a slow decrease. The proportion of synapses displaying a decrease in fluorescence was significantly increased after HFS compared to LFS.

Further analysis revealed that hippocampal cells also exhibited these differential responses after HFS and that the proportion of downwards traces was dramatically decreased during LFS. These results led me to hypothesise that VAMP4-pHluorin was indeed being internalised by ADBE, but only by a subset of synapses within each cell. This hypothesis correlated with the finding that only a subset of synapses

in both CGN and hippocampal cultures internalise dextran upon HFS (Clayton & Cousin 2009; Wenzel et al. 2012).

To investigate the effects of inhibiting ADBE on the retrieval of VAMP4-pH a two-stimulation protocol was used in which ADBE is inhibited upon a second stimulus, but not the first. Using this protocol it was observed that there were significantly fewer downwards traces upon inhibition of ADBE. This was seen in comparison to both a second stimulation when compared to control cells and when compared to the internal control. Blocking ADBE via syndapin knockdown also caused a near ablation of downwards traces. This further strengthened the hypothesis that downwards traces were indicative of VAMP4-pHluorin which has been internalised via ADBE into an endosome which is undergoing slow acidification.

One further experiment which would solidify the theory of synapses exhibiting downwards traces being equivalent to synapses undergoing (more) ADBE, would be via a combined dextran uptake/VAMP4-pHluorin experiment. This experiment could give very useful information providing the fluorescence of the dextran used does not overlap with that of VAMP4-pH and a system of dextran application and removal was devised that did not interfere with the live imaging of VAMP4-pH. One would be looking to see if those synapses which displayed downwards traces after HFS corresponded significantly with those which internalised dextran on the same stimulation.

The cause of the upwards fluorescence is also a matter of interest. VAMP4 specifically labels asynchronous pool SVs and it has also been shown that an overexpression of VAMP4 leads to a significant increase in asynchronous fusion

(Raingo et al. 2012). It is possible that the slow increase in fluorescence is due to the (enhanced) asynchronous release of vesicles labelled with VAMP4-pH. The inhibition of asynchronous release could reveal if this is the case. This could be achieved via application of the calcium chelator EGTA (Raingo et al. 2012). However, as EGTA application also causes an inhibition of ADBE (Morton et al. 2015), this would only be a useful stratagem during LFS.

The acid wash protocol previously used to show a lack of sequestered pHluorin after HFS when tagged to synaptophysin, was successful in revealing a significant proportion of sequestered VAMP4-pHluorin after HFS but not LFS in both hippocampal cells and CGNs.

Pharmacological and genetic methods to inhibit CME were utilised to observe any effects on the trafficking of VAMP4-pHluorin during HFS. The retrieval of VAMP4-pHluorin after HFS via the slowly acidifying route was not inhibited when used in a protocol which did not affect the incidence of ADBE. However, when used in conjunction with a knockdown of CHC in CGNs, which was individual in that it had an inhibitory effect on ADBE, a significantly reduced retrieval was observed. These observations also agreed with my theory that the slow decreases in VAMP4-pHluorin were indicative of ADBE.

As it appeared that VAMP4 was unusual in its uptake via ADBE I investigated any role that it may play in ADBE itself. Knocking down VAMP4 in CGNs resulted in an inhibition of ADBE as measured by dextran uptake but no effect of the retrieval of syp-pH via CME, revealing a particular requirement for VAMP4 in the normal function of ADBE but not CME.

To investigate the effects of ablating ADBE on exocytosis and CME, I next conducted a four-HFS experiment, monitoring the release and retrieval of syp-pH over each stimulation in comparison to the first stimulation (which is unaffected by VAMP4 knockdown - Figure 6.17). Interestingly, VAMP4 knockdown resulted in a steady and significant decrease of peak height upon stimulation across all stimulations from the second onwards. This was not due to an increased rate of CME and so was attributed to the reduction in fusion ready SVs due to the elimination of ADBE-derived SVs as a supplement to the RP and RRP during HFS.

This theory could be investigated using an HRP budding assay in conjunction with a culture wide infection using a lentiviral vector. If it was true that SV stocks are depleted due to a lack of ADBE, this should be apparent due to a lack of HRP-labelled SVs after a number of stimulations. The results using syp-pH would imply that this difference could be visible even after the first stimulation.

I next attempted to identify the protein interaction responsible for the uptake of VAMP4 into bulk endosomes. A VAMP4-pH containing a mutated di-leucine motif known to be essential for adaptor protein binding was used, and its retrieval during HFS was examined in hippocampal cells and CGNs. Both cell types exhibited a significant reduction of retrieval compared to wild-type VAMP4-pH. This was deemed not to be a dominant-negative effect of mutant VAMP4 expression, as overexpression of this mutant VAMP4 did not inhibit dextran uptake. This adaptor binding mutant was also incapable of rescuing ADBE inhibition as caused by VAMP4 knock down. This data together demonstrates a necessity for adaptor binding in both the role of VAMP4 in ADBE and its retrieval by this mode.

Hippocampal cultures consist of around 65% excitatory and 35% inhibitory synapses and inhibitory synapses are more likely to undergo ADBE (Wenzel et al. 2012). It is possible therefore that inhibitory synapses would exhibit a higher proportion of downstrokes. However, as hippocampal cells experience a much higher rate of transfection than CGNs, it is nearly impossible to study individual transfected cells in these cultures. As such it is possible that any difference in responses between inhibitory and excitatory neurons was not detected.

The vesicular GABA transporter (vGAT) is only expressed in inhibitory neurons and therefore the use of a fluorescently-labelled antibody for vGAT (vGAT-oyster488) (Wenzel et al. 2012) could make this comparison possible. This antibody recognises the luminal domain of vGAT and can be used during live cell imaging. Comparing the fluorescent responses of hippocampal cells transfected with both VAMP4-pH and mCer in the presence of vGAT-oyster488 would allow one to distinguish which synapses belonged to inhibitory neurons and compare the two populations for differences in their VAMP4-pH retrieval. This would only be possible if the pHluorin molecule tagged to VAMP4 was modified to mOrange to allow visualisation of all three fluorescent labels.

7.5 Model

The results accumulated within this thesis have allowed for the creation of a model of some of the essential components and cellular factors which must be present for the normal progression of ADBE during HFS (Figure 7.1).

HFS leads to a rapid and localised increase in Ca^{2+} concentration via voltage-gated calcium channels which are enriched at the active zone. This Ca^{2+} increase initiates a PI3K-mediated cascade, leading to activation of the kinase Akt via its phosphorylation. Akt then phosphorylates and de-activates GSK3, allowing the efficient dephosphorylation of the ADBE essential molecule dynamin I and potentially other ADBE substrates such as PI4KIIα. Inhibition of GSK3 has previously been shown to inhibit ADBE over sequential stimuli. GSK3 deactivation therefore plays an acute role in ADBE, which is mediated via a rapid change in the presynaptic environment in response to an intense stimulation.

PI4KIIα is essential for ADBE and its phosphorylation by GSK3 inhibits its function in the capacity. Therefore, GSK3 activity may also have a longer term role in the modulation of PI4KIIα levels in the synapse. The active form of GSK3 phosphorylates PI4KIIα, marking it for degradation via AP-3-mediated trafficking to the lysosome. This would be predicted to occur during low neuronal activity. This increased clearance of PI4KIIα may cause an inhibition of ADBE. Conversely, it is possible that GSK3 inhibition via intense activity results in more PI4KIIα at the synapse, possibly allowing a higher incidence of ADBE to compensate for the high rate of SV fusion, which would be another consequence of high activity in the synapse. Thus GSK3 phosphorylation may perform a dual role to ensure optimal

coupling of neuronal activity to ADBE. In addition, PI4KIIα plays discrete role in the regulation of CME potentially via its enzymatic activity.

SV proteins are predominantly recycled via CME and do not form a representative proportion of the cargo composition of bulk endosomes. VAMP4 is unusual in that it is retrieved in the majority by ADBE. VAMP4 is essential for ADBE, as is the presence of an adaptor-protein-specific binding site on the protein. As such, it is my theory that formation of a bulk endosome involves the use of specific adaptor proteins (potentially AP-1) which recognise VAMP4 to initiate ADBE. This leads to a distinct protein signature of SVs formed via ADBE and CME which may allow for their differential sorting to vesicle pools. It is still unknown how SVs from bulk endosomes become fusion-competent as they possess a much lower copy number of essential fusion proteins but it is possible that they are shuttled through another endosome to be equipped with this machinery after budding from the bulk endosome.

In conclusion, the work completed for this thesis has identified several new potential avenues for the continued research of ADBE. VAMP4-pH was designed to be the first specific, live-cell capable method of tracking ADBE. A potential adaptor protein interaction was identified for the initiation of ADBE. In addition, novel regulatory roles for PI4KIIα have been revealed for both CME and ADBE, with different aspects of the kinase serving different functions for both. The work here, taken together, should allow significant scope for the manipulation of ADBE and will allow simpler observation of the effects of cellular manipulations on ABDE in future experiments.

ADBE is of particular interest because of its role in synaptic exhaustion which takes place with high incidence of ADBE. In this instance ADBE sequesters large sections of plasma membrane and possibly SV cargo or adaptors, causing a run down in synaptic activity until SVs are formed from bulk endosomes. Synaptic exhaustion, if manipulated via the facilitation of ADBE, could allow the control of epileptic seizures. The identification of the active regions within these two, newly discovered ADBE-specific proteins may allow for this. Synthetic peptides which mimic these functional regions could be utilised and these tools are becoming an increasingly relevant tool for clinical use (Groß et al. 2015). Conversely, synaptic exhaustion could be ablated through the inhibition of ADBE, allowing a larger number of ready-made, readily-releasable SVs. This could be a useful tact for the treatment of conditions in which the efficacy of neurotransmission is affected such as neurodegenerative conditions.

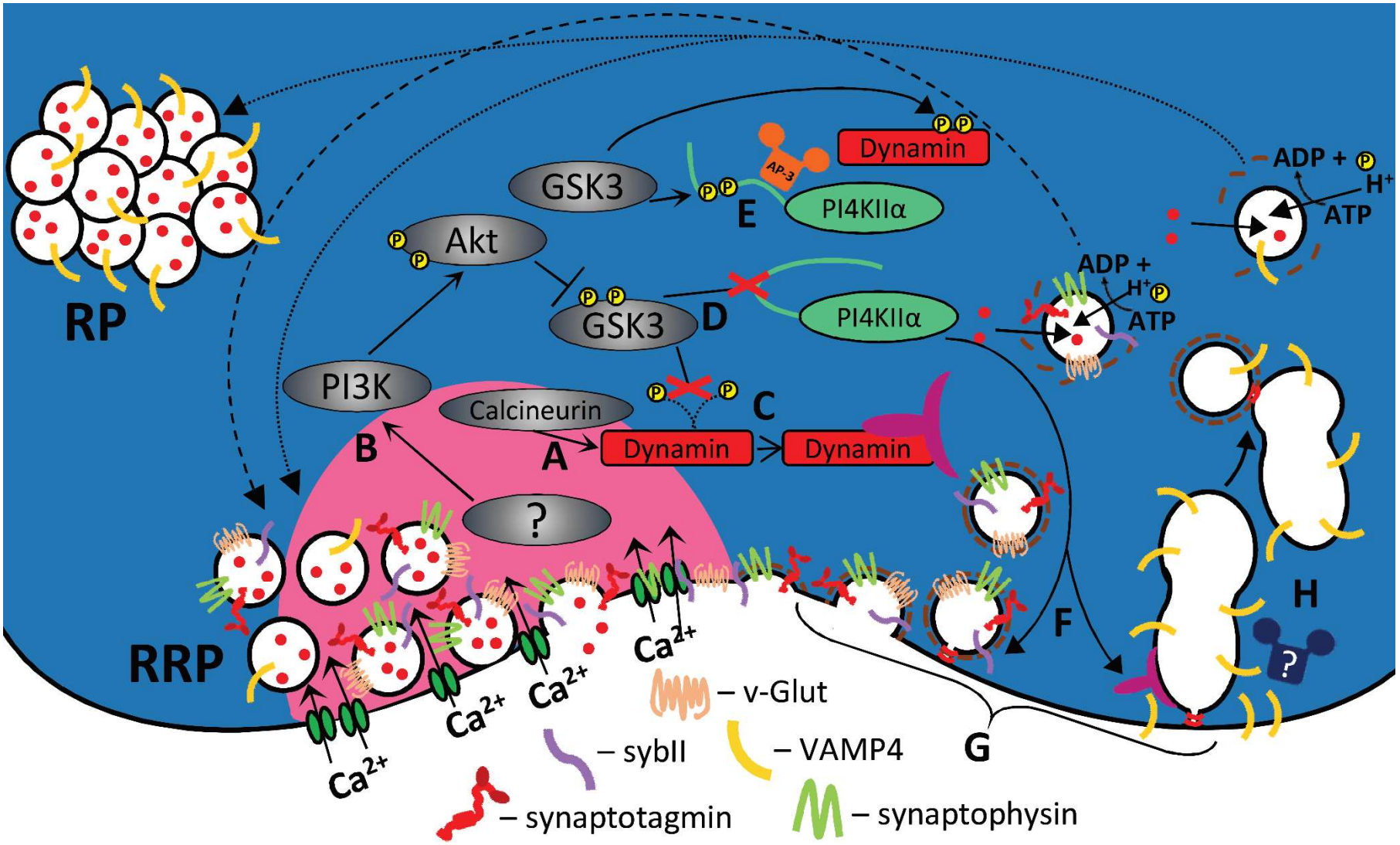
RP
RRP
GSK3
Akt
PI3K
GSK3
Calcineurin
Dynamin
Dynamin
Dynamin
AP-3
PI4KIIα
PI4KIIα
A
B
C
D
E
F
G
H
?
?
ADP +
H+
ATP
ADP +
H+
ATP
Ca2+
Ca2+
Ca2+
Ca2+
– v-Glut
– sybII
– VAMP4
– synaptotagmin
– synaptophysin

Figure 7.1 Model of Phosphorylation Cascades Relevant to ADBE and SV protein retrieval and Recycling

During HFS, increased calcium concentration in the presynapse causes simultaneous activation of calcineurin (by cytoplasmic increase) (A), leading to dephosphorylation as well as the activation of a signalling cascade which leads to the phosphorylation and de-activation of GSK3 via Akt and PI3K (by active zone increase) (B). This de-activation allows maximal dephosphorylation of dynamin during HFS and binding to syndapin (C). GSK3 de-activation also prevents the phosphorylation of PI4KIIα (D). This phosphorylation would normally lead to a removal of PI4KIIα from the presynapse via AP-3 binding (E). PI4KIIα is essential for ADBE and plays a distinct role in the modulation of CME (F). VAMP4 is specifically retrieved via ADBE whereas other SV proteins are not (G). VAMP4 recognition by an adaptor protein is also essential for ADBE (H).

8. References

Achiriloaie, M., Barylko, B. & Albanesi, J.P., 1999. Essential role of the dynamin pleckstrin homology domain in receptor-mediated endocytosis. *Mol Cell Biol*, 19(2), pp.1410–1415. Available at: http://www.ncbi.nlm.nih.gov/entrez/query.fcgi?cmd=Retrieve&db=PubMed&dopt=Citation&list_uids=9891074.

Adler, E.M. et al., 1991. Alien intracellular calcium chelators attenuate neurotransmitter release at the squid giant synapse. *The Journal of neuroscience : the official journal of the Society for Neuroscience*, 11(6), pp.1496–1507.

Agranoff, B.W., Davis, R.E. & Brink, J.J., 1965. Memory fixation in the goldfish. *Pnas*, 54, pp.788–793.

Ahle, S. & Ungewickell, E., 1986. Purification and properties of a new clathrin assembly protein. *the The European Molecular Biology Organization Journal*, 5(12), pp.3143–3149. Available at: http://www.ncbi.nlm.nih.gov/entrez/query.fcgi?cmd=Retrieve&db=PubMed&dopt=Citation&list_uids=3816757.

Aikawa, Y. & Martin, T.F.J., 2003. ARF6 regulates a plasma membrane pool of phosphatidylinositol(4,5)bisphosphate required for regulated exocytosis. *Journal of Cell Biology*, 162(4), pp.647–659.

Alessi, D.R. et al., 1997. Characterization of a 3-phosphoinositide-dependent protein kinase which phosphorylates and activates protein kinase Balpha. *Curr Biol*, 7(4), pp.261–269. Available at: http://www.ncbi.nlm.nih.gov/entrez/query.fcgi?cmd=Retrieve&db=PubMed&dopt=Citation&list_uids=9094314.

Andersson, F. et al., 2008. Perturbation of syndapin/PACSIN impairs synaptic vesicle recycling evoked by intense stimulation. *J Neurosci*, 28(15), pp.3925–3933. Available at: http://www.ncbi.nlm.nih.gov/pubmed/18400891\nhttp://www.jneurosci.org/content/28/15/3925.full.pdf.

Andres, P.G. et al., 2004. CD28 signals in the immature immunological synapse. *Journal of immunology (Baltimore, Md. : 1950)*, 172, pp.5880–5886.

Andres, S.F. et al., 2013. Insulin receptor isoform switching in intestinal stem cells, progenitors, differentiated lineages and tumors: evidence that IR-B limits proliferation. *Journal of cell science*, 126(Pt 24), pp.5645–56. Available at: http://www.ncbi.nlm.nih.gov/pubmed/24127567.

Anggono, V. et al., 2006. Syndapin I is the phosphorylation-regulated dynamin I partner in synaptic vesicle endocytosis. *Nature neuroscience*, 9(6), pp.752–760. Available at: http://www.pubmedcentral.nih.gov/articlerender.fcgi?artid=2082060&tool=pmcentrez&rendertype=abstract.

Aoyagi, K. et al., 2005. The activation of exocytotic sites by the formation of phosphatidylinositol 4,5-bisphosphate microdomains at syntaxin clusters. *Journal of Biological Chemistry*, 280(17), pp.17346–17352.

Araç, D. et al., 2006. Close membrane-membrane proximity induced by Ca(2+)-dependent multivalent binding of synaptotagmin-1 to phospholipids. *Nature structural & molecular biology*, 13(3), pp.209–217.

Ashby, M.C. et al., 2006. Lateral diffusion drives constitutive exchange of AMPA receptors at dendritic spines and is regulated by spine morphology. *The Journal of neuroscience : the official journal of the Society for Neuroscience*, 26(26), pp.7046–7055.

Atluri, P.P. & Ryan, T. a, 2006. The kinetics of synaptic vesicle reacidification at hippocampal nerve terminals. *The Journal of neuroscience : the official journal of the Society for Neuroscience*, 26(8), pp.2313–20. Available at: http://www.ncbi.nlm.nih.gov/pubmed/16495458.

Attree, O. et al., 1992. The Lowe's oculocerebrorenal syndrome gene encodes a protein highly homologous to inositol polyphosphate-5-phosphatase. *Nature*, 358(6383), pp.239–242.

Bähler, M. & Rhoads, A., 2002. Calmodulin signaling via the IQ motif. *FEBS Letters*, 513(1), pp.107–113.

Baird, D. et al., 2008. Assembly of the PtdIns 4-kinase Stt4 complex at the plasma membrane requires Ypp1 and Efr3. *The Journal of cell biology*, 183(6), pp.1061–74. Available at: http://jcb.rupress.org/cgi/content/long/183/6/1061 [Accessed September 3, 2016].

Bal, M. et al., 2013. Reelin Mobilizes a VAMP7-Dependent Synaptic Vesicle Pool and Selectively Augments Spontaneous Neurotransmission. *Neuron*, 80(4), pp.934–946.

Balaji, J. & Ryan, T. a, 2007. Single-vesicle imaging reveals that synaptic vesicle exocytosis and endocytosis are coupled by a single stochastic mode. *Proceedings of the National Academy of Sciences of the United States of America*, 104(51), pp.20576–20581.

Balla, A. & Balla, T., 2006. Phosphatidylinositol 4-kinases: old enzymes with emerging functions. *Trends in Cell Biology*, 16(7), pp.351–361.

Balla, T., 2013. Phosphoinositides: tiny lipids with giant impact on cell regulation. *Physiological reviews*, 93(3), pp.1019–137. Available at: http://www.ncbi.nlm.nih.gov/pubmed/23899561.

Barouch, W. et al., 1997. Auxilin-induced interaction of the molecular chaperone Hsc70 with clathrin baskets. *Biochemistry*, 36(14), pp.4303–4308.

Bartos, M., Vida, I. & Jonas, P., 2007. Synaptic mechanisms of synchronized gamma oscillations in inhibitory interneuron networks. *Nature reviews. Neuroscience*, 8(1), pp.45–56.

Barylko, B. et al., 1998. Synergistic activation of dynamin GTPase by Grb2 and

phosphoinositides. *Journal of Biological Chemistry*, 273(6), pp.3791–3797.

Barysch, S. V, Jahn, R. & Rizzoli, S.O., 2010. A fluorescence-based in vitro assay for investigating early endosome dynamics. *Nature protocols*, 5(6), pp.1127–1137. Available at: http://dx.doi.org/10.1038/nprot.2010.84.

Bashkirov, P. V. et al., 2008. GTPase Cycle of Dynamin Is Coupled to Membrane Squeeze and Release, Leading to Spontaneous Fission. *Cell*, 135(7), pp.1276–1286.

Benfenati, F. et al., 1992. Interaction of free and synaptic vesicle-bound synapsin I with F-actin. *Neuron*, 8(2), pp.377–386.

Benmerah, A. et al., 1998. Ap-2/Eps15 interaction is required for receptor-mediated endocytosis. *Journal of Cell Biology*, 140(5), pp.1055–1062.

Bennett, M.K., Calakos, N. & Scheller, R.H., 1992. Syntaxin: a synaptic protein implicated in docking of synaptic vesicles at presynaptic active zones. *Science (New York, N.Y.)*, 257(5067), pp.255–259.

Berman, D.E. et al., 2008. Oligomeric amyloid-beta peptide disrupts phosphatidylinositol-4,5-bisphosphate metabolism. *Nature neuroscience*, 11(5), pp.547–554.

Betz, W.J., 1970. Depression of transmitter release at the neuromuscular junction of the frog. *The Journal of physiology*, 206(3), pp.629–44. Available at: http://www.pubmedcentral.nih.gov/articlerender.fcgi?artid=1348669&tool=pmcentrez&rendertype=abstract.

Birks, R. & MacIntosh, F.C., 1961. ACETYLCHOLINE METABOLISM OF A SYMPATHETIC GANGLION. *Biochemistry and Cell Biology*, 39, pp.787–827.

Van Der Bliek, A.M. et al., 1993. Mutations in human dynamin block an intermediate stage in coated vesicle formation. *Journal of Cell Biology*, 122(3), pp.553–563.

Bloom, O. et al., 2003. Colocalization of synapsin and actin during synaptic vesicle recycling. *Journal of Cell Biology*, 161(4), pp.737–747.

Böcking, T. et al., 2011. Single-molecule analysis of a molecular disassemblase reveals the mechanism of Hsc70-driven clathrin uncoating. *Nature structural & molecular biology*, 18(3), pp.295–301. Available at: http://www.pubmedcentral.nih.gov/articlerender.fcgi?artid=3056279&tool=pmcentrez&rendertype=abstract.

Boucrot, E. et al., 2010. Roles of AP-2 in clathrin-mediated endocytosis. *PLoS ONE*, 5(5).

Boura, E. & Nencka, R., 2015. Phosphatidylinositol 4-kinases: Function, structure, and inhibition. *Experimental Cell Research*, 337(2), pp.136–145.

Bozek, K. et al., 2015. Organization and Evolution of Brain Lipidome Revealed by Large-Scale Analysis of Human, Chimpanzee, Macaque, and Mouse Tissues. *Neuron*, 85(4), pp.695–702.

Bozulic, L. & Hemmings, B.A., 2009. PIKKing on PKB: regulation of PKB activity by phosphorylation. *Current Opinion in Cell Biology*, 21(2), pp.256–261.

Brazil, D.P. & Hemmings, B.A., 2001. Ten years of protein kinase B signalling: A hard Akt to follow. *Trends in Biochemical Sciences*, 26(11), pp.657–664.

Brose, N., 2008. For better or for worse: Complexins regulate SNARE function and vesicle fusion. *Traffic*, 9(9), pp.1403–1413.

Brose, N. et al., 1992. Synaptotagmin: a calcium sensor on the synaptic vesicle surface. *Science (New York, N.Y.)*, 256(5059), pp.1021–1025.

Brunn, G.J. et al., 1996. Direct inhibition of the signaling functions of the mammalian target of rapamycin by the phosphoinositide 3-kinase inhibitors, wortmannin and LY294002. *The EMBO journal*, 15(19), pp.5256–5267.

Burgoyne, R.D. & Cambray-Deakin, M.A., 1988. The cellular neurobiology of neuronal development: the cerebellar granule cell. *Brain Research*, 472(1), pp.77–101. Available at: http://www.ncbi.nlm.nih.gov/pubmed/3277691.

Burkhardt, P. et al., 2008. Munc18a controls SNARE assembly through its interaction with the syntaxin N-peptide. *The EMBO journal*, 27(7), pp.923–33. Available at: http://emboj.embopress.org/content/27/7/923.abstract.

De Camilli, P. et al., 1983. Synapsin I (protein I), a nerve terminal-specific phosphoprotein. II. Its specific association with synaptic vesicles demonstrated by immunocytochemistry in agarose-embedded synaptosomes. *Journal of Cell Biology*, 96(5), pp.1355–1373.

Cantley, L.C., 2002. The Phosphoinositide 3-Kinase Pathway. *Science*, 296(5573), pp.1655–1657. Available at: http://www.sciencemag.org/content/296/5573/1655\nhttp://www.ncbi.nlm.nih.gov/pubmed/12040186\nhttp://www.sciencemag.org/content/296/5573/1655.full\nhttp://www.sciencemag.org/content/296/5573/1655.full.pdf.

Chaineau, M., Danglot, L. & Galli, T., 2009. Multiple roles of the vesicular-SNARE TI-VAMP in post-Golgi and endosomal trafficking. *FEBS Letters*, 583(23), pp.3817–3826.

Chang-Ileto, B. et al., 2011. Synaptojanin 1-mediated PI(4,5)P2 hydrolysis is modulated by membrane curvature and facilitates membrane fission. *Developmental Cell*, 20(2), pp.206–218. Available at: http://www.pubmedcentral.nih.gov/articlerender.fcgi?artid=3058127&tool=pmcentrez&rendertype=abstract.

Chapman, E.R., 2002. Synaptotagmin: a Ca(2+) sensor that triggers exocytosis? *Nature reviews. Molecular cell biology*, 3(7), pp.498–508.

Chasserot-Golaz, S. et al., 2010. Lipid dynamics in exocytosis. In *Cellular and Molecular Neurobiology*. pp. 1335–1342.

Chasserot-Golaz, S. et al., 1998. Possible involvement of phosphatidylinositol 3-kinase in regulated exocytosis: studies in chromaffin cells with inhibitor LY294002. *Journal of neurochemistry*, 70(6), p.2347–56. Available at: Jan's drive:Documents:Papers:Chasserot1998 PI3 chrom\npapers3://publication/uuid/186C7B88-4EE8-43BA-BA5D-61B4321AAB88.

Chen, D.Y. et al., 2012. Glucocorticoid receptors recruit the CaMKIIalpha-BDNF-CREB pathways to mediate memory consolidation. *Nat Neurosci*, 15(12), pp.1707–1714. Available at: http://www.ncbi.nlm.nih.gov/entrez/query.fcgi?cmd=Retrieve&db=PubMed&dopt=Citation&list_uids=23160045.

Chen, H. et al., 1998. Epsin is an EH-domain-binding protein implicated in clathrin-mediated endocytosis. *Nature*, 394(6695), pp.793–797.

Cheung, G. & Cousin, M. a, 2013. Synaptic vesicle generation from activity-dependent bulk endosomes requires calcium and calcineurin. *The Journal of neuroscience : the official journal of the Society for Neuroscience*, 33(8), pp.3370–9. Available at: http://www.pubmedcentral.nih.gov/articlerender.fcgi?artid=3589713&tool=pmcentrez&rendertype=abstract.

Cheung, G. & Cousin, M. a., 2012. Adaptor Protein Complexes 1 and 3 Are Essential for Generation of Synaptic Vesicles from Activity-Dependent Bulk Endosomes. *Journal of Neuroscience*, 32(17), pp.6014–6023.

Cheung, G., Jupp, O.J. & Cousin, M.A., 2010. Activity-dependent bulk endocytosis and clathrin-dependent endocytosis replenish specific synaptic vesicle pools in central nerve terminals. *The Journal of neuroscience : the official journal of the Society for Neuroscience*, 30(24), pp.8151–8161.

Chi, P., Greengard, P. & Ryan, T.A., 2001. Synapsin dispersion and reclustering during synaptic activity. *Nature neuroscience*, 4(12), pp.1187–1193.

Chi, P., Greengard, P. & Ryan, T.A., 2003. Synaptic vesicle mobilization is regulated by distinct synapsin I phosphorylation pathways at different frequencies. *Neuron*, 38(1), pp.69–78.

Chicka, M.C. et al., 2008. Synaptotagmin arrests the SNARE complex before triggering fast, efficient membrane fusion in response to Ca2+. *Nature structural & molecular biology*, 15(8), pp.827–835.

Chin, D. & Means, A.R., 2000. Calmodulin: A prototypical calcium sensor. *Trends in Cell Biology*, 10(8), pp.322–328.

Clayton, E.L. et al., 2010. Dynamin I phosphorylation by GSK3 controls activity-dependent bulk endocytosis of synaptic vesicles. *Nature neuroscience*, 13(7), pp.845–851.

Clayton, E.L. et al., 2009. The phospho-dependent dynamin-syndapin interaction triggers activity-dependent bulk endocytosis of synaptic vesicles. *The Journal of neuroscience : the official journal of the Society for Neuroscience*, 29(24), pp.7706–7717.

Clayton, E.L. & Cousin, M.A., 2009. Quantitative monitoring of activity-dependent bulk endocytosis of synaptic vesicle membrane by fluorescent dextran imaging. *Journal of Neuroscience Methods*, 185(1), pp.76–81.

Clayton, E.L. & Cousin, M.A., 2009. The molecular physiology of activity-dependent bulk endocytosis of synaptic vesicles. *Journal of Neurochemistry*, 111(4), pp.901–914.

Clayton, E.L. & Cousin, M. a., 2008. Differential labelling of bulk endocytosis in nerve terminals by FM dyes. *Neurochemistry International*, 53(3–4), pp.51–55.

Clayton, E.L., Evans, G.J.O. & Cousin, M. a, 2008. Bulk synaptic vesicle endocytosis is rapidly triggered during strong stimulation. *The Journal of neuroscience : the official journal of the Society for Neuroscience*, 28(26), pp.6627–6632.

Clayton, E.L., Minogue, S. & Waugh, M.G., 2013. Phosphatidylinositol 4-kinases and PI4P metabolism in the nervous system: Roles in psychiatric and neurological diseases. *Molecular Neurobiology*, 47, pp.361–372.

Colicos, M.A. et al., 2001. Remodeling of synaptic actin induced by photoconductive stimulation. *Cell*, 107(5), pp.605–616.

Collins, B.M. et al., 2002. Molecular architecture and functional model of the endocytic AP2 complex. *Cell*, 109(4), pp.523–535.

Cousin, M.A., 2009. Activity-dependent bulk synaptic vesicle endocytosis-A fast, high capacity membrane retrieval mechanism. *Molecular Neurobiology*, 39(3), pp.185–189.

Cousin, M.A. et al., 2003. Synapsin I-associated phosphatidylinositol 3-kinase mediates synaptic vesicle delivery to the readily releasable pool. *Journal of Biological Chemistry*, 278(31), pp.29065–29071.

Cousin, M.A., Nicholls, D.G. & Pocock, J.M., 1993. Flunarizine inhibits both calcium-dependent and -independent release of glutamate from synaptosomes and cultured neurones. *Brain Research*, 606(2), pp.227–236.

Cousin, M. a & Nicholls, D.G., 1997. Synaptic vesicle recycling in cultured cerebellar granule cells: role of vesicular acidification and refilling. *Journal of neurochemistry*, 69, pp.1927–35. Available at: http://www.ncbi.nlm.nih.gov/pubmed/9349537.

Craige, B., Salazar, G. & Faundez, V., 2008. Phosphatidylinositol-4-kinase type II alpha contains an AP-3-sorting motif and a kinase domain that are both required for endosome traffic. *Molecular Biology of the Cell*, 19(4), pp.1415–1426. Available at: http://www.ncbi.nlm.nih.gov/entrez/query.fcgi?db=pubmed&cmd=Retrieve&dopt=AbstractPlus&list_uids=18256276.

Cremona, O. et al., 1999. Essential Role of Phosphoinositide Metabolism in Synaptic Vesicle Recycling. *Cell*, 99(2), pp.179–188. Available at: http://www.sciencedirect.com/science/article/pii/S0092867400816499.

Davletov, B. a & Sudhof, T.C., 1993. a Single C2 Domain From Synaptotagmin-I Is Sufficient for High-Affinity Ca2+/Phospholipid Binding. *Journal of Biological*

Chemistry, 268(35), pp.26386–26390. Available at: <Go to ISI>://WOS:A1993MK42500057.

Davletov, B. & Montecucco, C., 2010. Lipid function at synapses. *Current Opinion in Neurobiology*, 20(5), pp.543–549.

Dawson, J.C., Legg, J.A. & Machesky, L.M., 2006. Bar domain proteins: a role in tubulation, scission and actin assembly in clathrin-mediated endocytosis. *Trends in Cell Biology*, 16(10), pp.493–498.

Debaisieux, S., et al., 2012. The ins and outs of HIV-1 Tat. *Traffic*, 13(3), p.355–63.

Dittman, J.S. & Kaplan, J.M., 2006. Factors regulating the abundance and localization of synaptobrevin in the plasma membrane. *Proceedings of the National Academy of Sciences of the United States of America*, 103(30), pp.11399–404. Available at: http://www.pubmedcentral.nih.gov/articlerender.fcgi?artid=1544097&tool=pmcentrez&rendertype=abstract.

Domin, J. et al., 1997. Cloning of a human phosphoinositide 3-kinase with a C2 domain that displays reduced sensitivity to the inhibitor wortmannin. *The Biochemical journal*, 326 (Pt 1, pp.139–147.

Dominguez, V. et al., 2011. Class II phosphoinositide 3-kinase regulates exocytosis of insulin granules in pancreatic β cells. *Journal of Biological Chemistry*, 286(6), pp.4216–4225.

Doussau, F. & Augustine, G.J., 2000. The actin cytoskeleton and neurotransmitter release: An overview. *Biochimie*, 82(4), pp.353–363.

Drake, M.T., Zhu, Y. & Kornfeld, S., 2000. The assembly of AP-3 adaptor complex-containing clathrin-coated vesicles on synthetic liposomes. *Molecular biology of the cell*, 11(11), pp.3723–36. Available at: http://www.pubmedcentral.nih.gov/articlerender.fcgi?artid=15032&tool=pmcentrez&rendertype=abstract.

Dulubova, I. et al., 1999. A conformational switch in syntaxin during exocytosis: Role of munc18. *EMBO Journal*, 18(16), pp.4372–4382.

Dulubova, I. et al., 2007. Munc18-1 binds directly to the neuronal SNARE complex. *Proceedings of the National Academy of Sciences of the United States of America*, 104(8), pp.2697–702. Available at: http://www.pubmedcentral.nih.gov/articlerender.fcgi?artid=1815244&tool=pmcentrez&rendertype=abstract.

Egashira, Y., Takase, M. & Takamori, S., 2015. Monitoring of Vacuolar-Type H+ ATPase-Mediated Proton Influx into Synaptic Vesicles. *The Journal of neuroscience : the official journal of the Society for Neuroscience*, 35(8), pp.3701–3710. Available at: http://www.jneurosci.org/cgi/doi/10.1523/JNEUROSCI.4160-14.2015.

Eldar-Finkelman, H., 2002. Glycogen synthase kinase 3: an emerging therapeutic target. *Trends in Molecular Medicine*, 8(3), pp.126–132. Available at: <Go to

ISI>://WOS:000174204600006.

Erzberger, J.P. & Berger, J.M., 2006. Evolutionary relationships and structural mechanisms of AAA+ proteins. *Annual review of biophysics and biomolecular structure*, 35, pp.93–114. Available at: http://www.ncbi.nlm.nih.gov/pubmed/16689629.

Evans, G.J.O. & Cousin, M. a, 2007. Activity-dependent control of slow synaptic vesicle endocytosis by cyclin-dependent kinase 5. *The Journal of neuroscience : the official journal of the Society for Neuroscience*, 27(2), pp.401–411.

Evstratova, A. et al., 2014. Vesicles derived via AP-3-dependent recycling contribute to asynchronous release and influence information transfer. *Nature communications*, 5, p.5530. Available at: http://www.ncbi.nlm.nih.gov/pubmed/25410111.

Farnsworth, C.L. et al., 1995. Calcium activation of Ras mediated by neuronal exchange factor Ras-GRF. *Nature*, 376(6540), pp.524–527.

Fasshauer, D. et al., 2002. SNARE assembly and disassembly exhibit a pronounced hysteresis. *Nature structural biology*, 9(2), pp.144–151.

Faúndez, V., Horng, J.T. & Kelly, R.B., 1998. A function for the AP3 coat complex in synaptic vesicle formation from endosomes. *Cell*, 93(3), pp.423–432.

Ferguson, S. et al., 2009. Coordinated Actions of Actin and BAR Proteins Upstream of Dynamin at Endocytic Clathrin-Coated Pits. *Developmental Cell*, 17(6), pp.811–822.

Ferguson, S.M. & De Camilli, P., 2012. Dynamin, a membrane-remodelling GTPase. *Nature Reviews Molecular Cell Biology*.

Fernández-Chacón, R. et al., 2001. Synaptotagmin I functions as a calcium regulator of release probability. *Nature*, 410(6824), pp.41–49.

Fernández-Medarde, A. & Santos, E., 2011. The RasGrf family of mammalian guanine nucleotide exchange factors. *Biochimica et Biophysica Acta - Reviews on Cancer*, 1815(2), pp.170–188.

Ford, M.G. et al., 2001. Simultaneous binding of PtdIns(4,5)P2 and clathrin by AP180 in the nucleation of clathrin lattices on membranes. *Science (New York, N.Y.)*, 291(5506), pp.1051–1055.

Ford, M.G.J. et al., 2002. Curvature of clathrin-coated pits driven by epsin. *Nature*, 419(6905), pp.361–366.

Foss, S.M. et al., 2013. Multiple dileucine-like motifs direct VGLUT1 trafficking. *Journal of Neuroscience*, 33(26), pp.10647–10660. Available at: http://eutils.ncbi.nlm.nih.gov/entrez/eutils/elink.fcgi?dbfrom=pubmed&id=23804088&retmode=ref&cmd=prlinks\nfile:///Users/balarampooja/Library/Application Support/Papers2/Articles/2013/Foss/Journal of Neuroscience 2013 Foss.pdf\npapers2://publication/doi/1.

Fotin, A. et al., 2004. Structure of an auxilin-bound clathrin coat and its implications for the

mechanism of uncoating. *Nature*, 432(7017), pp.649–653.

Frame, S. & Cohen, P., 2001. GSK3 takes centre stage more than 20 years after its discovery. *Biochemical Journal*, 359(Pt 1), pp.1–16. Available at: http://www.biochemj.org/content/359/1/1.abstract.

Gad, H. et al., 1998. Dissociation between Ca2+-triggered synaptic vesicle exocytosis and clathrin-mediated endocytosis at a central synapse. *Neuron*, 21(3), pp.607–616.

Gaidarov, I. & Keen, J.H., 1999. Phosphoinositide-AP-2 interactions required for targeting to plasma membrane clathrin-coated pits. *Journal of Cell Biology*, 146(4), pp.755–764.

Gallop, J.L. & McMahon, H.T., 2005. BAR domains and membrane curvature: bringing your curves to the BAR. *Biochemical Society symposium*, 231(72), pp.223–231. Available at: http://www.ncbi.nlm.nih.gov/pubmed/15649145?dopt=abstract\npapers3://publication/uuid/7249B715-6812-4392-8AAA-F2D0EFD204C2.

Gamper, N. & Shapiro, M.S., 2007. Regulation of ion transport proteins by membrane phosphoinositides. *Nature reviews. Neuroscience*, 8(12), pp.921–934.

Gao, X. et al., 2008. The Akt signaling pathway contributes to postconditioning's protection against stroke; the protection is associated with the MAPK and PKC pathways. *Journal of neurochemistry*, 105(3), pp.943–955. Available at: http://www.pubmedcentral.nih.gov/articlerender.fcgi?artid=2746404&tool=pmcentrez&rendertype=abstract.

Garcia, C.C. et al., 2004. Identification of a mutation in synapsin I, a synaptic vesicle protein, in a family with epilepsy. *Journal of medical genetics*, 41(3), pp.183–6. Available at: http://www.pubmedcentral.nih.gov/articlerender.fcgi?artid=1735688&tool=pmcentrez&rendertype=abstract.

Gasnier, B., 2000. The loading of neurotransmitters into synaptic vesicles. *Biochimie*, 82(4), pp.327–337.

Geppert, M. et al., 1994. Synaptotagmin I: A major Ca2+ sensor for transmitter release at a central synapse. *Cell*, 79(4), pp.717–727.

Gerasimenko, J. V et al., 1998. Calcium uptake via endocytosis with rapid release from acidifying endosomes. *Current biology : CB*, 8(24), pp.1335–1338.

Giraudo, C.G. et al., 2009. Alternative zippering as an on-off switch for SNARE-mediated fusion. *Science (New York, N.Y.)*, 323(5913), pp.512–6. Available at: http://www.pubmedcentral.nih.gov/articlerender.fcgi?artid=3736854&tool=pmcentrez&rendertype=abstract.

Gisselsson, L.L., Matus, A. & Wieloch, T., 2005. Actin redistribution underlies the sparing effect of mild hypothermia on dendritic spine morphology after in vitro ischemia. *Journal of cerebral blood flow and metabolism : official journal of the International Society of Cerebral Blood Flow and Metabolism*, 25(10), pp.1346–55. Available at:

http://www.ncbi.nlm.nih.gov/pubmed/15874974.

Gitler, D. et al., 2004. Different presynaptic roles of synapsins at excitatory and inhibitory synapses. *The Journal of neuroscience : the official journal of the Society for Neuroscience*, 24(50), pp.11368–80. Available at: http://www.jneurosci.org/content/24/50/11368.long.

Glyvuk, N. et al., 2010. AP-1/sigma1B-adaptin mediates endosomal synaptic vesicle recycling, learning and memory. *The EMBO journal*, 29(8), pp.1318–30. Available at: http://www.pubmedcentral.nih.gov/articlerender.fcgi?artid=2868567&tool=pmcentrez&rendertype=abstract.

Goldschmidt, H.L. et al., 2015. DGK?? Catalytic Activity Is Required for Efficient Recycling of Presynaptic Vesicles at Excitatory Synapses. *Cell Reports*.

Gormal, R.S. et al., 2015. An Acto-Myosin II Constricting Ring Initiates the Fission of Activity-Dependent Bulk Endosomes in Neurosecretory Cells. *Journal of Neuroscience*, 35(4), pp.1380–1389. Available at: http://www.jneurosci.org/cgi/doi/10.1523/JNEUROSCI.3228-14.2015.

Gracheva, E.O. et al., 2008. Direct interactions between C. elegans RAB-3 and Rim provide a mechanism to target vesicles to the presynaptic density. *Neuroscience Letters*, 444(2), pp.137–142.

Granseth, B. et al., 2007. Clathrin-mediated endocytosis: the physiological mechanism of vesicle retrieval at hippocampal synapses. *The Journal of physiology*, 585(Pt 3), pp.681–686.

Granseth, B.B. et al., 2006. Clathrin-Mediated Endocytosis Is the Dominant Mechanism of Vesicle Retrieval at Hippocampal Synapses. *Neuron*, 51(6), pp.773–786.

Groffen, A.J. et al., 2010. Doc2b is a high-affinity Ca2+ sensor for spontaneous neurotransmitter release. *Science (New York, N.Y.)*, 327(5973), pp.1614–8. Available at: http://science.sciencemag.org/content/327/5973/1614.abstract.

Groß, A. et al., 2015. Synthetic Peptides as Protein Mimics. *Frontiers in bioengineering and biotechnology*, 3, p.211. Available at: http://journal.frontiersin.org/article/10.3389/fbioe.2015.00211/abstract.

Gu, C. et al., 2010. Direct dynamin-actin interactions regulate the actin cytoskeleton. *EMBO J*, 29(21), pp.3593–3606. Available at: http://www.ncbi.nlm.nih.gov/pubmed/20935625\nhttp://emboj.embopress.org/content/embojnl/29/21/3593.full.pdf.

Guo, J. et al., 2003. Phosphatidylinositol 4-kinase type IIalpha is responsible for the phosphatidylinositol 4-kinase activity associated with synaptic vesicles. *Proceedings of the National Academy of Sciences of the United States of America*, 100(7), pp.3995–4000.

Haigh, J.R., Noremberg, K. & Parsons, S.M., 1994. Acetylcholine active transport by rat brain synaptic vesicles. *Neuroreport*, 5(7), pp.773–6. Available at:

http://www.ncbi.nlm.nih.gov/pubmed/8018848.

Halbach, A. et al., 2007. PACSIN 1 forms tetramers via its N-terminal F-BAR domain. *FEBS Journal*, 274(3), pp.773–782.

Hammond, G.R. V et al., 2012. PI4P and PI(4,5)P2 are essential but independent lipid determinants of membrane identity. *Science (New York, N.Y.)*, 337(6095), pp.727–30. Available at: http://www.pubmedcentral.nih.gov/articlerender.fcgi?artid=3646512&tool=pmcentrez&rendertype=abstract.

Hansen, S.B., Tao, X. & MacKinnon, R., 2011. Structural basis of PIP2 activation of the classical inward rectifier K+ channel Kir2.2. *Nature*, 477(7365), pp.495–8. Available at: http://www.pubmedcentral.nih.gov/articlerender.fcgi?artid=3324908&tool=pmcentrez&rendertype=abstract.

Hanson, P.I. et al., 1997. Structure and conformational changes in NSF and its membrane receptor complexes visualized by quick-freeze/deep-etch electron microscopy. *Cell*, 90(3), pp.523–535.

Hao, W. et al., 1999. AP180 and AP-2 interact directly in a complex that cooperatively assembles clathrin. *Journal of Biological Chemistry*, 274(32), pp.22785–22794.

Hao, W. et al., 1997. Regulation of AP-3 function by inositides. Identification of phosphatidylinositol 3,4,5-trisphosphate as a potent ligand. *Journal of Biological Chemistry*, 272(10), pp.6393–6398.

Hartmann-Petersen, R. et al., 2000. Individual cell motility studied by time-lapse video recording: Influence of experimental conditions. *Cytometry*, 40(4), pp.260–270.

Hata, Y., Slaughter, C.A. & Südhof, T.C., 1993. Synaptic vesicle fusion complex contains unc-18 homologue bound to syntaxin. *Nature*, 366, pp.347–351.

Haucke, V. & De Camilli, P., 1999. AP-2 recruitment to synaptotagmin stimulated by tyrosine-based endocytic motifs. *Science (New York, N.Y.)*, 285(5431), pp.1268–71. Available at: http://www.ncbi.nlm.nih.gov/pubmed/10455054.

Haucke, V., Neher, E. & Sigrist, S.J., 2011. Protein scaffolds in the coupling of synaptic exocytosis and endocytosis. *Nat Rev Neurosci*, 12(3), pp.127–138. Available at: http://www.ncbi.nlm.nih.gov/pubmed/21304549.

Hay, J.C. et al., 1995. ATP-dependent inositide phosphorylation required for Ca(2+)-activated secretion. *Nature*, 374(6518), pp.173–7. Available at: http://www.ncbi.nlm.nih.gov/pubmed/11208903.

Heerssen, H., Fetter, R.D. & Davis, G.W., 2008. Clathrin Dependence of Synaptic-Vesicle Formation at the Drosophila Neuromuscular Junction. *Current Biology*, 18, pp.401–409.

Helen E. M. Stimpson,* Christopher P. Toret,*† Aaron T. Cheng, Barbara S. Pauly, and

D.G.D. author, 2010. Early-Arriving Syp1p and Ede1p Function in Endocytic Site Placement and Formation in Budding Yeast. *Molecular biology of the cell*, 21(22), pp.4042–4056.

Henne, W.M. et al., 2010. FCHo proteins are nucleators of clathrin-mediated endocytosis. *Science (New York, N.Y.)*, 328(5983), pp.1281–4. Available at: http://www.pubmedcentral.nih.gov/articlerender.fcgi?artid=2883440&tool=pmcentrez&rendertype=abstract.

Henne, W.M. et al., 2007. Structure and Analysis of FCHo2 F-BAR Domain: A Dimerizing and Membrane Recruitment Module that Effects Membrane Curvature. *Structure*, 15(7), pp.839–852.

Heuser, J.E. & Reese, T.S., 1973. Evidence for recycling of synaptic vesicle membrane during transmitter release at the frog neuromuscular junction. *Journal of Cell Biology*, 57(2), pp.315–344.

Hilfiker, S. et al., 1999. Synapsins as regulators of neurotransmitter release. *Philosophical transactions of the Royal Society of London. Series B, Biological sciences*, 354(1381), pp.269–279.

Hinners, I. et al., 2003. AP-1 recruitment to VAMP4 is modulated by phosphorylation-dependent binding of PACS-1. *EMBO reports*, 4(12), pp.1182–9. Available at: http://embor.embopress.org.ezp-prod1.hul.harvard.edu/content/4/12/1182.abstract.

Hinshaw, J.E. & Schmid, S.L., 1995. Dynamin self-assembles into rings suggesting a mechanism for coated vesicle budding. *Nature*, 374(6518), pp.190–192.

Hirokawa, N. et al., 1989. The cytoskeletal architecture of the presynaptic terminal and molecular structure of synapsin 1. *Journal of Cell Biology*, 108(1), pp.111–126.

Hojjati, M.R. et al., 2007. Kinase activity is not required for alphaCaMKII-dependent presynaptic plasticity at CA3-CA1 synapses. *Nature neuroscience*, 10(9), pp.1125–7. Available at: http://www.pubmedcentral.nih.gov/articlerender.fcgi?artid=2804046&tool=pmcentrez&rendertype=abstract.

Holt, M. et al., 2003. Bulk membrane retrieval in the synaptic terminal of retinal bipolar cells. *The Journal of neuroscience : the official journal of the Society for Neuroscience*, 23(4), pp.1329–1339.

Holz, R.W. et al., 2000. A pleckstrin homology domain specific for phosphatidylinositol 4,5-bisphosphate (PtdIns-4,5-P2) and fused to green fluorescent protein identifies plasma membrane PtdIns-4,5-P2 as being important in exocytosis. *Journal of Biological Chemistry*, 275(23), pp.17878–17885.

de Hoop, M.J. et al., 1994. The involvement of the small GTP-binding protein Rab5a in neuronal endocytosis. *Neuron*, 13(1), pp.11–22.

Hoopmann, P. et al., 2010. Endosomal sorting of readily releasable synaptic vesicles. *Proceedings of the National Academy of Sciences of the United States of America*, 107,

pp.19055–19060.

Hori, A. et al., 2014. Msd1/SSX2IP-dependent microtubule anchorage ensures spindle orientation and primary cilia formation. *EMBO Reports*, 15(2), pp.175–184.

Hosaka, M., Hammer, R.E. & S??dhof, T.C., 1999. A phospho-switch controls the dynamic association of synapsins with synaptic vesicles. *Neuron*, 24(2), pp.377–387.

Hua, Y. et al., 2013. Blocking endocytosis enhances short-term synaptic depression under conditions of normal availability of vesicles. *Neuron*, 80, pp.343–349.

Huang, F.-D. et al., 2004. Rolling blackout, a newly identified PIP2-DAG pathway lipase required for Drosophila phototransduction. *Nature neuroscience*, 7(10), pp.1070–8. Available at: http://www.ncbi.nlm.nih.gov/pubmed/15361878.

Huang, F.-D. et al., 2006. Rolling blackout is required for synaptic vesicle exocytosis. *The Journal of neuroscience : the official journal of the Society for Neuroscience*, 26(9), pp.2369–79. Available at: http://www.ncbi.nlm.nih.gov/pubmed/16510714.

Hui, E. et al., 2009. Synaptotagmin-Mediated Bending of the Target Membrane Is a Critical Step in Ca2+-Regulated Fusion. *Cell*, 138(4), pp.709–721.

Ishizuka, T. et al., 1995. Synaphin: a protein associated with the docking/fusion complex in presynaptic terminals. *Biochemical and biophysical research communications*, 213(3), pp.1107–14. Available at: http://www.ncbi.nlm.nih.gov/pubmed/7654227.

Jahn, R. & Fasshauer, D., 2012. Molecular machines governing exocytosis of synaptic vesicles. *Nature*, 490(7419), pp.201–207. Available at: http://dx.doi.org/10.1038/nature11320.

Jensen, V. et al., 2007. A delayed response enhancement during hippocampal presynaptic plasticity in mice. *The Journal of physiology*, 583, pp.129–143.

Jiang, R.F. et al., 1997. Interaction of auxilin with the molecular chaperone, Hsc70. *Journal of Biological Chemistry*, 272(10), pp.6141–6145.

Jockusch, W.J. et al., 2005. Clathrin-dependent and clathrin-independent retrieval of synaptic vesicles in retinal bipolar cells. *Neuron*, 46(6), pp.869–878.

Jones, a T. & Clague, M.J., 1995. Phosphatidylinositol 3-kinase activity is required for early endosome fusion. *The Biochemical journal*, 311 (Pt 1, pp.31–4. Available at: http://www.pubmedcentral.nih.gov/articlerender.fcgi?artid=1136114&tool=pmcentrez&rendertype=abstract.

Jost, M. et al., 1998. Phosphatidylinositol-4,5-bisphosphate is required for endocytic coated vesicle formation. *Current Biology*, 8(25), pp.1399–1404. Available at: http://www.sciencedirect.com/science/article/pii/S0960982298000220.

Jovanovic, J.N. et al., 1996. Neurotrophins stimulate phosphorylation of synapsin I by MAP kinase and regulate synapsin I-actin interactions. *Proceedings of the National Academy of Sciences of the United States of America*, 93(8), pp.3679–3683.

Jovanovic, J.N. et al., 2001. Opposing changes in phosphorylation of specific sites in synapsin I during Ca2+-dependent glutamate release in isolated nerve terminals. *The Journal of neuroscience : the official journal of the Society for Neuroscience*, 21(20), pp.7944–7953.

Jović, M. et al., 2014. Endosomal sorting of VAMP3 is regulated by PI4K2A. *Journal of cell science*, 127(Pt 17), pp.3745–56. Available at: http://www.ncbi.nlm.nih.gov/pubmed/25002402.

Joyal, J.L. et al., 1997. Calmodulin activates phosphatidylinositol 3-kinase. *Journal of Biological Chemistry*, 272(45), pp.28183–28186.

Jung, G. et al., 2011. Stabilization of phosphatidylinositol 4-kinase type II?? by interaction with Hsp90. *Journal of Biological Chemistry*, 286(14), pp.12775–12784.

Kane, R.E., 1976. Actin polymerization and interaction with other proteins in temperature-induced gelation of sea urchin egg extracts. *The Journal of cell biology*, 71(3), pp.704–14. Available at: http://www.pubmedcentral.nih.gov/articlerender.fcgi?artid=2109792&tool=pmcentrez&rendertype=abstract.

Kantheti, P. et al., 2003. Genetic and phenotypic analysis of the mouse mutant mh2J, an Ap3d allele caused by IAP element insertion. *Mammalian Genome*, 14(3), pp.157–167.

Kantheti, P. et al., 1998. Mutation in AP-3 ?? in the mocha mouse links endosomal transport to storage deficiency in platelets, melanosomes, and synaptic vesicles. *Neuron*, 21(1), pp.111–122.

Kasprowicz, J. et al., 2008. Inactivation of clathrin heavy chain inhibits synaptic recycling but allows bulk membrane uptake. *The Journal of Cell Biology*, 182(5), pp.1007–1016. Available at: http://eutils.ncbi.nlm.nih.gov/entrez/eutils/elink.fcgi?dbfrom=pubmed&id=18762582&retmode=ref&cmd=prlinks\npapers2://publication/doi/10.1083/jcb.200804162.

Kavalali, E.T., 2006. Synaptic vesicle reuse and its implications. *The Neuroscientist : a review journal bringing neurobiology, neurology and psychiatry*, 12(1), pp.57–66. Available at: http://www.ncbi.nlm.nih.gov/pubmed/16394193.

Kelly, B.T. et al., 2008. A structural explanation for the binding of endocytic dileucine motifs by the AP2 complex. *Nature*, 456(7224), pp.976–79. Available at: http://dx.doi.org/10.1038/nature07422.

Kelly, B.T. & Owen, D.J., 2011. Endocytic sorting of transmembrane protein cargo. *Current Opinion in Cell Biology*, 23(4), pp.404–412. Available at: http://www.sciencedirect.com/science/article/pii/S0955067411000214\nhttp://pdn.sciencedirect.com/science?_ob=MiamiImageURL&_cid=272029&_user=1495569&_pii=S0955067411000214&_check=y&_origin=article&_zone=toolbar&_coverDate=31-Aug-2011&view=c&originContentF.

Kessels, M.M. et al., 2001. Mammalian Abp1, a signal-responsive F-actin-binding protein, links the actin cytoskeleton to endocytosis via the GTPase dynamin. *Journal of Cell*

Biology, 153(2), pp.351–366.

Kessels, M.M. & Qualmann, B., 2006. Syndapin oligomers interconnect the machineries for endocytic vesicle formation and actin polymerization. *Journal of Biological Chemistry*, 281(19), pp.13285–13299.

Kessels, M.M. & Qualmann, B., 2002. Syndapins integrate N-WASP in receptor-mediated endocytosis. *EMBO Journal*, 21(22), pp.6083–6094.

Ketel, K. et al., 2016. A phosphoinositide conversion mechanism for exit from endosomes. *Nature*. Available at: http://www.nature.com/nature/journal/vaop/ncurrent/full/nature16516.html?WT.ec_id=NATURE-20160114&spMailingID=50459781&spUserID=MjA1NTA3MzU3MQS2&spJobID=841825502&spReportId=ODQxODI1NTAyS0.

Khuong, T.M. et al., 2013. Synaptic PI(3,4,5)P3 Is Required for Syntaxin1A Clustering and Neurotransmitter Release. *Neuron*, 77(6), pp.1097–1108.

Khvotchev, M. et al., 2007. Dual modes of Munc18-1/SNARE interactions are coupled by functionally critical binding to syntaxin-1 N terminus. *The Journal of neuroscience : the official journal of the Society for Neuroscience*, 27(45), pp.12147–55. Available at: http://www.ncbi.nlm.nih.gov/pubmed/17989281.

Kim, S.H. & Ryan, T.A., 2010. CDK5 Serves as a Major Control Point in Neurotransmitter Release. *Neuron*, 67(5), pp.797–809.

Kim, S.H. & Ryan, T. a, 2009. Synaptic vesicle recycling at CNS snapses without AP-2. *The Journal of neuroscience : the official journal of the Society for Neuroscience*, 29(12), pp.3865–74. Available at: http://www.pubmedcentral.nih.gov/articlerender.fcgi?artid=2713063&tool=pmcentrez&rendertype=abstract.

Klein, D.E. et al., 1998. The pleckstrin homology domains of dynamin isoforms require oligomerization for high affinity phosphoinositide binding. *Journal of Biological Chemistry*, 273(42), pp.27725–27733.

Von Kleist, L. et al., 2011. Role of the clathrin terminal domain in regulating coated pit dynamics revealed by small molecule inhibition. *Cell*, 146(3), pp.471–484.

Koch, M. & Holt, M., 2012. Coupling exo- and endocytosis: An essential role for PIP 2 at the synapse. *Biochimica et Biophysica Acta - Molecular and Cell Biology of Lipids*, 1821(8), pp.1114–1132.

Kokotos, A.C. & Cousin, M.A., 2015. Synaptic vesicle generation from central nerve terminal endosomes. *Traffic*, 16(3), pp.229–240. Available at: http://doi.wiley.com/10.1111/tra.12235.

Kononenko, N.L. et al., 2014. Clathrin/AP-2 mediate synaptic vesicle reformation from endosome-like vacuoles but are not essential for membrane retrieval at central synapses. *Neuron*, 82(5), pp.981–988. Available at:

http://dx.doi.org/10.1016/j.neuron.2014.05.007.

Kononenko, N.L.L. & Haucke, V., 2015. Molecular mechanisms of presynaptic membrane retrieval and synaptic vesicle reformation. *Neuron*, 85(3), pp.484–496. Available at: http://linkinghub.elsevier.com/retrieve/pii/S0896627314010976.

Kosaka, T. & Ikeda, K., 1983. Reversible blockage of membrane retrieval and endocytosis in the garland cell of the temperature-sensitive mutant of Drosophila melanogaster, shibirets1. *Journal of Cell Biology*, 97(2), pp.499–507.

Koushika, S.P. et al., 2001. A post-docking role for active zone protein Rim. *Nature neuroscience*, 4(10), pp.997–1005.

Kuromi, H. & Kidokoro, Y., 1998. Two distinct pools of synaptic vesicles in single presynaptic boutons in a temperature-sensitive Drosophila mutant, shibire. *Neuron*, 20(5), pp.917–925.

Lafon-Cazal, M. et al., 2002. Akt mediates the anti-apoptotic effect of NMDA but not that induced by potassium depolarization in cultured cerebellar granule cells. *European Journal of Neuroscience*, 16(4), pp.575–583.

Larimore, J. et al., 2011. The schizophrenia susceptibility factor dysbindin and its associated complex sort cargoes from cell bodies to the synapse. *Molecular Biology of the Cell*, 22(24), pp.4854–4867.

Lauwers, E., Goodchild, R. & Verstreken, P., 2016. Membrane Lipids in Presynaptic Function and Disease. *Neuron*, 90(1), pp.11–25. Available at: http://www.sciencedirect.com/science/article/pii/S0896627316001707.

Lawlor, M. a & Alessi, D.R., 2001. PKB/Akt: a key mediator of cell proliferation, survival and insulin responses? *Journal of Cell Science*, 114, pp.2903–2910.

Lee, H.-K. et al., 2010. Dynamic Ca2+-dependent stimulation of vesicle fusion by membrane-anchored synaptotagmin 1. *Science (New York, N.Y.)*, 328(5979), pp.760–763.

Lee, S.Y. et al., 2004. Regulation of synaptojanin 1 by cyclin-dependent kinase 5 at synapses. *Proceedings of the National Academy of Sciences of the United States of America*, 101(4), pp.546–551.

Leibiger, B. et al., 2010. Insulin-feedback via PI3K-C2α activated PKBα/Akt1 is required for glucose-stimulated insulin secretion. *The FASEB Journal*, 24(6), pp.1824–1837. Available at: http://www.fasebj.org/content/24/6/1824.abstract\nhttp://www.fasebj.org/content/24/6/1824.full.pdf.

Li, C. et al., 1995. Ca(2+)-dependent and -independent activities of neural and non-neural synaptotagmins. *Nature*, 375(15), pp.594–599.

Li, J. et al., 2015. Identification of the Conformational transition pathway in PIP2 Opening Kir Channels. *Scientific Reports*, 5(October 2014), p.11289. Available at:

http://www.nature.com/doifinder/10.1038/srep11289.

Li, L. et al., 1995. Impairment of synaptic vesicle clustering and of synaptic transmission, and increased seizure propensity, in synapsin I-deficient mice. *Proceedings of the National Academy of Sciences of the United States of America*, 92(20), pp.9235–9. Available at: http://www.pubmedcentral.nih.gov/articlerender.fcgi?artid=40959&tool=pmcentrez&rendertype=abstract.

Li, S. et al., 2006. Distinct roles for Ras-guanine nucleotide-releasing factor 1 (Ras-GRF1) and Ras-GRF2 in the induction of long-term potentiation and long-term depression. *The Journal of neuroscience : the official journal of the Society for Neuroscience*, 26(6), pp.1721–1729.

Li, Z. et al., 2010. Caspase-3 activation via mitochondria is required for long-term depression and AMPA receptor internalization. *Cell*, 141(5), pp.859–871.

Lin, H.C. & Gilman, A.G., 1996. Regulation of dynamin I GTPase activity by G protein ???? subunits and phosphatidylinositol 4,5-bisphosphate. *Journal of Biological Chemistry*, 271(45), pp.27979–27982.

Lindner, R. & Ungewickell, E., 1991. Light-chain-independent binding of adaptors, AP180, and auxilin to clathrin. *Biochemistry*, 30(37), pp.9097–101. Available at: http://www.ncbi.nlm.nih.gov/pubmed/1909890.

Linne, M.-L. & Jalonen, T.O., 2003. Simulations of the cultured granule neuron excitability. *Neurocomputing*, 52–54, pp.583–590. Available at: http://www.sciencedirect.com/science/article/pii/S0925231202008044.

Liu, H. et al., 2009. Autapses and networks of hippocampal neurons exhibit distinct synaptic transmission phenotypes in the absence of synaptotagmin I. *The Journal of neuroscience : the official journal of the Society for Neuroscience*, 29(23), pp.7395–403. Available at: http://www.pubmedcentral.nih.gov/articlerender.fcgi?artid=2723061&tool=pmcentrez&rendertype=abstract.

Liu, K.S.Y. et al., 2011. RIM-Binding Protein, a Central Part of the Active Zone, Is Essential for Neurotransmitter Release. *Science*, 334(6062), pp.1565–1569.

López-Murcia, F.J., Royle, S.J. & Llobet, A., 2014. Presynaptic clathrin levels are a limiting factor for synaptic transmission. *Journal of neuroscience*, 34(25), pp.8618–29. Available at: http://www.ncbi.nlm.nih.gov/pubmed/24948816.

Loyet, K.M. et al., 1998. Specific binding of phosphatidylinositol 4,5-bisphosphate to calcium- dependent activator protein for secretion (CAPS), a potential phosphoinositide effector protein for regulated exocytosis. *Journal of Biological Chemistry*, 273(14), pp.8337–8343.

Macia, E. et al., 2006. Dynasore, a Cell-Permeable Inhibitor of Dynamin. *Developmental Cell*, 10(6), pp.839–850.

Mani, M. et al., 2007. The Dual Phosphatase Activity of Synaptojanin1 Is Required for Both Efficient Synaptic Vesicle Endocytosis and Reavailability at Nerve Terminals. *Neuron*, 56(6), pp.1004–1018.

Marks, B. & McMahon, H.T., 1998. Calcium triggers calcineurin-dependent synaptic vesicle recycling in mammalian nerve terminals. *Current biology : CB*, 8(13), pp.740–9. Available at: http://www.ncbi.nlm.nih.gov/pubmed/9651678.

Martens, S., Kozlov, M.M. & McMahon, H.T., 2007. How synaptotagmin promotes membrane fusion. *Science (New York, N.Y.)*, 316(5828), pp.1205–1208. Available at: http://eutils.ncbi.nlm.nih.gov/entrez/eutils/elink.fcgi?dbfrom=pubmed&id=17478680&retmode=ref&cmd=prlinks\npapers3://publication/doi/10.1126/science.1142614.

Martin, T.F. et al., 1997. The role of PtdIns(4,5)P2 in exocytotic membrane fusion. *Biochem Soc Trans*, 25(4), pp.1137–1141.

Martin, T.F.J., 2014. PI(4,5)P2-binding effector proteins for vesicle exocytosis. *Biochimica et Biophysica Acta - Molecular and Cell Biology of Lipids*, 1851(6), pp.785–793. Available at: http://dx.doi.org/10.1016/j.bbalip.2014.09.017.

Martin, T.F.J. et al., 2012. Role of PI(4,5)P2 in Vesicle Exocytosis and Membrane Fusion. *Subcellular Biochemistry*, 59, pp.111–130. Available at: http://link.springer.com/content/pdf/10.1007/978-94-007-3015-1.pdf.

Martinez-Arca, S. et al., 2003. A dual mechanism controlling the localization and function of exocytic v-SNAREs. *Proceedings of the National Academy of Sciences of the United States of America*, 100(15), pp.9011–6. Available at: http://www.pubmedcentral.nih.gov/articlerender.fcgi?artid=166429&tool=pmcentrez&rendertype=abstract.

Massol, R.H. et al., 2006. A burst of auxilin recruitment determines the onset of clathrin-coated vesicle uncoating. *Proceedings of the National Academy of Sciences of the United States of America*, 103(27), pp.10265–70. Available at: http://www.pubmedcentral.nih.gov/articlerender.fcgi?artid=1502446&tool=pmcentrez&rendertype=abstract.

Matsuda, N. et al., 2009. Differential activity-dependent secretion of brain-derived neurotrophic factor from axon and dendrite. *The Journal of neuroscience : the official journal of the Society for Neuroscience*, 29(45), pp.14185–14198.

Maximov, A. et al., 2009. Complexin controls the force transfer from SNARE complexes to membranes in fusion. *Science (New York, N.Y.)*, 323(5913), pp.516–21. Available at: http://www.pubmedcentral.nih.gov/articlerender.fcgi?artid=3235366&tool=pmcentrez&rendertype=abstract.

Maycox, P.R., Hell, J.W. & Jahn, R., 1990. Amino acid neurotransmission: spotlight on synaptic vesicles. *Trends in Neurosciences*, 13(3), pp.83–87.

Mazza, S. & Maffucci, T., 2011. Class ii phosphoinositide 3-kinase C2alpha: What we learned so far. *International Journal of Biochemistry and Molecular Biology*, 2(2), pp.168–182.

Mccluskey, A. et al., 2013. Building a better dynasore: The dyngo compounds potently inhibit dynamin and endocytosis. *Traffic*, 14(12), pp.1272–1289.

McCrea, H.J. & De Camilli, P., 2009. Mutations in phosphoinositide metabolizing enzymes and human disease. *Physiology (Bethesda, Md.)*, 24, pp.8–16. Available at: http://www.pubmedcentral.nih.gov/articlerender.fcgi?artid=3499097&tool=pmcentrez&rendertype=abstract.

McMahon, H.T. & Boucrot, E., 2011. Molecular mechanism and physiological functions of clathrin-mediated endocytosis. *Nature reviews. Molecular cell biology*, 12(8), pp.517–533. Available at: http://dx.doi.org/10.1038/nrm3151.

McPherson, P.S. et al., 1996. A presynaptic inositol-5-phosphatase. *Nature*, 379(June), pp.353–357.

McPherson, P.S. et al., 1994. p145, a major Grb2-binding protein in brain, is co-localized with dynamin in nerve terminals where it undergoes activity-dependent dephosphorylation. *Journal of Biological Chemistry*, 269(48), pp.30132–30139.

Medine, C.N. et al., 2007. Munc18-1 prevents the formation of ectopic SNARE complexes in living cells. *Journal of cell science*, 120, pp.4407–4415.

Menegon, A. et al., 2006. Protein kinase A-mediated synapsin I phosphorylation is a central modulator of Ca2+-dependent synaptic activity. *The Journal of neuroscience : the official journal of the Society for Neuroscience*, 26(45), pp.11670–11681.

Meunier, F.A. et al., 2005. Phosphatidylinositol 3-kinase C2alpha is essential for ATP-dependent priming of neurosecretory granule exocytosis. *Molecular biology of the cell*, 16(10), pp.4841–4851.

Micheva, K.D., Kay, B.K. & McPherson, P.S., 1997. Synaptojanin forms two separate complexes in the nerve terminal. Interactions with endophilin and amphiphysin. *Journal of Biological Chemistry*, 272(43), pp.27239–27245.

Miesendbock, G. et al., 1998. Visualizing secretino and synaptic transmissino with pH-sensitive green fluorescent proteins. *Nature*, 394(July), pp.192–195.

Miller, T.M. & Heuser, J.E., 1984. Endocytosis of synaptic vesicle membrane at the frog neuromuscular junction. *Journal of Cell Biology*, 98(2), pp.685–698.

Milosevic, I. et al., 2005. Plasmalemmal phosphatidylinositol-4,5-bisphosphate level regulates the releasable vesicle pool size in chromaffin cells. *The Journal of neuroscience : the official journal of the Society for Neuroscience*, 25(10), pp.2557–2565.

Minogue, S. & Waugh, M.G., 2012. The Phosphatidylinositol 4-Kinases: Don't Call it a Comeback. *Sub-cellular biochemistry*, 58, pp.1–24. Available at: http://link.springer.com/10.1007/978-94-007-3012-0\nhttp://www.ncbi.nlm.nih.gov/pubmed/22403072.

Minta, A., Kao, J.P.Y. & Tsien, R.Y., 1989. Fluorescent indicators for cytosolic calcium

based on rhodamine and fluorescein chromophores. *Journal of Biological Chemistry*, 264(14), pp.8171–8178.

Misura, K.M., Scheller, R.H. & Weis, W.I., 2000. Three-dimensional structure of the neuronal-Sec1-syntaxin 1a complex. *Nature*, 404(6776), pp.355–362.

Mittelstaedt, T., Alvaréz-Baron, E. & Schoch, S., 2010. RIM proteins and their role in synapse function. *Biological Chemistry*, 391(6), pp.599–606.

Morales, M., Colicos, M.A. & Goda, Y., 2000. Actin-Dependent Regulation of Neurotransmitter Release at Central Synapses. *Neuron*, 27(3), pp.539–550. Available at: http://www.sciencedirect.com/science/article/pii/S0896627300000647.

Morgan, J.R. et al., 2003. Eps15 homology domain-NPF motif interactions regulate clathrin coat assembly during synaptic vesicle recycling. *Journal of Biological Chemistry*, 278(35), pp.33583–33592.

Morris, S.A. et al., 1993. Clathrin assembly protein AP180: primary structure, domain organization and identification of a clathrin binding site. *The EMBO journal*, 12(2), pp.667–75. Available at: http://www.pubmedcentral.nih.gov/articlerender.fcgi?artid=413251&tool=pmcentrez&rendertype=abstract.

Morton, A., Marland, J.R.K. & Cousin, M.A., 2015. Synaptic vesicle exocytosis and increased cytosolic calcium are both necessary but not sufficient for activity-dependent bulk endocytosis. *Journal of Neurochemistry*, 134(3), pp.405–415.

Mössinger, J. et al., 2012. Phosphatidylinositol 4-kinase IIα function at endosomes is regulated by the ubiquitin ligase Itch. *EMBO reports*, 13(12), pp.1087–94. Available at: http://dx.doi.org/10.1038/embor.2012.164\nhttp://www.ncbi.nlm.nih.gov/pubmed/23146885.

Motley, A. et al., 2003. Clathrin-mediated endocytosis in AP-2-depleted cells. *Journal of Cell Biology*, 162(5), pp.909–918.

Murray, D.H. & Tamm, L.K., 2009. Clustering of syntaxin-1A in model membranes is modulated by phosphatidylinositol 4,5-bisphosphate and cholesterol. *Biochemistry*, 48(21), pp.4617–4625.

Nathanson, J.L. et al., 2009. Preferential labeling of inhibitory and excitatory cortical neurons by endogenous tropism of adeno-associated virus and lentivirus vectors. *Neuroscience*, 161(2), pp.441–50. Available at: http://www.pubmedcentral.nih.gov/articlerender.fcgi?artid=2728494&tool=pmcentrez&rendertype=abstract.

Neher, E., 2010a. Complexin: Does It Deserve Its Name? *Neuron*, 68(5), pp.803–806.

Neher, E., 2010b. What is rate-limiting during sustained synaptic activity: Vesicle supply or the availability of release sites. *Frontiers in Synaptic Neuroscience*, (SEP).

Newell-Litwa, K. et al., 2010. Hermansky-Pudlak protein complexes, AP-3 and BLOC-1,

differentially regulate presynaptic composition in the striatum and hippocampus. *The Journal of neuroscience : the official journal of the Society for Neuroscience*, 30(3), pp.820–31. Available at: http://www.pubmedcentral.nih.gov/articlerender.fcgi?artid=2824551&tool=pmcentrez&rendertype=abstract.

Newell-Litwa, K. et al., 2007. Neuronal and non-neuronal functions of the AP-3 sorting machinery. *Journal of cell science*, 120(Pt 4), pp.531–541.

Nguyen, T.H. et al., 2012. Actin- and dynamin-dependent maturation of bulk endocytosis restores neurotransmission following synaptic depletion. *PLoS ONE*, 7(5).

Nicholls, D.G., 1993. The glutamatergic nerve terminal. *European journal of biochemistry / FEBS*, 212(3), pp.613–631.

Nicholson-Fish, J.C.C. et al., 2015. VAMP4 Is an Essential Cargo Molecule for Activity-Dependent Bulk Endocytosis. *Neuron*, 88(5), pp.973–984. Available at: http://linkinghub.elsevier.com/retrieve/pii/S089662731500937X.

Oh, W.J. & Jacinto, E., 2011. mTOR complex 2 signaling and functions. *Cell Cycle*, 10(14), pp.2305–2316.

Osborne, S.L., Wen, P.J. & Meunier, F.A., 2006. Phosphoinositide regulation of neuroexocytosis: Adding to the complexity. *Journal of Neurochemistry*, 98(2), pp.336–342.

Pagano, A. et al., 2004. In vitro formation of recycling vesicles from endosomes requires adaptor protein-1/clathrin and is regulated by rab4 and the connector rabaptin-5. *Molecular biology of the cell*, 15(11), pp.4990–5000. Available at: http://www.molbiolcell.org/content/15/11/4990.short.

Pan, P.-Y., Marrs, J. & Ryan, T. a., 2015. Vesicular Glutamate Transporter 1 orchestrates recruitment of other synaptic vesicle cargo proteins during synaptic vesicle recycling. *Journal of Biological Chemistry*, 290(37), p.jbc.M115.651711. Available at: http://www.jbc.org/lookup/doi/10.1074/jbc.M115.651711.

Pang, Z.P. et al., 2006. A gain-of-function mutation in synaptotagmin-1 reveals a critical role of Ca2+-dependent soluble N-ethylmaleimide-sensitive factor attachment protein receptor complex binding in synaptic exocytosis. *The Journal of neuroscience : the official journal of the Society for Neuroscience*, 26(48), pp.12556–12565.

Di Paolo, G. et al., 2004. Impaired PtdIns(4,5)P2 synthesis in nerve terminals produces defects in synaptic vesicle trafficking. *Nature*, 431(7007), pp.415–422.

Park, R.J. et al., 2013. Dynamin triple knockout cells reveal off target effects of commonly used dynamin inhibitors. *Journal of cell science*, 126(Pt 22), pp.5305–12. Available at: http://www.pubmedcentral.nih.gov/articlerender.fcgi?artid=3828596&tool=pmcentrez&rendertype=abstract.

Park, Y. et al., 2015. Synaptotagmin-1 binds to PIP2-containing membrane but not to SNAREs at physiological ionic strength. *Nature structural & molecular biology*,

22(10), pp.815–823. Available at: http://www.ncbi.nlm.nih.gov/pubmed/26389740.

Patki, V. et al., 1997. Identification of an early endosomal protein regulated by phosphatidylinositol 3-kinase. *Proceedings of the National Academy of Sciences of the United States of America*, 94(14), pp.7326–30. Available at: http://www.pubmedcentral.nih.gov/articlerender.fcgi?artid=23820&tool=pmcentrez&rendertype=abstract.

Peden, A. a., Park, G.Y. & Scheller, R.H., 2001. The Di-leucine Motif of Vesicle-associated Membrane Protein 4 Is Required for Its Localization and AP-1 Binding. *Journal of Biological Chemistry*, 276(52), pp.49183–49187.

Peineau, S. et al., 2007. LTP Inhibits LTD in the Hippocampus via Regulation of GSK3β. *Neuron*, 53(5), pp.703–717.

Perin, M.S. et al., 1990. Phospholipid binding by a synaptic vesicle protein homologous to the regulatory region of protein kinase C. *Nature*, 345(6272), pp.260–263.

Peter, B.J. et al., 2004. BAR domains as sensors of membrane curvature: the amphiphysin BAR structure. *Science (New York, N.Y.)*, 303(5657), pp.495–499.

Pieribone, V. a et al., 1995. Distinct pools of synaptic vesicles in neurotransmitter release. *Nature*, 375(6531), pp.493–7. Available at: http://www.ncbi.nlm.nih.gov/pubmed/7777058.

Popova, N. V., Deyev, I.E. & Petrenko, A.G., 2011. Association of adaptor protein TRIP8b with clathrin. *Journal of Neurochemistry*, 118(6), pp.988–998.

Praefcke, G.J.K. et al., 2004. Evolving nature of the AP2 alpha-appendage hub during clathrin-coated vesicle endocytosis. *The EMBO journal*, 23(22), pp.4371–4383.

Prasad, K. et al., 1994. Complex formation between clathrin and uncoating ATPase. *Journal of Biological Chemistry*, 269(9), pp.6931–6939.

Prior, I. a. & Clague, M.J., 1997. Glutamate uptake occurs at an early stage of synaptic vesicle recycling. *Current Biology*, 7(5), pp.353–356. Available at: http://linkinghub.elsevier.com/retrieve/pii/S096098220600159X.

Pryor, P.R. et al., 2008. Molecular Basis for the Sorting of the SNARE VAMP7 into Endocytic Clathrin-Coated Vesicles by the ArfGAP Hrb. *Cell*, 134(5), pp.817–827.

Puchkov, D. & Haucke, V., 2013. Greasing the synaptic vesicle cycle by membrane lipids. *Trends in Cell Biology*, 23(10), pp.493–503.

Pyle, J.L. et al., 2000. Rapid reuse of readily releasable pool vesicles at hippocampal synapses. *Neuron*, 28(1), pp.221–31. Available at: http://www.ncbi.nlm.nih.gov/pubmed/11086996.

Raingo, J. et al., 2012. VAMP4 directs synaptic vesicles to a pool that selectively maintains asynchronous neurotransmission. *Nature Neuroscience*, 15(5), pp.738–745.

Rao, Y. et al., 2012. The early steps of endocytosis: From cargo selection to membrane deformation. *European Journal of Cell Biology*, 91(4), pp.226–233.

Reider, A. et al., 2009. Syp1 is a conserved endocytic adaptor that contains domains involved in cargo selection and membrane tubulation. *The EMBO journal*, 28(20), pp.3103–3116.

Reim, K. et al., 2001. Complexins regulate a late step in Ca2+-dependent neurotransmitter release. *Cell*, 104(1), pp.71–81.

Res, M.P.B.B., Prasad, K. & Lippoldt, R.E., 1988. Molecular Characterization of the AP180 Coated Vesicle Assembly Protein ? *Assembly*, (1987), pp.6098–6104.

Richards, D. a. et al., 2003. Synaptic vesicle pools at the frog neuromuscular junction. *Neuron*, 39, pp.529–541.

Richards, D. a. A., Guatimosim, C. & Betz, W.J.J., 2000. Two Endocytic Recycling Routes Selectively Fill Two Vesicle Pools in Frog Motor Nerve Terminals. *Neuron*, 27(3), pp.551–559. Available at: http://www.sciencedirect.com/science/article/pii/S0896627300000659.

Richards, D. a, Rizzoli, S.O. & Betz, W.J., 2004. Effects of wortmannin and latrunculin A on slow endocytosis at the frog neuromuscular junction. *The Journal of physiology*, 557(Pt 1), pp.77–91.

Rickman, C. et al., 2004. High Affinity Interaction of Syntaxin and SNAP-25 on the Plasma Membrane Is Abolished by Botulinum Toxin E. *Journal of Biological Chemistry*, 279(1), pp.644–651.

Ringstad, N., Nemoto, Y. & De Camilli, P., 1997. The SH3p4/Sh3p8/SH3p13 protein family: binding partners for synaptojanin and dynamin via a Grb2-like Src homology 3 domain. *Proceedings of the National Academy of Sciences of the United States of America*, 94(16), pp.8569–8574.

Rizzo, M.A. et al., 2004. An improved cyan fluorescent protein variant useful for FRET. *Nature biotechnology*, 22(4), pp.445–449.

Rizzoli, S.O. & Betz, W.J., 2005. Synaptic vesicle pools. *Nature reviews. Neuroscience*, 6(1), pp.57–69.

Robinson, J. et al., 2010. Phosphorylation of PI4KII α by GSK3 regulates trafficking. , (15), pp.1–11.

Robinson, J.W. et al., 2014. PI4KIIα phosphorylation by GSK3 directs vesicular trafficking to lysosomes. *The Biochemical journal*, 464(1), pp.145–56. Available at: http://www.ncbi.nlm.nih.gov/pubmed/25083612.

Robinson, M.S., Sahlender, D. a. & Foster, S.D., 2010. Rapid Inactivation of Proteins by Rapamycin-Induced Rerouting to Mitochondria. *Developmental Cell*, 18(2), pp.324–331. Available at: http://dx.doi.org/10.1016/j.devcel.2009.12.015.

Roseth, S., Fykse, E.M. & Fonnum, F., 1995. Uptake of L-glutamate into rat brain synaptic vesicles: effect of inhibitors that bind specifically to the glutamate transporter. *Journal of neurochemistry*, 65(1), pp.96–103. Available at: http://www.ncbi.nlm.nih.gov/pubmed/7790899.

Rothnie, A. et al., 2011. A sequential mechanism for clathrin cage disassembly by 70-kDa heat-shock cognate protein (Hsc70) and auxilin. *Proceedings of the National Academy of Sciences of the United States of America*, 108(17), pp.6927–32. Available at: http://www.pubmedcentral.nih.gov/articlerender.fcgi?artid=3084117&tool=pmcentrez&rendertype=abstract.

Roux, A. et al., 2006. GTP-dependent twisting of dynamin implicates constriction and tension in membrane fission. *Nature*, 441(7092), pp.528–531.

Roux, A., 2014. Reaching a consensus on the mechanism of dynamin? *F1000prime reports*, 6(86), p.86. Available at: http://f1000.com/prime/reports/b/6/86/#fig-001.

Royle, S.J., Bright, N. a & Lagnado, L., 2005. Clathrin is required for the function of the mitotic spindle. *Nature*, 434(7037), pp.1152–1157.

Royle, S.J. & Lagnado, L., 2003. Endocytosis at the synaptic terminal. *The Journal of physiology*, 553(2003), pp.345–355.

S??llner, T. et al., 1993. A protein assembly-disassembly pathway in vitro that may correspond to sequential steps of synaptic vesicle docking, activation, and fusion. *Cell*, 75(3), pp.409–418.

Saffarian, S., Cocucci, E. & Kirchhausen, T., 2009. Distinct dynamics of endocytic clathrin-coated pits and coated plaques. *PLoS Biology*, 7(9).

Saito, T. et al., 2001. Mutation analysis of SYNJ1: a possible candidate gene for chromosome 21q22-linked bipolar disorder. *Molecular psychiatry*, 6(4), pp.387–95. Available at: http://www.ncbi.nlm.nih.gov/pubmed/11443522.

Salazar, G. et al., 2005. Phosphatidylinositol-4-kinase type II alpha is a component of adaptor protein-3-derived vesicles. *Molecular biology of the cell*, 16(8), pp.3692–704. Available at: http://www.pubmedcentral.nih.gov/articlerender.fcgi?artid=1182308&tool=pmcentrez&rendertype=abstract.

Sang, Y.L. et al., 2005. Regulation of the interaction between PIPKIγ and talin by proline-directed protein kinases. *Journal of Cell Biology*, 168(5), pp.789–799.

Sankaranarayanan, S., Atluri, P.P. & Ryan, T. a, 2003. Actin has a molecular scaffolding, not propulsive, role in presynaptic function. *Nature neuroscience*, 6(2), pp.127–135.

Sankaranarayanan, S. & Ryan, T. a, 2000. Real-time measurements of vesicle-SNARE recycling in synapses of the central nervous system. *Nature cell biology*, 2(4), pp.197–204.

Sara, Y. et al., 2002. Fast vesicle recycling supports neurotransmission during sustained

stimulation at hippocampal synapses. *The Journal of neuroscience : the official journal of the Society for Neuroscience*, 22(5), pp.1608–1617.

Sarbassov, D.D. et al., 2005. Phosphorylation and regulation of Akt/PKB by the rictor-mTOR complex. *Science (New York, N.Y.)*, 307(5712), pp.1098–1101.

Sastry, P.S., 1985. Lipids of nervous tissue: Composition and metabolism. *Progress in Lipid Research*, 24(2), pp.69–176.

Schiavo, G. et al., 1996. Calcium-dependent switching of the specificity of phosphoinositide binding to synaptotagmin [published erratum appears in Proc Natl Acad Sci U S A 1997 Feb 4;94(3):1047]. *Proc Natl Acad Sci U S A*, 93(23), pp.13327–13332. Available at: http://www.ncbi.nlm.nih.gov/cgi-bin/Entrez/referer?http://www.pnas.org/cgi/content/full/93/23/13327.

Schiebler, W. et al., 1986. Characterization of synapsin I binding to small synaptic vesicles. *Journal of Biological Chemistry*, 261(18), pp.8383–8396.

Schikorski, T. & Stevens, C.F., 1997. Quantitative ultrastructural analysis of hippocampal excitatory synapses. *The Journal of neuroscience : the official journal of the Society for Neuroscience*, 17(15), pp.5858–5867.

Schlossman, D.M. et al., 1984. An enzyme that removes clathrin coats: Purification of an uncoating ATPase. *Journal of Cell Biology*, 99(2), pp.723–733.

Schoch, S. et al., 2006. Redundant functions of RIM1alpha and RIM2alpha in Ca(2+)-triggered neurotransmitter release. *The EMBO journal*, 25(24), pp.5852–5863.

Schoch, S. et al., 2002. RIM1α forms a protein scaffold for regulating neurotransmitter release at the active zone. *Nature*, 415(6869), pp.321–326.

Schonn, J.-S. et al., 2008. Synaptotagmin-1 and -7 are functionally overlapping Ca2+ sensors for exocytosis in adrenal chromaffin cells. *Proceedings of the National Academy of Sciences of the United States of America*, 105, pp.3998–4003.

Shaner, N.C. et al., 2008. Improving the photostability of bright monomeric orange and red fluorescent proteins. *Nature methods*, 5(6), pp.545–551.

Shi, X. et al., 2013. Ca2+ regulates T-cell receptor activation by modulating the charge property of lipids. *Nature*, 493(7430), pp.111–115. Available at: http://www.ncbi.nlm.nih.gov/pubmed/23201688.

Shih, W., Gallusser, A. & Kirchhausen, T., 1995. A clathrin-binding site in the hinge of the ??2 chain of mammalian AP-2 complexes. *Journal of Biological Chemistry*, 270(52), pp.31083–31090.

Shimada, A. et al., 2007. Curved EFC/F-BAR-Domain Dimers Are Joined End to End into a Filament for Membrane Invagination in Endocytosis. *Cell*, 129(4), pp.761–772.

Shisheva, A., 2008. Phosphoinositides in insulin action on GLUT4 dynamics: not just PtdIns(3,4,5)P3. *American journal of physiology. Endocrinology and metabolism*,

295(3), pp.E536-44. Available at: http://www.pubmedcentral.nih.gov/articlerender.fcgi?artid=2536738&tool=pmcentrez&rendertype=abstract.

Shupliakov, O. et al., 2002. Impaired recycling of synaptic vesicles after acute perturbation of the presynaptic actin cytoskeleton. *Proceedings of the National Academy of Sciences of the United States of America*, 99(22), pp.14476–14481.

Simons, J.P. et al., 2009. Loss of phosphatidylinositol 4-kinase 2alpha activity causes late onset degeneration of spinal cord axons. *Proceedings of the National Academy of Sciences of the United States of America*, 106(28), pp.11535–11539. Available at: http://www.pubmedcentral.nih.gov/articlerender.fcgi?artid=2710652&tool=pmcentrez&rendertype=abstract.

Sinha, R.K. et al., 2013. Type II phosphatidylinositol 4-kinase ?? is an integral signaling component of early T cell activation mechanisms. *Biochimie*, 95(8), pp.1560–1566.

Smillie, K.J. et al., 2013. Control of synaptic vesicle endocytosis by an extracellular signalling molecule. *Nature communications*, 4, p.2394. Available at: http://www.pubmedcentral.nih.gov/articlerender.fcgi?artid=3778765&tool=pmcentrez&rendertype=abstract.

Smillie, K.J. & Cousin, M.A., 2012. Akt/PKB Controls the Activity-Dependent Bulk Endocytosis of Synaptic Vesicles. *Traffic*, 13(7), pp.1004–1011.

Smillie, K.J. & Cousin, M.A., 2011. The Role of GSK3 in Presynaptic Function. *International journal of Alzheimer's disease*, 2011, p.263673.

Söllner, T. et al., 1993. SNAP receptors implicated in vesicle targeting and fusion. *Nature*, 362(6418), pp.318–324.

Sørensen, J.B., 2009. Conflicting views on the membrane fusion machinery and the fusion pore. *Annual review of cell and developmental biology*, 25, pp.513–537. Available at: http://www.annualreviews.org/doi/pdf/10.1146/annurev.cellbio.24.110707.175239\nhttp://www.annualreviews.org/doi/full/10.1146/annurev.cellbio.24.110707.175239?url_ver=Z39.88-2003&rfr_id=ori:rid:crossref.org&rfr_dat=cr_pub=pubmed.

Sørensen, J.B. et al., 2003. Examining synaptotagmin 1 function in dense core vesicle exocytosis under direct control of Ca2+. *The Journal of general physiology*, 122(3), pp.265–276. Available at: http://www.jgp.org/cgi/doi/10.1085/jgp.200308855.

Spector I, Shochet NR, Kashman Y, G.A. et al., 1983. Latrunculins: novel marine toxins that disrupt microfilament organization in cultured cells. *Science (New York, N.Y.)*, 5932(February), pp.493–495. Available at: http://www.ncbi.nlm.nih.gov/pubmed/6681676.

Stein, A. et al., 2009. Helical extension of the neuronal SNARE complex into the membrane. *Nature*, 460(7254), pp.525–528. Available at: http://dx.doi.org/10.1038/nature08156.

Stein, A. et al., 2007. Synaptotagmin activates membrane fusion through a Ca2+-dependent trans interaction with phospholipids. *Nature structural & molecular biology*, 14(10),

pp.904–911.

Stein, A. & Jahn, R., 2009. Complexins Living Up to Their Name- New Light on Their Role in Exocytosis. *Neuron*, 64(3), pp.295–297.

Stopkova, P. et al., 2004. Analysis of SYNJ1, a candidate gene for 21q22 linked bipolar disorder: A replication study. *Psychiatry Research*, 127(1–2), pp.157–161.

Stowell, M.H. et al., 1999. Nucleotide-dependent conformational changes in dynamin: evidence for a mechanochemical molecular spring. *Nature cell biology*, 1(1), pp.27–32.

Südhof, T.C., 2013. A molecular machine for neurotransmitter release: synaptotagmin and beyond. *Nature Medicine*, 19(10), pp.1227–1231. Available at: http://www.ncbi.nlm.nih.gov/pubmed/24100992\nhttp://www.nature.com/doifinder/10.1038/nm.3338.

Südhof, T.C., 2013. Neurotransmitter release: The last millisecond in the life of a synaptic vesicle. *Neuron*, 80(3), pp.675–690.

Südhof, T.C., 2012. The presynaptic active zone. *Neuron*, 75(1), pp.11–25.

Südhof, T.C., 2004. the Synaptic Vesicle Cycle. *Annual Review of Neuroscience*, 27(1), pp.509–547. Available at: http://www.annualreviews.org/doi/abs/10.1146/annurev.neuro.26.041002.131412.

Südhof, T.C., 2000. The Synaptic VesicleCycle Revisited. *Neuron*, 28(2), pp.317–320. Available at: http://www.sciencedirect.com/science/article/pii/S0896627300001094 [Accessed May 13, 2016].

Sudhof, T.C. & Rothman, J.E., 2009. Membrane fusion: grappling with SNARE and SM proteins. *Science*, 323(5913), pp.474–477. Available at: http://www.ncbi.nlm.nih.gov/entrez/query.fcgi?cmd=Retrieve&db=PubMed&dopt=Citation&list_uids=19164740\nhttp://www.sciencemag.org/content/323/5913/474.full.pdf.

Sun, F., Li, J. & Chen, C., 2014. Puzzle out the regulation mechanism of PI4KIIα activity. *Science China Life Sciences*, 57(6), pp.636–638. Available at: http://link.springer.com/10.1007/s11427-014-4656-8.

Sundborger, A. et al., 2011. An endophilin-dynamin complex promotes budding of clathrin-coated vesicles during synaptic vesicle recycling. *Journal of cell science*, 124(Pt 1), pp.133–143.

Sutton, R.B. et al., 1998. Crystal structure of a SNARE complex involved in synaptic exocytosis at 2.4 A resolution. *Nature*, 395(6700), pp.347–353.

Sutton, R.B. et al., 1995. Structure of the first C2 domain of synaptotagmin I: A novel Ca2+/phospholipid-binding fold. *Cell*, 80(6), pp.929–938.

Sweitzer, S.M. & Hinshaw, J.E., 1998. Dynamin undergoes a GTP-dependent conformational change causing vesiculation. *Cell*, 93(6), pp.1021–1029.

Takamori, S., Holt, M., Stenius, K., Lemke, E.A., et al., 2006. Molecular Anatomy of a Traf cking Organelle. *Cell*, 127(4), pp.831–846. Available at: http://www.ncbi.nlm.nih.gov/pubmed/17110340.

Takamori, S., Holt, M., Stenius, K., Lemke, E.A., et al., 2006. Molecular Anatomy of a Trafficking Organelle. *Cell*, 127(4), pp.831–846.

Takei, K. et al., 1998. Generation of coated intermediates of clathrin-mediated endocytosis on protein-free liposomes. *Cell*, 94(1), pp.131–141.

Takei, Y. et al., 1995. Synapsin I deficiency results in the structural change in the presynaptic terminals in the murine nervous system. *Journal of Cell Biology*, 131(6 II), pp.1789–1800.

Tan, T.C. et al., 2003. Cdk5 is essential for synaptic vesicle endocytosis. *Nature cell biology*, 5(8), pp.701–710.

Tang, J. et al., 2006. A Complexin/Synaptotagmin 1 Switch Controls Fast Synaptic Vesicle Exocytosis. *Cell*, 126(6), pp.1175–1187.

Tebar, F. et al., 1996. Eps15 is a component of clathrin-coated pits and vesicles and is located at the rim of coated pits. *Journal of Biological Chemistry*, 271(46), pp.28727–28730.

Torri-Tarelli, F. et al., 1990. Redistribution of synaptophysin and synapsin I during ??-latrotoxin-induced release of neurotransmitter at the neuromuscular junction. *Journal of Cell Biology*, 110(2), pp.449–459.

Tryoen-Toth, P. et al., 2013. HIV-1 Tat protein inhibits neurosecretion by binding to phosphatidylinositol 4,5-bisphosphate. *Journal of Cell Science*, 126(2), pp.454–463. Available at: http://www.ncbi.nlm.nih.gov/pubmed/23178941\nhttp://jcs.biologists.org/cgi/doi/10.1242/jcs.111658.

Tsien, R.Y., Rink, T.J. & Poenie, M., 1985. Measurement of cytosolic free Ca2+ in individual small cells using fluorescence microscopy with dual excitation wavelengths. *Cell calcium*, 6(1–2), pp.145–157.

Ungewickell, E. et al., 1995. Role of auxilin in uncoating clathrin-coated vesicles. *Nature*, 378(6557), pp.632–5. Available at: http://www.nature.com/nature/journal/v378/n6557/pdf/378632a0.pdf\nhttp://www.nature.com/nature/journal/v378/n6557/abs/378632a0.html\nhttp://www.ncbi.nlm.nih.gov/pubmed/8524399.

Vaillant, A.R. et al., 1999. Depolarization and neurotrophins converge on the phosphatidylinositol 3- kinase-Akt pathway to synergistically regulate neuronal survival. *Journal of Cell Biology*, 146(5), pp.955–966.

Vennekate, W. et al., 2012. Cis- and trans-membrane interactions of synaptotagmin-1. *Proceedings of the National Academy of Sciences*, 109(27), pp.11037–11042.

Verhage, M. et al., 2000. Synaptic assembly of the brain in the absence of neurotransmitter secretion. *Science (New York, N.Y.)*, 287(5454), pp.864–869.

Verhage, M. & S??rensen, J.B., 2008. Vesicle docking in regulated exocytosis. *Traffic*, 9(9), pp.1414–1424.

Vijayakrishnan, N., Phillips, S.E. & Broadie, K., 2010. Drosophila Rolling Blackout Displays Lipase Domain-Dependent and -Independent Endocytic Functions Downstream of Dynamin. *Traffic*, 11(12), pp.1567–1578.

Vijayakrishnan, N., Woodruff, E. a & Broadie, K., 2009. Rolling blackout is required for bulk endocytosis in non-neuronal cells and neuronal synapses. *Journal of cell science*, 122(Pt 1), pp.114–25. Available at: http://www.pubmedcentral.nih.gov/articlerender.fcgi?artid=2714403&tool=pmcentrez&rendertype=abstract.

Voglmaier, S.M. et al., 2006. Distinct Endocytic Pathways Control the Rate and Extent of Synaptic Vesicle Protein Recycling. *Neuron*, 51(1), pp.71–84.

Wang, J. et al., 2007. PI4P Promotes the Recruitment of the GGA Adaptor Proteins to the Trans-Golgi Network and Regulates Their Recognition of the Ubiquitin Sorting Signal. *Molecular Biology of the Cell*, 18(7), pp.2646–2655. Available at: http://www.molbiolcell.org/cgi/doi/10.1091/mbc.E06-10-0897.

Wang, L. et al., 2016. Eps15 membrane binding and bending activity acts redundantly with Fcho1 during clathrin-mediated endocytosis. *Molecular Biology of the Cell*, 1.

Wang, Y.J. et al., 2003. Phosphatidylinositol 4 phosphate regulates targeting of clathrin adaptor AP-1 complexes to the Golgi. *Cell*, 114(3), pp.299–310.

Watanabe, S. et al., 2014. Clathrin regenerates synaptic vesicles from endosomes. *Nature*, 515(V), pp.228–33. Available at: http://www.nature.com.328.han.fh-campuswien.ac.at/nature/journal/v515/n7526/full/nature13846.html.

Watanabe, S., Liu, Q., et al., 2013. Ultrafast endocytosis at Caenorhabditis elegans neuromuscular junctions. *eLife*, 2013(2).

Watanabe, S., Rost, B.R., et al., 2013. Ultrafast endocytosis at mouse hippocampal synapses. *Nature*, 504(7479), pp.242–7. Available at: http://www.ncbi.nlm.nih.gov/pubmed/24305055.

Wei, Y.J. et al., 2002. Type II phosphatidylinositol 4-kinase ?? is a cytosolic and peripheral membrane protein that is recruited to the plasma membrane and activated by Rac-GTP. *Journal of Biological Chemistry*, 277(48), pp.46586–46593.

Wen, P.J. et al., 2008. Ca2+-regulated pool of phosphatidylinositol-3-phosphate produced by phosphatidylinositol 3-kinase C2alpha on neurosecretory vesicles. *Molecular biology of the cell*, 19(12), pp.5593–5603.

Wen, P.J., Osborne, S.L. & Meunier, F.A., 2011. Dynamic control of neuroexocytosis by phosphoinositides in health and disease. *Progress in Lipid Research*, 50(1), pp.52–61.

Wenk, M.R. et al., 2001. PIP kinase I?? is the major PI(4,5)P2 synthesizing enzyme at the synapse. *Neuron*, 32(1), pp.79–88.

Wenzel, E.M. et al., 2012. Key physiological parameters dictate triggering of activity-dependent bulk endocytosis in hippocampal synapses. *PLoS ONE*, 7(6), p.e38188. Available at: http://www.pubmedcentral.nih.gov/articlerender.fcgi?artid=3366995&tool=pmcentrez&rendertype=abstract.

Whiteheart, S.W., Schraw, T. & Matveeva, E.A., 2001. N-ethylmaleimide sensitive factor (NSF) structure and function. *International Review of Cytology*, 207, pp.71–112.

Wienisch, M. & Klingauf, J., 2006. Vesicular proteins exocytosed and subsequently retrieved by compensatory endocytosis are nonidentical. *Nature neuroscience*, 9(8), pp.1019–27. Available at: http://www.ncbi.nlm.nih.gov/pubmed/16845386.

Wigge, P. et al., 1997. Amphiphysin heterodimers: potential role in clathrin-mediated endocytosis. *Molecular biology of the cell*, 8(10), pp.2003–2015.

Wilhelm, B.G. et al., 2014. Composition of isolated synaptic boutons reveals the amounts of vesicle trafficking proteins. *Science (New York, N.Y.)*, 344(6187), pp.1023–8. Available at: http://www.ncbi.nlm.nih.gov/pubmed/24876496.

Willox, A.K. & Royle, S.J., 2012. Stonin 2 is a major adaptor protein for clathrin-mediated synaptic vesicle retrieval. *Current Biology*, 22(15), pp.1435–1439.

Willox, A.K., Sahraoui, Y.M.E. & Royle, S.J., 2014. Non-specificity of Pitstop 2 in clathrin-mediated endocytosis. *Biology open*, 3, pp.326–31. Available at: http://www.pubmedcentral.nih.gov/articlerender.fcgi?artid=4021354&tool=pmcentrez&rendertype=abstract.

de Wit, H. et al., 2009. Synaptotagmin-1 Docks Secretory Vesicles to Syntaxin-1/SNAP-25 Acceptor Complexes. *Cell*, 138(5), pp.935–946.

Woodgett, J.R., 1990. Molecular cloning and expression of glycogen synthase kinase-3/factor A. *The EMBO journal*, 9(8), pp.2431–8. Available at: http://www.pubmedcentral.nih.gov/articlerender.fcgi?artid=552268&tool=pmcentrez&rendertype=abstract.

Woscholski, R. et al., 1998. Identification and characterisation of a novel splice variant of synaptojanin1. *FEBS Lett*, 432, pp.5–8.

Wragg, R.T. et al., 2013. Synaptic Vesicles Position Complexin to Block Spontaneous Fusion. *Neuron*, 77(2), pp.323–334.

Wu, L.-G., Ryan, T.A. & Lagnado, L., 2007. Modes of Vesicle Retrieval at Ribbon Synapses, Calyx-Type Synapses, and Small Central Synapses. *Journal of Neuroscience*, 27(44), pp.11793–11802. Available at: http://www.jneurosci.org/cgi/doi/10.1523/JNEUROSCI.3471-07.2007.

Wu, X.-S. et al., 2009. Ca(2+) and calmodulin initiate all forms of endocytosis during

depolarization at a nerve terminal. *Nature neuroscience*, 12(8), pp.1003–1010.

Wucherpfennig, T., Wilsch-Bräuninger, M. & González-Gaitán, M., 2003. Role of Drosophila Rab5 during endosomal trafficking at the synapse and evoked neurotransmitter release. *Journal of Cell Biology*, 161(3), pp.609–624.

Xu, J., Mashimo, T. & S??dhof, T.C., 2007. Synaptotagmin-1, -2, and -9: Ca2+ Sensors for Fast Release that Specify Distinct Presynaptic Properties in Subsets of Neurons. *Neuron*, 54(4), pp.567–581.

Xue, M. et al., 2008. The Janus-faced nature of the C(2)B domain is fundamental for synaptotagmin-1 function. *Nature structural & molecular biology*, 15(11), pp.1160–8. Available at: http://www.pubmedcentral.nih.gov/articlerender.fcgi?artid=2587052&tool=pmcentrez&rendertype=abstract.

Yang, X. et al., 2010. Complexin Clamps Asynchronous Release by Blocking a Secondary Ca2+ Sensor via Its Accessory ?? Helix. *Neuron*, 68(5), pp.907–920.

Yao, P.J., 2004. Synaptic frailty and clathrin-mediated synaptic vesicle trafficking in Alzheimer's disease. *Trends in neurosciences*, 27(1), pp.24–9. Available at: http://www.sciencedirect.com/science/article/pii/S0166223603003710 [Accessed May 24, 2016].

Yoshimura, T. et al., 2005. GSK-3β regulates phosphorylation of CRMP-2 and neuronal polarity. *Cell*, 120(1), pp.137–149.

Yuan, T.L. et al., 2011. Cell-to-cell variability in PI3K protein level regulates PI3K-AKT pathway activity in cell populations. *Current Biology*, 21(3), pp.173–183.

Zaydman, M.A. et al., 2013. Kv7.1 ion channels require a lipid to couple voltage sensing to pore opening. *Proceedings of the National Academy of Sciences of the United States of America*, 110(32), pp.13180–5. Available at: http://www.pubmedcentral.nih.gov/articlerender.fcgi?artid=3740903&tool=pmcentrez&rendertype=abstract.

Zhao, M. et al., 2015. Mechanistic insights into the recycling machine of the SNARE complex. *Nature*, 518(7537), pp.61–67. Available at: http://dx.doi.org/10.1038/nature14148.

Zhou, L., McInnes, J. & Verstreken, P., 2014. Ultrafast synaptic endocytosis cycles to the center stage. *Developmental Cell*, 28(1), pp.5–6.

Zhou, Q. et al., 2014. Molecular insights into the membrane-associated phosphatidylinositol 4-kinase IIα. *Nature communications*, 5(3552), pp.1–10. Available at: http://www.ncbi.nlm.nih.gov/pubmed/24675427.

Zhu, Y., Xu, J. & Heinemann, S.F., 2009. Two Pathways of Synaptic Vesicle Retrieval Revealed by Single-Vesicle Imaging. *Neuron*, 61(3), pp.397–411.

Zoncu, R. et al., 2007. Loss of endocytic clathrin-coated pits upon acute depletion of

phosphatidylinositol 4,5-bisphosphate. *Proceedings of the National Academy of Sciences of the United States of America*, 104(10), pp.3793–8. Available at: http://www.pubmedcentral.nih.gov/articlerender.fcgi?artid=1805489&tool=pmcentrez&rendertype=abstract.

Zumbrunn, J. et al., 2001. Binding of the adenomatous polyposis coli protein to microtubules increases microtubule stability and is regulated by GSK3β phosphorylation. *Current Biology*, 11(1), pp.44–49.